

BACTERIAL COLD STRESS AND ANTIBIOTIC DISCOVERY

**EXPLOITING COLD SENSITIVITY IN *ESCHERICHIA COLI* TO IDENTIFY
NOVEL ANTIBACTERIAL MOLECULES**

By Jonathan M. Stokes, B.H.Sc.

A thesis submitted to the School of Graduate Studies in partial fulfillment of the
requirements for the degree of Doctor of Philosophy

McMaster University © Jonathan M. Stokes, June 2016

PhD Thesis – J. M. Stokes; McMaster University – Biochemistry and Biomedical Science

DOCTOR OF PHILOSOPHY (2016) McMaster University

(Biochemistry and Biomedical Sciences) Hamilton, Ontario

TITLE: Exploiting cold sensitivity in *Escherichia coli* to identify novel antibacterial molecules

AUTHOR: Jonathan M. Stokes, B.H.Sc.

SUPERVISOR: Eric D. Brown, Ph.D.

PAGES: XI; 252

Abstract

The widespread emergence of antibiotic resistance determinants for nearly all drug classes threatens human health on a global scale. It is therefore essential to discover antibiotics with novel functions that are less likely to be influenced by pre-existing resistance mechanisms. An emerging approach to identify inhibitors of investigator-defined cellular processes involves screening compounds for antimicrobial activity under non-standard growth conditions. Indeed, by growing cells under conditions of stress, inhibitors of specific cellular targets can be enriched, thereby allowing for the identification of molecules with predictable activities in the complex environment of the cell. Here, I exploit cold stress in *Escherichia coli* to identify molecules targeting ribosome biogenesis and outer membrane biosynthesis. First, through a screen of 30,000 small molecules for growth inhibition exclusively at 15°C, I was able to identify the first small molecule inhibitor of bacterial ribosome biogenesis, lamotrigine. Second, by leveraging the idiosyncratic cold sensitivity of *E. coli* to vancomycin, I developed a novel screening technology designed to enrich for non-lethal inhibitors of Gram-negative outer membrane biosynthesis. From this platform, I identified pentamidine as an efficient outer membrane perturbant that was able to potentiate Gram-positive antibiotics against Gram-negative pathogens, similar to the polymyxins. Remarkably, however, this compound was able to overcome *mcr-1* mediated polymyxin resistance. Together, this thesis highlights the utility of exploiting the bacterial cold stress response in antibiotic discovery.

Acknowledgements

Dr. Eric Brown – thank you for your guidance and support. In the times of greatest uncertainty, your unwavering confidence in my work helped foster the ambition to pursue what I perceived as important questions. I am deeply indebted, and will work hard to elevate budding scientists throughout my career.

Drs. Gerry Wright, Mike Surette, and Justin Nodwell – a fine balance of valuable scientific input and persistent challenging of my conjectures has made me a more refined scientist, both in practice and in philosophy. Time and effort are valuable commodities, and for yours I am thankful.

Channel 4 – rarely will one meet a more foolish group of people who are able to accomplish so much. It's been a privilege working with you.

Mom and Vanessa – even in my long periods of absence, your love and affection are omnipresent. It's the comfort of family that has allowed me to focus on my work. I love you both.

Angela – I don't know what brings two distant people together in space and time, whether it's chance, or whether the happenings of the universe are predetermined. Much of the time I believe the former, but why I would be so lucky to have met you I can't understand. Your support throughout my studies has been perpetual, and no words of mine can capture my appreciation. I will love you until the final second of the final clock ticks. This is yours.

Me – Well done. Work harder.

Table of contents

Foreword	
Abstract	IV
Acknowledgements	V
Table of contents	VI
List of figures	VIII
List of tables	X
List of abbreviations	XI
Chapter I – Introduction	
A brief history of antibiotic discovery	2
The re-emergence of phenotypic screening	4
Chemical probes of the ribosome and its assembly	6
Ribosome biogenesis <i>in vivo</i>	9
Cold sensitivity	14
Membrane permeability in Gram-negative bacteria	15
LPS structure and biosynthesis	18
Chemical perturbation of LPS structure and biosynthesis	20
References	24
Figure legends	32
Figures	34
Chapter II – Discovery of a small molecule that inhibits bacterial ribosome biogenesis	
Preface	38
Abstract	39
Introduction	39
Results	42
Discussion	58
Materials and methods	63
Accession numbers	71
Acknowledgements	71
Author contributions	72
References	72
Figure legends	76
Figures	89
Chapter III – Chemical modulators of ribosome biogenesis as biological probes	
Preface	106
Abstract	107
Introduction	107
The methods that shaped our understanding of ribosome biogenesis	110
The pitfalls of current <i>in vivo</i> methods	114
The discovery and characterization of a specific inhibitor of bacterial ribosome biogenesis	118
Developing ribosome biogenesis inhibitors of diverse function	121

Concluding remarks	130
Acknowledgements	130
References	130
Figure legends.....	139
Table 1	143
Figures	144
Chapter IV – Cold stress makes <i>Escherichia coli</i> susceptible to glycopeptide antibiotics by altering outer membrane integrity	
Preface	149
Summary	150
Introduction.....	150
Results	154
Discussion	162
Significance	168
Experimental procedures	169
Author contributions	175
Acknowledgements	175
References	175
Figure legends.....	180
Supplemental figure legends	183
Table S1	187
Figures	188
Chapter V – An antiprotozoal drug overcomes <i>mcr-1</i> mediated colistin resistance	
Preface	201
Text.....	202
Methods.....	210
References	217
Acknowledgements	221
Author Contributions.....	221
Figure Legends	222
Extended Data Figure Legends.....	226
Table 1	230
Figures	231
Chapter VI – Conclusions	
Suggestions for future research	240
Is ribosome biogenesis an attractive drug target?.....	241
How should we target the Gram-negative outer membrane?.....	245
Concluding remarks	249
References	250

List of figures

Chapter I	
Figure 1 – Structure of the <i>E. coli</i> ribosome	34
Figure 2 – LPS transport in <i>E. coli</i>	35
Figure 3 – Assembly of lipid A and core OS.....	36
Chapter II	
Figure 1 – The ribosome is a primary targets of cold stress	89
Figure 1 supplement 1 – Primary data from the screen of the <i>E. coli</i> Keio collection	90
Figure 2 – Lamotrigine induces profound cold sensitivity in <i>E. coli</i>	91
Figure 2 supplement 1 – Primary data from the small molecule screen	92
Figure 2 supplement 2 – Temperature-dependence of lamotrigine activity in <i>E. coli</i>	93
Figure 3 – Lamotrigine treatment results in the accumulation of non-native ribosomal particles	94
Figure 3 supplement 1 – Temperature-dependent antibiotic activity in <i>E. coli</i>	95
Figure 4 – Non-native ribosomal particles are immature 30S and 50S subunits	96
Figure 4 supplement 1 – 5' primer extension of lamotrigine-treated <i>E. coli</i>	97
Figure 4 supplement 2 – R-protein mass spectrometry of ribosomal particles from lamotrigine-treated <i>E. coli</i>	98
Figure 5 – Lamotrigine binds to wild type but not mutant IF2 in a G-nucleotide-dependent manner	99
Figure 5 supplement 1 – Genetic determinants of lamotrigine activity	100
Figure 6 – Accumulation of immature ribosomal subunits is not the result of translation inhibition	101
Figure 6 supplement 1 – Effects of lamotrigine on translation in <i>E. coli</i>	102
Figure 7 – Immature ribosomal particles sediment as mature subunits upon removal of lamotrigine stress	104
Chapter III	
Figure 1 – Simplified overview of ribosome biogenesis	144
Figure 2 – Classical methods to study ribosome biogenesis	145
Figure 3- Genetic perturbation of ribosome biogenesis factors lacks temporal resolution and can lead to multiple unrelated phenotypic effects.....	146
Figure 4 – Small molecule inhibitors of ribosome biogenesis provide kinetic resolution of events following perturbation.....	147
Chapter IV	
Figure 1 – Vancomycin inhibits growth of <i>E. coli</i> in a temperature-dependent manner	188
Figure 2 – Genetic perturbations in outer membrane biosynthesis cause vancomycin resistance.....	189
Figure 3 – LPS profiles of vancomycin-sensitive and –resistant <i>E. coli</i> strains	190

Figure 4 – Modifications in LPS chemistry affect vancomycin activity in <i>E. coli</i>	191
Figure 5 – Proposed structures of core OS from wild type and Y324* mutant <i>E. coli</i>	192
Figure 6 – Proposed model for vancomycin activity in <i>E. coli</i> at low growth temperature	193
Figure S1 – Growth of <i>E. coli</i> at 37°C and 15°C	194
Figure S2 – Temperature-dependent activity of glycopeptides against <i>E. coli</i>	195
Figure S3 – Phenotypic characterization of the vancomycin resistant <i>E. coli</i> strains	196
Figure S4 – Antibiotic susceptibility of a core-OS deficient $\Delta rfaE$ strain of <i>E. coli</i>	197
Figure S5 – Charge-deconvoluted negative-ion ESI mass spectra of core OS isolated from wild type and Y324* mutant	198
Figure S6 – Charge-deconvoluted negative-ion ESI mass spectra of lipid A isolated from wild type <i>E. coli</i> and Y324* mutant	199
Chapter V	
Figure 1 – A vancomycin antagonism screening platform identifies pentamidine	231
Figure 2 – Pentamidine potentiates Gram-positive antibiotics in Gram-negative pathogens	232
Figure 3 – Pentamidine is an adjuvant in Gram-negative organisms containing <i>mcr-1</i>	233
Figure 4 – Pentamidine potentiates Gram-positive antibiotics against wild type and <i>mcr-1</i> positive <i>A. baumannii</i> in systemic murine infection models	234
ED Figure 1 – Cell surface analyses of <i>E. coli</i> treated with outer-membrane active molecules	235
ED Figure 2 – Pentamidine-dependent potentiation of antibiotics against <i>E. coli</i>	236
ED Figure 3 – Sensitivity of <i>mcr-1</i> positive <i>E. coli</i> to colistin	237
ED Figure 4 – <i>In vivo</i> efficacy of pentamidine against <i>A. baumannii</i>	238

List of tables

Chapter III	
Table 1 – Characterized whole cells-active small molecule inhibitors of ribosome biogenesis	143
Chapter IV	
Table S1 – <i>E. coli</i> Keio strains that displayed resistance to vancomycin at 15°C.	187
Chapter V	
Table 1 – Activity of pentamidine analogs against <i>E. coli</i>	230

List of abbreviations

ATP	adenosine triphosphate
GTP	guanosine triphosphate
GDP	guanosine diphosphate
UDP	uridine diphosphate
rRNA	ribosomal RNA
mRNA	messenger RNA
tRNA	transfer RNA
r-protein	ribosomal protein
IF2	translation initiation factor 2
eIF5b	eukaryotic initiation factor 5b
Pgm	phosphoglucosmutase
LPS	lipopolysaccharide
Core OS	LPS core oligosaccharide
Kdo	3-deoxy-D-manno-oct-2-ulosonic acid
Hep	L-glycero-D-manno-heptose
PEtN	phosphoethanolamine
PMBn	polymyxin B nonapeptide
DMSO	dimethyl sulfoxide
TCA	trichloroacetic acid
EDTA	ethylenediaminetetraacetic acid
PBS	phosphate buffered saline
MIC	minimum inhibitory concentration
FIC	fractional inhibitory concentration
OD	optical density
LB	lysogeny broth
M9	M9 minimal growth media
PCR	polymerase chain reaction
TEM	transmission electron microscopy
AFM	atomic force microscopy
ESI-TOF	electrospray ionization time-of-flight mass spectrometry

CHAPTER I - Introduction

A brief history of antibiotic discovery

The application of antibiotics to treat infection is perhaps the greatest achievement of medicine, dramatically increasing human longevity through non-invasive means. Penicillin, the first of our “modern” antibiotics, was discovered by Alexander Fleming in 1929 and developed as a clinical agent by Howard Florey and Ernst Chain prior to World War II. Remarkably, during World War I it is estimated that 12-15 percent of wounded soldiers treated in front-line hospitals died of infection, a figure that dropped to ~3 percent during World War II, due largely to the implementation of penicillin¹. In the wake of this success, a period spanning from the early-1940s to the early-1960s saw significant progress in antibiotic discovery, where some 20 structurally and functionally diverse classes of antibiotics were identified and characterized. Unfortunately, this golden era of antibiotic discovery was followed by a dramatic waning of productivity, and since 1961 only 7 new classes of clinically valuable antibiotics have been identified, the latest being the tuberculosis-specific bedaquiline in 2005^{2,3}.

This waning of discovery, if viewed as an isolated phenomenon, would be unlikely to pose a significant clinical concern due to the broad pathogen coverage of our current antibiotic arsenal. However, the simultaneous global dissemination of antibiotic resistance determinants due to drug overuse is rapidly eroding the efficacy of these compounds, threatening the re-emergence of a pre-antibiotic era. While anecdotal evidence suggests that the use of antibiotics in clinical and agricultural settings is becoming slightly more conservative, without the advent of

structurally and functionally novel compounds, untreatable infections are likely to become increasingly common.

Antibiotic discovery has evolved through several epochs aimed at maximizing productivity with available technologies⁴. Early research largely involved screening soil-dwelling actinomycetes for metabolites that caused bacterial cell killing or growth inhibition, without specific targets in mind. This route to antibiotic discovery defines the golden era, highlighting the value of empirical discovery of antibacterial molecules. Towards the mid-1960s, identifying novel antibiotic scaffolds through such methods became increasingly difficult. This ushered in a period dominated by medicinal chemistry, where structural analogs of existing antibiotics were synthesized in order to improve pathogen spectrum, decrease host toxicity, increase potency, and overcome resistance. Indeed, due to the success of this approach, structural modification of existing antibiotics remains essential.

The mid-1990s witnessed a hopeful era of novel drug discovery fueled by a combination of emerging resistance and new technologies. During this time, software-guided robotics were entering the laboratory, the first bacterial genomes were being sequenced, and breakthroughs in recombinant DNA technologies allowed investigators to purify large quantities of proteins for high-throughput screening of synthetic chemical libraries. In theory, the marriage of high-throughput *in vitro* technologies with the computational capabilities to recognize essential gene products should have resulted in a successful new wave of target-

based drug discovery. On the contrary, this era has been defined by repeated failures, primarily because highly potent *in vitro* inhibitors failed to display activity in whole-cell assays⁵. Poor membrane permeability of *in vitro* actives was largely to blame, although it may be that an under-appreciation for the complexity of cellular systems also contributed to this loss activity from *in vitro* to intracellular environments.

The re-emergence of phenotypic screening

Target-based screening is an inherently reductionist approach. Detailed knowledge of a protein of interest is paramount prior to developing a targeted screen, and failures to appreciate the essentiality of gene products in the context of infection have likely narrowed the scope of what investigators would consider druggable. It is therefore appropriate to once again focus on empirical screening for molecules that are growth-inhibitory against cells. However, where golden era discovery efforts largely aimed to identify molecules that displayed antibacterial activity under optimal growth conditions – rich media at 37°C – compounds with novel mechanisms of action that are unlikely to be affected by pre-existing antibiotic resistance determinants should be identified through non-conventional screening approaches. In this manner, bioactive molecules can be enriched for targeting investigator-defined cellular processes, while avoiding the re-discovery of old antibiotics.

To demonstrate this approach, Zlitni *et al.* conducted a screen of ~30,000 synthetic small molecules for those that specifically inhibited metabolic processes in wild type *Escherichia coli*⁶. This was accomplished by identifying compounds that displayed growth inhibition in minimal growth media, but not in rich defined conditions. Indeed, in this work the authors showed that 119 *E. coli* gene products that were dispensable for growth in rich media became essential in minimal media, highlighting a sizable target list that would be inaccessible under typical growth conditions. Using this approach, three novel molecules were identified that inhibited glycine metabolism, *p*-aminobenzoic acid biosynthesis, and biotin biosynthesis.

Furthermore, where the nutrient-limitation screening approach of Zlitni *et al.* allowed for broad access to a relatively large target set, work by Farha *et al.* highlights an alternative phenotypic screening platform aimed at targeting a narrower scope of cellular processes⁷. Here, the authors designed a screen to identify inhibitors of so-called early steps in Gram-positive wall teichoic acid biosynthesis. This was done by screening a small chemical library against *Staphylococcus aureus* and observing for cell growth in the presence of lethal concentrations of targocil – a known late step teichoic acid biosynthesis inhibitor⁸. Due to the well-characterized phenotype that lethal deletions in late step teichoic acid genes are rescued by concurrent deletions in early step genes⁹, this screen was able to be relatively specific in its predicted target list. Indeed, the authors successfully identified and characterized an inhibitor of *S. aureus* UppS, an

enzyme involved in the biosynthesis of a polyisoprenoid essential for peptidoglycan and teichoic acid biosynthesis.

These approaches – both of which have significantly influenced my thinking at various periods throughout my studies – in addition to recent others, demonstrate how investigators can enrich for inhibitors of specific cellular targets by modulating cellular growth conditions accordingly (reviewed in ¹⁰). Together, this growing body of work suggests that cell-based screens can be developed for most, if not all, cellular processes provided that a fairly specific and robust phenotype can be elucidated. This line of thinking fueled my studies.

Chemical probes of the ribosome and its assembly

The ribosome is an essential 2.4 MDa ribonucleoprotein complex responsible for translating the nucleotide sequences of mRNA into proteins¹¹ (Figure 1a). These universally conserved machines are composed of two subunits. The small subunit (30S in bacteria) contains a single 16S ribosomal RNA (rRNA) molecule and 21 ribosomal proteins (r-proteins), and mediates base-pairing interactions between mRNA and tRNA. The large subunit (50S in bacteria) contains a 23S rRNA, a 5S rRNA, and 33 r-proteins, and houses the center responsible for catalyzing peptide bond formation between adjacent amino acids.

The first inhibitor of the bacterial ribosome was the aminoglycoside streptomycin, isolated in 1943 by Albert Schatz, a graduate student under the

supervision of Selman Waksman¹². Since then, ~10 functionally unique classes of antibiotics targeting the ribosome have found clinical utility, with the most recent being the oxazolidinones discovered in 1978². Both natural product and synthetic translation inhibitors have been discovered that inhibit all three stages of translation – initiation, elongation, and termination/ribosome recycling – highlighting the complexity of the ribosome, as well as its intrinsic druggability¹³. Importantly, in addition to providing effective clinical treatments, these molecules have been essential to our increased understanding of the structure and function of the ribosome during the various stages of translation. However, in over a century of antibiotic discovery, no small molecules that directly and specifically inhibit the assembly of the bacterial ribosome have been reported. Given the important roles that translation inhibitors have played as antibiotics and as probes of ribosome biochemistry, this lack of small molecule perturbants of the assembly process is surely a hindrance in both arenas.

Ribosome biogenesis, which consumes ~40% of the cell's energy in rapidly growing *E. coli*¹⁴, involves (a) the coordinated transcription, modification, and folding of rRNA; (b) translation, modification, and folding of r-proteins; (c) binding of r-proteins to the appropriate rRNA scaffolds; and (d) the binding and release of ribosome biogenesis factors. *In vivo*, these events occur in parallel, and exemplify a highly dynamic system of interrelated processes that occur cooperatively to narrow the assembly landscape of the ribosome into a

translationally competent state¹⁵. In the context of a bacterial cell this process is highly efficient, requiring only ~2 minutes to occur¹⁶.

Intriguingly, while it has been shown that ribosomal subunits will spontaneously assemble *in vitro*¹⁷⁻²¹, this process requires inordinate durations, temperatures, and ionic conditions that are far from physiological. The significant difference between assembly efficiency *in vivo* and *in vitro* can be largely attributed to the action of ribosome biogenesis factors, which transiently bind immature ribosomal subunits to enhance the rate of assembly through wide-ranging putative functions^{15,22}. Historically, genetic manipulation of these ribosome biogenesis factors has been the primary method to elucidate the molecular events underlying ribosome assembly *in vivo*. Specifically, genetic perturbation of ribosome assembly factors inhibits or decreases the rate of assembly, making it possible to isolate and biochemically characterize the relatively abundant resultant particles. Indeed, assembly intermediates represent just ~2% of ribosomal particles in wild type cells¹⁶, prohibiting detailed biochemical analyses.

Often overlooked, however, are the consequences of genetic perturbation and the physiological relevance of the particles isolated from such genetic means. Previous work has shown that the phenotypes associated with mutations in ribosome biogenesis factors can be wide ranging²³⁻²⁷, making it difficult to unambiguously assign a specific function to a specific protein. Furthermore, immature subunits that accumulate in ribosome biogenesis factor mutants at

steady state may not be *bona fide* intermediates, but may instead represent aberrant products of a process gone awry. In this context, small molecule inhibitors of ribosome biogenesis factors have unique advantages over genetic techniques for understanding this process *in vivo*. Specifically, chemicals can exert their effects on a time scale of seconds, be added and removed from systems at will, and afford the critical opportunity to follow the impact of perturbation with kinetic resolution. Therefore, chemical perturbants can be elegant probes of complex cellular systems and the macromolecules that function therein.

Ribosome biogenesis *in vivo*

Bacterial ribosome biogenesis initiates with the production of a primary rRNA transcript containing 16S, 23S, and 5S rRNA, which is cleaved by a series of ribonucleases to release mature forms of each rRNA species (Figure 1b). Importantly, processing and assembly of the primary rRNA transcript begins before transcription is complete, with concurrent formation of secondary rRNA structures and association of r-proteins immediately upon exposure of the necessary binding sites. The first endoribonuclease to cleave the primary rRNA transcript is RNase III, which coarsely separates precursor rRNAs. The products of this cleavage are pre-16S rRNA (17S rRNA), pre-23S rRNA, pre-5S rRNA (9S rRNA), and depending on the *rrn* operon, a few pre-tRNAs^{28,29}. To generate mature 16S rRNA, 115 nucleotides are removed from the 5' end of 17S rRNA

through the sequential actions of RNase E and RNase G³⁰. A currently unknown RNase is responsible for cleaving 33 nucleotides from the 3' terminus³¹. After initial RNase III cleavage, 3 or 7 nucleotides from the 5' end and 7 or 9 nucleotides from the 3' end of pre-23S rRNA are further trimmed by RNase III. Final processing of the 3' terminus requires RNase T³², whereas maturation of the 5' terminus is conducted by an unknown enzyme. Lastly, 84 nucleotides from the 5' end of 9S rRNA, as well as 42 nucleotides from the 3' end are cleaved by RNase E, leaving 3 extra nucleotides at both termini³³. Final maturation at the 3' end has been shown to depend on RNase T³⁴, while the 5'-active RNase has yet to be determined.

In addition to 5' and 3' trimming, various conserved 16S and 23S rRNA nucleotides are covalently modified during maturation. In *E. coli*, 16S rRNA contains 11 modified positions, of which 10 are methylations and 1 is a pseudouridylation. Furthermore, 23S rRNA contains 25 known modifications – 14 methylations, 9 pseudouridylations, 1 methylated pseudouridylation, and 1 that is currently unknown¹⁵. Most of these modifications cluster to the 30S decoding region and 50S peptidyl transferase center, suggesting their importance for accurate and efficient translation³⁵. Indeed, while *in vitro* unmodified 16S rRNA and all of the natural 30S r-proteins can reconstitute active 30S subunits, these display significantly reduced activity relative to wild type particles³⁶. Furthermore, *in vitro* unmodified transcripts of 23S rRNA occupied by natural 50S r-proteins are unable to be reconstituted into catalytically active subunits³⁷. However, while

decreased translation efficiency and/or deficiencies in subunit assembly *in vitro* have been observed, our understanding of the precise functions of these modifications is generally poor, and efforts aimed at determining their precise roles during assembly and translation continue.

In addition to rRNA nucleotides, it has been observed that 5 r-proteins from the 30S subunit and 6 r-proteins from the 50S subunit are post-translationally modified²². It is important to note that additional modifications may exist but have yet to be identified. The fact that numerous r-proteins are modified, and that many of these contain multiple modifications, suggest that covalent modifications are important for ribosome structure and function, similar to those on rRNA. Specifically, these may optimize the specificity of r-protein binding to specific rRNA regions on the assembling ribosome. Additionally, it has been hypothesized that the modifications present in sub-stoichiometric quantities may be a mechanism to signal the physiological state of the cell³⁸. Despite their predicted significance, the only r-protein modification known to produce a phenotype when absent *in vivo* is the methylation of the 50S subunit r-protein L3, which results in cold sensitivity and an accumulation of ribosomal subunit precursors, suggesting a role in ribosome biogenesis^{39,40}.

Beyond the enzymes necessary for proper rRNA processing and covalent modification of rRNA and r-proteins, upwards of 30 additional ribosome biogenesis factors perform an array of putative functions to narrow the assembly landscape of 30S and 50S subunits *in vivo*. Consider that as the length of an

RNA molecule increases, so too does the number of secondary structures it can access⁴¹. In the context of large rRNA molecules, local mis-folded regions may be quite stable, explaining the low rate of spontaneous assembly *in vitro*, as immature subunits must sample numerous conformations prior to proceeding to subsequent assembly events. *In vivo*, ribosome biogenesis factors are hypothesized to limit the folding landscape of rRNA, facilitate r-protein/rRNA interactions, and function as checkpoints during the assembly process, thereby dramatically increasing the rate and accuracy of subunit maturation.

Depending on function, ribosome biogenesis factors are generally classified as DEAD-box RNA helicases, ribosome-dependent GTPases, and/or general maturation factors. While an exhaustive discussion of the putative functions of each protein is unnecessary in the context of this thesis, a number of important concepts should be recognized: (a) ribosome biogenesis factors drive discrete molecular events on both subunits; (b) genetic interactions are frequently observed between assembly factors with putatively divergent functions; and (c) the precise functions of all ribosome biogenesis factors discovered to date remain somewhat ill-defined.

These notions can be captured through investigations that have involved two well-studied canonical ribosome biogenesis factors, RsgA and EngA. RsgA is a non-essential ribosome-stimulated GTPase that assists in 30S subunit assembly⁴². Previous work has shown that RsgA associates with 30S subunits when in the presence of the non-hydrolyzable GTP analog GMP-PNP⁴³, and that

a $\Delta rsgA$ strain of *E. coli* displays sensitivity to growth at low temperatures⁴⁴ and accumulates free 30S and 50S subunits⁴⁵. Furthermore, deletion of *rsgA* leads to the accumulation of 17S rRNA, strongly suggesting a role in the late stages of 30S subunit biogenesis⁴⁶. Interestingly, overexpression of the essential 30S biogenesis factor Era partially suppresses the slow growth phenotype of a $\Delta rsgA$ strain, and decreases the abundance of free 30S and 50S subunits with a concurrent increase in 70S ribosomes⁴⁵. Overexpression of a mutant form of the 30S assembly factor RbfA similarly suppresses the defects in an *rsgA* deletion background⁴⁷. Contrarily, deletion of the 30S assembly factors RimM and KsgA enhances the deleterious effects of a $\Delta rsgA$ strain⁴⁵.

Where RsgA is non-essential, the ribosome biogenesis factor EngA is an essential enzyme necessary for maturation of the 50S subunit. Previous work has shown that EngA associates with 50S subunits in the presence of a non-hydrolyzable GTP analog⁴⁸, and that EngA depletion leads to cold sensitivity⁴⁹ and the accumulation of free 30S and 50S subunits at the expense of 70S ribosomes⁵⁰. Furthermore, a $\Delta engA$ strain of *E. coli* displays an abundance of unprocessed 16S and 23S rRNA species⁴⁸. Together, these data are consistent with a role during the later stages of 50S subunit maturation. Additionally, and similarly to the genetic interactions observed in the $\Delta rsgA$ background, it has been shown that overexpression of EngA rescues the slow-growth phenotype of a $\Delta rrmJ$ strain of *E. coli*, which also facilitates 50S subunit biogenesis⁵¹.

Together, these observations explicitly show that both RsgA and EngA play important roles in 30S and 50S subunit biogenesis, respectively. However, absent from the above discussions are detailed mechanistic descriptions of their specific roles during ribosome assembly. Indeed, this is the case for all bacterial ribosome biogenesis factors. As alluded to earlier, it is likely that only general functional assignments have been made due to a lack of proper biochemical tools with which to probe ribosome assembly. Therefore, chemical probes of bacterial ribosome biogenesis may offer essential advantages toward enhancing our understanding of the molecular events underlying this dynamic and time-dependent process.

Cold sensitivity

Where ribosome biogenesis factors are hypothesized to perform a wide array of functions, and result in numerous phenotypes upon deletion or depletion, one commonality amongst many of these proteins is their temperature-dependent essentiality. Here, this is defined as the phenotype where mutants do not display significant perturbations in cell growth at 37°C, but are severely attenuated at higher or lower temperatures. As we and others have shown⁴⁴, loss of various assembly factors in *E. coli* results in cold and heat sensitivity, with the former being significantly more common. It is hypothesized that as temperature decreases, rRNA transcripts can assume a greater number of non-native stable secondary and tertiary structures, necessitating the action of ribosome

biogenesis factors to release immature subunits from kinetic traps, thereby allowing for proper assembly.

As will be described in chapters 2 and 3, identifying small molecules that inhibited the growth of *E. coli* exclusively at low temperatures proved to be a suitable phenotype toward identifying molecules that targeted ribosome biogenesis. Excitingly, it was through this approach that we discovered the first small molecule inhibitor of bacterial ribosome biogenesis, lamotrigine. However, rarely do phenotypic assays isolate a single cellular process. Indeed, while our work has shown that screening for cold sensitivity significantly enriched for proteins involved in ribosome biogenesis, a sizable array of additional targets was found to be accessible using this phenotype. Surprisingly, the Gram-negative outer membrane was amongst these.

Membrane permeability in Gram-negative bacteria

Gram-negative bacteria synthesize an inner membrane that encloses the cytoplasm, and an outer membrane that is exposed to the extracellular milieu. The outer membrane, which is essential for life in Gram-negative species, is a highly selective barrier against extracellular solutes. This characteristic prevents the diffusion of large and hydrophobic molecules in particular, many of which are potent antibiotics against Gram-positive organisms that lack an outer membrane. Indeed, numerous reports from the pharmaceutical sector have highlighted the extreme challenges in identifying novel Gram-negative antibiotics, and attribute

this lack of success to poor outer membrane permeability of *in vitro* active molecules^{5,52}. For instance, a recent paper by Tommasi *et al.*⁵² described the relationship between *in vitro* potency of lead antibacterial molecules, and activity in whole cell assays. Here, small molecules were synthesized towards enhanced activity against purified *Pseudomonas aeruginosa* MurC, an enzyme involved in early events of peptidoglycan biosynthesis. Compounds that displayed increased *in vitro* potency tended to increase in hydrophobicity, however increasing hydrophobicity correlated with decreased activity against whole cells.

This inverse relationship between activity *in vitro* versus that *in vivo* may represent one of the primary challenges in Gram-negative antibiotic discovery. From a medicinal chemistry perspective, one possible solution may involve designing highly potent – and generally hydrophobic – *in vitro* inhibitors with the hypothesis that this may overcome poor permeability. Alternatively, one could imagine developing slightly more hydrophilic compounds with decreased *in vitro* potency, with the goal of improving permeability to reach effective intracellular concentrations of inhibitor. Unfortunately, both approaches have encountered difficulties. However, it is likely that reconciling the opposing chemical requirements for enzyme-based and cell-based activity is possible through an increased understanding of the fundamental principles of outer membrane permeability.

A chief contributor to the selective permeability of the Gram-negative outer membrane is lipopolysaccharide (LPS). This molecule is found exclusively in the

outer leaflet of the outer membrane, and $\sim 2 \times 10^6$ copies cover 75% of the *E. coli* cell surface⁵³. LPS is an amphipathic molecule that contains a fatty acyl moiety – lipid A – covalently linked to a core oligosaccharide (core OS), which is bound to a chemically variable long-chain O-antigenic polysaccharide in many species. It is important to note that *E. coli* K-12 and its derivatives are largely lacking O polysaccharide, and contain only lipid A and core OS⁵⁴; the lipid A – core OS complex will be the primary focus of subsequent discussions.

Under normal laboratory conditions, lipid A of *E. coli* consists of a β -1'-6-linked glucosamine disaccharide that is phosphorylated at the 1 and 4' positions, and contains 6 fatty acyl chains with lengths of 12 or 14 carbons. Attached to this disaccharide at the 6' position is core OS, which has been conceptually divided into inner core and outer core based on carbohydrate composition. The inner core is composed of 3-deoxy-D-manno-oct-2-ulosonic acid (Kdo) and L-glycero-D-manno-heptose (Hep), and the outer core contains primarily hexose and acetamidohexose sugars⁵⁵. The lipid A – core OS complex is assembled on the cytoplasmic face of the inner membrane, and is subsequently flipped to the periplasmic surface by the essential ATP-binding cassette transporter MsbA^{56,57}. Once situated on the periplasmic face of the inner membrane, LPS is transported to the outer leaflet of the outer membrane through the LPS transport pathway, consisting of 7 essential proteins – LptA, LptB₂, LptC, LptD, LptE, LptF, and LptG⁵⁸ (Figure 2).

LPS structure and biosynthesis

Lipid A – Kdo₂ is essential for life in most Gram-negative bacteria and is synthesized through the 9-step Raetz pathway (Figure 3a). The first step of lipid A biosynthesis involves the addition of a C14 acyl chain to the 3-OH group of uridine diphosphate N-acetylglucosamine (UDP-GlcNAc) by LpxA. In *E. coli*, this enzyme is specific for β -hydroxymyristate (3-OH-C14:0)^{59,60}. Next, the zinc metalloamidase LpxC deacetylates UDP-3-O-acyl-GlcNAc. Due to the unfavorable equilibrium constant for UDP-GlcNAc acylation by LpxA, the LpxC-mediated reaction is the first committed step of lipid A biosynthesis⁶¹. As is discussed below, LpxC is currently the only canonical LPS biosynthetic enzyme against which whole cell-active small molecules exist.

The removal of an acetyl group from UDP-3-O-acyl-GlcNAc exposes a free amino group for the addition of a second β -hydroxymyristate residue, forming UDP-2,3-diacyl-GlcN. This reaction is catalyzed by LpxD⁶². Subsequent cleavage of UDP-2,3-diacyl-GlcN by LpxH releases UMP and the resulting lipid A precursor, lipid X⁶³. After the generation of lipid X, the cell is able to form the characteristic β -1'-6-linked glucosamine disaccharide of lipid A⁶⁴. To this end, the glycosyltransferase LpxB condenses one molecule of lipid X with one molecule of UDP-2,3-diacyl-GlcN, releasing UDP as a byproduct. Upon formation of the disaccharide, lipid X is the origin of the position-1 phosphate found on *E. coli* lipid A. The second lipid A phosphate at the 4' position is subsequently added through ATP-dependent phosphorylation by LpxK⁶⁵, producing lipid IV_A.

The next step in the Raetz pathway, and also the last essential event within Lipid A – Kdo₂ biosynthesis, involves the addition of two Kdo residues to lipid IV_A by WaaA⁶⁶. Although Kdo₂ is formally a constituent of core OS, its addition to lipid A is considered an integral part of lipid A biosynthesis since the subsequent addition of two non-essential secondary acyl chains requires the presence of this moiety⁶⁷⁻⁶⁹. These final acylation events involve the addition of a lauryl group to the 2' acyl group by LpxL, followed by the addition of a myristoyl group to the 3' acyl group by LpxM^{68,69}. The product of these final reactions is the conventional hexa-acylated lipid A – Kdo₂ species found in *E. coli* when grown under standard laboratory conditions.

Upon synthesis of lipid A – Kdo₂, core OS is subsequently assembled onto KdoI by sequential glycosyl transfer reactions that occur on the cytoplasmic face of the inner membrane (Figure 3b). These reactions are catalyzed by a series of membrane-associated glycosyltransferases, using nucleotide sugars as donor substrates. In *E. coli*, core OS distal to Kdo₂ is non-essential, although atypical growth phenotypes under various environmental stressors are often observed in mutants deficient in native core OS composition.

WaaC, WaaF, and WaaQ are three non-essential heptosyltransferases that are responsible for the addition of HepI, HepII, and side-chain HepIII of inner core OS⁷⁰⁻⁷². HepI and HepII are additionally phosphorylated by core OS kinases WaaP and WaaY, respectively. Interestingly, functional interactions have been observed between WaaQ, WaaP, and WaaY, where addition of each modification

must proceed in the order WaaP → WaaQ → WaaY. Indeed, loss of WaaP obviates WaaQ and WaaY activities, resulting in the cumulative deficiency of both core OS phosphates as well as side chain HepIII⁷². Biosynthesis of outer core OS subsequently initiates with the addition of the first glucose residue (GlcI) to HepII of inner core by WaaG⁷³, followed by the addition of a side chain galactose (Gal) to GlcI by WaaB⁷⁴. The presence of this side chain Gal allows for efficient addition of GlcII to GlcI by WaaO⁷¹, and WaaJ subsequently transfers GlcIII to GlcII⁷⁴. Lastly, WaaU catalyzes the addition of HepIV to GlcIII⁵⁵, thereby completing core OS biosynthesis native to wild type *E. coli* K-12.

Chemical perturbation of LPS structure and biosynthesis

While the above discussion details the canonical structure and biosynthetic pathways of *E. coli* LPS, it is important to note that both lipid A and core OS are heavily modified in response to changing environmental conditions, and that perturbations to its structure greatly impact the ability of cells to resist exogenous stressors. This is further discussed in chapter 4, with a focus on cold-induced modifications to LPS. Of particular importance in the context of antibiotic permeability, LPS provides Gram-negative species a highly selective barrier against compounds that are large and hydrophobic. Indeed, genetic inhibition of LPS biosynthesis, particularly core OS, has been shown to sensitize a wide array of species to Gram-positive-active molecules⁷⁵, as well as components of innate immunity such as complement and host-borne cationic antimicrobial peptides⁷⁶.

Therefore, as is described in chapters 4 and 5, core OS biosynthetic enzymes represent excellent targets for the development of antibiotic adjuvants against Gram-negative pathogens.

Given the important role that LPS plays in intrinsic antibiotic resistance, it is intriguing that such a small repertoire of drugs targeting this molecule exists. As briefly mentioned above, the only LPS biosynthetic enzyme that has been successfully targeted by small molecules is LpxC, which catalyzes the committing step in lipid A biosynthesis. The first inhibitor of LpxC – L-573,655 – was identified by the Raetz lab in the mid-1990s through a screen analyzing [U-¹⁴C]-galactose incorporation into acid-precipitable material in living cells⁷⁷. Over the ensuing 2 decades, numerous hydroxamate-based analogs have been synthesized, displaying varied *in vitro* and whole-cell activities. CHIR-090 may be the most thoroughly studied of these, owing to its high potency both *in vitro* and *in vivo* against numerous Gram-negative pathogens, including *P. aeruginosa*⁷⁸. *In vitro* biochemical analysis of the mechanism of inhibition has shown that binding to LpxC occurs in a two-step process defined by the formation of a fast reversible encounter complex, followed by a time-dependent induced fit event⁷⁹. It has been suggested that this time-dependent mechanism of inhibition may be the cause of its significant potency *in vitro* and *in vivo*, due to prolonged target residence times. Additionally, structural data has revealed that the hydroxamate moiety of CHIR-090 coordinates a LpxC-associated Zn²⁺ ion, with the hydrophobic extension of CHIR-090 projecting through a hydrophobic tunnel on LpxC that is

critical for catalysis⁸⁰. Together, these data have presented a strong foundation on which rational SAR campaigns can build towards the development of highly potent, non-toxic inhibitors.

While LpxC is the only canonical LPS biosynthetic enzyme against which small molecules exist, it should be noted that whole-cell active small molecule inhibitors of the LPS transport pathway are beginning to emerge. Of the proteins involved in this pathway, the most advanced from a drug discovery perspective is LptD, which forms an outer membrane β -barrel necessary for delivery of LPS to the cell surface. Recently, a family of peptidomimetic molecules based on the antimicrobial peptide protegrin I were synthesized, and shown to bind LptD in actively growing *P. aeruginosa*⁸¹. While the precise mechanism of action of these molecules has yet to be determined, it is likely that occupation of LptD sterically hinders the progression of LPS to the outer membrane. Importantly, many of these peptidomimetic analogs displayed potent and selective activity against *Pseudomonas* species both in broth microdilution assays and in a mouse model of septicemia. Here, it is important to note that recent progress has also been made in identifying inhibitors of LptB, the ATPase that provides energy for LPS transport⁸². However, these are only moderately active against purified LptB, and display low activity against *E. coli*, likely due to poor permeability.

The last family of molecules that target LPS, the polymyxins, do not inhibit assembly or transport, but rather bind to lipid A and perturb the organization of the outer membrane. In general, cationic nitrogen atoms found on the cyclic

peptide of polymyxins associate with lipid A phosphate residues, thereby disrupting lateral inter-LPS interactions and destabilizing the outer membrane. This allows for subsequent self-promoted uptake into the periplasm, where a hydrophobic extension dissolves the cytoplasmic membrane, resulting in lysis⁸³. Despite being hailed as the last-line of defense against drug-resistant Gram-negative pathogens, their clinical use is limited due to the potential for severe kidney injury during treatment. As such, recent efforts have focused on developing analogs with significantly decreased nephrotoxicity. To this end, one advance was the development of polymyxin B nonapeptide, which lacks the fatty acid tail common to other polymyxin derivatives⁸⁴. Interestingly, this molecule does not display intrinsic antimicrobial activity due to the lack of an inner membrane-active hydrophobic moiety, but acts as a potent antibiotic adjuvant owing to its ability to bind lipid A and disrupt the organization of the outer membrane⁸⁵. However, a growing threat to the utility of polymyxins, both those that display intrinsic bactericidal activity and those that function as adjuvants, is the emergence of plasmid-borne resistance determinants, notably *mcr-1*⁸⁶. This is a phosphoethanolamine transferase responsible for addition of phosphoethanolamine to lipid A. The presence of a cationic moiety on lipid A decreases the affinity of polymyxins to the cell surface through charge-charge repulsion, rendering cells displaying this modification resistant to these last-line antibiotics.

Chapters 4 and 5 of this thesis aim to address (a) the lack of core OS

biosynthesis inhibitors and (b) the emergence of plasmid-borne polymyxin resistance determinants. Specifically, chapter 4 describes the development of a novel screening platform to identify non-lethal perturbants of core OS biosynthesis and outer membrane integrity; this screen leverages the idiosyncratic sensitivity of *E. coli* to vancomycin during cold stress. Subsequently, using the approach outlined in chapter 4, the fifth chapter highlights the discovery of an antibiotic adjuvant that potentiates Gram-positive antibiotics against Gram-negative pathogens, and overcomes *mcr-1* mediated polymyxin resistance.

Lastly, chapter 6 concludes this thesis with a brief discussion of suggestions for future research, based on the observations described herein.

References

1. Neushul, P. Science, government, and the mass production of penicillin. *J Hist Med Allied Sci.* **48**, 371–395 (1993).
2. Silver, L. L. Challenges of antibacterial discovery. *Clin Microbiol Rev.* **24**, 71–109 (2011).
3. Andries, K. *et al.* A diarylquinoline drug active on the ATP synthase of *Mycobacterium tuberculosis*. *Science* **307**, 223–227 (2005).
4. Brown, E. D. & Wright, G. D. Antibacterial drug discovery in the resistance era. *Nature* **529**, 336–343 (2016).
5. Brown, D. G., May-Dracka, T. L., Gagnon, M. M. & Tommasi, R. Trends and exceptions of physical properties on antibacterial activity for Gram-positive and Gram-negative pathogens. *J Med Chem.* **57**, 10144–10161 (2014).
6. Zlitni, S., Ferruccio, L. F. & Brown, E. D. Metabolic suppression identifies new antibacterial inhibitors under nutrient limitation. *Nat Chem Biol.* **9**, 796–804 (2013).

7. Farha, M. A. *et al.* Antagonism screen for inhibitors of bacterial cell wall biogenesis uncovers an inhibitor of undecaprenyl diphosphate synthase. *Proc Natl Acad Sci U.S.A.* (2015).
8. Campbell, J. *et al.* An antibiotic that inhibits a late step in wall teichoic acid biosynthesis induces the cell wall stress stimulon in *Staphylococcus aureus*. *Antimicrob Agents Chemother.* **56**, 1810–1820 (2012).
9. Sewell, E. W. & Brown, E. D. Taking aim at wall teichoic acid synthesis: new biology and new leads for antibiotics. *J Antibiot.* **67**, 43–51 (2014).
10. Farha, M. A. & Brown, E. D. Unconventional screening approaches for antibiotic discovery. *Ann N Y Acad Sci.* (2015).
11. Moore, P. B. How should we think about the ribosome? *Annu Rev Biophys.* **41**, 1–19 (2012).
12. Rawlins, M. The disputed discovery of streptomycin. *Lancet* **380**, 207 (2012).
13. Wilson, D. N. The A-Z of bacterial translation inhibitors. *Crit Rev Biochem Mol Biol.* **44**, 393–433 (2009).
14. Maguire, B. A. Inhibition of bacterial ribosome assembly: a suitable drug target? *Microbiol Mol Biol Rev.* **73**, 22–35 (2009).
15. Shajani, Z., Sykes, M. T. & Williamson, J. R. Assembly of bacterial ribosomes. *Annu Rev Biochem.* **80**, 501–526 (2011).
16. Lindahl, L. Intermediates and time kinetics of the in vivo assembly of *Escherichia coli* ribosomes. *J Mol Biol.* **92**, 15–37 (1975).
17. Hosokawa, K., Fujimura, R. K., Nomura, M. Reconstitution of functionally active ribosomes from inactive subparticles and proteins. *Proc Natl Acad Sci U.S.A.* **55**, 198–204 (1966).
18. Traub, P. & Nomura, M. Structure and function of *Escherichia coli* ribosomes. *J Mol Biol.* **40**, 391–413 (1969).
19. Mizushima, S. & Nomura, M. Assembly mapping of 30S ribosomal proteins from *E. coli*. *Nature* **226**, 1214 (1970).
20. Nierhaus, K. H. & Dohme, F. Total reconstitution of functionally active 50S ribosomal subunits from *Escherichia coli*. *Proc Natl Acad Sci U.S.A.* **71**,

4713–4717 (1974).

21. Röhl, R. & Nierhaus, K. H. Assembly map of the large subunit (50S) of *Escherichia coli* ribosomes. *Proc Natl Acad Sci U.S.A.* **79**, 729–733 (1982).
22. Kaczanowska, M. & Rydén-Aulin, M. Ribosome biogenesis and the translation process in *Escherichia coli*. *Microbiol Mol Biol Rev.* **71**, 477–494 (2007).
23. Gollop, N. & March, P. E. A GTP-binding protein (Era) has an essential role in growth rate and cell cycle control in *Escherichia coli*. *J Bacteriol.* **173**, 2265–2270 (1991).
24. Britton, R. A. *et al.* Cell cycle arrest in Era GTPase mutants: a potential growth rate-regulated checkpoint in *Escherichia coli*. *Mol Microbiol.* **27**, 739–750 (1998).
25. Sayed, A., Matsuyama, S. I. & Inouye, M. Era, an essential *Escherichia coli* small G-protein, binds to the 30S ribosomal subunit. *Biochem Biophys Res Commun.* **264**, 51–54 (1999).
26. Inoue, K., Alsina, J., Chen, J. & Inouye, M. Suppression of defective ribosome assembly in a rbfA deletion mutant by overexpression of Era, an essential GTPase in *Escherichia coli*. *Mol Microbiol.* **48**, 1005–1016 (2003).
27. Sharma, M. R. *et al.* Interaction of Era with the 30S ribosomal subunit: implications for 30S subunit assembly. *Mol Cell* **18**, 319–329 (2005).
28. Bram, R. J., Young, R. A. & Steitz, J. A. The ribonuclease III site flanking 23S sequences in the 30S ribosomal precursor RNA of *E. coli*. *Cell* **19**, 393–401 (1980).
29. Young, R. A. & Steitz, J. A. Complementary sequences 1700 nucleotides apart form a ribonuclease III cleavage site in *Escherichia coli* ribosomal precursor RNA. *Proc Natl Acad Sciences U.S.A.* **75**, 3593–3597 (1978).
30. Li, Z., Pandit, S. & Deutscher, M. P. RNase G (CafA protein) and RNase E are both required for the 5' maturation of 16S ribosomal RNA. *EMBO J.* **18**, 2878–2885 (1999).
31. Hayes, F. & Vasseur, M. Processing of the 17-S *Escherichia coli* precursor RNA in the 27S pre-ribosomal particle. *Eur J Biochem.* **61**, 433–442 (1976).
32. Li, Z., Pandit, S. & Deutscher, M. P. Maturation of 23S ribosomal RNA

- requires the exoribonuclease RNase T. *RNA* **5**, 139–146 (1999).
33. Roy, M. K., Singh, B., Ray, B. K. & Apirion, D. Maturation of 5-S rRNA: ribonuclease E cleavages and their dependence on precursor sequences. *Eur J Biochem.* **131**, 119–127 (1983).
 34. Li, Z. & Deutscher, M. P. The tRNA processing enzyme RNase T is essential for maturation of 5S RNA. *Proc Natl Acad Sci U.S.A.* **92**, 6883–6886 (1995).
 35. Decatur, W. A. & Fournier, M. J. rRNA modifications and ribosome function. *Trends Biochem Sci.* **27**, 344–351 (2002).
 36. Krzyzosiak, W. *et al.* In vitro synthesis of 16S ribosomal RNA containing single base changes and assembly into a functional 30S ribosome. *Biochemistry* **26**, 2353–2364 (2002).
 37. Alix, J. H., Hayes, D. & Nierhaus, K. H. Properties of ribosomes and RNA synthesized by *Escherichia coli* grown in the presence of ethionine: V. Methylation dependence of the assembly of *E. coli* 50 S ribosomal subunits. *J Mol Biol* **127**, 375–395 (1979).
 38. Ramagopal, S. & Subramanian, A. R. Growth-dependent regulation in production and utilization of acetylated ribosomal protein L7. *J Mol Biol.* **94**, 633–641 (1975).
 39. Colson, C., Lhoest, J. & Urlings, C. Genetics of ribosomal protein methylation in *Escherichia coli*. *Mol Gen Genet.* **169**, 245–250 (1979).
 40. Lhoest, J. & Colson, C. Cold-sensitive ribosome assembly in an *Escherichia coli* mutant lacking a single methyl group in ribosomal protein L3. *Eur J Biochem.* **121**, 33–37 (1981).
 41. Wuchty, S., Fontana, W., Hofacker, I. L. & Schuster, P. Complete suboptimal folding of RNA and the stability of secondary structures. *Biopolymers* **49**, 145–165 (1999).
 42. Jomaa, A. *et al.* Cryo-electron microscopy structure of the 30S subunit in complex with the YjeQ biogenesis factor. *RNA* **17**, 2026–2038 (2011).
 43. Daigle, D. M. & Brown, E. D. Studies of the interaction of *Escherichia coli* YjeQ with the ribosome in vitro. *J Bacteriol.* **186**, 1381–1387 (2004).
 44. Stokes, J. M., Davis, J. H., Mangat, C. S., Williamson, J. R. & Brown, E. D.

- Discovery of a small molecule that inhibits bacterial ribosome biogenesis. *Elife* **3**, e03574 (2014).
45. Campbell, T. L. & Brown, E. D. Genetic interaction screens with ordered overexpression and deletion clone sets implicate the *Escherichia coli* GTPase YjeQ in late ribosome biogenesis. *J Bacteriol.* **190**, 2537–2545 (2008).
 46. Himeno, H. *et al.* A novel GTPase activated by the small subunit of ribosome. *Nucleic Acids Res.* **32**, 5303–5309 (2004).
 47. Goto, S., Kato, S., Kimura, T., Muto, A. & Himeno, H. RsgA releases RbfA from 30S ribosome during a late stage of ribosome biosynthesis. *EMBO J.* **30**, 104–114 (2011).
 48. Hwang, J. & Inouye, M. The tandem GTPase, Der, is essential for the biogenesis of 50S ribosomal subunits in *Escherichia coli*. *Mol Microbiol.* **61**, 1660–1672 (2006).
 49. Bharat, A. & Brown, E. D. Phenotypic investigations of the depletion of EngA in *Escherichia coli* are consistent with a role in ribosome biogenesis. *FEMS Microbiol Lett.* **353**, 26–32 (2014).
 50. Bharat, A., Jiang, M., Sullivan, S. M., Maddock, J. R. & Brown, E. D. Cooperative and critical roles for both G domains in the GTPase activity and cellular function of ribosome-associated *Escherichia coli* EngA. *J Bacteriol.* **188**, 7992–7996 (2006).
 51. Tan, J., Jakob, U. & Bardwell, J. C. A. Overexpression of two different GTPases rescues a null mutation in a heat-induced rRNA methyltransferase. *J Bacteriol.* **184**, 2692–2698 (2002).
 52. Tommasi, R., Brown, D. G., Walkup, G. K., Manchester, J. I. & Miller, A. A. ESKAPEing the labyrinth of antibacterial discovery. *Nat Rev Drug Discov.* **14**, 529–542 (2015).
 53. Whitfield, C. & Trent, M. S. Biosynthesis and Export of Bacterial Lipopolysaccharides*. *Annu Rev Biochem.* **83**, 99–128 (2014).
 54. Stevenson, G. *et al.* Structure of the O antigen of *Escherichia coli* K-12 and the sequence of its rfb gene cluster. *J Bacteriol.* **176**, 4144–4156 (1994).
 55. Heinrichs, D. E., Yethon, J. A. & Whitfield, C. Molecular basis for structural diversity in the core regions of the lipopolysaccharides of *Escherichia coli*

- and *Salmonella enterica*. *Mol Microbiol.* **30**, 221–232 (1998).
56. Zhou, Z. M., White, K. A., Polissi, A., Georgopoulos, C. & Raetz, C. R. Function of *Escherichia coli* MsbA, an essential ABC family transporter, in lipid A and phospholipid biosynthesis. *J Biol Chem.* **273**, 12466–12475 (1998).
 57. Doerrler, W. T., Gibbons, H. S. & Raetz, C. R. MsbA-dependent translocation of lipids across the inner membrane of *Escherichia coli*. *J Biol Chem.* **279**, 45102–45109 (2004).
 58. Okuda, S., Sherman, D. J., Silhavy, T. J., Ruiz, N. & Kahne, D. Lipopolysaccharide transport and assembly at the outer membrane: the PEZ model. *Nat Rev Microbiol.* **14**, 337–345 (2016).
 59. Anderson, M. S., Bulawa, C. E. & Raetz, C. R. The biosynthesis of gram-negative endotoxin. Formation of lipid A precursors from UDP-GlcNAc in extracts of *Escherichia coli*. *J Biol Chem.* **260**, 15536–15541 (1985).
 60. Anderson, M. S. & Raetz, C. R. Biosynthesis of lipid A precursors in *Escherichia coli*. A cytoplasmic acyltransferase that converts UDP-N-acetylglucosamine to UDP-3-O-(R-3-hydroxymyristoyl)-N-acetylglucosamine. *J Biol Chem.* **262**, 5159–5169 (1987).
 61. Young, K. *et al.* The *envA* permeability/cell division gene of *Escherichia coli* encodes the second enzyme of lipid A biosynthesis. *J Biol Chem.* **270**, 30384–30391 (1995).
 62. Kelly, T. M., Stachula, S. A., Raetz, C. R. & Anderson, M. S. The *firA* gene of *Escherichia coli* encodes UDP-3-O-(R-3-hydroxymyristoyl)-glucosamine N-acyltransferase. The third step of endotoxin biosynthesis. *J Biol Chem.* **268**, 19866–19874 (1993).
 63. Babinski, K. J., Ribeiro, A. A. & Raetz, C. R. The *Escherichia coli* gene encoding the UDP-2,3-diacylglucosamine pyrophosphatase of lipid A biosynthesis. *J Biol Chem.* **277**, 25937–25946 (2002).
 64. Crowell, D. N., Anderson, M. S. & Raetz, C. R. Molecular cloning of the genes for lipid A disaccharide synthase and UDP-N-acetylglucosamine acyltransferase in *Escherichia coli*. *J Bacteriol.* **168**, 152–159 (1986).
 65. Garrett, T. A., Kadmas, J. L. & Raetz, C. R. Identification of the gene encoding the *Escherichia coli* lipid A 4'-kinase. *J Biol Chem.* **272**, 21855–21864 (1997).

66. Clementz, T. & Raetz, C. R. A gene coding for 3-deoxy-D-manno-octulosonic-acid transferase in *Escherichia coli*. Identification, mapping, cloning, and sequencing. *J Biol Chem.* **266**, 9687–9696 (1991).
67. Hankins, J. V. & Trent, M. S. Secondary acylation of *Vibrio cholerae* lipopolysaccharide requires phosphorylation of Kdo. *J Biol Chem.* **284**, 25804–25812 (2009).
68. Clementz, T., Bednarski, J. J. & Raetz, C. R. Function of the htrB high temperature requirement gene of *Escherichia coli* in the acylation of lipid A. HtrB catalyzed incorporation of laurate. *J Biol Chem.* **271**, 12095–12102 (1996).
69. Clementz, T., Zhou, Z. & Raetz, C. R. Function of the *Escherichia coli* msbB gene, a multicopy suppressor of htrB knockouts, in the acylation of lipid A. Acylation by MsbB follows laurate incorporation by HtrB. *J Biol Chem.* **272**, 10353–10360 (1997).
70. Kadrmaz, J. L. & Raetz, C. R. Enzymatic synthesis of lipopolysaccharide in *Escherichia coli*. Purification and properties of heptosyltransferase i. *J Biol Chem.* **273**, 2799–2807 (1998).
71. Schnaitman, C. A. & Klena, J. D. Genetics of lipopolysaccharide biosynthesis in enteric bacteria. *Microbiol Rev.* **57**, 655–682 (1993).
72. Yethon, J. A., Heinrichs, D. E., Monteiro, M. A., Perry, M. B. & Whitfield, C. Involvement of waaY, waaQ, and waaP in the modification of *Escherichia coli* lipopolysaccharide and their role in the formation of a stable outer membrane. *J Biol Chem.* **273**, 26310–26316 (1998).
73. Parker, C. T. *et al.* Role of the rfaG and rfaP genes in determining the lipopolysaccharide core structure and cell surface properties of *Escherichia coli* K-12. *J Bacteriol.* **174**, 2525–2538 (1992).
74. Pradel, E., Parker, C. T. & Schnaitman, C. A. Structures of the rfaB, rfaI, rfaJ, and rfaS genes of *Escherichia coli* K-12 and their roles in assembly of the lipopolysaccharide core. *J Bacteriol.* **174**, 4736–4745 (1992).
75. Liu, A. *et al.* Antibiotic sensitivity profiles determined with an *Escherichia coli* gene knockout collection: generating an antibiotic bar code. *Antimicrob Agents Chemother.* **54**, 1393–1403 (2010).
76. Loutet, S. A., Flannagan, R. S., Kooi, C., Sokol, P. A. & Valvano, M. A. A

- complete lipopolysaccharide inner core oligosaccharide is required for resistance of *Burkholderia cenocepacia* to antimicrobial peptides and bacterial survival in vivo. *J Bacteriol.* **188**, 2073–2080 (2006).
77. Onishi, H. R. *et al.* Antibacterial agents that inhibit lipid A biosynthesis. *Science* **274**, 980–982 (1996).
 78. Tomaras, A. P. *et al.* LpxC inhibitors as new antibacterial agents and tools for studying regulation of lipid a biosynthesis in Gram-negative pathogens. *mBio* **5**, e01551–14 (2014).
 79. McClerren, A. L. *et al.* A slow, tight-binding inhibitor of the zinc-dependent deacetylase LpxC of lipid A biosynthesis with antibiotic activity comparable to ciprofloxacin. *Biochemistry* **44**, 16574–16583 (2005).
 80. Barb, A. W., Jiang, L., Raetz, C. R. & Zhou, P. Structure of the deacetylase LpxC bound to the antibiotic CHIR-090: Time-dependent inhibition and specificity in ligand binding. *Proc Natl Acad Sci U.S.A.* **104**, 18433–18438 (2007).
 81. Srinivas, N. *et al.* Peptidomimetic antibiotics target outer-membrane biogenesis in *Pseudomonas aeruginosa*. *Science* **327**, 1010–1013 (2010).
 82. Sherman, D. J., Okuda, S., Denny, W. A. & Kahne, D. Validation of inhibitors of an ABC transporter required to transport lipopolysaccharide to the cell surface in *Escherichia coli*. *Bioorg Med Chem.* **21**, 4846–4851 (2013).
 83. Olaitan, A. O., Morand, S. & Rolain, J.M. Mechanisms of polymyxin resistance: acquired and intrinsic resistance in bacteria. *Front Microbiol.* **5**, 643 (2014).
 84. Viljanen, P. & Vaara, M. Susceptibility of gram-negative bacteria to polymyxin B nonapeptide. *Antimicrob Agents Chemother.* **25**, 701–705 (1984).
 85. Ofek, I. *et al.* Antibacterial synergism of polymyxin B nonapeptide and hydrophobic antibiotics in experimental gram-negative infections in mice. *Antimicrob Agents Chemother.* **38**, 374–377 (1994).
 86. Liu, Y.Y. *et al.* Emergence of plasmid-mediated colistin resistance mechanism MCR-1 in animals and human beings in China: a microbiological and molecular biological study. *Lancet Infect Dis.* **16**, 161–168 (2015).

Figure Legends

Figure 1. Structure of the *E. coli* ribosome. (a) The 30S subunit is shown on the left, with rRNA in yellow and r-proteins in orange. On the right is the 50S subunit, with 23S rRNA in light blue, 5S rRNA in green, and r-proteins in dark blue. Structures were assembled from PDB: 4V4Q. (b) Depiction of nucleolytic processing of the *rnmB* transcript. The promoters P1 and P2, as well as terminators T1 and T2 are shown, as are the relative locations of cleavage sites for RNase III (III), RNase E (E), RNase G (G), and RNase T (T). Processing events mediated by unknown enzymes are denoted with “?”.

Figure 2. LPS transport in *E. coli*. LPS is synthesized on the inner leaflet of the inner membrane and subsequently flipped to the periplasmic leaflet by the ATP-binding cassette transporter MsbA. LPS is then transported to the outer membrane through the LPS transport pathway, which consists of 7 essential proteins. The LptB₂FG complex removes LPS from the inner membrane in an ATP-dependent manner, and transports this extracted LPS to LptC. This protein forms a periplasmic bridge with LptA and the N-terminus of LptD, through which LPS traverses to reach the β -barrel C-terminus of LptD and LptE. Together, the C-terminus of LptD and LptE form the translocon responsible for inserting LPS into the outer leaflet of the outer membrane.

Figure 3. Assembly of lipid A and core OS. (a) The Raetz pathway depicting the biosynthesis of Kdo₂-lipid A in *E. coli*. The first 3 steps mediated by LpxA,

LpxC, and LpxD occur in the cytoplasm, whereas those mediated by LpxH onward occur on the inner leaflet of the inner membrane. Black numbers indicate predominant acyl-chain lengths under standard laboratory conditions. (b) The structure of *E. coli* K-12 core OS and the gene products necessary for its biosynthesis. Core OS assembly occurs on the inner leaflet of the inner membrane.

Figure 1

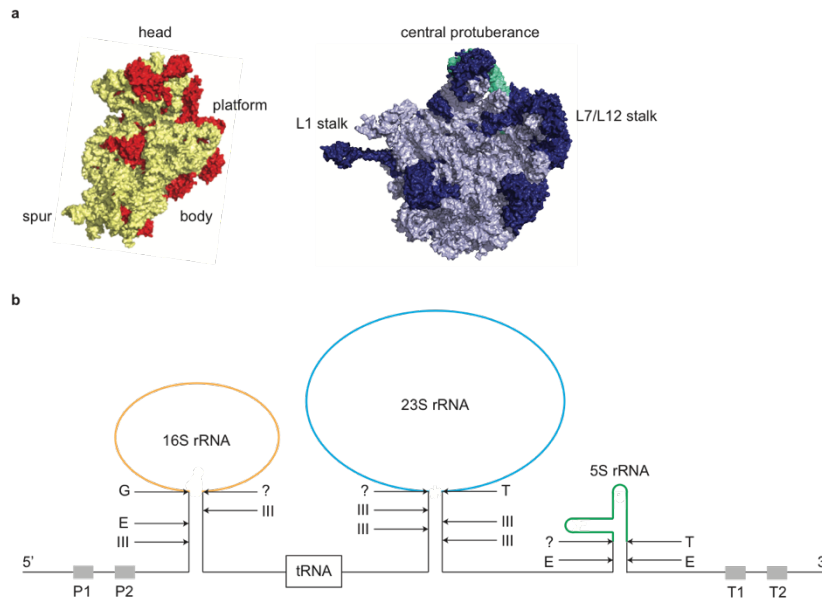


Figure 2

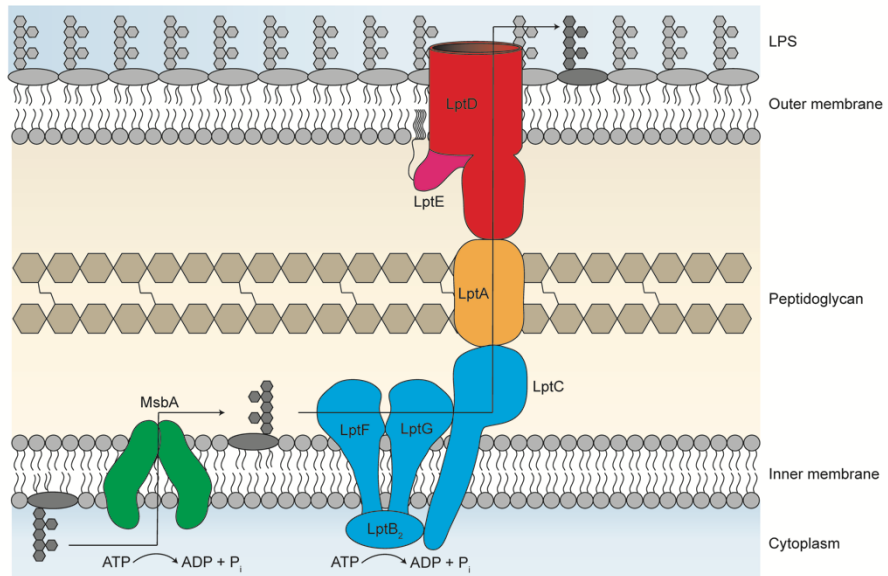
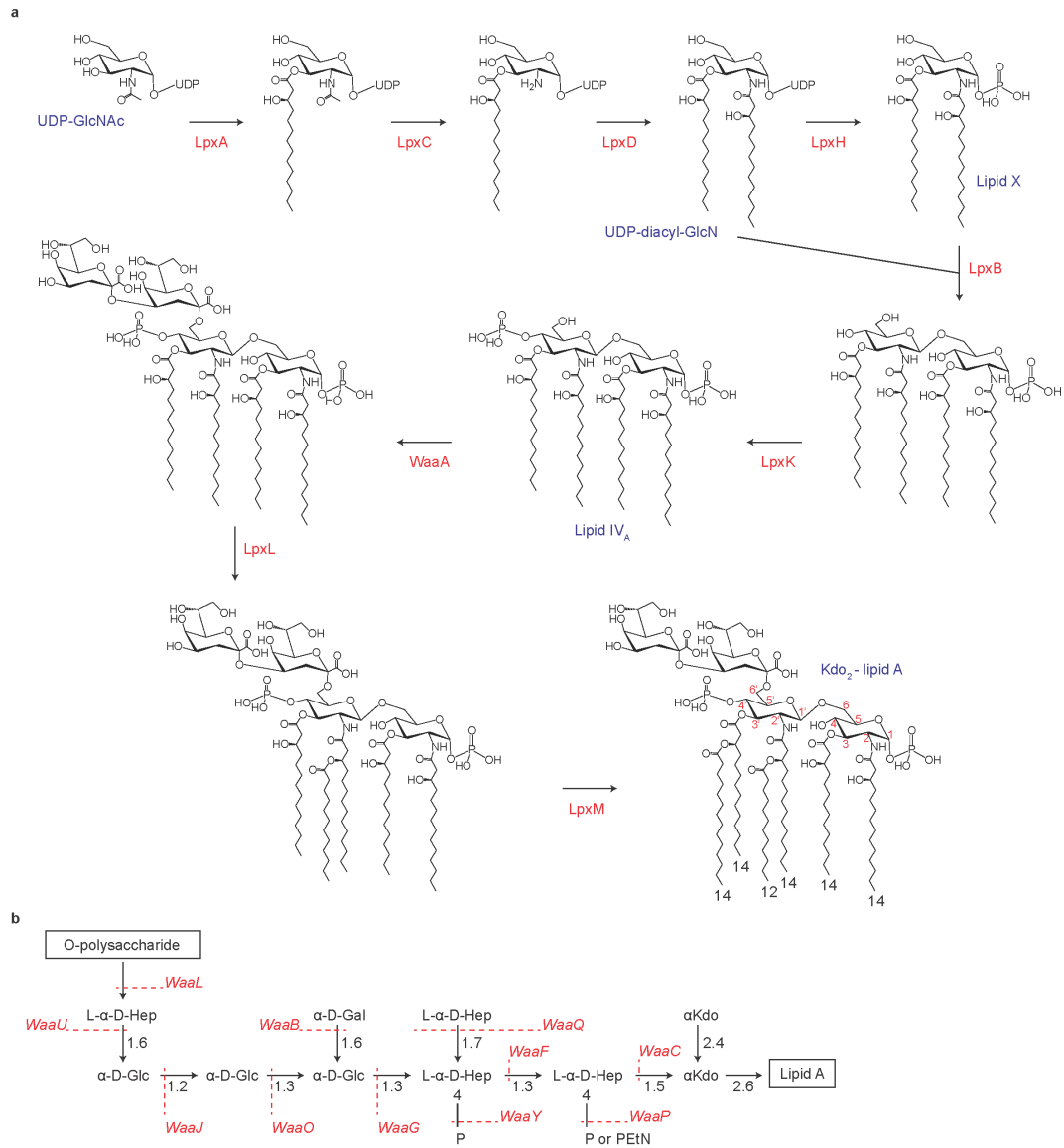


Figure 3



**CHAPTER II – Discovery of a small molecule that inhibits bacterial
ribosome biogenesis**

Preface

The work presented in this chapter was previously published in:

Stokes JM, Davis JH, Mangat CS, Williamson JR, Brown ED. Discovery of a small molecule that inhibits bacterial ribosome biogenesis. *Elife* **3**, e03574 (2014).

Permission has been granted by the publisher to reproduce the material herein.

I performed all experiments with the exception of mass spectrometry, which was conducted by Davis JH. Mangat CS assisted with screening experiments. I wrote and edited the manuscript with input from all authors.

Abstract

While small molecule inhibitors of the bacterial ribosome have been instrumental in understanding protein translation, no such probes exist to study ribosome biogenesis. We screened a diverse chemical collection that included previously approved drugs for compounds that induced cold sensitive growth inhibition in the model bacterium *Escherichia coli*. Among the most cold sensitive was lamotrigine, an anticonvulsant drug. Lamotrigine treatment resulted in the rapid accumulation of immature 30S and 50S ribosomal subunits at 15°C. Importantly, this was not the result of translation inhibition, as lamotrigine was incapable of perturbing protein synthesis *in vivo* or *in vitro*. Spontaneous suppressor mutations blocking lamotrigine activity mapped solely to the poorly characterized domain II of translation initiation factor IF2, and prevented the binding of lamotrigine to IF2 *in vitro*. This work establishes lamotrigine as a widely available chemical probe of bacterial ribosome biogenesis and suggests a role for *E. coli* IF2 in ribosome assembly.

Introduction

The bacterial ribosome is a 2.6 MDa ribonucleoprotein complex responsible for protein translation, which sediments as a 70S particle composed of a small (30S) and a large (50S) subunit. While there is a relatively thorough understanding of the structure and function of the ribosome during translation¹, the molecular events underlying its assembly remain largely enigmatic. Ribosome

biogenesis, which consumes up to 40% of the cell's energy in rapidly growing *E. coli*², involves the coordinated transcription, modification, and folding of rRNA transcripts; translation, modification, and folding of r-proteins; binding of r-proteins to the appropriate rRNA scaffolds; and binding and release of ribosome biogenesis factors. *In vivo*, these events occur in parallel and represent a highly dynamic system of interrelated processes that occur cooperatively to narrow the assembly landscape of the ribosome³⁻⁵.

Ribosome biogenesis factors are proteins that transiently bind to assembling ribosomal particles to increase the efficiency of subunit maturation⁶ and prevent the entry of immature subunits into the translation cycle⁷⁻¹⁰. *E. coli* has approximately 60 of such factors. Genetic perturbation has been the conventional route to probe the function of these proteins but has drawbacks. Genetic inactivation is typically permanent, often 'all or none' in scope, and for essential genes is fraught with the difficulty of creating conditional alleles. Further, due to the coordination of 30S and 50S subunit biogenesis, and regulatory feedback from the translational capacity of the cell^{11,12}, genetic probes of ribosome assembly are prone to wide-ranging impacts and pleiotropic phenotypes¹³.

Small molecules are finding increasing use in a research paradigm that emphasizes the value of these as probes of biology. Such chemicals can exert their effects on a time scale of seconds and be added or removed from cell systems at will. Further, small molecules can be dosed to achieve varying levels

of target inhibition and as such can be elegant probes of protein function. While existing antibiotics provide a surfeit of probes for on-going efforts to understand the mechanistic details of protein translation, no chemical probes exist for the study of ribosome biogenesis. Small molecule inhibitors of ribosome biogenesis could provide important new tools for the study this complex process, particularly those events controlled by uncharacterized protein assembly factors. Additionally, chemical inhibitors of bacterial ribosome biogenesis might serve as leads for an entirely new mechanistic class of antibiotics¹⁴.

Here, we report the discovery and characterization of a chemical inhibitor of bacterial ribosome biogenesis. Using a diverse chemical library that included previously approved drugs and compounds of known bioactivity, we enriched for molecules that induced cold sensitive growth inhibition in the model bacterium *E. coli*. Indeed, numerous studies have revealed that genetic defects in ribosome assembly result in cold sensitive growth phenotypes¹⁵⁻²⁰. We too performed validating efforts, reported herein, of the cold sensitivity of strains from the Keio collection, a comprehensive compendium of *E. coli* deletion strains. A subsequent chemical screen determined that the anticonvulsant drug lamotrigine induced a strongly cold sensitive growth phenotype. Treatment with this molecule resulted in the accumulation of immature ribosomal subunits in a time-dependent manner without inhibiting protein translation. Spontaneous suppressors of lamotrigine activity mapped exclusively to translation initiation factor IF2, encoded by *infB*. These mutations, found in the poorly characterized and evolutionarily

divergent domain II of IF2, obviated the binding of lamotrigine to IF2 *in vitro*. This work establishes lamotrigine as a widely available chemical probe of bacterial ribosome biogenesis and suggests a role for *E. coli* IF2 in this process.

Results

The ribosome is a primary target of cold stress. Where cold sensitive growth has previously been identified as a dominant phenotype for defects in ribosome biogenesis, we set out to first validate such an enrichment strategy with a screen of the *E. coli* Keio collection²¹, a comprehensive set of non-essential gene deletion strains. We looked for strains that were sensitized to growth at 15°C compared to 37°C (Figure 1 – figure supplement 1A, B). A cold sensitivity factor was subsequently generated for each clone, defined as the ratio of growth at 37°C to growth at 15°C, normalized to the mean growth ratio measured for the entire collection (Figure 1A). Strains that displayed a cold sensitivity factor in the top 3.5% (155 clones) were analyzed using clusters of orthologous groups^{22,23} to categorize the cellular function of each deleted gene (Figure 1 – figure supplement 1C). To highlight the relative proportion of genes in each functional class, the number of cold sensitive genes in each was divided by the total number of non-essential genes in that same category (Figure 1B). This normalization procedure highlighted ribosome-related genes as exceptionally sensitive to low temperatures, as >20% of genes in this functional class were found to be cold sensitive. Importantly, this screen was also successful in

identifying the vast majority of previously reported cold sensitive ribosome biogenesis genes, providing support that screening compounds for cold sensitivity would enrich for those related to ribosome function and biogenesis.

Lamotrigine induces profound cold sensitivity in *E. coli*. Having validated our cold sensitivity enrichment strategy, we proceeded to screen a diverse chemical collection to identify molecules that exhibited a cold sensitive growth inhibition phenotype. This collection, assembled from a variety of vendors, included some 30,000 compounds. These were largely diverse synthetic molecules with a subset of 3,500 previously approved drugs and chemicals with known biological activity. *E. coli* was grown in LB media at 15°C and 37°C in the presence of 10 µM of each compound (Figure 2 – figure supplement 1). To select compounds for follow-up, we identified those that strongly inhibited growth at 15°C ($>3\sigma$ below the mean OD₆₀₀ at 15°C), yet displayed little growth inhibition at 37°C ($<2\sigma$ below the mean OD₆₀₀ at 37°C). These criteria resulted in 49 active compounds (Figure 2A). We removed all antibiotics with known mechanisms of action and filtered the active molecules for diversity in chemical structure. This led to a short-list of 38 active molecules, which were analyzed in dose at 37°C and 15°C. The anticonvulsant drug lamotrigine displayed the largest change in minimum inhibitory concentration (MIC) upon temperature downshift, increasing in potency more than 50-fold from >512 µM at 37°C to 7.8 µM at 15°C (Figure 2B, Figure 2 – figure supplement 2).

Lamotrigine treatment results in the accumulation of non-native ribosomal particles. To determine whether lamotrigine resulted in cold sensitivity through perturbation of the ribosome, we harvested ribosomal particles from early-log cultures of *E. coli* treated with 2x MIC of lamotrigine for 1 hour and 6 hours at 15°C in LB media, and resolved them using sucrose density centrifugation. We note that the doubling time of wild type *E. coli* at 15°C in LB media was 6 hours. Cultures were pulse labeled with [¹⁴C]-uridine immediately upon drug treatment to visualize the accumulation of newly synthesized particles. Since previous reports have shown that inhibitors of protein translation can cause accumulation of immature ribosomal particles²⁴⁻²⁶ we also tested a panel of antibiotics (Figure 3 – figure supplement 1A-D) with known mechanism of action for comparison.

Mock treatment of cells with DMSO and simultaneous pulsing with [¹⁴C]-uridine allowed for the visualization of 30S, 50S, and 70S particle accumulation after 1 hour and 6 hours of growth post-treatment (Figure 3A). After 1 hour of treatment, small quantities of newly synthesized particles were present, and after 6 hours cells had accumulated labeled ribosomal particles to near steady-state levels. Cultures treated with chloramphenicol (Figure 3B), erythromycin (Figure 3C), and tetracycline (Figure 3D) displayed a substantial accumulation of non-native ribosomal particles after just 1 hour of treatment, illustrating that inhibition of translation can indirectly inhibit ribosomal subunit assembly by limiting the availability of r-proteins. Interestingly, we found that addition of 2x MIC of

vancomycin to *E. coli* resulted in a detectable perturbation of the ribosome profile (Figure 3E). However, the presence of a ~40S particle after 6 hours of treatment is likely the result of cell lysis induced by the inhibition of peptidoglycan synthesis (Stokes and Brown, unpublished data). Treatment with lamotrigine resulted in the accumulation of non-native ribosomal particles after 1 hour of incubation, and did so in a time-dependent manner (Figure 3F). Further investigations revealed that treatment of *E. coli* with 2x MIC of lamotrigine for only 5 minutes (~1% of the doubling time) caused a significant accumulation of these non-native particles (Figure 3G, H). Consistent with the cold sensitive phenotype induced by lamotrigine, these pre-30S and pre-50S particles that accumulated at 15°C were not present after treatment at 37°C (Figure 3 – figure supplement 1E, F).

To determine if lamotrigine directly associated with ribosomal particles, early-log cultures of *E. coli* were treated with [³H]-lamotrigine in the absence (Figure 3 – figure supplement 1G) or presence (Figure 3 – figure supplement 1H) of 1x MIC of unlabeled lamotrigine. Ribosomal particles were then separated on a sucrose gradient, and individual fractions counted to localize [³H]-lamotrigine. Radiolabeled compound was found exclusively in the soluble fractions eluting early in the gradient, suggesting that lamotrigine does not interact directly with mature or non-native ribosomal particles.

Non-native ribosomal particles are immature 30S and 50S subunits.

We reasoned that ribosomal particles accumulating during treatment could be immature subunits or degradation products of weakly assembled ribosomes.

Thus, we analyzed rRNA processing and r-protein content of all particles that accumulated upon lamotrigine treatment. Because previous investigations have shown that the cleavage of 5' and 3' termini of rRNA is among the final events in ribosomal subunit assembly²⁷⁻²⁹, we first performed 5' primer extension reactions using rRNA purified from sucrose gradients of lamotrigine-treated cells. Early-log cultures of *E. coli* were grown in the presence of 2x MIC of lamotrigine at 15°C in LB media for 5 minutes, 1 hour, and 6 hours, at which time the ribosomal particles were resolved on sucrose gradients and the rRNA corresponding to each discrete particle was purified and reverse transcribed using 5' carboxyfluorescein-tagged primers. A 16S rRNA-specific primer was used to analyze the 30S subunit rRNA in pre-30S, 30S, and 70S fractions, whereas a 23S rRNA-specific primer was used to analyze the 50S subunit rRNA in pre-30S, pre-50S, 50S and 70S fractions. Figure 4A displays the 5' cleavage events during the processing of 16S and 23S rRNAs³⁰. We note here that our experiments were unable to detect the first 16S cleavage event of 49 nucleotides by Rnase E, and that all immature 16S rRNA species described contain a full-length 5' terminus of 115 nucleotides.

Primer extension analysis of cells treated with DMSO for 6 hours is depicted in Figure 4B (top panel). Analysis of the pre-30S, 30S, and 70S regions of the gradient using the 16S rRNA-specific primer revealed that increasing sedimentation rate correlated with a decreased proportion of immature 16S rRNA relative to total 16S rRNA. The presence of immature 16S rRNA sedimenting in

the pre-30S region suggested a heterogeneous composition of 30S particles at various stages of maturation. At the maximum of the 30S peak approximately 40% of 16S rRNA was unprocessed. The 16S rRNA found in fractions corresponding to the 70S subunit was >95% processed, as expected. Overall, a similar trend was seen when analyzing the processing of 23S rRNA in the pre-30S, pre-50S, 50S, and 70S regions of the gradient; increasing sedimentation rate correlated with a decreased proportion of immature 23S rRNA relative to total 23S rRNA. The pre-30S and pre-50S regions of the gradient were devoid of quantifiable 23S rRNA, suggesting very little 50S precursor accumulation in unperturbed cells.

Compared to cells treated with DMSO, those treated with 2x MIC of lamotrigine for 5 minutes (Figure 4B – bottom panel), 1 hour (Figure 4 – figure supplement 1A), and 6 hours (Figure 4 – figure supplement 1B) contained similar proportions of immature to total 16S and 23S rRNA in the 30S, 50S, and 70S regions of the gradient. Furthermore, lamotrigine-treated cells displayed almost identical proportions of immature to total 16S rRNA in the pre-30S region, relative to DMSO-treated cells. Unlike DMSO-treatment, however, lamotrigine treatment resulted in the accumulation of immature 23S rRNA in the pre-30S and pre-50S regions. While the presence of unprocessed 23S rRNA in the pre-50S region strongly suggested an immature 50S subunit sedimenting at ~40S, its presence in the pre-30S region raised questions of whether the dominant species in the pre-30S peak (Figure 3F) was derived from 16S or 23S rRNA.

While calculating proportions of immature to total rRNA of the same species ($[\text{immature } 16\text{S} / \text{total } 16\text{S}]$ and $[\text{immature } 23\text{S} / \text{total } 23\text{S}]$) provides detail of rRNA processing efficiency in each region of the gradient, it does not inform on the absolute quantity of one species (16S rRNA) relative to the other (23S rRNA). To answer this question, we quantified absolute cDNA fluorescence from 5' primer extension reactions (Figure 4C, Figure 4 – figure supplement 1C). Samples of rRNA purified from single fractions of sucrose gradients were reverse transcribed in parallel reactions using either the 16S- or 23S-specific primer. Here, cDNA production is proportional to the amount of rRNA transcript in the sample, and therefore reflects absolute quantities of each rRNA species (16S and 23S) present. The quantity of immature 16S rRNA from DMSO-treated cells was minor relative to cells treated with lamotrigine. This is consistent with previous reports, which have shown that immature ribosomal particles in unperturbed cells account for only a small proportion of total ribosomal material^{31,32}. Furthermore, while immature 23S rRNA slowly accumulated in this region as a function of lamotrigine treatment length, immature 16S rRNA did so at a significantly greater rate. These results indicate that, by far, the major species of rRNA residing within the pre-30S region in lamotrigine-treated cells was unprocessed 16S rRNA. Thus, 5' primer extension results strongly suggested that lamotrigine treatment results in the accumulation of an immature 30S subunit that sediments at ~25S and an immature 50S subunit that sediments at ~40S.

To further test this hypothesis, we used quantitative mass spectrometry to determine the relative stoichiometry of r-proteins across sucrose gradients of DMSO- and lamotrigine-treated cells. Early-log cultures of *E. coli* grown at 15°C in ¹⁴N-labeled LB media were treated with DMSO or 2x MIC of lamotrigine for 6 hours, lysed, and the ribosomal particles were separated through sucrose gradients. Fractions spanning the pre-30S to the 70S regions were spiked with a fixed concentration of 70S ribosomes purified from cells grown in ¹⁵N-labeled media. These spiked samples were then digested with trypsin and prepared for mass spectrometry. This approach resulted in multiple independent peptide measurements for each r-protein in every fraction (Figure 4D, Figure 4 – figure supplement 2A, B). Protein occupancy was calculated as $^{14}\text{N} / [^{14}\text{N} + ^{15}\text{N}]$. Direct inspection of the protein occupancy profiles revealed distinct patterns for early- (e.g. S15, L24) and late- (e.g. S3, L28) binding proteins. In the DMSO samples, all r-proteins within a given subunit displayed highly correlated occupancy patterns with maximal occupancy corresponding to “peak” fractions as determined by rRNA absorbance (Figure 4D). In contrast, treatment with lamotrigine resulted in significant occupancy of the early-binding proteins in pre-30S and pre-50S fractions, whereas the late-binding r-proteins exhibited relatively unperturbed profiles. Indeed, protein S15 is found at significantly greater occupancy in the pre-30S fractions upon lamotrigine treatment (dark blue). This effect on early binding proteins is particularly pronounced in the L24 profile with peak occupancy shifted six fractions earlier in the gradient (from orange to

green). To facilitate further analysis, this large dataset (~20,000 measurements) was compressed to a 53-protein x 28-fraction heat map using the median protein occupancy value for each protein in each fraction (Figure 4E). As expected, the 70S peak from both DMSO- and lamotrigine-treated cells exhibited stoichiometric occupancy of each r-protein.

In both DMSO- and lamotrigine-treated samples, we observed sub-stoichiometric occupancy of the late-binding r-proteins S21, S2, and to a lesser extent S3, within the 30S peak. Notably, this effect was enhanced in the lamotrigine-treated samples. The depletion of these proteins is consistent with prior *in vivo* analysis of small subunit biogenesis at 37°C, which found S2, S3, and S21 to be the latest-binding small subunit proteins (Figure 4 – figure supplement 2C)³³. Consistent with sucrose gradient traces monitoring UV absorbance and [¹⁴C]-uridine incorporation, we observed a subtle broadening of the 30S protein occupancy peak upon treatment with lamotrigine. Analysis of the leading edge of this peak revealed an enrichment of relatively early-binding proteins S13, S7, S16, S8, S15, S6, and S18, consistent with the presence of 30S subunit assembly intermediates in lamotrigine-treated cells. Inspection of large subunit protein occupancy revealed drastic changes as a result of lamotrigine treatment, resulting in the accumulation of an immature particle depleted of the late-binding r-proteins L35, L36, L16, L30, and L28 as well as earlier-binding proteins, L34, L6, and L21 (Figure 4 – figure supplement 2D). Particles with this heterogeneous protein composition could not be found in the

DMSO-treated samples, indicating that if they do form they rapidly convert to mature particles that migrate later in the gradient.

Formally, these r-protein occupancy patterns could have resulted either from immature assembly intermediates, or from the degradation of mature particles initiated by the removal of late-binding proteins. To distinguish between these possibilities, we used mass spectrometry to determine the occupancy pattern for the ribosome biogenesis factors RbfA and DeaD (Figure 4F). These proteins were completely absent from mature 70S particles, and thus we reasoned that their presence could be used as markers of immature particles. The 30S-specific maturation factor RbfA co-sedimented with the 30S particles in both DMSO- and lamotrigine-treated samples. Further, the 50S-biogenesis factor DeaD co-migrated with the pre-50S peak in the lamotrigine-treated samples and the 50S peak in the DMSO-treated samples. These data further suggest that the pre-30S and pre-50S particles are immature subunits and not the result of degradation of mature ribosomal particles.

Lamotrigine binds to wild type but not mutant IF2 in a G-nucleotide-dependent manner. To identify lamotrigine's target *in vivo*, we generated suppressor mutants and sequenced the resulting genomes to identify the mutation(s) that were responsible for resistance. Briefly, *E. coli* BW25113 was grown at 15°C in the presence of 5x MIC (39 µM) of lamotrigine in LB media to saturation. Putative suppressors were then serially passaged in the presence and absence of lamotrigine to purify and to ensure mutation stability. After 20

independent strains had been isolated, 3 were selected at random, sequenced using an Illumina MiSeq platform, and analyzed against the *E. coli* MG1655 genome using BreSeq. At this time, the chromosome of BW25113 had yet to be sequenced, thus this strain was sequenced in parallel to be used as a reference genome. The sequencing data revealed mutations solely in domain II of initiation factor IF2 (Figure 5A, Figure 5 – figure supplement 1A). Subsequent Sanger sequencing of the *infB* genes from each of the remaining 17 suppressor strains revealed that all mutations mapped to domain II of IF2, and fell into only four categories. Three classes of mutant contained in-frame chromosomal deletions in this region and one mutant class contained a short duplication.

To understand the phenotypic characteristics of these four unique lamotrigine suppressor strains, cells from each class were first analyzed for growth rate and resistance to lamotrigine. All displayed wild type growth at 15°C in the absence of lamotrigine, and little sensitivity to lamotrigine treatment up to 512 µM in LB media (Figure 5 – figure supplement 1B, C). We subsequently analyzed these strains to determine the composition of ribosomal particles upon lamotrigine treatment. Suppressor strains were grown to early-log phase, treated with 2x MIC of lamotrigine, and grown for 6 hours at 15°C. Immediately after the addition of lamotrigine to the cultures, cells were pulse-labeled with [¹⁴C]-uridine to monitor accumulation of non-native ribosomal particles. Treatment of suppressor strains with lamotrigine did not result in the accumulation of non-native ribosomal particles (Figure 5 – figure supplement 1D).

To test the hypothesis that IF2 was the target of lamotrigine, we conducted *in vitro* binding studies using recombinant *E. coli* IF2 and [³H]-lamotrigine (Figure 5B). Wild type and mutant forms of *E. coli* IF2 were purified and incubated with [³H]-lamotrigine in the presence of GDP or GTP. After incubation for 3 hours at 15°C, the reaction mixtures were passed through a pre-cooled Sephadex G-25 column, and the flow-through was collected and scintillation counted to detect the presence of lamotrigine-IF2 complexes. Lamotrigine was found to associate with wild type *E. coli* IF2 in a G-nucleotide-dependent manner, with lamotrigine-IF2 complex formation favored in the presence of GDP over GTP (Figure 5C). We note here that previous studies have not reported measurable GTP turnover by IF2 in the absence of ribosomal subunits³⁴. Analyses of lamotrigine binding with mutant IF2 in the presence of GTP and GDP failed to reveal association (Figure 5C). Consistent with these results, lamotrigine was found to have activity solely against members of the Enterobacteriaceae, which is the only bacterial family that contains the domain II sequence outlined in Figure 5A. Interestingly, the potency of lamotrigine at 15°C against the Enterobacteriaceae was directly correlated with IF2-α sequence homology (data not shown), further suggesting that the sequence of domain II defines essential structural features for lamotrigine association (Figure 5 – figure supplement 1E, F).

Accumulation of immature ribosomal subunits is not the result of translation inhibition. Given the known role of IF2 in protein translation, we tested whether lamotrigine was indirectly perturbing ribosome biogenesis by

inhibiting IF2-dependent translation. We first monitored [³⁵S]-methionine incorporation into bulk cellular protein. Early-log cultures of *E. coli* grown in M9 minimal media were treated with lamotrigine and a collection of known antibiotics for 2.6 hours at 15°C (doubling time = 16hrs). Immediately after the addition of drug, cells were pulsed with [³⁵S]-methionine to monitor the production of newly synthesized proteins. Cells were then pelleted, washed, lysed, and treated with TCA. The precipitated proteins were captured on glass filters and counted. These investigations revealed that lamotrigine had no impact on [³⁵S]-methionine incorporation, even when cells were treated with 8x MIC of lamotrigine (Figure 6A, 6C – black dots). Similarly, cells treated with these same concentrations of lamotrigine at 37°C for 3 doublings did not display any inhibition of translation (Figure 6 – figure supplement 1A). We found that when cells were treated with 8x MIC of tetracycline, chloramphenicol, and erythromycin, there was a marked decrease in protein labeling. As expected given its known mechanism of action, cells treated with 8x MIC of vancomycin did not display inhibition of protein biosynthesis after 2.6 hours of treatment.

To determine if lamotrigine had a direct effect on protein biosynthesis *in vitro*, we employed a commercially available *E. coli* K-12 cell-free transcription/translation system producing luciferase. Reactions in the presence of 8x MIC of lamotrigine and the aforementioned antibiotics were incubated at 15°C for 4 hours (see Figure 6 – figure supplement 1C for *in vitro* translation kinetics at 15°C), at which time luciferin was added to quantify the luciferase

produced. As expected, all translation inhibitors blocked the production of luciferase while vancomycin did not (Figure 6B). Lamotrigine failed to block the production of luciferase at either 15°C or 37°C (Figure 6B, 6C – white dots, Figure 6 – figure supplement 1B). To ensure that the *in vitro* translation assay required IF2 activity, we tested the effect of evernimicin, an oligosaccharide antibiotic known to inhibit IF2-dependent 70S initiation complex formation^{35,36}. Evernimicin prevented luciferase synthesis *in vitro* at both 15°C and 37°C (Figure 6D).

Having ruled out a direct effect on bulk protein biosynthesis, we wondered if lamotrigine might have a specific effect on r-protein synthesis that could lead to accumulation of immature ribosome subunits. To test this, we measured the synthesis rate of each r-protein *in vivo* using a mass spectrometry-based pulse labeling technique. At 15°C, cells were grown in ¹⁴N-labeled M9 minimal media to mid-log phase at which point they were diluted 2-fold into ¹⁵N-labeled M9 media and concurrently treated with DMSO, lamotrigine, or chloramphenicol. Cells were harvested after 1 hour, 2.6 hours, 4 hours, 8 hours, and 16 hours and spiked with equal quantities of ¹⁵N-labeled 70S ribosomes as an internal reference standard. After cell lysis, these spiked samples were digested with trypsin for analysis by mass spectrometry. Using a Fourier-transform deconvolution algorithm^{32,37}, we independently quantified the r-proteins produced before the pulse (¹⁴N) and those synthesized post-pulse (50% ¹⁵N) from the cellular lysate (Figure 6 – figure supplement 1D).

Inspection of ^{14}N abundance as a function of time revealed that most ribosomal proteins were stable over this time course (Figure 6 – figure supplement 1E, G, I), consistent with our prior work³². We then carefully inspected the rate of 50% ^{15}N incorporation into each ribosomal protein in each treatment condition. Using a linear approximation of the synthesis rate based on the 4-, 8-, and 16-hour time points, we found that each protein was synthesized at a similar rate in the DMSO- and lamotrigine-treated cells up to 6x MIC. However, we found significant inhibition of r-protein synthesis with increasing concentrations of chloramphenicol, our positive control compound (Figure 6E, Figure 6 – figure supplement 1F, H, J).

Immature ribosomal particles sediment as mature subunits upon removal of lamotrigine stress. To establish if the pre-30S and pre-50S particles that accumulate upon lamotrigine treatment represented immature subunits on pathway to maturity, we endeavored to monitor the impact of relieving inhibition by lamotrigine. We hypothesized that cells relieved of lamotrigine stress would assemble immature 30S and 50S particles into mature 30S and 50S subunits. *E. coli* was grown to early-log phase in LB media at 15°C and treated with either 2x MIC of lamotrigine or DMSO as a mock treatment. After 5 minutes, [^{14}C]-uridine was added and the cells were grown an additional 3 hours, at which point cells were pelleted, washed, and resuspended in fresh LB media supplemented with a 1000-fold excess of non-labeled uridine. Cells were harvested immediately

preceding the chase, and after 30 minutes, 1 hour, 2 hours, and 3 hours of this chase period (Figure 7A).

In each DMSO-treated sample (Figure 7B), we found significant quantities of [¹⁴C]-uridine-labeled 30S and 50S subunits. Because the quantity of labeled subunits did not change as a function of the length of the chase, these particles likely represent fully mature subunits that have simply dissociated. Interestingly, DMSO-treated cells harvested immediately after the 3-hour pulse and before the addition of the chase show a slight decrease in the levels of complete 70S ribosomes relative to any of the samples harvested post-chase (Figure 7B). This small but significant change likely results from the presence of an intracellular pool of [¹⁴C]-uridine, which is incorporated into 70S particles during the initial 30-minute chase. This pool may consist of free nucleotides that are not washed away during the chase or, as described previously, may exist as transcribed rRNA that has not completed the assembly process^{32,33}. Cells harvested at subsequent times during the chase period showed no change in the quantities of 30S, 50S, and 70S particles, indicating that all newly synthesized rRNA is incorporating exclusively non-labeled uridine. This result allowed us to analyze the maturation of the lamotrigine-induced pre-30S and pre-50S particles, confident that they were generated during the initial pulse and not synthesized *de novo* between 30 minutes and 3 hours post-pulse.

We next analyzed the ability of cells treated with lamotrigine to process pre-30S and pre-50S particles (Figure 7C). Cells harvested immediately after the

3-hour pulse period displayed a significant accumulation of pre-30S and pre-50S material. As shown earlier (Figure 3F), we also noticed a large decrease in the relative accumulation of 70S ribosomes during drug treatment. Some 30 minutes after removal of lamotrigine and non-labeled uridine chase, the relative proportions of ribosomal particles began to adjust. Specifically, the levels of pre-30S and pre-50S particles decreased with a corresponding increase in 70S ribosomes. This trend continued throughout the 3-hour chase period, after which there were no apparent differences between DMSO-treated, and lamotrigine-treated cells. Interestingly, after 1 hour of non-labeled uridine chase, a cluster of three particles that sedimented at approximately 40S (discussed above as the pre-50S), 45S, and 50S appeared. With each successive time point, the levels of 50S increased at the expense of the other particles, suggesting our time course had captured cells actively assembling the pre-50S particles into 50S subunits.

Discussion

Understanding bacterial ribosome assembly has proven to be a challenging undertaking. Involving nearly 60 protein factors, the process is rapid, highly efficient, and studies to date suggest that assembly intermediates are elusive and do not accumulate in significant amounts^{31,32}. The genetic inactivation of ribosome biogenesis factors has provided an opportunity to perturb the process in order to better understand the action of chemical modification and chaperone functions in the assembly process³⁰. Nevertheless, many of these

factors are essential and resist genetic manipulation. Further, genetic inactivation has poor temporal resolution and is not ideally suited to probe the coordinated action of these factors in time and space. Indeed, our understanding of ribosome function has benefited enormously from a great number and variety of small molecule probes of chemical and conformational steps of protein translation^{38,39}. Chemical inhibitors of the assembly process would similarly provide important new probes of ribosome biogenesis. Herein, we report the discovery and characterization of a small molecule inhibitor of ribosome assembly in *E. coli* under cold temperature growth conditions. The inhibitor, lamotrigine, is a widely available anticonvulsant drug whose target in *E. coli* is domain II of initiation factor IF2. In all, this work provides the first small molecule probe of ribosome assembly and points to a novel role for IF2 in *E. coli* ribosome biogenesis.

To find small molecule inhibitors of ribosome assembly we developed a cell-based platform to first enrich for inhibitors of ribosome assembly and function by screening for compounds that led to a cold sensitive growth phenotype. The screen was inspired by numerous previous reports of cold sensitive mutants in ribosome-related genes, and was validated with a screen of the *E. coli* Keio collection. In our screen of the Keio collection, ribosome genes were overwhelmingly enriched and, of the known cold sensitive ribosome biogenesis genes, we were successful in identifying the vast majority of these. We next screened a diverse collection of ~30,000 small molecules, including many known drugs and bioactive compounds, to identify growth inhibitory compounds with

increased potency at 15°C relative to 37°C. Of 38 structurally diverse active compounds from this screen, lamotrigine induced the most profound cold sensitive growth inhibition. Sedimentation analysis revealed that lamotrigine induced the rapid accumulation of non-native ribosomal particles with apparent sedimentation rates of ~25S (pre-30S) and ~40S (pre-50S), prompting an in-depth analysis of their composition. Using 5' primer extension of rRNA and r-protein mass spectrometry, these particles were found to be immature 30S and 50S subunits, respectively. These immature subunits lacked r-proteins associated with the neck of the 30S subunit and the body of the 50S subunit around the L1 arm, central protuberance, and L11 arm (Figure 4 – figure supplement 2C, D). With these regions encompassing the functional centers of each subunit, it is tempting to speculate that lamotrigine may perturb late steps in 30S and 50S subunit assembly. It has recently been suggested that these sites are among the last to mature⁴⁰⁻⁴³, consistent with this hypothesis.

Whole genome sequencing of spontaneous suppressor mutants capable of robust growth in the presence of lamotrigine revealed mutations in domain II near the N-terminus of initiation factor IF2. Further, *in vitro* binding studies indicated that lamotrigine binds to IF2 in a nucleotide dependent fashion and that suppressor mutations abrogated binding. Interestingly, domain II is conserved solely among IF2 proteins from the Enterobacteriaceae and has yet to be assigned a definitive function. Indeed, only one study suggests a role for this region in binding strongly to 30S, 50S, and 70S ribosomal particles relative to the

other Enterobacteriaceae IF2 domains⁴⁴. While lamotrigine treatment resulted in the rapid accumulation of immature 30S and 50S subunits, the target IF2 led us to wonder if lamotrigine might be an inhibitor of protein translation. We speculated that the observed ribosome biogenesis phenotype might be an indirect effect of blocking r-protein production, as described previously for antibiotics known to inhibit translation²⁴⁻²⁶. Using multiple orthogonal approaches, both *in vitro* and *in vivo*, we were unable to detect any translational inhibition by lamotrigine even when using concentrations far above the MIC. These results were in contrast to assays with known translational inhibitors, including evernimicin, a known inhibitor of IF2-dependent 70S initiation complex formation.

The finding that IF2 is the target of lamotrigine is intriguing in light of emerging information on the role of its eukaryotic counterpart, eIF5B, in 40S subunit assembly in yeast^{8,9}. In *Saccharomyces cerevisiae*, eIF5B associates with immature 40S subunits in a translation-like checkpoint, wherein immature 40S particles bind to mature 60S subunits prior to final maturation. Given that pre-30S and pre-50S particles accumulate during lamotrigine stress, a bacterial model may include association of two immature particles prior to maturation of the functional centers within the 30S and 50S subunits. Alternatively, it is possible that IF2 is involved in the maturation of 30S and 50S subunits independently. Regardless of the precise events mediated by IF2, our data strongly supports a central role for the enigmatic and divergent domain II of *E. coli* IF2 in the assembly of both subunits. Interestingly, our observations help rationalize the

previously unexplained finding that overexpression of IF2 in a $\Delta yjeQ$ background of *E. coli* partially suppresses the mutant slow growth phenotype and restores ribosome profiles to wild type⁴⁵. Similarly to lamotrigine-treated cells, the 30S particles of cells lacking YjeQ display significantly depleted occupancy of S21, S1, S2, and S3⁴³, suggesting that IF2 may perform an overlapping role in late 30S maturation during cold stress. Our results also parallel work dating back almost two decades, which showed that truncation of the N-terminus of *E. coli* IF2, containing domain II, led to cold sensitive growth^{46,47}. With much of the machinery involved in ribosome biogenesis^{48,49} and translation⁵⁰ conserved among bacteria and eukaryotes, the maintenance of IF2/eIF5B function in ribosome biogenesis through evolution is surely plausible. Given that domain II of IF2 is highly divergent, this work raises questions of how diverse bacterial species carry out the temperature-dependent functions of IF2 described herein. Domain II may have a purpose that is uniquely important to the Enterobacteriaceae under cold stress or, alternatively, species-specific proteins that mimic the N-terminus of IF2 from Enterobacteriaceae may perform this activity.

Taken together, this work establishes the lamotrigine as a first-in-class small molecule inhibitor of bacterial ribosome biogenesis. Moreover, we have identified domain II of IF2 as the molecular target of lamotrigine, suggesting an as-yet-uncharacterized ribosome assembly function for this canonical translation initiation factor. We posit that lamotrigine will serve as an important tool in

expanding our understanding of the molecular details of IF2 in ribosome biogenesis, and functions as a proof-of-concept molecule in the development of novel antibiotics.

Materials and Methods

Screening for cold sensitivity. Overnight cultures of *E. coli* BW25113 (including Keio strains) grown in LB media at 37°C were diluted 1/1000 in fresh LB, and incubated at 15°C (48 hours) and 37°C (24 hours) in duplicate without shaking in a final volume of 100 µL. Cells were grown in Corning (Corning, NY) Costar 96-well clear-bottom plates. For the small molecule screen, compounds were added to *E. coli* BW25113 to a final concentration of 10 µM. All screens were performed in duplicate. Molecules, dissolved in DMSO, were sourced from ChemBridge (San Diego, CA), Maybridge (Waltham, MA), MicroSource Discovery Systems (Gaylordsville, CT), Prestwick Chemicals (Washington, DC), and Biomol-Enzo Life Sciences (Farmingdale, NY). Liquid handling was performed using a Beckman Coulter (Brea, CA) FX^P Laboratory Automated Workstation. After incubation, plates were read using a Perkin Elmer (Waltham, MA) EnVision plate reader at 600nm.

Sucrose density gradient analysis. 25 mL cultures of early-log *E. coli* BW25113 (OD=0.2) grown in LB media at 15°C were treated with the appropriate concentration of each antibiotic (purchased from Sigma, St. Louis, MO) and, when applicable, pulse labeled with [¹⁴C]-uridine (purchased from American

Radiolabeled Chemicals, St. Louis, MO) to a final concentration of 0.2 $\mu\text{Ci/mL}$ (specific activity 55 mCi/mmol). Cells were incubated as necessary, harvested by centrifugation, and lysed using a Constant Systems (Daventry, England) cell disruptor at 13 kpsi in 3 mL ice-cold ribosome buffer (20 mM Tris-HCl, pH 7.0, 10.5 mM MgOAc, 100 mM NH_4Cl , 3 mM β -mercaptoethanol). Cell lysates were clarified using a Beckman Coulter MLA-80 rotor at 24,000 rpm for 45 minutes, at which time they were loaded onto 35 mL 10%-40% sucrose gradients and centrifuged for 18 hours at 18,700 rpm in a Thermo (Waltham, MA) SureSpin rotor. The volume of lysate added to each gradient was adjusted based on OD_{600} of the DMSO-treated control culture to ensure reproducibility across experiments. Gradients were either fractionated using an AKTA Prime FPLC (GE Healthcare, Little Chalfont, England) outfitted with a continuous flow UV cell at 260 nm, or analyzed via continuous flow UV and scintillation counting using an AKTA Prime FPLC in series with a Perkin Elmer 150TR flow scintillation analyzer.

5' primer extension analysis of rRNA. Sucrose density gradients, loaded with clarified cell lysates normalized for OD_{600} , were ran as described above. Total rRNA from 500 μL sucrose gradient fractions was purified using phenol chloroform extraction followed by sodium acetate precipitation, and dissolved in 5 μL of water. 1 μL of rRNA from each sample was added to 9 μL of water, and 1 μL (2.4 pmol) of the necessary primer was added. Each 11 μL reaction was incubated at 80°C for 10 minutes and allowed to cool to room temperature in order to denature the rRNA. rRNA was subsequently reverse transcribed at 45°C

for 24 hours using RevertAid H Minus Reverse Transcriptase from Thermo Scientific in a reaction volume of 20 μ L according to the manufacturers instructions. cDNA products from each reaction were precipitated using sodium acetate and 90% ethanol, and washed once in 70% ethanol. Purified cDNA samples were analyzed via capillary electrophoresis using a GeneScan 350 TAMRA size standard. 16S rRNA and 23S rRNA primers containing a 5' 6-oxyfluorescein marker were purchased from Sigma. 16S rRNA primer sequence: 5'-CTGTTACCGTTCGACTTG-3'. 23S rRNA primer sequence: 5'-CTTATCGCAGATTAGCACG-3'.

R-protein quantitation using mass spectrometry. Reference standard ribosomal particles were prepared by growing *E. coli* strain NCM3722 in supplemented M9 [48 mM Na_2HPO_4 , 22 mM KH_2PO_4 , 8.5 mM NaCl 10 mM MgCl_2 , 10 mM MgSO_4 , 5.6 mM glucose, 50 μ M Na_3EDTA , 25 mM CaCl_2 , 50 μ M FeCl_3 , 0.5 μ M ZnSO_4 , 0.5 μ M CuSO_4 , 0.5 μ M MnSO_4 , 0.5 μ M CoCl_2 , 0.04 μ M d-biotin, 0.02 μ M folic acid, 0.08 μ M vitamin B1, 0.11 μ M calcium pantothenate, 0.4 nM vitamin B12, 0.2 μ M nicotinamide, and 0.07 μ M riboflavin] bearing 7.6 mM of either ^{14}N or ^{15}N -labeled $(\text{NH}_4)_2\text{SO}_4$. Cells were harvested at OD=0.5 and lysed in Buffer A [20 mM Tris-HCl, 100 mM NH_4Cl , 10 mM MgCl_2 , 0.5 mM EDTA, 6 mM β -mercaptoethanol; pH 7.5] using a mini bead beater. Clarified lysates (5 mL) were layered above a 5 mL sucrose cushion [20 mM Tris-HCl, 500 mM NH_4Cl , 10 mM MgCl_2 , 0.5 mM EDTA, 6 mM β -mercaptoethanol, 37% sucrose; pH 7.5] and were spun for 22 hours at 37.2krpm in a Ti 70.1 rotor. Pellets bearing 70S

ribosomes were solubilized in buffer A at 4°C and saved at -80°C. Lamotrigine- and DMSO-treated ribosomal particles were separated on a sucrose density gradient and fractions were collected as described above. A mixed reference standard bearing 10 pmol of ¹⁴N-labeled and 30 pmol of ¹⁵N-labeled 70S ribosomal particles was added to 20 pmol of each experimental fraction. The use of this mixed reference ensured that every ¹⁵N-labeled peptide bore a ¹⁴N-labeled peptide pair irrespective of the abundance of that peptide in the experimental sample. Additionally, one sample bearing only the reference standard was mixed with an equal volume of buffer A. These samples were then prepared for LC/MS via precipitation, reduction, alkylation and tryptic digestion as described previously⁴⁰. Peptides were eluted from a C18 column using a concave acetonitrile gradient and detected using first an Agilent (Santa Clara, CA) G1969A ESI-TOF and second, to improve proteomic coverage and to identify non-ribosomal proteins, using an AB/Sciex (Framingham, MA) 5600 Triple-TOF run in MS² mode. In each case, the entire isotope distribution of each extracted MS¹ spectrum was fit using a Least Squares Fourier Transform Convolution algorithm³⁷ providing accurate quantitation of the ¹⁴N and ¹⁵N species' abundance. To account for the reference standard's contribution to the measured ¹⁴N peptide abundance, each spectrum was normalized using the paired ¹⁵N abundance. Having measured the reference standard alone in triplicate, we then subtracted these normalized spectra, resulting in the corrected peptide abundance for each peptide in each experimental sample. Datasets from the ESI-

TOF and Triple-TOF were merged and filtered for interference from co-eluting peptides. As a proof of principle, a series of standards bearing various quantities of ^{14}N -labeled 70S particles were also analyzed to assess the linearity of our detection technique⁵¹. Non-ribosomal proteins were quantified across the gradient using the aforementioned MS² Triple-TOF datasets. These datasets were acquired as IDA experiments with 200 ms MS¹ scans followed by 50 MS² scans, each with 50 ms of ion accumulation. Precursor ions were excluded from MS² analysis 12 seconds after one occurrence. In each fraction, spectral counts for each non-ribosomal protein were normalized to the total number of spectral counts in that fraction. These values were then normalized to the maximal spectral counts in any gradient fraction and the occupancy profile was smoothed using a 3-fraction sliding Gaussian window.

^{15}N pulse labeling. 30 mL mid-log cultures of *E. coli* BW25113 (OD=0.4) grown in M9 media were pulsed with 50% ^{15}N by adding 30 mL of M9 containing ^{15}N ammonium chloride as the sole nitrogen source. Cells were introduced to the necessary concentrations of chloramphenicol or lamotrigine during the pulse by supplementing the ^{15}N M9 with antibiotic. Cells were pulsed for 0 hours, 1 hour, 2.6 hours, 4 hours, 8 hours, and 16 hours, at which times 10 mL of each culture was removed and the cells harvested via centrifugation. Cell pellets were frozen at -80°C prior to processing for mass spectrometry.

R-protein synthesis measured by pulse-labeling quantitative mass

spectrometry. Pulse-labeled cells were spiked with 20 pmol of ^{15}N -labeled 70S

ribosomal particles and prepared for analysis on the ESI-TOF as described above. Extracted MS¹ spectra were fit using Least Squares Fourier Transform Convolution algorithm with three species: 0% ¹⁵N (pre-pulse), 50% ¹⁵N (post-pulse), and 100% ¹⁵N³⁷. Each species was normalized to the reference resulting in the following: pre-pulse material [0%/100%], post-pulse synthesis [50%/100%], and total material [(0%+50%)/100%]. Synthesis rates were calculated for each r-protein independently by fitting the median post-pulse synthesis measurement for the 0, 4, 8, 16-hour time points to a line. The synthesis rate of each of r-protein in the lamotrigine or chloramphenicol treatment was normalized to that of the DMSO treatment and log-transformed. The resultant values were presented as notched box and whisker plots, centered at the growth rate for each treatment (Figure 6E). Whiskers extend to the most extreme data point within 1.5 times the inner quartile range (IQR) whereas notches extend from the median $1.57 \cdot \text{IQR} / [\text{number of points}]^{1/2}$. All aforementioned data analysis was performed using a series of Python scripts available at https://github.com/joeydavis/StokesDavis_eLife_2014.

Lamotrigine suppressor isolation and whole genome sequencing. Dense overnight cultures of *E. coli* BW25113 were diluted 1/1000 in 10 mL of LB media supplemented with 39 μM lamotrigine and grown at 15°C until cultures became dense. This occurred after 7 days of incubation. Potential suppressor clones from these cultures were subsequently passaged three times on LB agar. Single colonies from LB agar plates were then re-streaked onto LB agar supplemented

with 39 μM lamotrigine to assess mutation stability and purify individual suppressor clones. Individual colonies were isolated based on colony diameter, and analyzed via UV absorbance at 600 nm in liquid LB media to determine growth kinetics and lamotrigine MICs at 15°C. Kinetic growth assays were conducted in a temperature-controlled Tecan (Mannedorf, Switzerland) Sunrise plate reader. The ribosomal particles of these clones were analyzed using sucrose density gradient centrifugation as described above. Genomic DNA from wild type *E. coli* BW25113 and lamotrigine suppressor mutants was purified using a Qiagen (Venlo, Netherlands) Genra Puregene kit and sequenced using an Illumina (San Diego, CA) MiSeq platform. Paired-end 250bp read data for wild type and mutant samples was aligned to the *E. coli* MG1655 chromosome (NC_000913) using BowTie2, and mutations were visualized and annotated using BreSeq and Tablet.

[³H]-lamotrigine binding assays. Wild type and mutant #3 *E. coli* *infB* genes were cloned into the pDEST17 plasmid containing an N-terminal His tag using the Invitrogen (Carlsbad, CA) Gateway cloning system. Protein expression was conducted in *E. coli* BL21-AI cells grown in LB at 15°C. Expression was induced at OD~0.6 using 0.2% arabinose, and cells were harvested after 16 hours of induction. Cells were lysed using a Constant Systems cell disruptor at 20 kpsi in IF2 lysis buffer (50 mM HEPES-KOH, pH 7.4, 1 M NH₄Cl, 10 mM MgCl₂, 0.1% Triton X-100, 7 mM β -mercaptoethanol) containing EDTA-free protease inhibitor tablets from Roche. Cell lysates were clarified via centrifugation at 20,000 rpm for

45 minutes in a Beckman Coulter JA-25.50 rotor. Clarified lysates were loaded onto a 1 mL GE Healthcare HisTrap FF column and eluted with IF2 elution buffer (50 mM HEPES-KOH, pH 7.4, 1 M NH₄Cl, 10 mM MgCl₂, 7 mM β-mercaptoethanol, 400 mM imidazole). Purified wild type and mutant IF2 was buffer exchanged into ice-cold ribosome buffer using an Amicon (Millipore, Billerica, MA) Ultracel filtration unit with a 50 kDa cutoff filter. 50 µL reactions containing 2 mg/mL BSA, 20 µM IF2, 200 nM [³H]-lamotrigine (specific activity 5 Ci/mmol; purchased from American Radiolabeled Chemicals), and 30 mM G-nucleotide (purchased from Sigma) were incubated at 15°C in ribosome buffer for 3 hours. Reactions were loaded onto 200 µL pre-wet Sephadex G-25 resin beds (resin purchased from GE Healthcare) and centrifuged at 400 x g for 3 minutes. Flow-through samples were scintillation counted using Perkin Elmer Ultima Gold scintillation fluid.

In vivo translation analysis. 1 mL early-log cultures of *E. coli* BW25113 (OD=0.2) grown in M9 media were treated with 8x MIC of various antibiotics and were concurrently pulse labeled with [³⁵S]-methionine (purchased from Perkin Elmer) to a final concentration of 5 µCi/mL (specific activity 1175 Ci/mmol). Cells were incubated for 2.6 hours at 15°C, at which time they were harvested via centrifugation and washed twice in 1 mL 0.85% saline. Cells were lysed using 100 µL Millipore BugBuster Master Mix reagent and proteins were precipitated using 25 µL ice-cold 25% TCA. Protein pellets were then washed twice in 25 µL ice-cold 10% TCA and passed through Whatman (GE Healthcare) GF/C filters

using a Millipore vacuum manifold. Filters were washed three times in ice-cold 10% TCA, dried overnight at room temperature, and scintillation counted using Perkin Elmer Ultima Gold scintillation fluid.

***In vitro* translation analysis.** Cell-free translation was conducted using the *E. coli* S30 transcription-translation system for circular DNA from Promega (Finchburg, WI) according the manufacturer's instructions. 10 μ L reactions containing the necessary antibiotics and plasmid DNA encoding the firefly luciferase gene were incubated either at 15°C for 4 hours or 37°C for 1 hour. Reactions were halted on ice for 5 minutes prior to addition of 25 μ L of room-temperature luciferin (purchased from Promega). Immediately after the addition of luciferin, samples were analyzed for luminescence output in a Nunc (Roskilde, Denmark) 384-well clear bottom plate using a Tecan Ultra Evolution luminometer.

Accession Numbers

The GenBank accession numbers for the IF2 variants described in this paper are KJ752767 (wild type *E. coli* BW25113 IF2); KJ52768 (mutant #1 IF2); KJ752769 (mutant #2 IF2); KJ752770 (mutant #3 IF2); and KJ752771 (mutant #4 IF2).

Acknowledgments

We thank Dr. Mike Surette and Nicholas Waglechner from McMaster University for assistance with genome analysis; members of the Center for Microbial Chemical Biology at McMaster University for technical assistance with screening

robotics; Dr. Stephan Nord, formerly in the lab of E.D.B., for assistance in 5' primer extension and lamotrigine suppressor generation; and Kella Kapnisi, formerly in the lab of E.D.B., for assistance with small molecule screening.

Author Contributions

J.M.S., J.H.D., C.S.M, and E.D.B. conceived and designed the study. J.M.S., J.H.D., and C.S.M. acquired data. J.M.S, J.H.D., C.S.M., J.R.W, and E.D.B. analyzed and interpreted data. J.M.S., J.H.D., J.R.W., and E.D.B. drafted and revised the manuscript.

References

1. Moore, P. B. How should we think about the ribosome? *Annu Rev Biophys.* **41**, 1–19 (2012).
2. Maguire, B. A. Inhibition of bacterial ribosome assembly: a suitable drug target? *Microbiol Mol Biol Rev.* **73**, 22–25 (2009).
3. Williamson, J. R. Assembly of the 30S ribosomal subunit. *Q Rev Biophys.* **38**, 397–403 (2005).
4. Holmes, K. L. & Culver, G. M. Analysis of conformational changes in 16S rRNA during the course of 30S subunit assembly. *J Mol Biol.* **354**, 340–357 (2005).
5. Kim, H. *et al.* Protein-guided RNA dynamics during early ribosome assembly. *Nature* **506**, 334–338 (2014).
6. Bunner, A. E., Nord, S., Wikström, P. M. & Williamson, J. R. The effect of ribosome assembly cofactors on *in vitro* 30S subunit reconstitution. *J Mol Biol.* **398**, 1–7 (2010).
7. Strunk, B. S. *et al.* Ribosome assembly factors prevent premature translation initiation by 40S assembly intermediates. *Science* **333**, 1449–1453 (2011).

8. Strunk, B. S., Novak, M. N., Young, C. L., & Karbstein, K. A translation-like cycle is a quality control checkpoint for maturing 40S ribosome subunits. *Cell* **150**, 111–121 (2012).
9. Lebaron, S. *et al.* Proofreading of pre-40S ribosome maturation by a translation initiation factor and 60S subunits. *Nat Struct Mol Biol.* **19**, 744–753 (2012).
10. Boehringer, D., O'Farrell, H. C., Rife, J. P. & Ban, N. Structural insights into methyltransferase KsgA function in 30S ribosomal subunit biogenesis. *J Biol Chem.* **287**, 10453–10459 (2012).
11. Yamagishi, M. & Nomura, M. Effects of induction of rRNA overproduction on ribosomal protein synthesis and ribosome subunit assembly in *Escherichia coli*. *J Bacteriol.* **170**, 5042–5050 (1988).
12. Gaal, T., Bartlett, M. S., Ross, W., Turnbough, C. L. & Gourse, R. L. Transcription regulation by initiating NTP concentration: rRNA synthesis in bacteria. *Science.* **278**, 2092–2097 (1997).
13. Lerner, C. G. & Inouye, M. Pleiotropic changes resulting from depletion of Era, an essential GTP-binding protein in *Escherichia coli*. *Mol Microbiol.* **5**, 951–957 (1991).
14. Comartin, D. J. & Brown, E. D. Non-ribosomal factors in ribosome subunit assembly are emerging targets for new antibacterial drugs. *Curr Opin Pharmacol.* **6**, 453–458 (2006).
15. Dammel, C. S. & Noller, H. F. Suppression of a cold-sensitive mutation in 16S rRNA by overexpression of a novel ribosome-binding factor, RbfA. *Genes Dev.* **9**, 626–637 (1995).
16. Jones, P. G., Mitta, M., Kim, Y., Jiang, W. & Inouye, M. Cold shock induces a major ribosomal-associated protein that unwinds double-stranded RNA in *Escherichia coli*. *Proc Natl Acad Sci U.S.A.* **93**, 76–80 (1996).
17. Bubunencko, M. *et al.* 30S ribosomal subunits can be assembled in vivo without primary binding ribosomal protein S15. *RNA* **12**, 1229–1239 (2006).
18. Connolly, K., Rife, J. P. & Culver, G. Mechanistic insight into the ribosome biogenesis functions of the ancient protein KsgA. *Mol Microbiol.* **70**, 1062–1075 (2008).
19. Clatterbuck Soper, S. F., Dator, R. P., Limbach, P. A. & Woodson, S. A. *In vivo* X-ray footprinting of pre-30S ribosomes reveals chaperone-

- dependent remodeling of late assembly intermediates. *Mol Cell*. **52**, 506–516 (2013).
20. Bryant, R. E. & Sypherd, P. S. Genetic analysis of cold-sensitive ribosome maturation mutants of *Escherichia coli*. *J Bacteriol*. **117**, 1082–1092 (1974).
 21. Baba, T. *et al.* Construction of *Escherichia coli* K-12 in-frame, single-gene knockout mutants: the Keio collection. *Mol Syst Biol*. 2006;2:2006.0008.
 22. Tatusov, R. L., Koonin, E. V. & Lipman, D. J. A genomic perspective on protein families. *Science* **278**, 631–637.
 23. Tatusov, R. L. *et al.* The COG database: an updated version includes eukaryotes. *BMC Bioinformatics*. **4**, 41 (2003).
 24. Siibak, T. *et al.* Erythromycin- and chloramphenicol-induced ribosomal assembly defects are secondary effects of protein synthesis inhibition. *Antimicrob Agents Chemother*. **53**, 563–571 (2009).
 25. Sykes, M. T., Shajani, Z., Sperling, E., Beck, A. H. & Williamson, J. R. Quantitative proteomic analysis of ribosome assembly and turnover *in vivo*. *J Mol Biol*. **403**, 331–345 (2010).
 26. Siibak, T. *et al.* Antibiotic-induced ribosomal assembly defects result from changes in the synthesis of ribosomal proteins. *Mol Microbiol*. **80**, 54–67 (2011).
 27. Lindahl, L. Two new ribosomal precursor particles in *E. coli*. *Nat New Biol*. **243**, 170–172 (1973).
 28. Mangiarotti, G., Turco, E., Ponzetto, A. & Altruda, F. Precursor 16S RNA in active 30S ribosomes. *Nature*. **247**, 147–148 (1974).
 29. Srivastava, A. K. & Schlessinger, D. Coregulation of processing and translation: mature 5' termini of *Escherichia coli* 23S ribosomal RNA form in polysomes. *Proc Natl Acad Sci U.S.A.* **85**, 7144–7148 (1988).
 30. Shajani, Z., Sykes, M. T. & Williamson, J. R. Assembly of bacterial ribosomes. *Annu Rev Biochem*. **80**, 501–526 (2011).
 31. Mulder, A. M. *et al.* Visualizing ribosome biogenesis: parallel assembly pathways for the 30S subunit. *Science*. **330**, 673–677 (2010).
 32. Chen, S. S., Sperling, E., Silverman, J. M., Davis, J. H. & Williamson, J. R. Measuring the dynamics of *E. coli* ribosome biogenesis using pulse-labeling and quantitative mass spectrometry. *Mol Biosyst*. **8**, 3325–3334 (2012).

33. Chen, S. S. & Williamson, J. R. Characterization of the ribosome biogenesis landscape in *E. coli* using quantitative mass spectrometry. *J Mol Biol.* **425**, 767–779 (2013).
34. Severini, M., Spurio, R., La Teana, A., Pon, C. L. & Gualerzi, C. O. Ribosome-independent GTPase activity of translation initiation factor IF2 and of its G-domain. *J Biol Chem.* **266**, 22800–22802 (1991).
35. McNicholas, P. M. *et al.* Evernimicin binds exclusively to the 50S ribosomal subunit and inhibits translation in cell-free systems derived from both gram-positive and gram-negative bacteria. *Antimicrob Agents Chemother.* **44**, 1121–1126 (2000).
36. Belova, L., Tenson, T., Xiong, L., McNicholas, P. M. & Mankin, A. S. A novel site of antibiotic action in the ribosome: interaction of evernimicin with the large ribosomal subunit. *Proc Natl Acad Sci U.S.A.* **98**, 3726–3731 (2001).
37. Sperling, E., Bunner, A. E., Sykes, M. T. & Williamson, J. R. Quantitative analysis of isotope distributions in proteomic mass spectrometry using least-squares Fourier transform convolution. *Anal Chem.* **80**, 4906–4917 (2008).
38. Tenson, T. & Mankin, A. Antibiotics and the ribosome. *Mol Microbiol.* **59**, 1664–1677 (2006).
39. Wilson, D. N. The A-Z of bacterial translation inhibitors. *Crit Rev Biochem Mol Biol.* **44**, 393–433 (2009).
40. Jomaa, A., *et al.* Functional domains of the 50S subunit mature late in the assembly process. *Nucleic Acids Res.* **42**, 3419–3435 (2014).
41. Li, N. *et al.* Cryo-EM structures of the late-stage assembly intermediates of the bacterial 50S ribosomal subunit. *Nucleic Acids Res.* **41**, 7073–7083 (2013).
42. Guo, Q. *et al.* Dissecting the *in vivo* assembly of the 30S ribosomal subunit reveals the role of RimM and general features of the assembly process. *Nucleic Acids Res.* **41**, 2609–2620 (2013).
43. Jomaa, A. *et al.* Understanding ribosome assembly: the structure of *in vivo* assembled immature 30S subunits revealed by cryo-electron microscopy. *RNA* **17**, 697–709 (2011).
44. Moreno, J. M., Drskjøtersen, L., Kristensen, J. E., Mortensen, K. K. & Sperling-Petersen, H. U. Characterization of the domains of *E. coli* initiation factor IF2 responsible for recognition of the ribosome. *FEBS Lett.* **455**, 130–

134 (1999).

45. Campbell, T. L. & Brown, E. D. Genetic interaction screens with ordered overexpression and deletion clone sets implicate the *Escherichia coli* GTPase YjeQ in late ribosome biogenesis. *J Bacteriol.* **190**, 2537–2545 (2008).
46. Laalami, S., Putzer, H., Plumbridge, J. A. & Grunberg-Manago, M. A severely truncated form of translational initiation factor 2 supports growth of *Escherichia coli*. *J Mol Biol.* **220**, 335–349 (1991).
47. Laalami, S. *et al.* Structural and functional domains of *E. coli* initiation factor IF2. *Biochimie.* **73**, 1557–1566 (1991).
48. Schaefer, L. *et al.* Multiple GTPases participate in the assembly of the large ribosomal subunit in *Bacillus subtilis*. *J Bacteriol.* **188**, 8252–8258 (2006).
49. Bharat, A., Jiang, M., Sullivan, S. M., Maddock, J. R. & Brown, E. D. Cooperative and critical roles for both G domains in the GTPase activity and cellular function of ribosome-associated *Escherichia coli* EngA. *J Bacteriol.* **188**, 7992–7996 (2006).
50. Anger, A. M. *et al.* Structures of the human and *Drosophila* 80S ribosome. *Nature* **497**, 80–85 (2013).
51. Gulati, M., Jain, N., Davis, J. H., Williamson, J. R. & Britton, R. A. Functional interaction between ribosomal protein L6 and RbgA during ribosome assembly. *PLOS Genet.* **10**, e1004694 (2014).
52. Held, W. A., Ballou, B., Mizushima, S. & Nomura, M. Assembly mapping of 30S ribosomal proteins from *Escherichia coli*. *J Biol Chem.* **249**, 3103–3111 (1974).
53. Herold, M. & Nierhaus, K. H. Incorporation of six additional proteins to complete the assembly map of the 50S subunit from *Escherichia coli* ribosomes. *J Biol Chem.* **262**, 8826–8833 (1987).

Figure Legends

Figure 1. The ribosome is a primary target of cold stress. (A) Screen of the *E. coli* Keio collection for cold sensitivity. Each strain's cold sensitivity factor is

defined as the ratio of growth at 37°C to growth at 15°C. Cold sensitivity factors for each strain were normalized to 1, based on the mean of all cold sensitivity factors calculated for the entire collection. Growth at each temperature was calculated based on the average of two replicates. A grey box highlights strains exhibiting cold sensitivity in the top 3.5% (155 strains). (B) The 155 cold sensitive genes from (A) were grouped based on clusters of orthologous groups classifications. The percentage of cold sensitive genes in each functional class was defined as the number of cold sensitive genes in that class divided by the total number of non-essential *E. coli* genes in that same functional class. By permuting the classification assignments, we determined that the proportion of cold sensitive genes in the Translation class (21%) was significant with a bootstrapped p-value $< 1e^{-6}$.

Figure 1 – figure supplement 1. Primary data from the screen of the *E. coli* Keio collection. (A) Replicate plot of Keio strains grown in duplicate at 37°C for 24 hours. (B) Replicate plot of Keio strains grown in duplicate at 15°C for 48 hours. Cells were grown in LB media supplemented with 50 µg/mL kanamycin for the aforementioned durations and subsequently read at 600 nm using a Perkin Elmer EnVision 96-well plate reader. Cells were grown in a final volume of 100 µL per well. (C) Distribution of functional classes amongst the top 3.5% of strains identified as cold sensitive. Classes are grouped according to the following: information storage and transfer (light grey); cellular processes (mid grey);

metabolism (dark grey); genes of unknown function (very dark grey) according to clusters of orthologous groups.

Figure 2. Lamotrigine induces profound cold sensitivity in *E. coli*. (A)

Screen of ~30,000 small molecules at 10 μ M against *E. coli* for cold sensitivity. Compounds found within the grey region were selected for secondary screening. Hit inclusion boundaries are defined as molecules residing $>3\sigma$ below the mean OD₆₀₀ at 15°C, and $<2\sigma$ below the mean OD₆₀₀ at 37°C. Growth at each temperature was calculated based on the average of two replicates. (B) Dose-response analysis of lamotrigine at 37°C (black dots) and 15°C (white dots). Error bars represent the error of two biological replicates.

Figure 2 – figure supplement 1. Primary data from the small molecule

screen. (A) Replicate plot of *E. coli* BW25113 grown in the presence of 10 μ M of each molecule from a collection of ~30,000 at 37°C for 24 hours, in duplicate. (B) Replicate plot of *E. coli* BW25113 grown in the presence of 10 μ M of each molecule from a collection of ~30,000 at 15°C for 48 hours, in duplicate. Cells were grown in LB media and subsequently read at 600 nm using a Perkin Elmer EnVision 96-well plate reader. Cells were grown in a final volume of 100 μ L per well.

Figure 2 – figure supplement 2. Temperature-dependence of lamotrigine

activity in *E. coli*. (A) *E. coli* BW25113 was grown in M9 (left column) and LB (middle column) until early stationary phase in the presence of varying concentrations of lamotrigine at 42°C. Cells were also grown at 37°C (B), 30°C

(C), 25°C (D), 20°C (E), and 15°C (F). Blue lines represent no-drug control cultures. Black lines represent cultures treated with MIC quantities of lamotrigine. Dose-response curves of cells grown in LB (black dots) and M9 (white dots) in the presence of lamotrigine are also shown for each temperature. Cells were grown in a final volume of 100 µL with continuous shaking, and read at 600nm every 10 minutes using a Tecan Sunrise 96-well plate reader.

Figure 3. Lamotrigine treatment results in the accumulation of non-native ribosomal particles. (A) Cells were treated with DMSO (vehicle) and immediately pulse labeled with [¹⁴C]-uridine. Cells were harvested after 1 hour (left) and 6 hours (right) of treatment and ribosomal particle accumulation was monitored using UV absorbance at 260 nm (black trace) and scintillation counting (gray trace). Also shown are treatments with 2x MIC chloramphenicol (B); 2x MIC erythromycin (C); 2x MIC tetracycline (D); 2x MIC vancomycin (E); and 2x MIC lamotrigine (F). (G) Early-log cultures of *E. coli* were treated with DMSO (solid line) or 2x MIC lamotrigine (hashed line), pulse labeled with [¹⁴C]-uridine, and incubated for 5 minutes. Ribosomal particles were separated on a sucrose gradient and monitored using UV absorbance. (H) These gradients were also analyzed via scintillation counting.

Figure 3 – figure supplement 1. Temperature-dependent antibiotic activity in *E. coli*. (A) *E. coli* BW25113 was grown in LB media at 37°C for 24 hours (black dots) and 15°C for 48 hours (white dots) in duplicate in the presence of varying concentrations of chloramphenicol, (B) erythromycin, (C) tetracycline, and

(D) vancomycin. Cells were grown in a final volume of 100 μ L. Minimum inhibitory concentration is defined as the lowest concentration of antibiotic required to prevent growth by >95%, as analyzed by OD₆₀₀. Error bars represent the error of two biological replicates. (E) Sucrose gradients of ribosomal particles from early-log cultures of *E. coli* treated with DMSO at 37°C. Cells were treated with DMSO and immediately pulse labeled with [¹⁴C]-uridine. Cells were harvested after 1 hour (~3 doublings) of treatment and ribosomal particle accumulation was monitored using UV absorbance at 260 nm (black trace) and scintillation counting (grey trace). (F) Cells were also treated with 2x MIC (15.6 μ M) of lamotrigine and ribosomes analyzed in the same manner. (G) Sucrose gradients of ribosomal particles from early-log cultures of *E. coli* treated with DMSO and immediately labeled with [³H]-lamotrigine to a final concentration of 0.2 μ Ci/mL. Cells were grown at 15°C in 25 mL of LB and harvested after 6 hours of treatment, after which they were lysed and the ribosomal particles separated through a sucrose gradient. The gradient was passed through a UV cell measuring absorbance at 260 nm (black trace), and 500 μ L fractions were subsequently collected and scintillation counted to localize [³H]-lamotrigine (grey dots). (H) Same as (G), except cells were treated with 1x MIC unlabeled lamotrigine in place of DMSO.

Figure 4. Non-native ribosomal particles are immature 30S and 50S

subunits. (A) 5' cleavage sites of 16S and 23S rRNA. (B) 5' primer extension analysis of ribosomal particles harvested from DMSO- and lamotrigine-treated *E. coli*. Early-log cells were treated with DMSO for 6 hours or 2x MIC lamotrigine for

5 minutes, ribosomal particles were separated on a sucrose gradient, and rRNA was fractionated according to increasing sedimentation rates as indicated (pre-30S, 30S, pre-50S, 50S and 70S). Particle detection by reverse transcription used a 16S rRNA specific primer (light grey) or a 23S rRNA specific primer (grey and dark grey). Proportion of immature rRNA was calculated as [immature 16S rRNA species / total 16S rRNA species] and [immature 23S rRNA species / total 23S rRNA species]. +7 and +3 represent immature 23S rRNA containing an additional 7 nucleotides and 3 nucleotides at the 5' terminus, respectively. Error bars represent the error of two biological replicates. (C) Quantitative cDNA production of rRNA species within pre-30S regions from DMSO- and lamotrigine-treated *E. coli*. Early-log cells were treated with DMSO for 6 hours or 2x MIC lamotrigine for 5 minutes, 1 hour, and 6 hours. Ribosomal particles were separated on a sucrose gradient, and rRNA purified from a single pre-30S fraction from each treatment was reverse transcribed in parallel using 16S- and 23S-specific primers. p16S represents immature 16S rRNA. Error bars represent the error of two biological replicates. (D) Quantitation of ribosomal protein occupancy within individual fractions collected from sucrose gradients. Fractions are colored from blue (lowest density portion of the gradient) to red (highest density portion of the gradient). Each open circle represents a unique peptide measurement; closed circles denote median values. Occupancy profiles for early (S15, L24) and late binding (S3, L28) proteins are compared between sucrose gradients analyzed using DMSO (top) or lamotrigine treated (bottom) cells. (E) R-

protein occupancy of ribosomal particles harvested from sucrose density gradient fractions of DMSO- (red) and lamotrigine-treated (green) *E. coli*. Data are plotted as a heat map using the median occupancy values (see results) corrected for the amount of sample analyzed in each fraction, and normalized to scale from 0 (white) to 1.0 (darkest shade). Small subunit (left) fractions span the pre-30S to the pre-50S regions of the sucrose gradient. Large subunit fractions (right) span the late-30S to the late-50S regions of the sucrose gradient. A representative 70S fraction is included in each dataset. Absorbance measured at 260 nm is plotted for the region analyzed above each heat map. (F) Mass spectrometric localization of RbfA and DeaD in sucrose density gradient fractions of DMSO- (red) and lamotrigine-treated (green) *E. coli*. Relative protein abundance was calculated as described in Materials and Methods.

Figure 4 – figure supplement 1. 5' primer extension of lamotrigine-treated *E. coli*. (A) 5' primer extension analysis of ribosomal particles harvested from *E. coli* treated with 2x MIC lamotrigine for 1 hour. Early-log cells were treated with lamotrigine, ribosomal particles were separated on a sucrose gradient, and rRNA was fractionated according to increasing sedimentation rates as indicated (pre-30S, 30S, pre-50S, 50S and 70S). Particle detection by reverse transcription used a 16S rRNA specific primer (light grey) or a 23S rRNA specific primer (grey and dark grey). Proportion of immature rRNA is calculated as [immature 16S rRNA species / total 16S rRNA species] and [immature 23S rRNA species / total 23S rRNA species]. +7 and +3 represent immature 23S rRNA containing an

additional 7 nucleotides and 3 nucleotides at the 5' terminus, respectively. Error bars represent the error of two biological replicates. (B) Same as (A), except cells were treated with 2x MIC lamotrigine for 6 hours. (C) Quantitative cDNA production of rRNA species within pre-30S regions from DMSO- and lamotrigine-treated *E. coli*. Early-log cells were treated with DMSO for 6 hours or 2x MIC lamotrigine for 5 minutes, 1 hour, and 6 hours. Ribosomal particles were separated on a sucrose gradient, and rRNA purified from a single pre-30S fraction from each treatment was reverse transcribed in parallel using 16S- and 23S-specific primers. p16S represents immature 16S rRNA. Error bars represent the error of two biological replicates.

Figure 4 – figure supplement 2. R-protein mass spectrometry of ribosomal particles from lamotrigine-treated *E. coli*. (A) R-protein occupancy of small subunit proteins across sucrose gradients from DMSO (top) and lamotrigine-treated (bottom) cells. Each open circle represents a unique peptide measurement in a given fraction. Closed circles highlight the median value for each peptide in a given fraction. Individual fractions are colored from blue (lowest density portion of the gradient) to red (highest density portion of the gradient). (B) Same as (A), except monitoring abundance of large subunit proteins. (C) Over-represented (green) and under-represented (red) small subunit r-proteins of the pre-30S particle that accumulates during lamotrigine treatment are highlighted on the Nomura assembly map^{32,52}. Assembly groups are colored according to Chen and Williamson³³. Low occupancy proteins highlighted on the 30S subunit (PDB

2AVY) cluster around the neck of the 30S subunit. (D) Under-represented (red) large subunit r-proteins from the pre-50S particle that accumulates during lamotrigine treatment are highlighted on the Nierhaus assembly map^{32,53}. Depleted proteins highlighted on the 50S subunit (PDB 2Y11) generally cluster in a ring around the L1 arm, central protuberance, and L11 arm.

Figure 5. Lamotrigine binds to wild type but not mutant IF2 in a G-nucleotide-dependent manner. (A) General domain organization of Enterobacteriaceae IF2- α with lamotrigine suppressor mutations mapped against the parental *E. coli* BW25113 sequence. (B) Experimental design of [³H]-lamotrigine association assay. (C) Relative association of [³H]-lamotrigine to wild type *E. coli* IF2 and lamotrigine suppressor IF2 (mutant #3) under varying conditions. CPMs of the experimental samples were normalized to the baseline flow-through of [³H]-lamotrigine in buffer. Error bars represent the error of three biological replicates.

Figure 5 – figure supplement 1. Genetic determinants of lamotrigine activity. (A) Structures of *E. coli* IF2N (PDB 1ND9) and *Methanothermobacter thermautotrophicus* IF2/eIF5B (PDB 1G7R), depicting the location of lamotrigine suppressor mutations in *E. coli* IF2. All mutations are localized within domain II. (B) Example growth curves of *E. coli* BW25113 (black trace) and lamotrigine suppressor mutant #3 (grey trace) in 150 μ L LB media at 15°C, shaking at 200 rpm. Cells were read at OD₆₀₀ every 10 minutes throughout the duration of the experiment. (C) Example potency analysis of lamotrigine against *E. coli*

BW25113 (white dots) and lamotrigine suppressor mutant #3 (black dots) at 15°C in LB media. Cells were grown for 48 hours prior to reading OD₆₀₀. Error bars represent the error of two biological replicates. (D) Example sucrose gradient of ribosomal particles from early-log cultures of lamotrigine suppressor mutant #3 treated with 2x MIC of lamotrigine at 15°C. Cells were treated with lamotrigine and immediately pulse labeled with [¹⁴C]-uridine. Cells were harvested after 6 hours of treatment and ribosomal particle accumulation was monitored using UV absorbance at 260 nm (black trace) and scintillation counting (grey trace). (E) IF2 homologs from various bacterial species were aligned using the MuscleWS multiple sequence alignment plugin through Jalview version 2.8. Residues 181 to 206 (*E. coli* numbering) are shown, depicting the conservation of this region exclusively in the Enterobacteriaceae. (F) Using Jalview, a distance tree relating the various IF2 homologs was calculated based on average distance using percent identity. IF2 homology between the Enterobacteriaceae predicts lamotrigine potency at 15°C.

Figure 6. Accumulation of immature ribosomal subunits is not the result of translation inhibition. (A) [³⁵S]-methionine incorporation into early-log cells grown for 2.6 hours in M9 media at 15°C. Immediately prior to the radioactivity pulse, cultures were treated with 8x MIC of each antibiotic. [³⁵S]-methionine incorporation was quantified by liquid scintillation counting. Error bars represent the error of two biological replicates. (B) Cell-free coupled transcription/translation reactions in the presence of 8x MIC of each antibiotic. Samples were incubated

at 15°C for 4 hours, at which time reactions were halted on ice, excess luciferin was added, and luminescence was monitored. Error bars represent the error of two biological replicates. (C) [³⁵S]-methionine incorporation (black dots) and cell-free luminescence (white dots) as a function of lamotrigine concentration.

Samples were prepared as described in (A) and (B). (D) Cell-free coupled transcription/translation reactions in the presence of increasing concentrations of evernimicin at 37°C (black dots) and 15°C (white dots). Reactions were assembled and analyzed as in (B). (E) Analysis of growth rate and r-protein synthesis rate as a function of lamotrigine and chloramphenicol concentrations. Synthesis rates were determined for each ribosomal protein using quantitative mass spectrometry. For each condition, r-protein synthesis rates (50 measurements per treatment) are presented as a notched box and whisker plot centered at the growth rate (1/hours) observed for that treatment (see Materials and Methods). Black dots represent synthesis rates of individual proteins in excess of [1.5 x inner quartile range] of that dataset. Light to dark shades of red represent 2x, 3x, 4x, 5x, and 6x MIC of chloramphenicol. Light to dark shades of green represent 2x, 3x, 4x, 5x, and 6x MIC of lamotrigine. Values were normalized to the DMSO control and log transformed.

Figure 6 – figure supplement 1. Effects of lamotrigine on translation in *E.*

coli. (A) [³⁵S]-methionine incorporation into early-log cells grown for 2 hours (~3 doublings) in M9 media at 37°C. Immediately prior to the radioactivity pulse, cultures were treated with increasing concentrations of lamotrigine. [³⁵S]-

methionine incorporation was quantified by liquid scintillation counting. Error bars represent the error of two biological replicates. (B) Cell-free coupled transcription/translation reactions in the presence of increasing concentrations of lamotrigine. Samples were incubated at 37°C for 1 hour, at which time reactions were halted on ice, excess luciferin was added, and luminescence was monitored. Error bars represent the error of two biological replicates. (C) Kinetics of cell-free transcription/translation system at 15°C. 10 µL reactions containing 1% DMSO were read every 30 minutes for 5 hours to establish a linear range of luciferase production. Error bars represent the error of two biological replicates. (D) Example pulse-labeling data showing the incorporation of 50% ¹⁵N into an r-protein peptide as a function of time. Similar data was gathered for all r-protein peptides from cells treated with DMSO; 2x, 3x, 4x, 5x, and 6x MIC lamotrigine; and 2x, 3x, 4x, 5x, and 6x MIC chloramphenicol. (E) R-protein degradation as a function of time in DMSO-treated cultures. Protein degradation is defined as [¹⁴N intensity / ¹⁵N intensity] for each peptide. Light shades to dark shades represent 0, 4, 8, and 16 hours of 50% ¹⁵N pulse. Small circles represent individual peptide measurements. Large circles denote the median measurement for that sample. (F) R-protein synthesis as a function of time in DMSO-treated cultures. Protein synthesis is defined as [50% ¹⁵N intensity / ¹⁵N intensity] for each peptide. Light shades to dark shades represent 0, 4, 8, and 16 hours of 50% ¹⁵N pulse. (G) and (I) are the same as (E), except for 6x MIC lamotrigine, and 6x MIC

chloramphenicol, respectively. (H) and (J) are the same as (F), except for 6x MIC lamotrigine, and 6x MIC chloramphenicol, respectively.

Figure 7. Immature ribosomal particles sediment as mature subunits upon removal of lamotrigine stress. Particles were analyzed by sedimentation over sucrose gradients and analyzed with radioactivity detection. (A) Experimental design of pulse-chase analysis of *E. coli* treated with 2x MIC lamotrigine. (B) Cells were treated with DMSO and concurrently pulsed with [¹⁴C]-uridine for 3 hours in LB media at 15°C prior to media exchange and unlabeled uridine chase. This time course reveals that no additional radiolabel was incorporated into ribosomal subunits during the chase period. (C) Cells were treated as in (B), except with 2x MIC lamotrigine in place of DMSO, revealing that radiolabeled pre-30S and pre-50S particles matured to 30S and 50S particles over the duration of chase period.

Figure 1

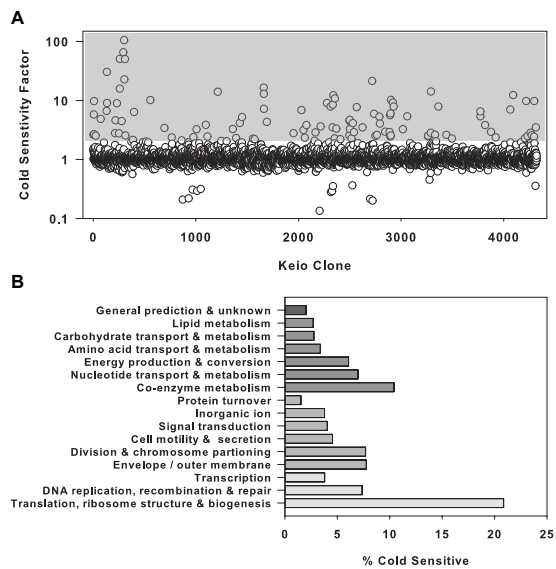


Figure 1 – figure supplement 1

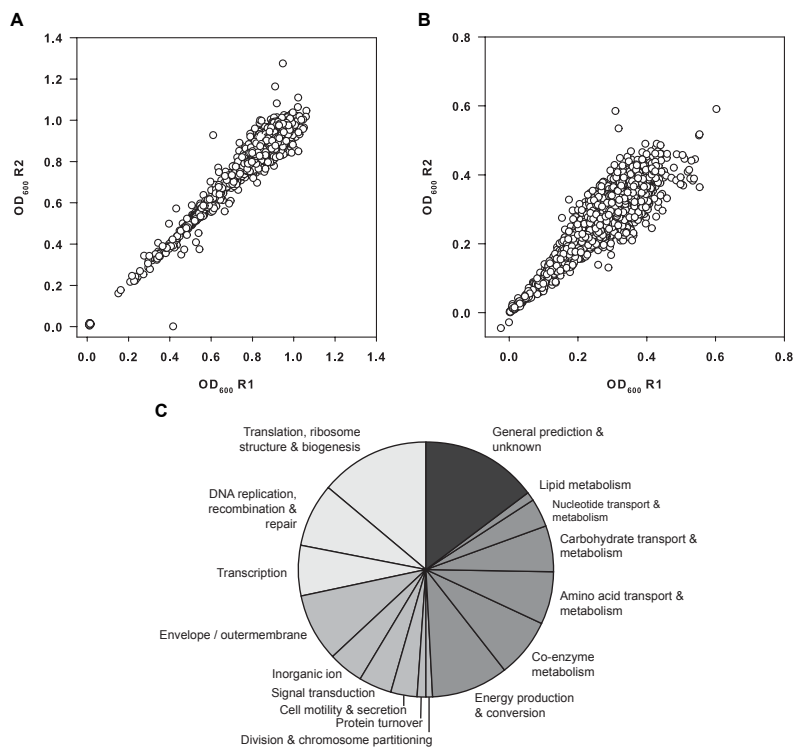


Figure 2

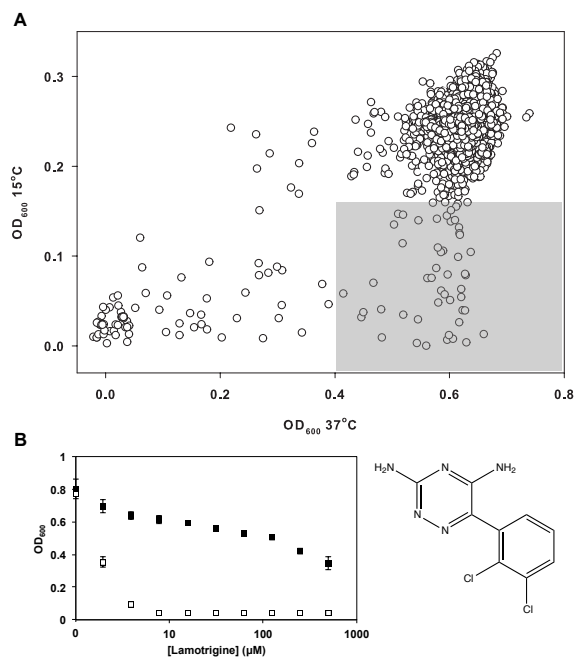


Figure 2 – figure supplement 1

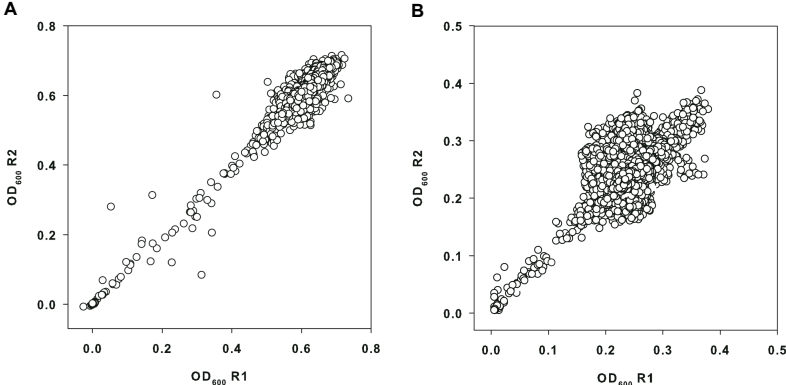


Figure 2 – figure supplement 2

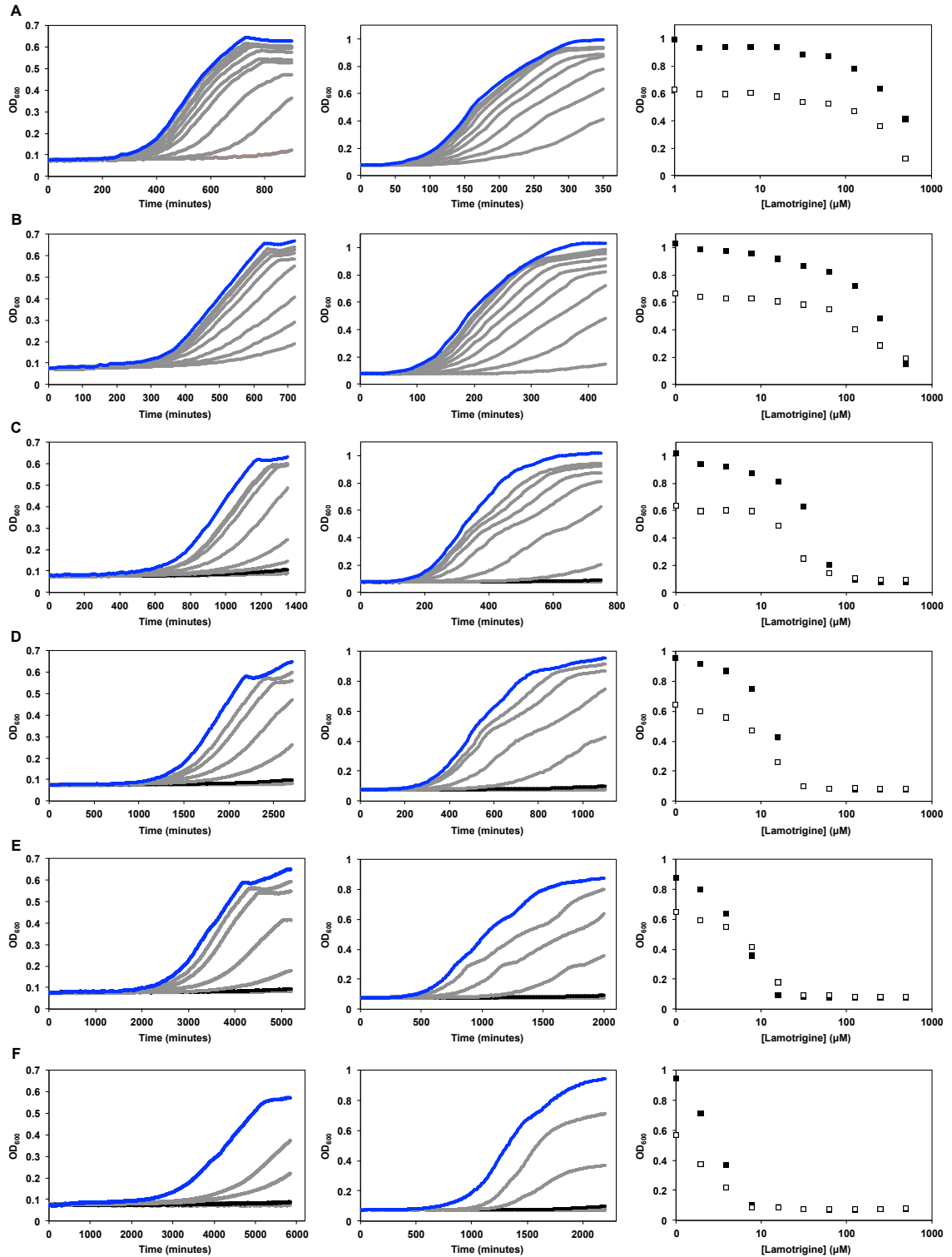


Figure 3

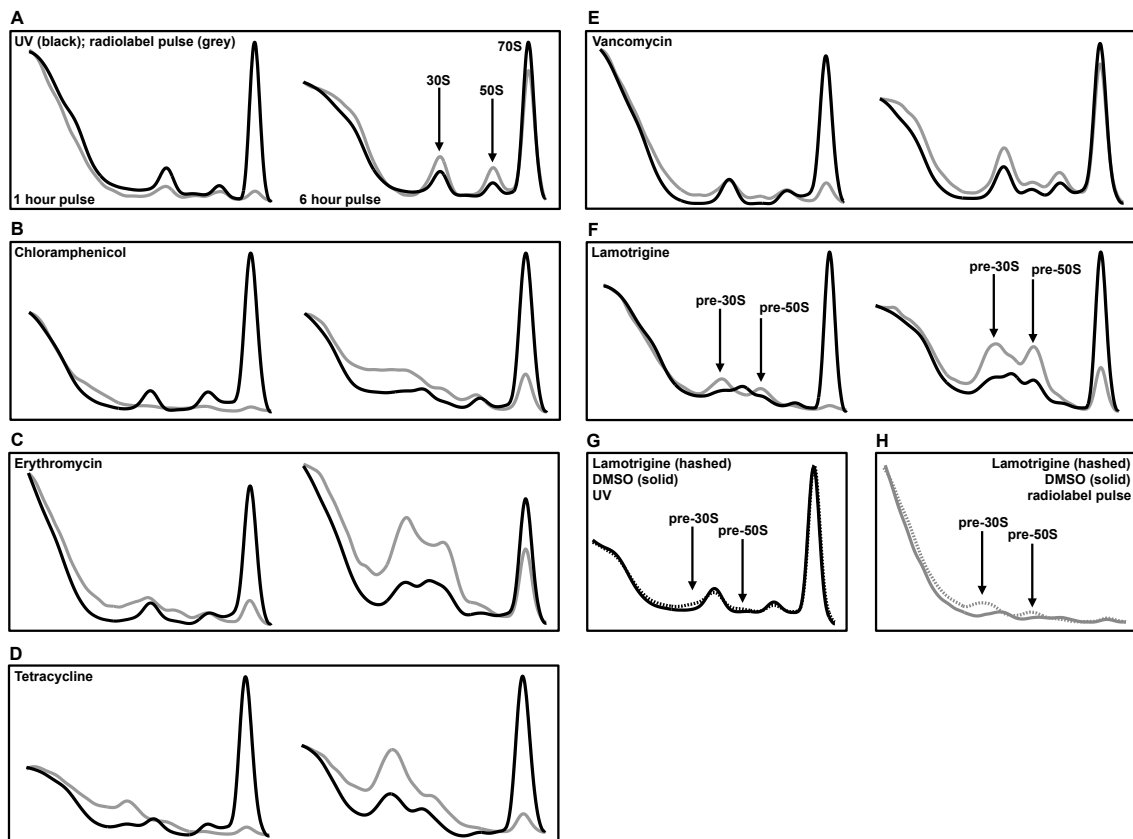


Figure 3 – figure supplement 1

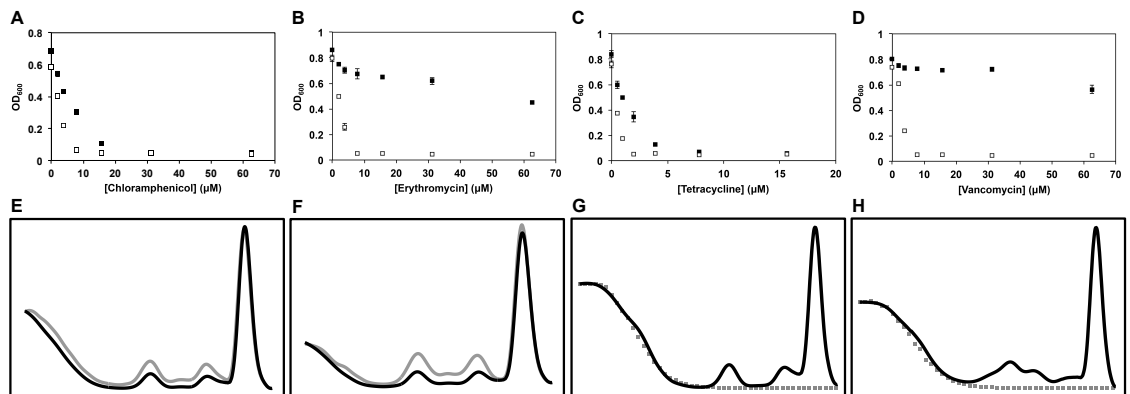


Figure 4

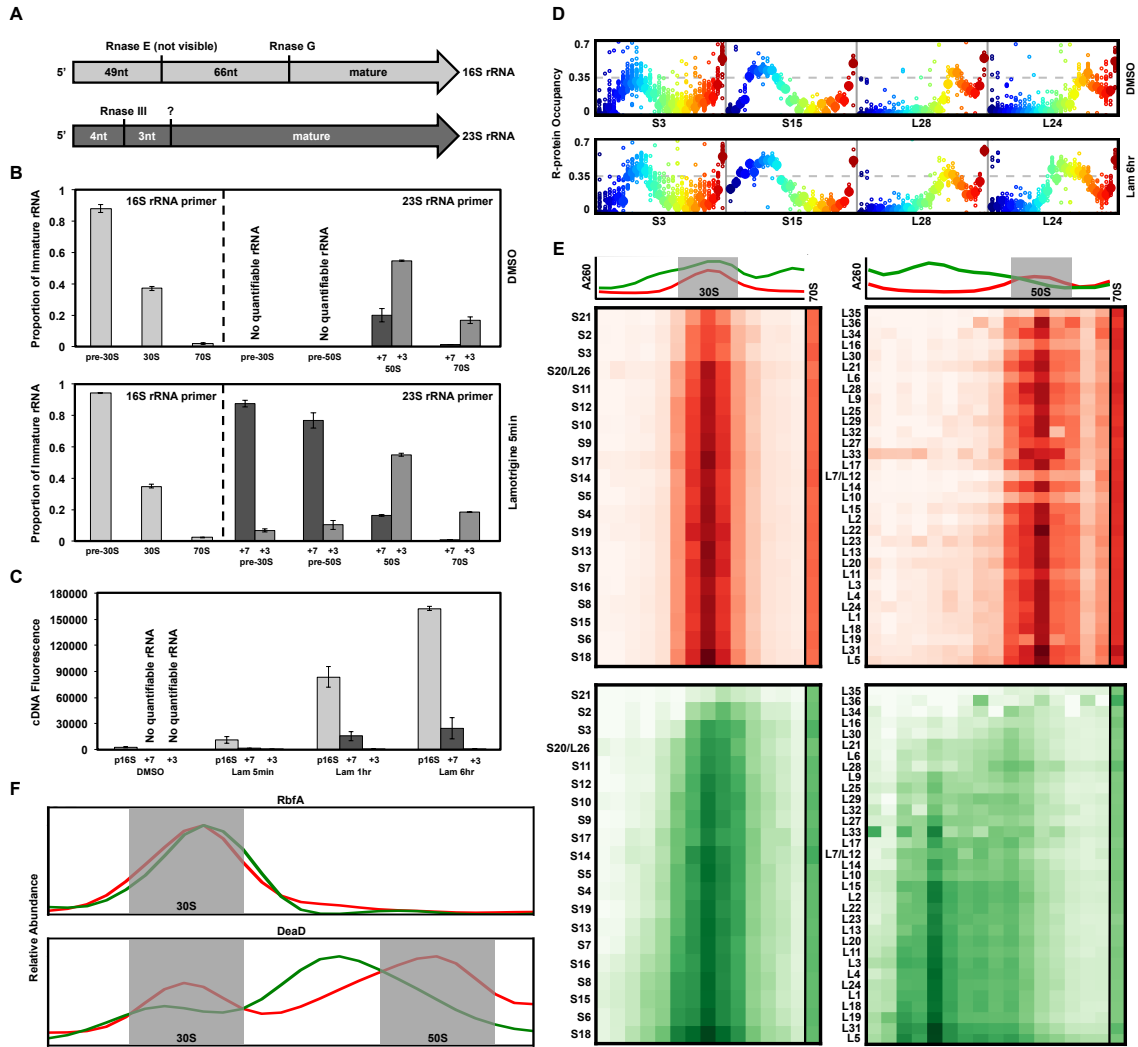


Figure 4 – figure supplement 1

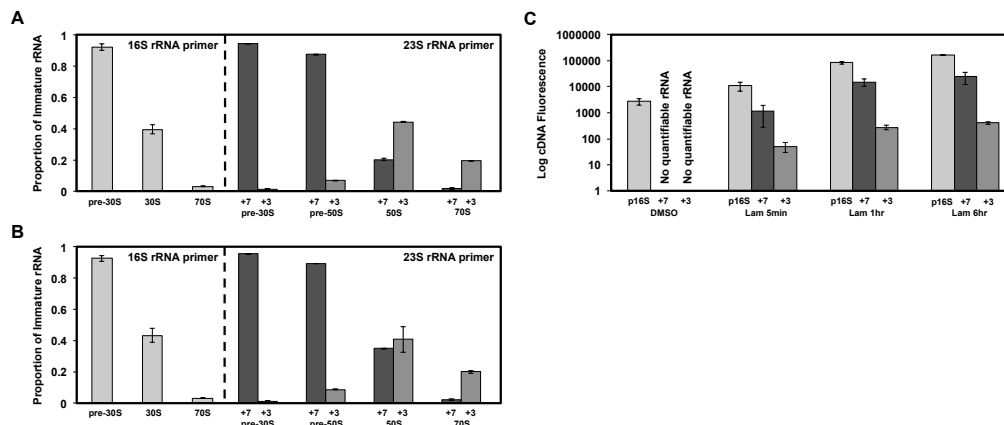


Figure 4 – figure supplement 2

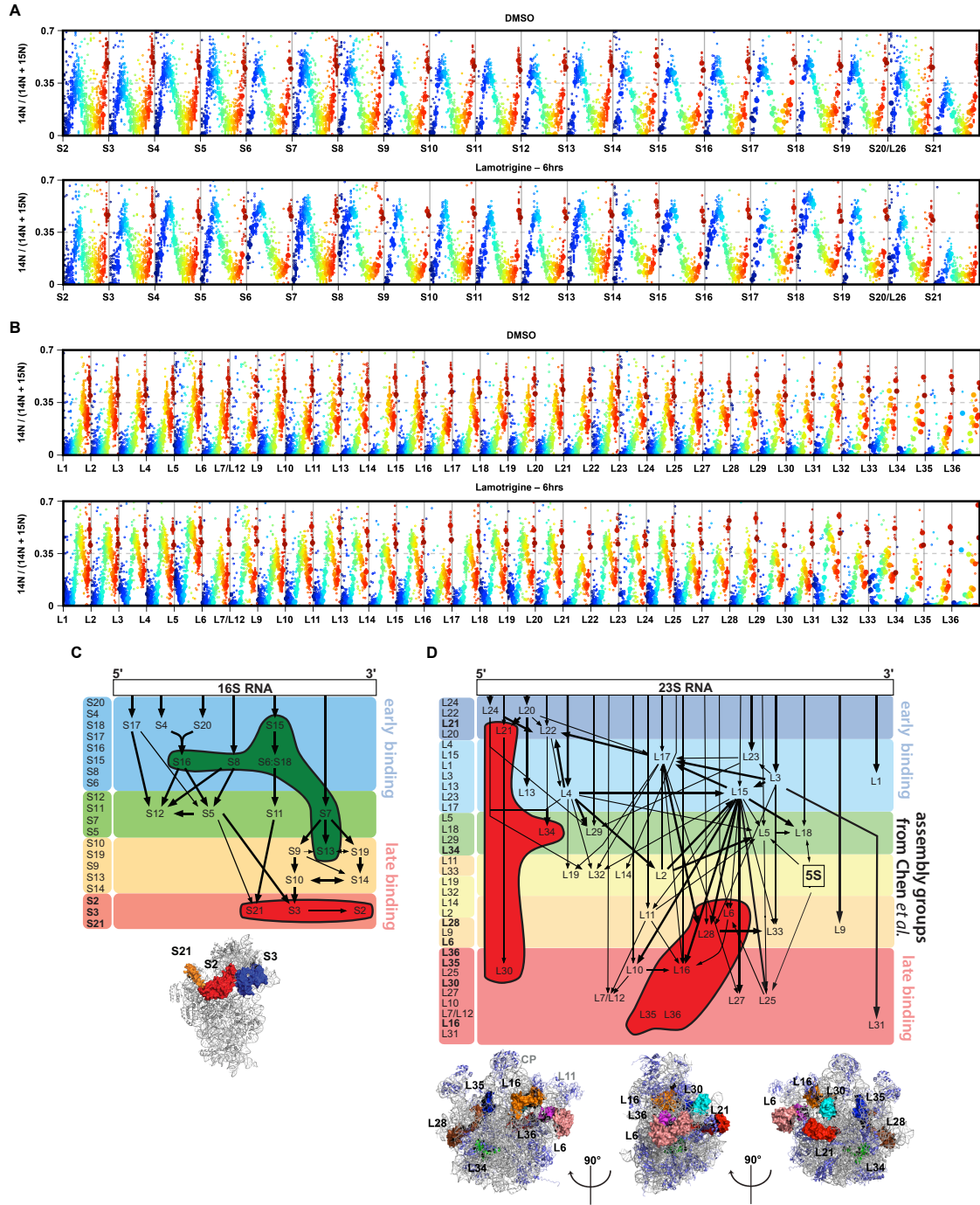


Figure 5

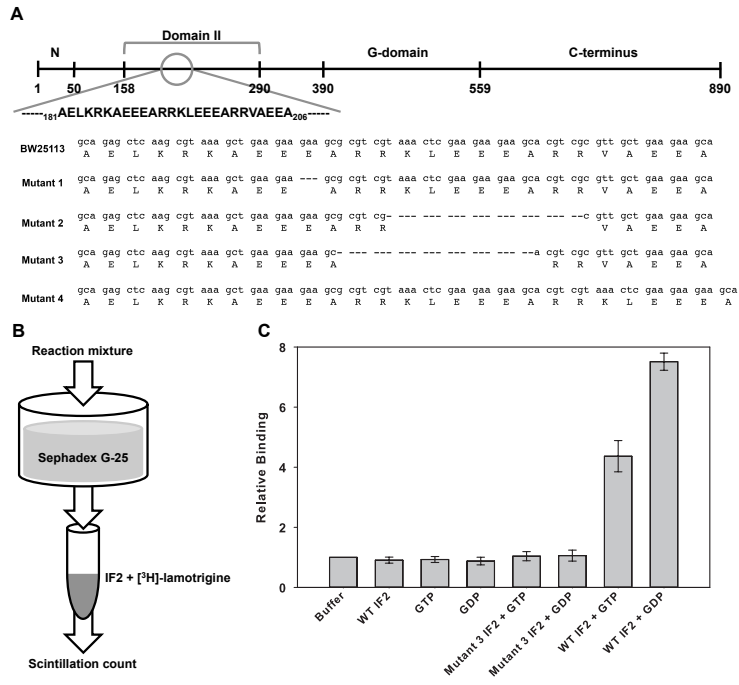


Figure 5 – figure supplement 1

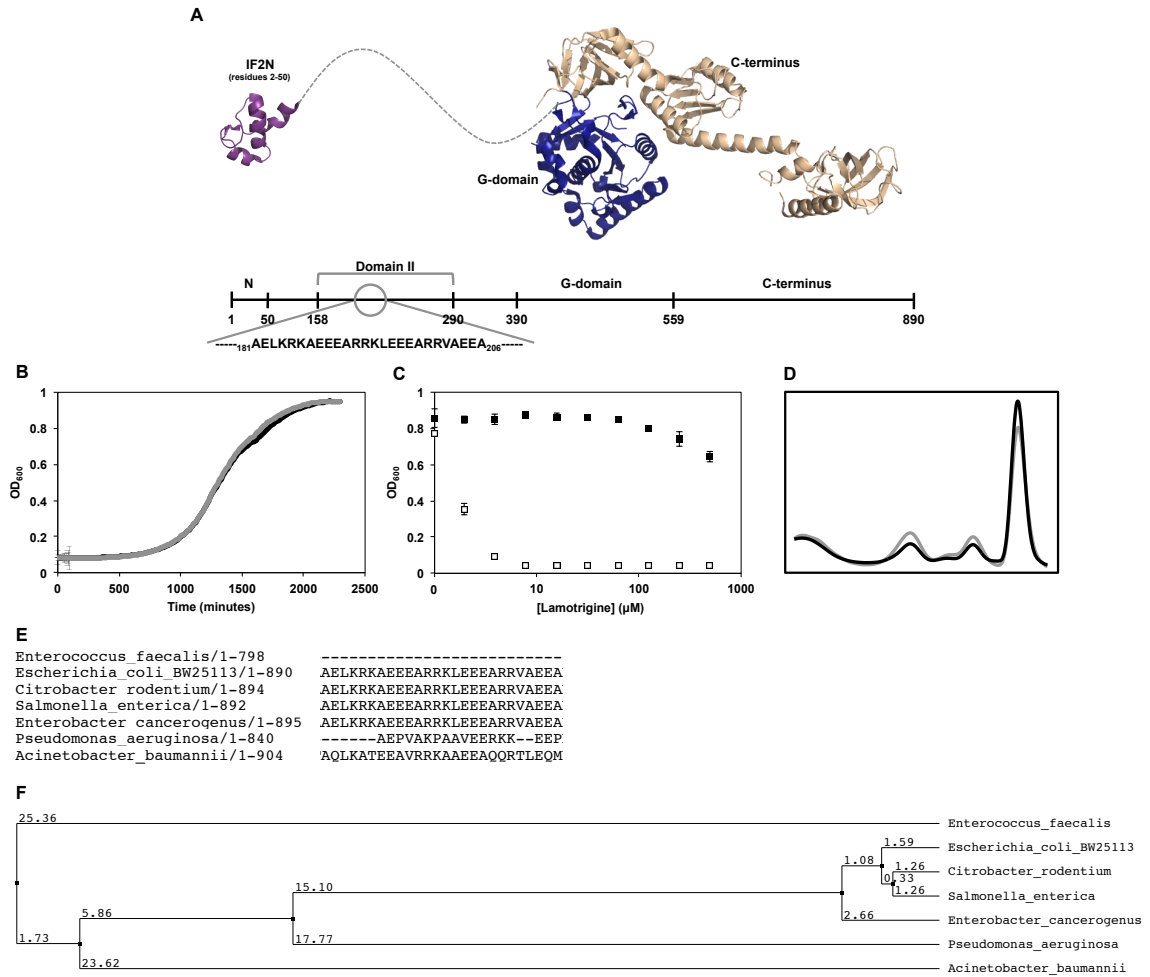


Figure 6

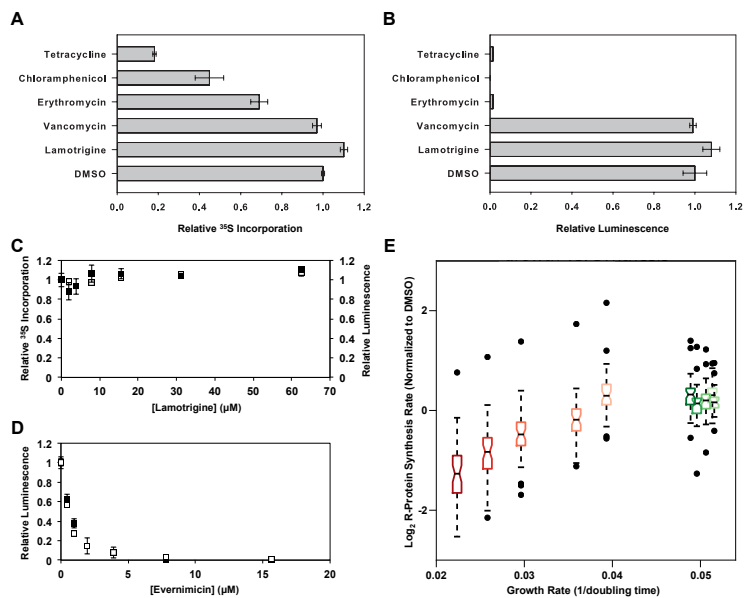


Figure 6 – figure supplement 1

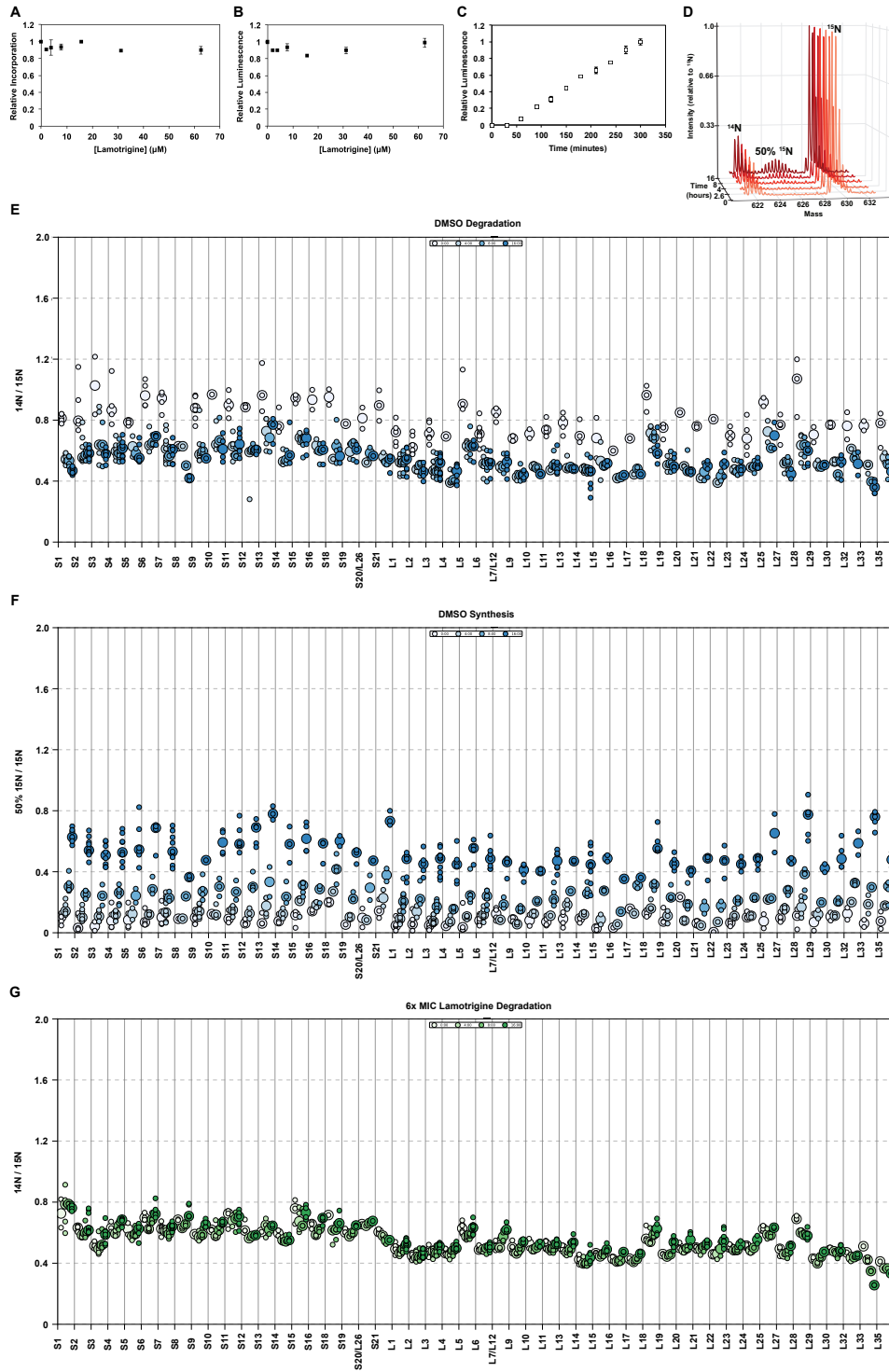


Figure 6 – figure supplement 1 continued

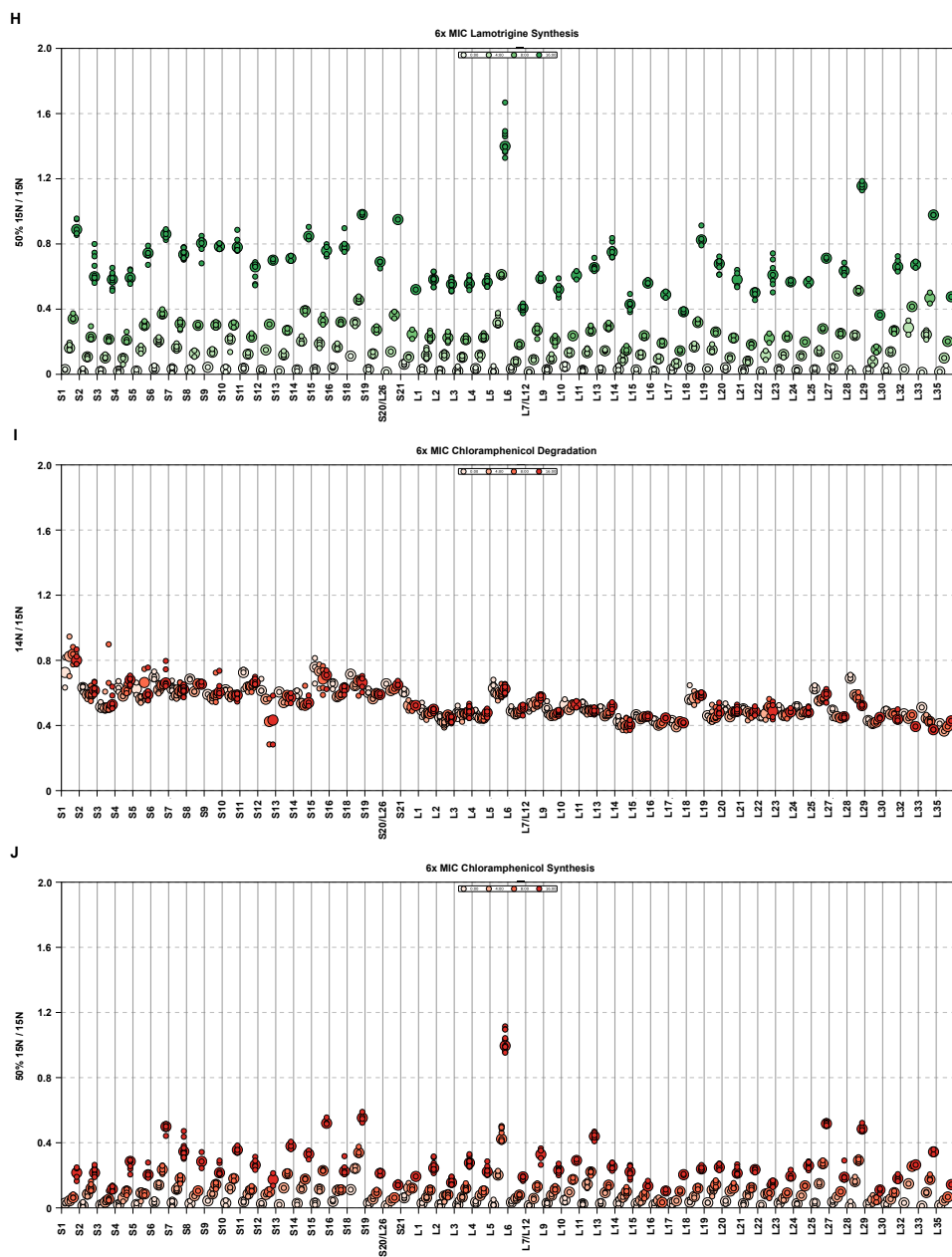
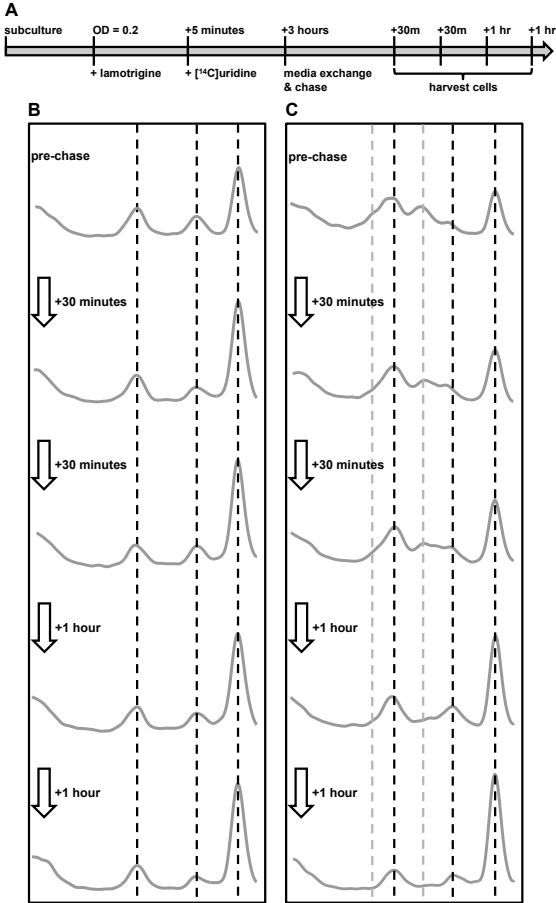


Figure 7



**CHAPTER III – Chemical modulators of ribosome biogenesis as biological
probes**

Preface

The concepts presented in this chapter were previously published in:

Stokes JM, Brown ED. Chemical modulators of ribosome biogenesis as biological probes. *Nature Chemical Biology* **11**, 924–932 (2015).

Permission has been granted by the publisher to reproduce the material herein.

I wrote and edited the manuscript with Brown, ED.

Abstract

Small molecule inhibitors of protein biosynthesis have been instrumental in dissecting the complexities of ribosome structure and function. Ribosome biogenesis, on the other hand, is a complex and largely enigmatic process for which there is a paucity of chemical probes. Indeed, ribosome biogenesis has been studied almost exclusively using genetic and biochemical approaches without the benefit of small molecule inhibitors of this process. Here, we provide a perspective on the promise of chemical inhibitors of ribosome assembly. We explore key obstacles that complicate the interpretation of studies aimed at perturbing ribosome biogenesis *in vivo* using genetic methods, and argue that chemical inhibitors are especially powerful because they can be used to induce perturbations in a manner that obviates these difficulties. Thus, in combination with leading-edge biochemical and structural methods, chemical probes offer unique advantages toward elucidating the molecular events that define the assembly of ribosomes.

Introduction

Ribosomes are ribonucleoprotein particles responsible for translating the nucleotide sequences of mRNA into proteins. These universally conserved machines are composed of two subunits. The small subunit (30S in bacteria and 40S in eukaryotes) is responsible for mediating base-pairing interactions between mRNA and tRNA, whereas the large subunit (50S in bacteria and 60S in

eukaryotes) contains the center responsible for catalyzing peptide bond formation between adjacent amino acids. Since the publication of the first atomic resolution structures in 2000¹⁻³, our understanding of the ribosome during the various stages of translation has advanced at an astonishing rate. Nevertheless, these structures have provided little insight into the events underlying the biogenesis of this massive complex.

Ribosome biogenesis is the process where ribosomal RNA (rRNA) transcripts and ribosomal proteins (r-proteins) are synthesized and assembled into functional ribosomes. Broadly, this process consists of (1) the coordinated transcription, modification, and folding of rRNA transcripts; (2) translation, modification, and folding of r-proteins; (3) binding of r-proteins to the appropriate rRNA scaffolds; and (4) binding and release of ribosome assembly factors⁴. *In vivo*, however, these events occur in parallel and represent a highly dynamic system of interrelated processes that occur cooperatively to narrow the assembly landscape of the ribosome⁵⁻⁸. While significant differences in this process are observed between bacteria and eukaryotes, i.e., eukaryotic ribosome biogenesis uniquely involves nuclear export⁹ and a pre-translational quality control checkpoint^{10,11}, the general principles underlying the process are evolutionarily conserved (Figure 1a,b).

Landmark investigations into ribosome biogenesis have employed simplified *in vitro* systems consisting of purified r-proteins and rRNA to understand the fundamental biochemical principles underlying assembly.

Nevertheless, a great deal of our knowledge of ribosome biogenesis *in vivo* has come from classical genetic approaches. Upwards of 60 ribosome biogenesis factors in bacteria and ~200 in yeast have been identified using such methods, and these factors have been variously leveraged to provide insights into a complex process that occurs on a timescale of minutes *in vivo*. Indeed, studies of ribosome assembly in cells are challenging because the assembly process is highly efficient and intermediates do not accumulate in significant amounts¹²⁻¹⁴. Genetic manipulation of ribosome assembly factors has been used to disable or slow down assembly and make it possible to isolate and characterize immature subunits that are the products of perturbation. Unclear, however, are the consequences of genetic perturbation and the nature of the isolated particles. In fact, the phenotypes associated with mutations in such factors can be wide ranging^{15,16} and often make it difficult to unambiguously assign a specific function in ribosome assembly. Further, immature subunits that are accumulated in such mutants at steady state may not be *bona fide* intermediates, but instead may represent aberrant products of a process gone awry.

In this context, we believe that small molecule inhibitors of ribosome biogenesis have particular advantages over genetic perturbation for understanding this process *in vivo*. Chemicals can exert their effects on a time scale of seconds, be added or removed from cell systems at will, and afford the opportunity to follow the impact of perturbation with kinetic resolution. As such they can be elegant probes of complex cellular systems and the macromolecules

that function therein¹⁷. Indeed, our understanding of protein translation has benefited enormously from the plethora of chemical probes that are available to study this process^{18,19}.

Herein, we aim to highlight the potential of small molecule inhibitors of ribosome biogenesis as probes of this complex process. We begin with a brief discussion of the techniques used to study ribosome biogenesis both *in vitro* and *in vivo*, with an emphasis on the genetic methods that have been employed to probe the molecular events therein. These methods are contrasted with small molecule approaches, where we describe, in particular, the thinking and difficulties to be considered. Lastly we explore possible molecular targets, as well as practical applications of ribosome biogenesis inhibitors.

The methods that shaped our understanding of ribosome biogenesis

The earliest studies into the composition of ribosomes occurred in the late 1950s, where investigators revealed that the bacterial 70S ribosome was a single species composed of two smaller, independent subunits that associated in a Mg^{2+} -dependent manner²⁰. Groundbreaking efforts into the study of the assembly of these macromolecules first came from Nomura and colleagues²¹⁻²³, who in the late 1960s began investigating the thermodynamic r-protein binding dependencies of the 30S subunit *in vitro* (Figure 2a – left panel). Starting with naked 16S rRNA and purified radiolabeled 30S subunit r-proteins, this group was able to elucidate the iconic 30S ribosomal subunit assembly map by

systematically monitoring which radiolabeled r-proteins were able to occupy small subunit particles containing various combinations of non-labeled r-proteins. Subsequent work^{24,25} used analogous approaches to reveal the considerably more complex r-protein binding dependencies of the 50S subunit (Figure 2a – right panel). Together, these investigations revealed that ribosome assembly occurred in a hierarchal manner, and that all of the information necessary for this process was contained in the rRNA and r-proteins themselves, without the necessity for exogenous factors.

These vintage studies were followed many years later by modern cell-free investigations, which have further advanced our understanding of the forces shaping rRNA/r-protein interactions during ribosomal subunit assembly (Figure 2b). Recent observations suggest that r-protein binding to rRNA drives folding and stabilizes local rRNA structure⁷, induces long-range conformational changes in rRNA²⁶, and creates new binding sites for subsequent r-proteins²⁷.

Furthermore, data also suggests that assembly occurs through multiple parallel pathways without significant rate-limiting steps²⁸, hinting at a process of remarkable complexity and redundancy that ensures proper assembly under even suboptimal conditions. These conclusions were reached through the use of leading-edge structural and biochemical methods capable of obtaining high-resolution kinetic data from simplified *in vitro* systems. For example, recent studies have made use of single-molecule fluorescence resonance energy transfer (FRET) to quantify real-time interactions between 30S subunit protein S4

and the 5' domain of 16S rRNA⁷, showing that local rRNA structure is affected by transient and stable r-protein encounters. Furthermore, millisecond time-scale x-ray footprinting techniques have been used to define how local rRNA/r-protein interactions affect global structures within the 30S subunit²⁶. These kinetic analyses were elaborated further using time-resolved cryo-EM to identify the structures of 14 distinct 30S subunit intermediates *in vitro*²⁸, suggesting that 30S subunit maturation progressed through multiple parallel pathways, largely without rate-limiting steps. This latter work agreed well with conclusions gathered using quantitative ESI-TOF mass spectrometry to monitor the association rates of individual r-proteins to purified 16S rRNA *in vitro*²⁷ and *in vivo*⁸.

In addition to charting the complex thermodynamic and kinetic constraints of r-protein binding and rRNA folding, these investigations also clearly exposed a need for additional factors during ribosome assembly *in vivo*. Experimental conditions necessary for ribosomal subunit assembly in cell-free systems are far from physiological, requiring inordinate durations, temperatures, and Mg²⁺ concentrations in order to progress⁴. Advances in identifying these accessory factors were made around the same time that the first *in vitro* 30S assembly map was initially being developed; it was then that the earliest links between stochastic mutagen-induced genetic mutations and aberrant ribosome biogenesis phenotypes were observed^{29,30}. Over the ensuing decades, investigators began to use more precise genetic and biochemical methods to identify and characterize protein factors necessary for the efficient assembly of ribosomes.

These efforts included the identification of enzymes responsible for separating and processing 16S, 23S, and 5S rRNA transcripts during ribosome biogenesis³¹⁻³⁵; investigators also found that many rRNA nucleotides and r-protein residues were modified during this process³⁶⁻⁴⁰, and came to understand how ribosomal precursor particles produced *in vivo* related to those observed during *in vitro* assembly of 30S and 50S subunits^{12,13,41}.

By the late-1980s, the first canonical ribosome assembly factors were being discovered and characterized. The 50S subunit assembly factor SrmB was arguably the prototype. Overexpression of SrmB rescued the growth of a temperature-sensitive lethal mutation in large subunit protein L24, and suggested a role for this protein in 50S subunit biogenesis⁴². Similar research⁴³ revealed that overexpression of the 30S subunit assembly factor RbfA in *E. coli* was able to suppress the cold sensitive growth phenotype associated with the C23U 16S rRNA point mutation, implying that this protein had a role late in 30S subunit assembly. This hypothesis was subsequently strengthened by showing that a deletion mutant of *rbfA* was cold sensitive, and accumulated free 30S and 50S subunits at the expense of 70S ribosomes. Furthermore, RbfA was found associated specifically with 30S subunits *in vivo*. Such cell-based investigations paved the way for efforts aimed at discovering new factors in ribosome biogenesis, and helped establish the principle that these accessory factors performed wide-ranging functions at various stages of ribosome assembly to increase the efficiency of this process beyond that observed in minimal cell-free

systems. Indeed, evidence to date suggests that accessory proteins involved in ribosome biogenesis include RNA processing enzymes, rRNA and r-protein modifying enzymes, rRNA chaperones/helicases, and in eukaryotes an array of proteins required for transport of pre-ribosomes from the nucleus to the cytoplasm. The functional breadth of accessory factors involved in ribosome biogenesis highlights the importance of efficient ribosome production *in vivo*.

The pitfalls of current *in vivo* methods

Since the mid-1990s, a large number of new ribosome assembly factors have been discovered (reviewed in ^{4,44-48}). Elucidating the functions of these assembly factors is a daunting goal that will be critical in understanding ribosome biogenesis in the context of the cell. The premise of using genetics to perturb ribosome biogenesis factors is that mutations in these proteins can disable or slow down assembly, making it possible to isolate and study immature subunits that are the products of perturbation (Figure 2c). An underlying assumption is that a non-native particle that accumulates in a specific mutant strain represents a *bona fide* intermediate, and that the aberrant product is a substrate for the missing assembly factor. However, the steady state nature of genetic perturbation is inherently ambiguous on this question. Particles that accumulate in genetically modified backgrounds may in fact be thermodynamically stable off-pathway products, or they might be derived from suppressor mutations that arise at high frequency in some genetic backgrounds. Further, these particles could be

the result of genetic pleiotropy, where a single mutation has multiple phenotypic effects. This pleiotropy may be at the level of ribosome biogenesis, such as the inhibition of multiple sequential steps within subunit assembly, or more broadly across wide-ranging aspects of cell biology.

Consider the history of the 30S bacterial ribosome assembly factor Era. In the early-1990s, Lerner and Inouye investigated the phenotypes associated with a temperature-sensitive mutant of *era* in *E. coli* and found that cells were impaired for the synthesis of heat shock proteins, the induction of ppGpp, and had increased capacity for carbon source metabolism through the TCA cycle¹⁵. Ensuing studies over almost a decade continued to associate wide-ranging functions to Era^{49,50}, until it was observed that Era bound to 16S rRNA and co-sedimented with 30S ribosomal subunits, leading to the hypothesis that this protein was a translation factor⁵¹. Subsequent work suggested that Era was not a translation factor, but a 30S subunit assembly factor, because its depletion resulted in the accumulation of immature 16S rRNA. Further, Era overexpression partially alleviated the cold sensitive phenotype associated with deleting the 30S ribosome assembly factor RbfA, and Era was able to bind the 30S subunit⁵². More recently, a cryo-EM co-structure of Era with the mature 30S subunit has led to the hypothesis that Era functions late in 30S subunit biogenesis, and may inhibit the premature formation of translation initiation complexes⁵³.

Pleiotropic phenotypes are exceptionally confounding to studies of ribosome assembly factors (Figure 3a). In particular, ribosome biogenesis and

protein translation are processes that are inextricably linked and difficult to differentiate *in vivo*. Consider a ribosome assembly factor such as RsgA (YjeQ), which results in cold sensitivity⁵⁴ and the accumulation of immature ribosomal subunits when deleted⁵⁵⁻⁵⁷. These phenotypes are not unique to perturbations in ribosome biogenesis machinery. Indeed, numerous investigations have revealed that treatment of *E. coli* with translation inhibiting antibiotics results in phenotypes that are nearly identical to mutations in ribosome assembly factors^{54,58-60}. This is because inhibition of protein translation causes sub-stoichiometric production of r-proteins relative to rRNA, resulting in the accumulation of non-native ribosomal subunits that are unable to mature until the antibiotic stress is removed. Recently, an elegant study by Siibak *et al.* explored the relationship between r-protein occupancy on immature ribosomal subunits and r-protein production during stress under chloramphenicol and erythromycin treatment⁶⁰. By growing *E. coli* in the presence of chloramphenicol or erythromycin and subjecting purified ribosomal particles to quantitative mass spectrometry, the investigators were able to reveal a positive correlation between r-protein occupancy on immature subunits and total synthesis of each r-protein, thereby providing strong evidence that decreased synthesis of a subset of r-proteins was responsible for the apparent inhibition of ribosome biogenesis.

Another example of the close relationship between ribosome biogenesis and translation can be seen in the controversial hypothesis that many classes of translation inhibitors inhibit both protein biosynthesis and ribosome biogenesis

directly^{59,61-64}. Two exhaustive reviews have previously provided detailed descriptions of this notion, including the specific ribosome biogenesis phenotypes associated with various classes of translation inhibitors, as well as extensive descriptions of radiolabeled rRNA pulse-chase experiments that have been employed to monitor the approximate rates of subunit synthesis under these stressors^{48,65}. Briefly, while it remains contentious, this theory was supported by the coincidence of translation inhibition *in vivo* with numerous ribosome biogenesis phenotypes. Additionally, radiolabeled erythromycin had been shown to co-sediment with immature 50S subunits during sucrose density centrifugation⁵⁹, providing biochemical support for this hypothesis. Nevertheless, the comprehensive mass spectrometry experiments described above provide compelling evidence that the coincidence of ribosome biogenesis and translation phenotypes during treatment with these antibiotics is the result of pleiotropy associated with translation inhibition. So too are data showing that both 30S and 50S subunits are inhibited for maturation on treatment with erythromycin or chloramphenicol, and that the expression of a macrolide resistance peptide that functions exclusively on mature ribosomes can rescue erythromycin-induced assembly defects⁵⁸.

It is humbling to consider that our understanding of the functions of ribosome assembly factors *in vivo* may be hazy at best. We believe that this is because investigations to date have largely been limited to analyzing ribosomal particles harvested using steady state methods, providing little or no temporal

data that could account for how a specific perturbation led to the accumulation of a non-native particle over time (Figure 3b). Indeed, clean deletions of ribosome biogenesis factors lack temporal resolution altogether, and chemically inducible or temperature-sensitive conditional alleles are plagued by slow protein accumulation/diminution rates that can obscure the interpretation of observed phenotypes *in vivo*. Because of the rapid assembly rates of ribosomes in cells, we require methods to kinetically monitor a cell's response immediately after perturbation of ribosome biogenesis with high temporal precision. Whole cell-active small molecule inhibitors of ribosome assembly, we believe, are uniquely suited to this kinetic approach.

The discovery and characterization of a specific inhibitor of bacterial ribosome biogenesis

Small molecules have been enormously beneficial as probes of almost all aspects of cell biology, and have provided a wealth of data that has greatly improved our understanding of biological complexity¹⁷. Studies of the function of the assembled ribosome, in particular, have been enabled by a surfeit of small molecule inhibitors of this cellular machine^{18,19}. As elegant probes of macromolecular function, these compounds have captured ribosomes in numerous conformational states, moving us closer to a complete understanding of protein translation. Thus, while small molecules have offered precise tools to carefully dissect the translationally competent ribosome, studies of ribosome

biogenesis *in vivo* have been mainly limited to classical genetic methods as a means of perturbation.

Optimally growing *E. coli* assembles ribosomal subunits in ~2 minutes¹², and at any given time there are on the order of 10^3 ribosomes at various stages of maturation (~5% of ~70,000 ribosomes^{12,66}). To better understand the molecular events during ribosome biogenesis, ideally we would follow the assembly of ribosomal subunits as a function of time, and give specific timestamps to all of the events during maturation, including rRNA processing, binding of r-proteins, binding and release of ribosome assembly factors, rRNA remodeling, and so on. This would allow for a global kinetic understanding of ribosome biogenesis. As discussed above, recent studies using leading-edge biochemical and structural methods have illuminated the precise kinetics of r-protein binding to rRNA scaffolds both *in vitro* and *in vivo*^{7,8,26-28,67,68}. However, while these investigations have been instrumental in defining the kinetic parameters of rRNA/r-protein interactions, they fall short in elucidating the roles that ribosome assembly factors play in this process.

Small molecules are uniquely suited to elucidating the molecular details and kinetic timestamps for these events because of the ability to monitor the system immediately after their introduction to cells, and with high temporal precision thereafter (Figure 4). Indeed, the high rate of subunit assembly *in vivo* limits the usefulness of conditional alleles and gene deletions in probing the process. This thinking drove our group to search for specific inhibitors of

ribosome assembly⁵⁴. Since mutations in many canonical ribosome assembly factors display cold sensitivity, we screened a diverse chemical collection that included previously approved drugs for compounds that induced cold sensitive growth inhibition in *E. coli*. Indeed, cold temperatures are hypothesized to capture thermodynamically stable, yet non-functional rRNA conformations⁶⁹, thereby challenging numerous steps in the assembly process and making essential the factors that promote these events under sub-optimal conditions. After screening a collection of ~30,000 small molecules, we identified 49 compounds that inhibited growth, and were enhanced in this phenotype at low temperature. Interestingly, a well-characterized anticonvulsant drug, lamotrigine, was among the most potent inducers of cold sensitive growth in *E. coli*. To understand the effect of this compound on ribosome assembly, ribosomes from lamotrigine-treated cells were analyzed using a myriad of approaches after growth for ~1% of a doubling, ~15% of a doubling, and after one complete doubling. These investigations, which would not have been possible using genetic approaches, revealed that immediately after drug treatment (~1% of a doubling), cells began accumulating two distinct particles, an immature 30S subunit that sedimented at ~25S and an immature 50S subunit that sedimented at ~40S.

Surprisingly, spontaneous mutations suppressing growth inhibition by lamotrigine at low temperature mapped to the gene encoding translation initiation factor IF2. These and further biochemical experiments suggested that IF2 was the target of lamotrigine (Table 1), and raised the possibility that this compound

might have a secondary effect on ribosome assembly by inhibiting protein translation. Indeed, it was necessary to determine if the ribosome assembly defects we observed were simply due to substoichiometric production of r-proteins^{58,60}. Thus we monitored the rates of production of all r-proteins, as well as the growth rate, of *E. coli* cells treated with either lamotrigine or the control compound chloramphenicol over one doubling time. The hypothesis was this: within this timeframe, increasing concentrations of chloramphenicol should proportionately decrease r-protein translation and growth rate. However, if lamotrigine was inhibiting ribosome biogenesis directly, increasing concentrations of lamotrigine should not have an immediate impact on r-protein production or growth rate, since exponentially growing *E. coli* has a large pool of functional ribosomes⁶⁶ that can sustain protein production within one doubling. Indeed, our results confirmed this hypothesis, consistent with the conclusion that lamotrigine inhibited a hitherto unrecognized function of IF2⁷⁰ in ribosome assembly.

Developing ribosome biogenesis inhibitors of diverse function

Our studies of the action of lamotrigine on bacterial ribosome assembly shed light on the utility of small molecules as probes of this process. Chemicals facilitate perturbation with precise temporal resolution, which is essential to dissect the tightly linked processes of assembly, translation, and, more generally, to avoid pleiotropy that follows the inhibition of ribosome assembly in cells. In this way, chemical inhibitors of ribosome biogenesis have particular utility in the

discovery of new factors and in understanding the complexity of the process as a whole. Importantly, the target specificity of ribosome biogenesis inhibitors will be key to avoid confounding pleiotropy and allow for the generation of meaningful conclusions regarding ribosome biogenesis factor function⁷¹. Furthermore, we envision additional applications as a means to purify low-abundance ribosomal particles. In all, we believe that the field is now ripe for a concerted effort in identifying and characterizing functionally diverse and target-specific chemical inhibitors of ribosome biogenesis. Such compounds will have great utility as probes and ultimately may have potential as leads for therapeutic applications.

Currently, however, a paucity of chemical probes of ribosome biogenesis is known and, apart from lamotrigine, these are active in eukaryotes (Table 1). Diazaborine for example, is a well-characterized inhibitor of the AAA-ATPase Drg1 in yeast⁷²⁻⁷⁴ (Figure 1a). Drg1 is the first ribosome biogenesis factor to function during cytoplasmic maturation of the 60S subunit. During this stage of assembly, Drg1 is recruited and activated by Rlp24, a paralog of large subunit protein L24⁷⁵. Upon activation, Drg1 removes Rlp24 from the assembling 60S subunit, as well as the assembly factors Nog1 and Bud20, thereby allowing binding of L24. Binding of L24 subsequently permits the recruitment of Rei1, and the progression of 60S subunit assembly⁷⁶. Inhibition of ATP hydrolysis in the D2 domain of Drg1 by diazaborine prevents the release of Rlp24 from pre-60S particles, blocking the further cytoplasmic maturation events of the 60S subunit.

In addition to diazaborine, CX-5461 is an antineoplastic agent that prevents RNA polymerase I pre-initiation complex formation by inhibiting the binding of the transcription initiation factor SL1 to rDNA promoters^{77,78}. This results in decreased production of 47S pre-rRNA transcripts, and subsequent r-protein/Mdm2/p53-mediated cell cycle arrest⁷⁹. Similarly, CX-3543 is a fluoroquinolone derivative that specifically disrupts nucleolin/rDNA G-quadruplex complexes in the nucleolus of mammalian cells, preventing RNA polymerase I transcription through rDNA operons, and leading to apoptosis⁸⁰. To date, neither CX-5461 nor CX-3543 have been reported to show activity in yeast, though the model eukaryote is surely susceptible to such perturbation. Indeed, among the three RNA polymerases in yeast, RNA polymerase I is the most active, being solely responsible for transcribing the pre-rRNA containing 18S, 5.8S, and 25S rRNAs, which accounts for ~60% of total cellular transcription⁴⁶. The development of specific inhibitors of rRNA biosynthesis in yeast may allow for a detailed temporal understanding of the earliest events during 40S and 60S subunit assembly at the level of co-transcriptional assembly. Furthermore, this approach may assist in revealing currently undiscovered factors that are necessary for early events during eukaryotic ribosome biogenesis.

With so few inhibitors available to probe ribosome biogenesis, and given the large number of targets available, the potential for probe discovery is high where capable assays can be developed. For instance, identifying inhibitors of rRNA processing might be accomplished through direct inhibition of the

processing enzymes themselves, or through RNA interference (RNAi). For the former, *in vitro* biochemical screens could be developed to identify compounds that inhibit rRNA cleavage. One caveat to this approach is that cell-free biochemical approaches rarely yield compounds that are permeable to cells⁸¹. Therefore, chemical optimization of promising hit compounds will be an important component of the workflow in order to achieve whole cell activity. Intriguingly, previous investigations have shown that the non-specific RNase inhibitor ribonucleoside vanadyl complex prevents ribosomal subunit maturation in *Staphylococcus aureus*⁸² and *E. coli*⁸³, potentially offering a foundation on which to develop specific inhibitors rRNA maturation to target ribosome biogenesis exclusively. Additionally, an *in vivo* screening approach may involve identifying compounds that potentiate the activity of macrolides, due to the increased sensitivity of ribosomal RNase-deficient *E. coli* strains to these antibiotics⁸⁴. An RNAi strategy, on the other hand, might involve the design of oligonucleotide sequences complementary to regions of rRNA that undergo cleavage during ribosome biogenesis, or to those that form regions essential for r-protein binding and subsequent rRNA folding events⁸⁵. Interestingly, a peptide nucleic acid has previously been described that targets domain II of 23S rRNA, inhibits translation *in vitro* and prevents the growth of *E. coli*⁸⁶. Thus, whole cell-active RNAi probes may have promise in elucidating the molecular details of rRNA cleavage and the recognition of rRNA scaffolds by r-proteins.

Related to this approach, screens for small molecule inhibitors of rRNA/r-protein interactions and rRNA folding have potential. For instance, an *in vitro* three-fluorophore FRET system to monitor the association of 30S subunit protein S15 to 16S rRNA has previously been used to identify perturbants of the folding of a three-way junction that forms early during 30S subunit assembly⁸⁷. Similar FRET-based assays could presumably be developed for any combination of interacting rRNA/r-protein pairs. One well-characterized rRNA/r-protein interaction that has recently been described is that involving the 30S subunit protein S4 and the 5' domain of 16S rRNA⁷. Furthermore, where detailed structural and biochemical data are available for the S4/16S interaction, it may be feasible in this instance to leverage structure-based drug design to help identify whole cell-active molecules inhibiting this event.

Lastly, and perhaps most obvious in the context of this perspective piece, identifying compounds active against canonical ribosome assembly factors can be accomplished *in vitro* by screening compound libraries against the purified protein. A pilot screen of some 30,000 diverse compounds, for example, was carried out for the essential 50S biogenesis factor and GTPase EngA⁸⁸. Similar screening methods could be used for the many ribosome assembly factors that hydrolyze GTP or ATP. Additionally, as we have shown, many of such factors, both essential and non-essential, are susceptible in phenotypic screens to cold sensitive growth inhibition^{54,89}.

Inhibition of the aforementioned processes would cover many events in ribosome biogenesis that are common to both eukaryotic bacterial organisms. However, one event that is unique to eukaryotic cells is nuclear export of pre-40S and pre-60S subunits. Indeed, the partitioning of eukaryotic cells by a nuclear membrane ensures that immature ribosomal subunits do not interact with the translating pool of ribosomes, and that those exported to the cytoplasm are ready for the final stages of maturation⁹. This is a complex and carefully choreographed process that has yet to be completely dissected, and the development of small molecule perturbants of this event could be exceptionally useful. Interestingly, a microscopy-based technique to monitor pre-60S subunit export from the nucleus has previously been developed to analyze genetic mutants deficient in this process⁹⁰. In that work, eukaryotic green fluorescent protein (eGFP) was fused to the yeast large subunit protein Rpl25p, which is present on nuclear pre-60S subunits, and export defects were studied by fluorescence microscopy. In a similar manner, it may be possible to conduct a microscopy-based screen for chemicals that prevent nuclear export of eGFP-labeled pre-ribosomes in yeast. While inhibitors of early pre-40S and pre-60S biogenesis would also prevent export, secondary screens could be conducted to identify molecules that were specific inhibitors of export. Since the protein content of pre-ribosomal particles has largely been characterized^{9,46,90,91}, this could be done, for example, through mass spectrometry of purified pre-40S or pre-60S particles of chemical-treated cells, with the hypothesis that compounds preventing nuclear export, but not

protein addition to immature subunits, may be specific inhibitors of the nuclear export machinery.

Quality control checkpoints are emerging as important processes in the assembly of ribosomes in both bacteria and eukaryotes, and these too could be probed with small molecules. For instance, in both kingdoms, ribosome biogenesis factors prevent the premature binding of r-proteins to immature subunits, as well as inhibit premature association of subunits with mRNA and tRNA⁹². Furthermore, in yeast it has been shown that 40S subunits undergo an eIF5B-mediated pre-translation quality control checkpoint, where pre-40S subunits initiate a translation-like cycle with mature 60S subunits prior to final maturation and entry into the translating pool¹¹. Small molecules that prevent this eIF5B-dependent pre-translation checkpoint might be discovered by looking for inhibition of GTP hydrolysis by eIF5B *in vitro*, or through analyzing pre-40S particles for the presence of the biogenesis factor Rio2 *in vivo*, which dissociates immediately following eIF5B-mediated 60S subunit joining^{10,11}. Interestingly, identifying inhibitors of the eukaryotic pre-translation checkpoint may aid in identifying a similar process in bacteria, which has yet to be observed.

Another universal method of ribosome quality control involves degradation of those subunits that fail to properly mature⁹²⁻⁹⁵. The identification of compounds that inhibit ribosome degradation could provide additional tools to dissect the mechanisms underlying ribosomal subunit mis-assembly, which remain largely elusive. In bacteria, for example, the ribonucleases YbeY, RNase R, and

polynucleotide phosphorylase have been shown to play important roles in this process^{93,94}. Inhibitors of these enzymes could be identified using *in vitro* biochemical assays of rRNA processing. Alternatively, one can envision whole cell screens using idiosyncratic mutants. For example, inhibitors of YbeY should show enhanced potency in an RNase R knockout strain relative to wild type, as previous investigations have shown that the *E. coli* double mutant $\Delta ybeY\Delta rnr$ shows synthetic lethality⁹⁶.

Indeed, while not exhaustive, these examples highlight the many opportunities to probe the molecular events underlying ribosome biogenesis using chemicals. In addition, we see unique prospects for the discovery of novel ribosome assembly factors and the purification of immature ribosomal subunits. Indeed, having established a cryptic role for IF2 in bacterial ribosome biogenesis with the chemical probe lamotrigine, we note that this function had previously eluded detection. Elucidating a role for this protein in ribosome assembly would have been extremely difficult using conventional approaches due to its known role in translation. Further exploration into the discovery and characterization of small molecule inhibitors of ribosome biogenesis is likely to identify compounds that inhibit unexplored factors. Furthermore, compounds that inhibit ribosome biogenesis factors may also be suited for development as affinity tags to purify low-abundance ribosomal particles from wild type cells, thereby obviating the need for mutants in this process. Current methods to purify immature ribosomal subunits have relied on genetic mutants, or on the incorporation of streptavidin

binding tags into 16S⁹⁷ or 23S⁹⁸ rRNA, as well as TAP tags to ribosome-associated proteins⁹⁹ which may alter the assembly of the 30S and 50S subunit, respectively. The use of a small molecule affinity tag to purify low abundance intermediates from wild type cells would be arguably less perturbing to the process, and may facilitate the purification of native particles for subsequent study.

While we have emphasized the utility of chemical inhibitors of ribosome biogenesis as probes to understand this complex process, also important is the therapeutic potential of such compounds. Small molecule inhibitors of ribosome biogenesis factors may prove to be exciting leads in the development of an entirely novel mechanistic class of antibiotics¹⁰⁰. Further, inhibitors of eukaryotic ribosome biogenesis have potential for the treatment of diverse hyperproliferative disorders. For instance, while current cancer-therapeutic discovery efforts involving ribosome biogenesis are focused on targeting rRNA transcription, the development of non-transcription factor-based compounds that directly inhibit ribosome assembly factors may provide an alternate route in the treatment of various malignancies. Indeed, recent evidence shows that inhibitors of casein kinase 1 δ/ϵ (Hrr25 in yeast), which is implicated in 40S subunit biogenesis, have promise in numerous preclinical animal models for cancer¹⁰¹. Therefore, while inhibitors of ribosome biogenesis will serve to enhance our understanding of this complex process in the context of the cell, these molecules may also have important therapeutic value for a wide array of diseases.

Concluding remarks

A half-century of research into ribosome biogenesis has given us a general understanding of the principles governing this immensely complex process, but the molecular details remain elusive due to a lack of probes suitable for insightful perturbation. Thus, we suggest that an intensive effort in identifying new chemical inhibitors of ribosome biogenesis is in order. Chemical probes are likely to play a crucial role, along with systems, biochemical, and structural methods, to more thoroughly understand the molecular details of ribosome biogenesis.

Acknowledgements

This work was supported by the Natural Sciences and Engineering Research Council (Discovery Grant to E.D.B.), by a salary award to E.D.B. from the Canada Research Chairs program, and by scholarships awarded to J.M.S. from the Canadian Institutes of Health Research and the Ontario Graduate Scholarships program.

References

1. Ban, N., Nissen, P., Hansen, J., Moore, P. B. & Steitz, T. A. The complete atomic structure of the large ribosomal subunit at 2.4 Å resolution. *Science* **289**, 905–920 (2000).
2. Wimberly, B. T. *et al.* Structure of the 30S ribosomal subunit. *Nature* **407**, 327–339 (2000).

3. Yusupov, M. M. *et al.* Crystal structure of the ribosome at 5.5 Å resolution. *Science* **292**, 883–896 (2001).
4. Shajani, Z., Sykes, M. T. & Williamson, J. R. Assembly of bacterial ribosomes. *Annu. Rev. Biochem.* **80**, 501–526 (2011).
5. Holmes, K. L. & Culver, G. M. Analysis of conformational changes in 16S rRNA during the course of 30S subunit assembly. *J. Mol. Biol.* **354**, 340–357 (2005).
6. Williamson, J. R. Assembly of the 30S ribosomal subunit. *Q. Rev. Biophys.* **38**, 397–403 (2005).
7. Kim, H. *et al.* Protein-guided RNA dynamics during early ribosome assembly. *Nature* **506**, 334–338 (2014).
8. Bunner, A. E., Beck, A. H. & Williamson, J. R. Kinetic cooperativity in *Escherichia coli* 30S ribosomal subunit reconstitution reveals additional complexity in the assembly landscape. *Proc. Natl. Acad. Sci. U.S.A.* **107**, 5417–5422 (2010).
9. Johnson, A. W., Lund, E. & Dahlberg, J. Nuclear export of ribosomal subunits. *Trends Biochem. Sci.* **27**, 580–585 (2002).
10. Strunk, B. S. *et al.* Ribosome assembly factors prevent premature translation initiation by 40S assembly intermediates. *Science* **333**, 1449–1453 (2011).
11. Strunk, B. S., Novak, M. N., Young, C. L. & Karbstein, K. A translation-like cycle is a quality control checkpoint for maturing 40S ribosome subunits. *Cell* **150**, 111–121 (2012).
12. Lindahl, L. Intermediates and time kinetics of the in vivo assembly of *Escherichia coli* ribosomes. *J. Mol. Biol.* **92**, 15–37 (1975).
13. Lindahl, L. Two new ribosomal precursor particles in *E. coli*. *Nat. New Biol.* **243**, 170–172 (1973).
14. Sykes, M. T., Shajani, Z., Sperling, E., Beck, A. H. & Williamson, J. R. Quantitative proteomic analysis of ribosome assembly and turnover in vivo. *J. Mol. Biol.* **403**, 331–345 (2010).
15. Lerner, C. G. & Inouye, M. Pleiotropic changes resulting from depletion of

- Era, an essential GTP-binding protein in *Escherichia coli*. *Mol. Microbiol.* **5**, 951–957 (1991).
16. Armistead, J. & Triggs-Raine, B. Diverse diseases from a ubiquitous process: the ribosomopathy paradox. *FEBS Lett.* **588**, 1491–1500 (2014).
 17. Falconer, S. B., Czarny, T. L. & Brown, E. D. Antibiotics as probes of biological complexity. *Nat. Chem. Biol.* **7**, 415–423 (2011).
 18. Wilson, D. N. The A-Z of bacterial translation inhibitors. *Crit. Rev. Biochem. Mol. Biol.* **44**, 393–433 (2009).
 19. Wilson, D. N. Ribosome-targeting antibiotics and mechanisms of bacterial resistance. *Nat. Rev. Microbiol.* **12**, 35–48 (2014).
 20. Tissieres, A. & Watson, J. D. Ribonucleoprotein particles from *Escherichia coli*. *Nature* **182**, 778–780 (1958).
 21. Hosokawa, K., Fujimura, R. K. & Nomura, M. Reconstitution of functionally active ribosomes from inactive subparticles and proteins. *Proc. Natl. Acad. Sci. U.S.A.* **55**, 198–204 (1966).
 22. Traub, P. & Nomura, M. Structure and function of *Escherichia coli* ribosomes. *J. Mol. Biol.* **40**, 391–413 (1969).
 23. Mizushima, S. & Nomura, M. Assembly mapping of 30S ribosomal proteins from *E. coli*. *Nature* **226**, 1214 (1970).
 24. Nierhaus, K. H. & Dohme, F. Total reconstitution of functionally active 50S ribosomal subunits from *Escherichia coli*. *Proc. Natl. Acad. Sci. U.S.A.* **71**, 4713–4717 (1974).
 25. Röhl, R. & Nierhaus, K. H. Assembly map of the large subunit (50S) of *Escherichia coli* ribosomes. *Proc. Natl. Acad. Sci. U.S.A.* **79**, 729–733 (1982).
 26. Adilakshmi, T., Bellur, D. L. & Woodson, S. A. Concurrent nucleation of 16S folding and induced fit in 30S ribosome assembly. *Nature* **455**, 1268–1272 (2008).
 27. Bunner, A. E., Trauger, S. A., Siuzdak, G. & Williamson, J. R. Quantitative ESI-TOF analysis of macromolecular assembly kinetics. *Anal. Chem.* **80**, 9379–9386 (2008).

28. Mulder, A. M. *et al.* Visualizing ribosome biogenesis: parallel assembly pathways for the 30S ubunit. *Science* **330**, 673–677 (2010).
29. Tai, P. C., Kessler, D. P. & Ingraham, J. Cold-sensitive mutations in *Salmonella typhimurium* which affect ribosome synthesis. *J. Bacteriol.* **97**, 1298–1304 (1969).
30. MacDonald, R. E., Turnock, G. & Forchhammer, J. The synthesis and function of ribosomes in a new mutant of *Escherichia coli*. *Proc. Natl. Acad. Sci. U.S.A.* **57**, 141–147 (1967).
31. Nikolaev, N., Silengo, L. & Schlessinger, D. A role for ribonuclease III in processing of ribosomal ribonucleic acid and messenger ribonucleic acid precursors in *Escherichia coli*. *J. Biol. Chem.* **248**, 7967–7969 (1973).
32. Ginsburg, D. & Steitz, J. A. The 30 S ribosomal precursor RNA from *Escherichia coli*. A primary transcript containing 23 S, 16 S, and 5 S sequences. *J. Biol. Chem.* **250**, 5647–5654 (1975).
33. Sirdeshmukh, R. & Schlessinger, D. Ordered processing of *Escherichia coli* 23S rRNA in vitro. *Nucleic Acids Res.* **13**, 5041–5054 (1985).
34. Ghora, B. K. & Apirion, D. Identification of a novel RNA molecule in a new RNA processing mutant of *Escherichia coli* which contains 5 S rRNA sequences. *J. Biol. Chem.* **254**, 1951–1956 (1979).
35. Li, Z., Pandit, S. & Deutscher, M. P. RNase G (CafA protein) and RNase E are both required for the 5' maturation of 16S ribosomal RNA. *EMBO J.* **18**, 2878–2885 (1999).
36. Bakin, A. & Ofengand, J. Four newly located pseudouridylate residues in *Escherichia coli* 23S ribosomal RNA are all at the peptidyltransferase center: analysis by the application of a new sequencing technique. *Biochemistry* **32**, 9754–9762 (1993).
37. Green, R. & Noller, H. F. In vitro complementation analysis localizes 23S rRNA posttranscriptional modifications that are required for *Escherichia coli* 50S ribosomal subunit assembly and function. *RNA* **2**, 1011–1021 (1996).
38. Decatur, W. A. & Fournier, M. J. rRNA modifications and ribosome function. *Trends Biochem. Sci.* **27**, 344–351 (2002).
39. Cumberlidge, A. G. & Isono, K. Ribosomal protein modification in *Escherichia coli*. I. A mutant lacking the N-terminal acetylation of protein S5

- exhibits thermosensitivity. *J. Mol. Biol.* **131**, 169–189 (1979).
40. Kushner, S. R., Maples, V. F. & Champney, W. S. Conditionally lethal ribosomal protein mutants: characterization of a locus required for modification of 50S subunit proteins. *Proc. Natl. Acad. Sci. U.S.A.* **74**, 467–471 (1977).
 41. Nierhaus, K. H. The assembly of prokaryotic ribosomes. *Biochimie* **73**, 739–755 (1991).
 42. Nishi, K., Morel-Deville, F., Hershey, J. W., Leighton, T. & Schnier, J. An eIF-4A-like protein is a suppressor of an *Escherichia coli* mutant defective in 50S ribosomal subunit assembly. *Nature* **336**, 496–498 (1988).
 43. Dammel, C. S. & Noller, H. F. Suppression of a cold-sensitive mutation in 16S rRNA by overexpression of a novel ribosome-binding factor, RbfA. *Genes Dev.* **9**, 626–637 (1995).
 44. Karbstein, K. Role of GTPases in ribosome assembly. *Biopolymers* **87**, 1–11 (2007).
 45. Britton, R. A. Role of GTPases in bacterial ribosome assembly. *Annu. Rev. Microbiol.* **63**, 155–176 (2009).
 46. Woolford, J. L. & Baserga, S. J. Ribosome biogenesis in the yeast *Saccharomyces cerevisiae*. *Genetics* **195**, 643–681 (2013).
 47. Kaczanowska, M. & Rydén-Aulin, M. Ribosome biogenesis and the translation process in *Escherichia coli*. *Microbiol. Mol. Biol. Rev.* **71**, 477–494 (2007).
 48. Maguire, B. A. Inhibition of bacterial ribosome assembly: a suitable drug target? *Microbiol. Mol. Biol. Rev.* **73**, 22–35 (2009).
 49. Gollop, N. & March, P. E. A GTP-binding protein (Era) has an essential role in growth rate and cell cycle control in *Escherichia coli*. *J. Bacteriol.* **173**, 2265–2270 (1991).
 50. Britton, R. A. *et al.* Cell cycle arrest in Era GTPase mutants: a potential growth rate-regulated checkpoint in *Escherichia coli*. *Mol. Microbiol.* **27**, 739–750 (1998).
 51. Sayed, A., Matsuyama, S. I. & Inouye, M. Era, an essential *Escherichia coli* small G-protein, binds to the 30S ribosomal subunit. *Biochem. Biophys.*

- Res. Commun.* **264**, 51–54 (1999).
52. Inoue, K., Alsina, J., Chen, J. & Inouye, M. Suppression of defective ribosome assembly in a *rbfA* deletion mutant by overexpression of Era, an essential GTPase in *Escherichia coli*. *Mol. Microbiol.* **48**, 1005–1016 (2003).
 53. Sharma, M. R. *et al.* Interaction of Era with the 30S ribosomal subunit implications for 30S subunit assembly. *Mol. Cell* **18**, 319–329 (2005).
 54. Stokes, J. M., Davis, J. H., Mangat, C. S., Williamson, J. R. & Brown, E. D. Discovery of a small molecule that inhibits bacterial ribosome biogenesis. *Elife* **3**, e03574 (2014).
 55. Campbell, T. L. & Brown, E. D. Genetic interaction screens with ordered overexpression and deletion clone sets implicate the *Escherichia coli* GTPase YjeQ in late ribosome biogenesis. *J. Bacteriol.* **190**, 2537–2545 (2008).
 56. Jomaa, A. *et al.* Cryo-electron microscopy structure of the 30S subunit in complex with the YjeQ biogenesis factor. *RNA* **17**, 2026–2038 (2011).
 57. Himeno, H. *et al.* A novel GTPase activated by the small subunit of ribosome. *Nucleic Acids Res.* **32**, 5303–5309 (2004).
 58. Siibak, T. *et al.* Erythromycin- and chloramphenicol-induced ribosomal assembly defects are secondary effects of protein synthesis inhibition. *Antimicrob. Agents Chemother.* **53**, 563–571 (2009).
 59. Usary, J. & Champney, W. S. Erythromycin inhibition of 50S ribosomal subunit formation in *Escherichia coli* cells. *Mol. Microbiol.* **40**, 951–962 (2001).
 60. Siibak, T. *et al.* Antibiotic-induced ribosomal assembly defects result from changes in the synthesis of ribosomal proteins. *Mol. Microbiol.* **80**, 54–67 (2011).
 61. Champney, W. S. & Burdine, R. 50S ribosomal subunit synthesis and translation are equivalent targets for erythromycin inhibition in *Staphylococcus aureus*. *Antimicrob. Agents Chemother.* **40**, 1301–1303 (1996).
 62. Champney, W. S. & Burdine, R. Azithromycin and clarithromycin inhibition of 50S ribosomal subunit formation in *Staphylococcus aureus* cells. *Curr. Microbiol.* **36**, 119–123 (1998).

63. Champney, W. S. & Tober, C. L. Evernimicin (SCH27899) inhibits both translation and 50S ribosomal subunit formation in *Staphylococcus aureus* cells. *Antimicrob. Agents Chemother.* **44**, 1413–1417 (2000).
64. McGaha, S. M. & Champney, W. S. Hygromycin B inhibition of protein synthesis and ribosome biogenesis in *Escherichia coli*. *Antimicrob. Agents Chemother.* **51**, 591–596 (2007).
65. Champney, W. S. The other target for ribosomal antibiotics: inhibition of bacterial ribosomal subunit formation. *Infect. Disord. Drug. Targets* **6**, 377–390 (2006).
66. Bremer, H. & Dennis, P. P. Modulation of chemical composition and other parameters of the cell by growth rate. In: *Escherichia coli and Salmonella: cellular and molecular biology*. 2nd ed. (ASM Press, Washington, D.C., 1996)
67. Chen, S. S. & Williamson, J. R. Characterization of the ribosome biogenesis landscape in *E. coli* using quantitative mass spectrometry. *J. Mol. Biol.* **425**, 767–779 (2012).
68. Chen, S. S., Sperling, E., Silverman, J. M., Davis, J. H. & Williamson, J. R. Measuring the dynamics of *E. coli* ribosome biogenesis using pulse-labeling and quantitative mass spectrometry. *Mol. Biosyst.* **8**, 3325–3334 (2012).
69. Charollais, J., Dreyfus, M. & Iost, I. CsdA, a cold-shock RNA helicase from *Escherichia coli*, is involved in the biogenesis of 50S ribosomal subunit. *Nucleic Acids Res.* **32**, 2751–2759 (2004).
70. Moreno, J. M., Drskjøtersen, L., Kristensen, J. E., Mortensen, K. K. & Sperling-Petersen, H. U. Characterization of the domains of *E. coli* initiation factor IF2 responsible for recognition of the ribosome. *FEBS Lett.* **455**, 130–134 (1999).
71. Arrowsmith, C. H. *et al.* The promise and peril of chemical probes. *Nat. Chem. Biol.* **11**, 536–541 (2015).
72. Loibl, M. *et al.* The drug diazaborine blocks ribosome biogenesis by inhibiting the AAA-ATPase Drg1. *J. Biol. Chem.* **289**, 3913–3922 (2013).
73. Pertschy, B. *et al.* Diazaborine treatment of yeast cells inhibits maturation of the 60S ribosomal subunit. *Mol. Cell. Biol.* **24**, 6476–6487 (2004).

74. Pertschy, B. *et al.* Cytoplasmic recycling of 60S preribosomal factors depends on the AAA protein Drg1. *Mol. Cell. Biol.* **27**, 6581–6592 (2007).
75. Kappel, L. *et al.* Rlp24 activates the AAA-ATPase Drg1 to initiate cytoplasmic pre-60S maturation. *J. Cell Biol.* **199**, 771–782 (2012).
76. Saveanu, C. *et al.* Sequential protein association with nascent 60S ribosomal particles. *Mol. Cell. Biol.* **23**, 4449–4460 (2003).
77. Drygin, D. *et al.* Targeting RNA polymerase I with an oral small molecule CX-5461 inhibits ribosomal RNA synthesis and solid tumor growth. *Cancer Res.* **71**, 1418–1430 (2011).
78. Bywater, M. J. *et al.* Inhibition of RNA polymerase I as a therapeutic strategy to promote cancer-specific activation of p53. *Cancer Cell* **22**, 51–65 (2012).
79. Deisenroth, C. & Zhang, Y. Ribosome biogenesis surveillance: probing the ribosomal protein-Mdm2-p53 pathway. *Oncogene* **29**, 4253–4260 (2010).
80. Drygin, D. *et al.* Anticancer activity of CX-3543: a direct inhibitor of rRNA biogenesis. *Cancer Res.* **69**, 7653–7661 (2009).
81. Lewis, K. Platforms for antibiotic discovery. *Nat. Rev. Drug Discov.* **12**, 371–387 (2013).
82. Frazier, A. D. & Champney, W. S. The vanadyl ribonucleoside complex inhibits ribosomal subunit formation in *Staphylococcus aureus*. *J. Antimicrob. Chemother.* **67**, 2152–2157 (2012).
83. Frazier, A. D. & Champney, W. S. Inhibition of ribosomal subunit synthesis in *Escherichia coli* by the vanadyl ribonucleoside complex. *Curr. Microbiol.* **67**, 226–233 (2013).
84. Silvers, J. A. & Champney, W. S. Accumulation and turnover of 23S ribosomal RNA in azithromycin-inhibited ribonuclease mutant strains of *Escherichia coli*. *Arch. Microbiol.* **184**, 66–77 (2005).
85. Rasmussen, L. C., Sperling-Petersen, H. U. & Mortensen, K. K. Hitting bacteria at the heart of the central dogma: sequence-specific inhibition. *Microb. Cell Fact.* **6**, 24 (2007).
86. Xue-Wen, H., Jie, P., Xian-Yuan, A. & Hong-Xiang, Z. Inhibition of bacterial translation and growth by peptide nucleic acids targeted to domain II of 23S

- rRNA. *J. Pept. Sci.* **13**, 220–226 (2007).
87. Klostermeier, D., Sears, P., Wong, C. H., Millar, D. P. & Williamson, J. R. A three-fluorophore FRET assay for high-throughput screening of small-molecule inhibitors of ribosome assembly. *Nucleic Acids Res.* **32**, 2707–2715 (2004).
 88. Bharat, A., Blanchard, J. E. & Brown, E. D. A high-throughput screen of the GTPase activity of *Escherichia coli* EngA to find an inhibitor of bacterial ribosome biogenesis. *J. Biomol. Screen.* **18**, 830–836 (2013).
 89. Bharat, A. & Brown, E. D. Phenotypic investigations of the depletion of EngA in *Escherichia coli* are consistent with a role in ribosome biogenesis. *FEMS Microbiol. Lett.* **353**, 26–32 (2014).
 90. Gadad, O. *et al.* Rlp7p is associated with 60S preribosomes, restricted to the granular component of the nucleolus, and required for pre-rRNA processing. *J. Cell Biol.* **157**, 941–951 (2002).
 91. Grandi, P. *et al.* 90S pre-ribosomes include the 35S pre-rRNA, the U3 snoRNP, and 40S subunit processing factors but predominantly lack 60S synthesis factors. *Mol. Cell* **10**, 105–115 (2002).
 92. Karbstein, K. Quality control mechanisms during ribosome maturation. *Trends Cell Biol.* **23**, 242–250 (2013).
 93. Cheng, Z. F. & Deutscher, M. P. Quality control of ribosomal RNA mediated by polynucleotide phosphorylase and RNase R. *Proc. Natl. Acad. Sci. U.S.A.* **100**, 6388–6393 (2003).
 94. Jacob, A. I., Köhrer, C., Davies, B. W., Rajbhandary, U. L. & Walker, G. C. Conserved bacterial RNase YbeY plays key roles in 70S ribosome quality control and 16S rRNA maturation. *Mol. Cell* **49**, 427–438 (2012).
 95. Cole, S. E., LaRiviere, F. J., Merrikh, C. N. & Moore, M. J. A convergence of rRNA and mRNA quality control pathways revealed by mechanistic analysis of nonfunctional rRNA decay. *Mol. Cell* **34**, 440–450 (2009).
 96. Davies, B. W. *et al.* Role of *Escherichia coli* YbeY, a highly conserved protein, in rRNA processing. *Mol. Microbiol.* **78**, 506–518 (2010).
 97. Golovina, A. Y., Bogdanov, A. A., Dontsova, O. A. & Sergiev, P. V. Purification of 30S ribosomal subunit by streptavidin affinity chromatography. *Biochimie* **92**, 914–917 (2010).

98. Leonov, A. A., Sergiev, P. V., Bogdanov, A. A., Brimacombe, R. & Dontsova, O. A. Affinity purification of ribosomes with a lethal G2655C mutation in 23 S rRNA that affects the translocation. *J. Biol. Chem.* **278**, 25664–25670 (2003).
99. Bassler, J. *et al.* Identification of a 60S preribosomal particle that is closely linked to nuclear export. *Mol. Cell* **8**, 517–529 (2001).
100. Stokes, J. M., Selin, C., Cardona, S. T. & Brown, E. D. Chemical inhibition of bacterial ribosome biogenesis shows efficacy in a worm infection model. *Antimicrob. Agents Chemother.* **59**, 2918–2920 (2015).
101. Ghalei, H. *et al.* Hrr25/CK1 δ -directed release of Ltv1 from pre-40S ribosomes is necessary for ribosome assembly and cell growth. *J. Cell Biol.* **208**, 745–759 (2015).

Figure Legends

Figure 1. Simplified overview of ribosome biogenesis. (a) In yeast, ribosome biogenesis initiates with transcription of 18S, 5.8S, and 25S rRNA by Pol I. 5S rRNA, transcribed by Pol III, is omitted for clarity. Co-transcriptional assembly and modification of the pre-43S particle occurs until the emergence of the A₂ RNA cleavage site, at which time the pre-43S particle is released and transcription continues through the 60S subunit rRNA genes. The 40S and 60S subunits are then independently assembled with the assistance of ~200 assembly factors. Upon export of the pre-ribosomal particles into the cytoplasm, mature 60S subunits bind pre-40S particles in an eIF5B-dependent pre-translation quality control checkpoint prior to final 40S maturation. Representative ribosome assembly factors are depicted with pink, yellow, and purple circles. (b) Bacterial ribosome biogenesis begins with transcription of 16S, 23S, and 5S

rRNA as a single transcript prior to cleavage by a series of RNases to release pre-30S and pre-50S particles. As in yeast, rRNA transcripts are co-transcriptionally assembled and modified (omitted for clarity). 30S and 50S subunits are subsequently modified by ~60 biogenesis factors, and mature through multiple parallel assembly pathways prior to translation initiation. Unlike eukaryotic ribosome biogenesis, this process in bacteria does not necessitate a nuclear export event, and a pre-translation quality control checkpoint has yet to be observed. Representative ribosome assembly factors are depicted with pink and yellow circles.

Figure 2. Classical methods to study ribosome biogenesis in *E. coli*. (a)

Classic *in vitro* investigations into ribosome biogenesis. The Nomura assembly map (left) shows the thermodynamic r-protein binding dependencies of the 30S subunit. A clear hierarchy of binding is seen where primary binding proteins interact directly with rRNA, secondary binding proteins require the previous addition of primary proteins, and tertiary binding proteins require the addition of primary and secondary binding proteins. Furthermore, r-proteins generally bind in a 5'-3' direction along 16S rRNA, thereby supporting a co-transcriptional assembly hypothesis. The Nierhaus assembly map (right) depicts the thermodynamic r-protein binding dependencies of the 50S subunit. R-proteins L5, L15, and L18 associate with 5S rRNA within the 50S subunit (orange). (b)

Modern *in vitro* approaches to monitor the kinetics of 30S subunit assembly. 30S r-proteins are introduced to 16S rRNA transcripts, incubated for varying

durations, and analyzed using mass spectrometry to quantify rates of r-protein addition to rRNA; cryo-EM to visualize assembling subunits; or x-ray footprinting to determine rRNA protection sites during folding. Not depicted here is the Woodson lab single-molecule FRET system, where the 5' domain of 16S rRNA was covalently bound to a quartz slide, and the dynamics of S4 association was monitored over time by introduction of this protein to the immobilized rRNA. (c) *In vivo* investigations into ribosome biogenesis. Commonly, putative ribosome biogenesis factors are deleted (or depleted), and the resulting cells are analyzed for cold sensitive growth and intracellular accumulation of rRNA, common phenotypes that prompt further investigation into the ribosomal composition of these cells. Ribosomal particles from the strain under investigation can be separated based on sedimentation rate, and in the event of aberrant ribosome profiles relative to wild type, non-native particles are commonly purified and analyzed for unique biochemical and structural features to define the possible function(s) of the deleted protein.

Figure 3. Genetic perturbation of ribosome biogenesis factors lacks temporal resolution and can lead to multiple unrelated phenotypic effects.

(a) Depletion of the essential 30S assembly factor Era in *E. coli* results in wide-ranging phenotypes, making it difficult to elucidate the function of this protein. Further, genetic methods generally have poor temporal resolution, preventing investigators from determining the series of events leading from genetic perturbation to the observed steady state phenotypes. (b) When analyzing

ribosomal particles from gene-deletion mutants as described in Figure 2c, investigators are generally able to thoroughly study only highly populous particles. Given that genetic methods have low temporal resolution, it is difficult to determine whether non-native ribosomal particles from genetically perturbed cells are on-pathway intermediates that have halted at the stage assisted by the deleted protein, or whether they are thermodynamically stable off-pathway particles. Representative ribosome assembly factors are depicted with pink circles.

Figure 4. Small molecule inhibitors of ribosome biogenesis provide kinetic resolution of events following perturbation. Co-treatment of cells with an inhibitor and a radioactive probe (yellow star) at time t_0 , enables kinetic investigations, i.e., t_1 to t_n , of events following perturbation, including how the composition of ribosomal particles changes as a function of time. In this example, *bona fide* intermediates accumulate soon after perturbation, but convert to thermodynamically stable off-pathway particles over time. In contrast, genetic methods of perturbation might conclude that the off-pathway particle was a true maturation intermediate due to the inability to visualize events over time. The maturation event inhibited by the molecule is depicted with a red line. Representative ribosome assembly factors are depicted with pink circles.

Table 1. Characterized whole cell-active small molecule inhibitors of ribosome biogenesis

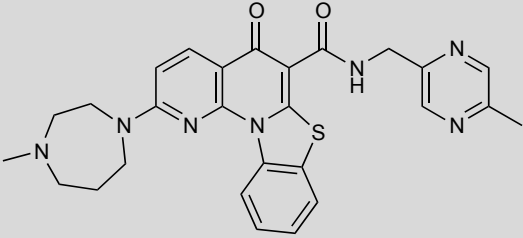
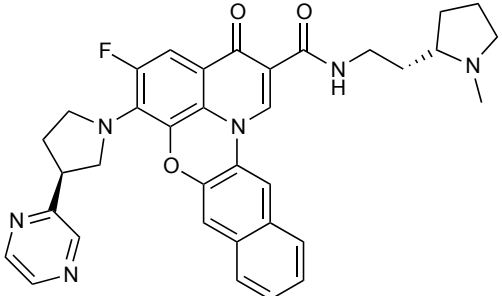
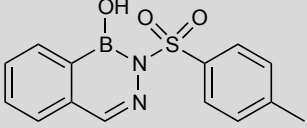
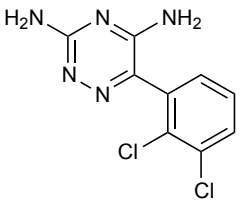
Compound	Target	Organism
CX-5461 	Pol I	Mammal
CX-3543 	Nucleolin/rDNA complexes	Mammal
Diazaborine 	Drg1	Yeast
Lamotrigine 	IF2	Bacteria

Figure 1

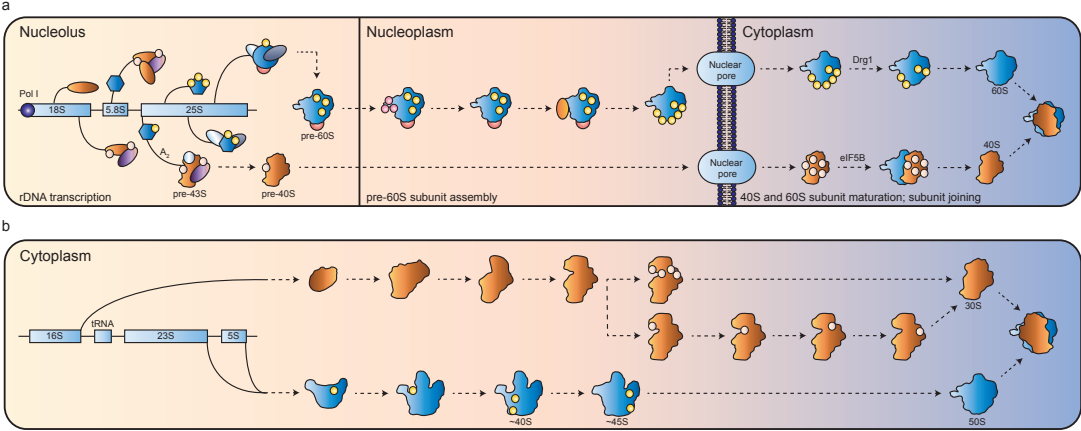


Figure 2

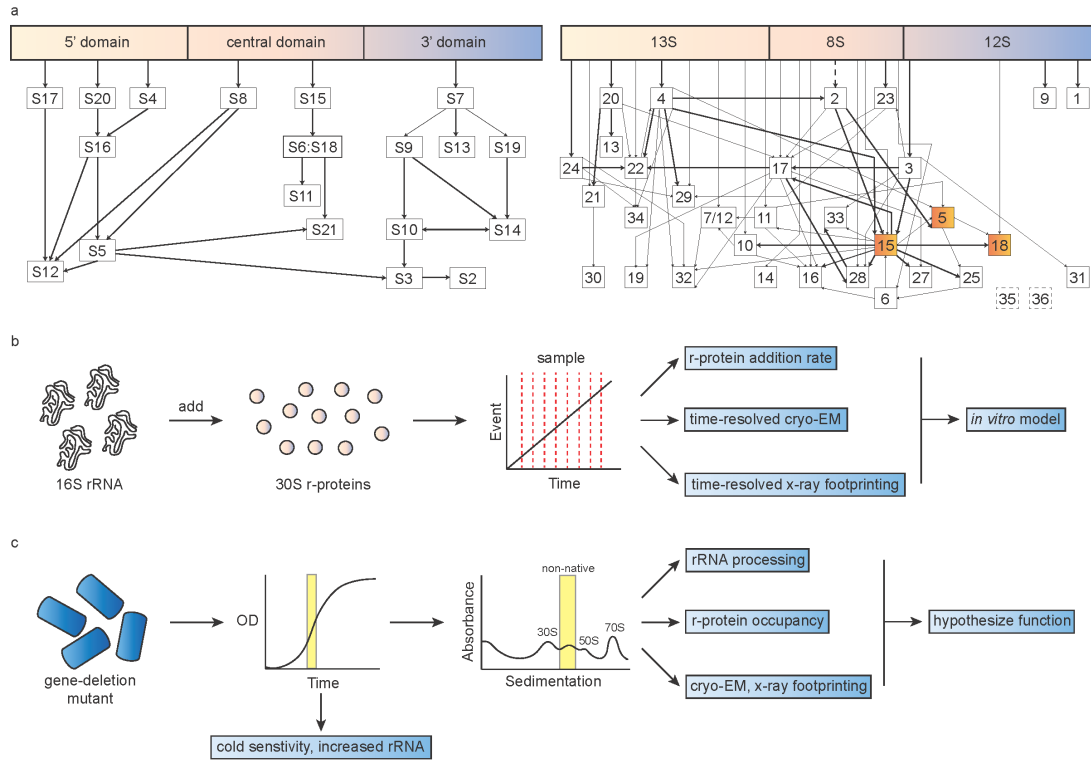


Figure 3

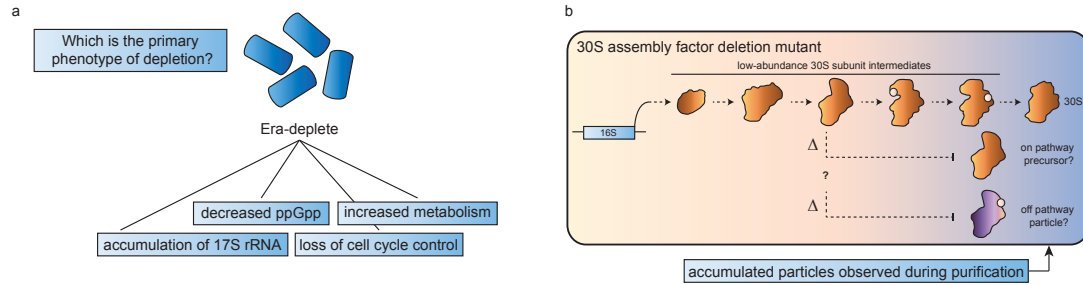
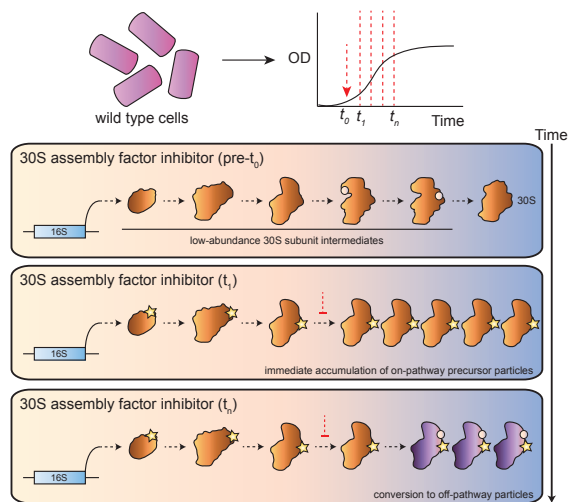


Figure 4



CHAPTER IV – Cold stress makes *Escherichia coli* susceptible to glycopeptide antibiotics by altering outer membrane integrity

Preface

The work presented in this chapter was previously published in:

Stokes JM, French S, Ovchinnikova OG, Bouwman C, Whitfield C, Brown ED. Cold stress makes *Escherichia coli* susceptible to glycopeptide antibiotics by altering outer membrane integrity. *Cell Chemical Biology* **23**, 267–277 (2016).

Permission has been granted by the publisher to reproduce the material herein.

I performed all experiments with the exception of LPS gel electrophoresis and LPS mass spectrometry, which was conducted by Bouwman C and Ovchinnikova OG. French S assisted in acquiring atomic force micrographs and with screening experiments. I wrote and edited the manuscript with assistance from all authors.

Summary

A poor understanding of the mechanisms by which antibiotics traverse the outer membrane remains a considerable obstacle to the development of novel Gram-negative antibiotics. Herein, we demonstrate that the Gram-negative bacterium *Escherichia coli* becomes susceptible to the narrow-spectrum antibiotic vancomycin during growth at low temperatures. Heterologous expression of an *Enterococcus vanHBX* vancomycin resistance cluster in *E. coli* confirmed that the mechanism of action was through inhibition of peptidoglycan biosynthesis. To understand the nature of vancomycin permeability, we screened for strains of *E. coli* that displayed resistance to vancomycin at low temperature. Surprisingly, we observed that mutations in outer membrane biosynthesis suppressed vancomycin activity. Subsequent chemical analysis of lipopolysaccharide from vancomycin-sensitive and -resistant strains confirmed that suppression was correlated with truncations in the core oligosaccharide of lipopolysaccharide. These unexpected observations challenge current understanding of outer membrane permeability, and provide new chemical insights into the susceptibility of *E. coli* to glycopeptide antibiotics.

Introduction

The outer membrane of Gram-negative bacteria is an effective barrier against extracellular solutes, providing intrinsic resistance to a plethora of clinically useful antibiotics¹. Compounded by the widespread dissemination of

acquired resistance genes, this results in dramatically decreased treatment options for patients with Gram-negative infections, resulting in high morbidity and mortality². This is a global problem, further potentiated by a lack of recent progress in discovering and characterizing novel Gram-negative antibiotics. Numerous reports have detailed the extreme challenges in identifying Gram-negative-active compounds using common drug screening approaches, and attribute this lack of productivity to an insufficient understanding of how chemicals traverse the outer membrane³⁻⁵. In response to this problem, the New Drugs for Bad Bugs initiative has, for example, recently launched TRANSLOCATION, a \$30 million program aimed at understanding the mechanisms through which small molecules navigate the Gram-negative cell envelope⁶. Indeed, with increased efforts directed at elucidating the fundamental properties of outer membrane permeability, ongoing Gram-negative antibiotic screening initiatives will benefit from the development of compound libraries and isolation of natural products with chemical characteristics necessary to traverse this surface.

A chief contributor to the intrinsic resistance displayed by Gram-negative organisms is lipopolysaccharide (LPS)⁷. Found exclusively in the outer membrane, LPS is composed of a highly conserved hydrophobic lipid A moiety, a core oligosaccharide (core OS), and in many species a long chain O-antigenic polysaccharide. *Escherichia coli* K-12 and its derivatives are largely lacking O polysaccharide, and contain only lipid A and core OS⁸. Lipid A of *E. coli* consists of a β -1'-6-linked glucosamine disaccharide that is phosphorylated at the 1 and 4'

positions, and contains six fatty acyl chains under routine laboratory conditions. Attached to the disaccharide of lipid A at the 6' position is core OS, which has been conceptually divided into two regions, inner and outer core, based on sugar composition. The inner core is composed of 3-deoxy-D-*manno*-oct-2-ulosonic acid (Kdo) and L-*glycero*-D-*manno*-heptopyranose, while the outer core contains primarily hexose and acetamidohexose sugars⁹. Given that both lipid A and inner core OS are negatively charged, ionic interactions of divalent cations provide membrane stability^{10,11} and help explain the impermeability of this surface to large molecular weight compounds.

Gram-negative bacteria modify LPS to maintain membrane stability in response to environmental stress. For instance, in *E. coli* and *Salmonella*, lipid A undergoes phosphate modification by ArnT and EptA, which catalyze the addition of 4-amino-4-deoxy arabinose and phosphoethanolamine, respectively¹². These modifications are primarily responsible for cationic antimicrobial peptide resistance. Similarly, the addition of palmitate to lipid A by PagP can be activated by cationic peptide challenge¹³⁻¹⁵, and palmitoleate can be added in place of laurate by LpxP during low temperature growth conditions as a means of improving membrane fluidity^{16,17}. Furthermore, in the Enterobacteriaceae the basic inner core structure can be modified by substitution of the heptose-Kdo backbone with residues such as rhamnose and phosphoethanolamine¹⁸.

Modification of native LPS chemistry greatly impacts antibiotic susceptibility. Generally, mutations inhibiting LPS biosynthesis have been shown

to decrease resistance to antimicrobial agents, with the primary hypothesis that this phenotype is the result of increased permeability through a structurally compromised outer membrane. This has been shown for Gram-positive specific antibiotics such as macrolides¹⁹, glycopeptides^{20,21}, and rifamycins²², as well as broad-spectrum inhibitors²³. Recently, we observed that the glycopeptide vancomycin is able to inhibit growth of wild type *E. coli* at low temperatures²⁴. Gram-negative organisms display intrinsic resistance to this class of antibiotics under normal growth conditions. Thus, we reasoned that the idiosyncratic cold sensitivity of *E. coli* to vancomycin presented a unique opportunity to further our understanding of glycopeptide permeability in this model Gram-negative bacterium.

Here, we expand on our previous observation with a mechanistic study of the determinants of glycopeptide activity in *E. coli*. Briefly, we observed that vancomycin potency increases between 2- and 4-fold with every 5°C to 7°C decrease in temperature. To confirm that this molecule prevented peptidoglycan assembly in *E. coli*, as it does in Gram-positive bacteria, we expressed an *Enterococcus vanHBX* vancomycin resistance cluster and observed the restoration of high-level resistance. Subsequent screening of an ordered *E. coli* gene deletion collection and generation of spontaneous suppressor mutants revealed, paradoxically, that mutations in outer membrane biosynthesis suppressed vancomycin activity. Lastly, chemical analysis of LPS from various gene deletion strains as well as from a strong suppressor mutant revealed that

the presence of truncated core OS species correlated with vancomycin resistance. Taken together, this work highlights an unexpected paradox where mutations that prevented native outer membrane biosynthesis in *E. coli* led to vancomycin impermeability, providing new chemical insights into the permeability of the Gram-negative outer membrane to glycopeptide antibiotics.

Results

Vancomycin inhibits growth of *E. coli* in a temperature-dependent manner. Initial observations of the temperature-dependent activity of vancomycin were made at 37°C and 15°C²⁴. To determine whether potency increased gradually as a function of temperature or dramatically after traversing a strict temperature threshold, *E. coli* was grown in LB media at 42°C, 37°C, 30°C, 25°C, 20°C, and 15°C in the presence of varying concentrations of vancomycin (Figure 1a – top, S1a, b). This revealed that vancomycin potency increased between 2- and 4-fold as temperature decreased 5°C to 7°C. To understand the chemical restrictions of permeability, we tested an additional five glycopeptides for activity (Figure S2a). Two analogs of vancomycin, balhimycin²⁵ and aglycovancomycin²⁶ (Figure S2b), showed at least 128-fold and 16-fold increases in potency between 37°C and 15°C, respectively. Three teicoplanins, which differ in peptide core structure from the vancomycins²⁷, were also tested (Figure S2a, b). Teicoplanin did not display activity against *E. coli* at any temperature. However, teicoplanin analogs A47934 and DSA-A47934 showed at least 2-fold and 8-fold increases in

potency between 37°C and 15°C respectively, albeit at high concentrations. These data suggest that both peptide core and sugar composition affect glycopeptide activity to an extent, although the vancomycin core appears to support higher activity against *E. coli* than that of teicoplanin.

Next, we set out to understand whether vancomycin inhibited peptidoglycan assembly in *E. coli*, rather than acting via an unanticipated mechanism. To this end, we optimized the codon usage of a *vanHBX* vancomycin resistance cluster from *Enterococcus faecalis*²⁸ for *E. coli* expression. This cluster is responsible for converting D-ala-D-ala termini of peptidoglycan into D-ala-D-lac, for which vancomycin has low affinity²⁹⁻³¹. Expression of *vanHBX* in *E. coli* at 15°C and concurrent treatment with vancomycin revealed that cells regained high-level resistance (Figure 1a – bottom, S2c), showing that growth inhibition occurred through the known peptidoglycan-dependent mechanism. Additionally, expression of *vanHBX* at 37°C resulted in increased vancomycin resistance over non-induced and empty-vector controls (Figure S2c, d).

Observing that vancomycin activity in *E. coli* was peptidoglycan-dependent, we reasoned that cell morphology would be altered by antibiotic treatment. Therefore, *E. coli* was grown in LB media at 15°C in the presence of varying concentrations of vancomycin. Cells were then stained with the lipophilic dye FM4-64 and visualized (Figure 1b). Treatment with increasing concentrations of vancomycin caused perturbed cell shape characterized by membrane blebbing

and loss of rod morphology. Subsequent imaging using transmission electron microscopy (TEM) revealed that cells treated with vancomycin lost native cell envelope architecture, and displayed severe separation of the outer membrane from the inner membrane (Figure 1c).

Since treatment of Gram-negative bacteria with EDTA has been shown to decrease outer membrane stability³², we hypothesized that increased concentrations of divalent cations may enhance vancomycin resistance through phosphate bridging of adjacent LPS molecules. *E. coli* was grown in LB media at 37°C and 15°C in the presence of varying concentrations of vancomycin and either Ca²⁺ or Mg²⁺ using checkerboard dilution assays. At 15°C (Figure 1d – blue), we observed striking antagonism between vancomycin and both species of divalent cation, suggesting that temperature-dependent drug activity could be overcome by increasing the association between adjacent LPS molecules. Antagonism was also observed at 37°C (Figure 1d – red), albeit to a lesser degree. This slightly decreased antagonism may be the result of altered outer membrane protein/lipid/LPS interactions between 15°C and 37°C, or by vancomycin lethality at 37°C being caused by off-target effects at high concentrations.

Genetic perturbations in outer membrane biosynthesis cause vancomycin resistance. We endeavored to dissect the genetic determinants of vancomycin activity to understand the outer membrane constituents that were necessary for permeability. To this end, we screened the *E. coli* Keio collection³³,

a comprehensive set of ~4200 non-essential gene deletion strains, to identify those that were resistant to vancomycin at low temperatures. Briefly, mutants were pinned onto solid LB media supplemented with vancomycin, grown at 37°C and 15°C, and visualized to quantify colony size and density (Figure 2a, S3a). In parallel, strains were pinned onto solid LB without antibiotic to assess intrinsic growth abnormalities displayed by any mutants in the collection (Figure S3a). Intriguingly, we observed vancomycin suppression by 41 mutants at 15°C, as defined by growth 3σ or greater above the mean of the entire collection (Table S1).

To determine which functional classes of genes were enriched for vancomycin suppression, all mutants were binned based on clusters of orthologous groups assignments^{34,35} (Figure 2b). Paradoxically, we observed a significant enrichment for genes involved in cell envelope biosynthesis and carbohydrate metabolism, two classes that are essential for generating a structurally integral cell surface (Table S1). To further strengthen these observations, we subsequently generated spontaneous suppressor mutants against vancomycin. One high-level mutant was then sequenced to reveal a point mutation in *pgm* (Y324stop), the gene encoding phosphoglucomutase, which is responsible for the interconversion of α -D-glucose-1-phosphate and α -D-glucose-6-phosphate³⁶ and has been implicated in the biosynthesis of UDP-linked hexose precursors used in LPS assembly³⁷⁻⁴⁰. Importantly, the Δ *pgm* strain from the Keio

collection also displayed vancomycin resistance, confirming the validity of both suppressor identification strategies.

To understand the phenotypic characteristics of vancomycin resistance, we tested our suppressor mutant (referred to herein as Y324*) for vancomycin suppression across a range of temperatures and drug concentrations. Here, the Y324* mutant was grown in LB media at 42°C, 37°C, 30°C, 25°C, 20°C, and 15°C in the presence of varying concentrations of vancomycin (Figure 2c), revealing that vancomycin suppression was temperature-independent. FM4-64 (Figure 2d) and TEM (Figure S3b) analysis of vancomycin-treated Y324* mutant revealed that cell morphology was unaltered in the presence of drug. Additionally, as in the wild type background, we observed vancomycin antagonism by both Ca^{2+} and Mg^{2+} in the Y324* mutant, consistent with the notion that cation-mediated phosphate bridging on LPS further increased antibiotic exclusion similar to that of wild type cells grown at 37°C (Figure S3c).

To determine whether resistance was unique to vancomycin, we tested the antibiotic sensitivity profile of the Y324* mutant relative to wild type at 37°C and 15°C (Figure S3d). The Y324* mutant displayed high-level resistance to the vancomycin analog balhimycin at low temperature. Furthermore, we observed resistance to rifampicin at 15°C in our mutant, whereas wild type *E. coli* was 64-fold more sensitive to this compound at low temperature relative to 37°C. Third, the Y324* mutant displayed extreme sensitivity to the core OS-binding antibiotic polymyxin B at both 37°C and 15°C relative to wild type, likely due to increased

accessibility of lipid A⁴¹, consistent with previous investigations^{41,42}. Taken together, these antibiotic susceptibility data suggest that the cell surface of the Y324* mutant may be proficient at excluding large molecular weight antibiotics by counteracting cold-induced perturbations in the outer membrane. Importantly, a vancomycin-resistant inner core OS-deficient $\Delta rfaE$ strain of *E. coli* displayed sensitivity and resistance phenotypes that were similar to the Y324* mutant (Figure S4), further supporting this hypothesis. One exception to the above observations is erythromycin, where wild type and the Y324* mutant displayed identical susceptibility phenotypes at 37°C and 15°C. However, temperature-dependent activity of this antibiotic may be significantly influenced by temperature sensitivity that is common to the ribosome^{43,44}.

Modifications in LPS chemistry affect vancomycin activity in *E. coli*.

We analyzed the LPS phenotypes of numerous resistant and sensitive *E. coli* mutants from the Keio collection to understand the chemistry governing vancomycin permeability. Here, 16 strains with mutations in outer membrane biosynthesis were grown in LB media at 37°C and 15°C, and LPS was analyzed using SDS-PAGE of proteinase K-treated whole cell lysates. Broadly, we observed that mutants showing wild type-like LPS profiles were sensitive to vancomycin (Figure 3a), and those displaying lower molecular mass LPS species were resistant at low temperatures (Figure 3b). Indeed, of the seven sensitive strains selected for analysis five displayed LPS profiles nearly identical to wild type, and of the nine resistant strains tested seven contained truncated LPS

species. In exception to this observation, $\Delta waaQ$ and $\Delta waaY$ mutants were resistant to vancomycin, yet did not show significant changes in LPS profiles relative to wild type. WaaQ is a transferase responsible for the addition of the side-chain heptose III to heptose II⁴⁵, whereas WaaY is a kinase that phosphorylates heptose II⁴⁵ (Figure 3d). The absence of large differences in band migration can be accounted for by mass changes insufficient to resolve via SDS-PAGE and/or by the activation of alternative LPS modifications in response to these mutations. On the other hand, $\Delta waaO$ and $\Delta waaP$ strains displayed vancomycin sensitivity at 15°C, although the LPS migrated subtly faster than wild type. With respect to WaaP (a kinase responsible for adding phosphate to O-4 of heptose I)⁴⁵, previous reports have shown that loss of this enzyme obviates WaaQ and WaaY activity^{45,46}, resulting in the cumulative deficiency of both core OS phosphates and a heptose residue, thereby explaining the observed band migrations (Figure 3d). Further, the loss of WaaO (a glucosyltransferase that adds glucose II to glucose I) results in the absence of distal outer core OS hexose residues, truncating core OS to a degree consistent with the observed migration rate⁴⁷ (Figure 3d). As expected, the LPS profile of the Y324* mutant was similar to the Δpgm strain (Figure 3c).

To build on these observations, we used electrospray ionization (ESI) mass spectrometry to analyze the core OS composition of wild type and Y324* mutant cells. Briefly, cultures were grown in LB at 37°C and 15°C, and LPS was isolated via hot water-phenol extraction. Mild acid hydrolysis of LPS liberated the

water-soluble carbohydrate portion of LPS. Core OS was subsequently isolated by size exclusion chromatography and analyzed by negative ion ESI mass spectrometry. Fractionation of the core OS of wild type *E. coli* LPS by size exclusion chromatography resulted in one oligosaccharide fraction (fraction II; see Experimental Procedures). As observed by ESI mass spectrometry, the predominant compounds in fraction II at 37°C (Figure 4a – left, 5a, S5a) corresponded to Kdo₁Hep₄Hex₄P₂ and Kdo₁Hep₃Hex₃P₂ core OS species, representing the two major *E. coli* K-12 core glycoforms I and IV, respectively⁴⁸. Some structural heterogeneity was noted and this was largely due to the presence of molecules having one or two additional phosphate and/or phosphoethanolamine residues. The same core OS species were observed in fraction II from wild type cells grown at 15°C (Figure 4a – right, 5a, S5a), however the predominant core species were found to contain three and four phosphate groups as opposed to the common two. The locations of the third and fourth phosphate groups are currently unknown.

Fractionation of core OS of the Y324* mutant by size exclusion chromatography resulted in two fractions: fraction IIa, which eluted in the same volume as fraction II of wild type, and fraction IIb, which contained lower molecular weight oligosaccharides (see Experimental Procedures). Composition of fraction IIa of the Y324* mutant grown at 37°C was similar to that found in wild type grown in the same conditions (Figure 4b – left, 5a, S5b). The mass spectrum of fraction IIb, on the other hand, showed the predominant peak corresponding to

a truncated core OS that contained two heptose residues decorated with phosphate and phosphoethanolamine (Figure 4c – left, 5b, S5c). While the overall structure was similar to wild type, oligosaccharides observed in fraction IIa at low temperature were found to be highly heterogeneous with respect to the content of phosphate, phosphoethanolamine, hexose, and heptose residues (Figure 4b – right, 5a, S5b). The higher molecular weight core species were dramatically reduced in the mutant, although the predominant core OS (Kdo₁Hep₃Hex₃P₃) was the same as that observed in wild type *E. coli* grown at 15°C. Lastly, fraction IIb of the Y324* mutant grown at 15°C contained three major truncated core OS species. The highest molecular mass oligosaccharide corresponded to Kdo₁Hep₂Hex₂P₁PEtN₁ and was accompanied by two compounds that lacked either phosphoethanolamine or two hexose residues (Figure 4c – right, 5b, S5c).

Taken together, the mass spectrometric data are in agreement with the observed SDS-PAGE LPS profiles, and further support the hypothesis that truncated core OS provides vancomycin resistance during cold stress. Indeed, ESI mass spectra of lipid A isolated from wild type and the Y324* mutant *E. coli* grown at 37°C and 15°C revealed no significant differences between these strains (Figure S6), leaving variances in core OS as the primary contributor to vancomycin permeability.

Discussion

Perhaps the most significant obstacle to the development of Gram-negative active antibiotics is a poor understanding of outer membrane permeability. Herein, we have taken advantage of the surprising observation that vancomycin is active against the model Gram-negative bacterium *E. coli* during cold stress. Vancomycin is a large hydrophilic molecule that is neither transported through membrane porins nor is it free to diffuse across the outer membrane⁴⁹. We observed that vancomycin displays temperature-dependent activity, where potency and temperature were inversely related. Recognizing that bioactive molecules can have varying and cryptic activities in diverse biological systems, we first set out to confirm that vancomycin was inhibiting the growth of *E. coli* through its canonical peptidoglycan-dependent mechanism. Expression of the *E. faecalis vanHBX* resistance cluster in *E. coli* resulted in high-level resistance, indicating that the mechanism of action of this molecule had been retained. Furthermore, vancomycin-treated cells exhibited morphological hallmarks of peptidoglycan disruption.

With phenotypic data implying that cold-induced changes in outer membrane characteristics were influencing vancomycin permeability, we endeavored to identify chemical and genetic modulators of drug activity. Interestingly, an analysis of various glycopeptide antibiotics revealed that vancomycin analogs showed activity against *E. coli* at reduced temperature, while teicoplanin was inactive, suggesting that the structure of the peptide core was key to permeability. This is perhaps most clear through comparison of

aglycovancomycin and DSA-A47934, which consist solely of the vancomycin and teicoplanin cores, respectively. However, these activity data also suggested a role for sugar composition of the antibiotic in outer membrane permeability, as can be seen through the varying activities of structural analogs within each glycopeptide class.

We subsequently set out to identify genetic modulators of vancomycin activity. Surprisingly, we observed that mutations in outer membrane biosynthesis conferred vancomycin resistance. This was paradoxical in the context of a conventional understanding of outer membrane integrity. Indeed, a large body of literature has shown that perturbations in LPS biosynthesis decrease intrinsic resistance towards antibiotics. For instance, it has been shown that mutations inhibiting core OS biosynthesis result in increased susceptibility to rifampicin, erythromycin, vancomycin, and others when cells are grown at 37°C²³. Furthermore, deletion of the cold-induced lipid A palmitoleate transferase LpxP from hyperpermeable *E. coli* results in significant vancomycin and rifampicin sensitivity during growth at 12°C¹⁶.

To resolve this apparent paradox, we investigated the composition of LPS from wild type and vancomycin resistant *E. coli* grown at both 37°C and 15°C, where we observed that truncated core OS was generally associated with vancomycin resistance. Nevertheless, $\Delta waaQ$ and $\Delta waaY$ strains were resistant to vancomycin yet displayed LPS phenotypes similar to wild type, and $\Delta waaO$ and $\Delta waaP$ strains were statistically sensitive yet displayed LPS species with

subtly lower molecular weight relative to wild type. Interestingly, while the LPS phenotypes of these strains may be inconsistent with the aforementioned correlation between LPS migration and vancomycin resistance, inspection of the functions of these enzymes within the LPS biosynthetic pathway is largely consistent with the overall model (Figure 3d). Our data suggest that residues distal to glucose I of outer core have little impact on vancomycin permeability, whereas the opposite is true for core OS residues closer in proximity to lipid A. With regards to the $\Delta waaP$ strain, vancomycin sensitivity at low temperature may have been observed due to unexplored biophysical consequences of additionally losing WaaQ and WaaY activities in this genetic background⁴⁵, and/or because of the potential activation of alternative core OS modifications. Further investigation will be important to understand the vancomycin sensitivity phenotype of the $\Delta waaP$ mutant.

We subsequently analyzed core OS and lipid A from wild type and the Y324* mutant by mass spectrometry. We focused on the Y324* mutant because of the strength of the suppressor phenotype and full characterization of its genome. Y324* contains a single nucleotide polymorphism in *pgm*, encoding phosphoglucomutase, converting tyrosine-324 to a premature stop codon. Previous studies have shown that *pgm* is required for LPS biosynthesis³⁷⁻⁴⁰. We observed that the mutant displayed a heterogeneous population of core OS, with a propensity to generate small molecular weight core species. Intriguingly, this strain was still capable of producing a small, yet measurable, quantity of full-

length core OS species without Pgm activity. This suggests that an alternative enzyme was able to perform the α -D-glucose-1-phosphate/ α -D-glucose-6-phosphate interconversion reaction, albeit less efficiently than Pgm. While the LPS composition of the Y324* mutant had little effect on vancomycin resistance relative to wild type at 37°C, it was clear that this was advantageous at low temperatures. Furthermore, we observed the presence of additional phosphate groups in core OS from wild type and Y324* grown at 15°C, suggesting a role for this additional negative charge during cold stress⁵⁰.

Interestingly, during growth at low temperatures many Gram-negative organisms dramatically remodel lipid A in order to maintain optimum membrane fluidity^{16,17}. Given the possibility that lipid A modifications may differ between wild type *E. coli* and the Y324* mutant, we analyzed lipid A from both strains at 37°C and 15°C. Lipid A composition was identical in these strains at both temperatures, suggesting that the chemistry of this region was not a factor in vancomycin permeability between these strains. However, checkerboard dilution assays showing that Ca²⁺ and Mg²⁺ potentially antagonize vancomycin highlights the importance of lipid A and core OS phosphates in this process¹.

Taken together, we propose a model in which heterogeneous or truncated core OS provides vancomycin resistance at low temperatures by generating an outer membrane that is resistant to cold-induced outer membrane “cracking”⁵¹. Figure 6a depicts the 3-dimensional structure of partial LPS from *E. coli* as a model for the orientation of core OS relative to lipid A⁵². In the side plane (Figure

6a – right), wild type core OS spans ~20 Å, preventing close association of individual LPS molecules at low temperatures (Figure 6b). However, in strains where core OS is heterogeneous as in the Y324* mutant, or more uniformly truncated, some or all of the resulting LPS molecules may associate more closely, thereby facilitating stronger intermolecular interactions (Figure 6c). At 37°C, inter-LPS interactions are clearly sufficiently stable as to prevent vancomycin permeability in all but the most extreme LPS perturbations. However, at low temperature, even with palmitoleate modification to increase membrane fluidity and additional core OS phosphates to promote intermolecular bridging, the outer membrane may be insufficiently dynamic to prevent outer membrane “cracking” in wild type backgrounds.

Importantly, this model fits well within the framework set by previous investigations into outer membrane permeability. It is well documented that at 37°C, mutants displaying truncated core OS are susceptible to large hydrophobic antibiotics (Figure S4, ²²). In extreme cases of core OS truncation²³, and perturbations in lipid A biosynthesis²², hydrophilic antibiotics are also able to cross the outer membrane. For the latter, it has been hypothesized that “cracks” in the outer membrane provide hydrophilic regions through which vancomycin can pass⁵¹. This may be why lipid A mutants are significantly more sensitive to hydrophilic antibiotics relative to those with defects in core OS biosynthesis²². Our observations of temperature-dependent vancomycin sensitivity in wild type *E. coli* may best be explained then by the presence of transient “cracks” in the outer

membrane that allow for the diffusion of hydrophilic molecules into the periplasm (Figure 6b), as has been previously suggested^{16,51}. It is therefore possible that vancomycin sensitivity is the result of an imperfect outer membrane response to cold-induced decreases in membrane fluidity. Intriguingly, the Y324* mutant, which displays heterogeneous LPS, as well as core OS-deficient strains such as the $\Delta rfaE$ mutant, appear to be better suited to maintain outer membrane integrity during cold stress, as is evidenced by these strains being more resistant to both vancomycin and rifampicin at 15°C relative to wild type. Here, despite decreased membrane fluidity during cold stress, robust inter-LPS bridging as a result of decreased steric hindrance may maintain exclusion properties more similar to that of wild type at 37°C.

Significance

The outer membrane of Gram-negative bacteria is a formidable barrier against antibiotics, and limits treatment options for patients with multi-drug resistant infections. Indeed, developing antibiotics that target these organisms is extremely challenging due to a poor understanding of the factors governing the permeability of Gram-negative pathogens. Glycopeptide antibiotics, for example, are extremely potent against Gram-positive organisms, which lack an outer membrane, but do not display activity against Gram-negatives. Here, we show that the model Gram-negative bacterium *Escherichia coli* becomes susceptible to the glycopeptide vancomycin during cold stress, and that this molecule inhibits

the growth of *E. coli* through the same peptidoglycan-dependent mechanism as in Gram-positives. Paradoxically, this cold-induced susceptibility is reversed through mutations that inhibit outer membrane biosynthesis, particularly that of lipopolysaccharide. We propose a model where decreased membrane fluidity during cold stress causes outer membrane “cracks”, and that inhibition of lipopolysaccharide synthesis results in an outer membrane that is resistant to this perturbation. Our observations challenge current understanding of lipopolysaccharide chemistry and antibiotic exclusion, provide new chemical insights into the susceptibility of a model Gram-negative bacterium to glycopeptide antibiotics, and offer novel phenotypes to leverage in the development of antibiotics and antibiotic adjuvants active against Gram-negative bacteria.

Experimental Procedures

Antibiotic potency analysis. Overnight cultures of wild type *E. coli* BW25113 and Y324* mutant were diluted 1000-fold in fresh LB media and introduced compound diluted in 2-fold increments. Glycopeptides were a generous gift from Dr. Gerry Wright. All other antibiotics were purchased from Sigma Aldrich. Cells were incubated to early-stationary phase at 42°C (16 hours), 37°C (18 hours), 30°C (24 hours), 25°C (36 hours), 20°C (48 hours), and 15°C (72 hours) in a stationary Eppendorf Innova 44 incubator (Eppendorf) and read using a Perkin

Elmer EnVision plate reader at 600 nm (Perkin Elmer). Cells were grown in Costar 96-well plates in a final volume of 100 μ l (Costar).

vanHBX cloning and expression. The *vanH*, *vanB*, and *vanX* genes from the *E. faecalis* pMG2200 plasmid²⁸ were codon optimized for *E. coli* and cloned behind the arabinose-inducible promoter in the pBAD30 expression vector (pBAD30-*vanHBX* GenBank accession number: KM013476). To test for vancomycin resistance, overnight cultures of *E. coli*-pBAD30-*vanHBX* were diluted 1000-fold in fresh LB media containing 100 μ g/ml ampicillin and 0.2% arabinose. Cells were grown to mid log (OD=0.5) at either 15°C or 37°C, at which time cells were diluted 100-fold into fresh LB containing 100 μ g/ml ampicillin and 0.2% arabinose, and introduced to vancomycin. Cells were incubated at 37°C (18 hours) or 15°C (72 hours) and read at 600 nm. Unless otherwise stated, cells were outgrown to mid log and incubated with vancomycin at the same temperature.

Fluorescence microscopy. Overnight cultures of wild type *E. coli* BW25113 and Y324* mutant were diluted 1000-fold in fresh LB media and introduced to varying concentrations of vancomycin (0-7 μ g/ml) in a final volume of 5 ml. Cells were grown at 15°C to early log phase (OD=0.2) and subsequently stained with FM4-64 (Life Technologies), and imaged using an inverted Nikon Eclipse TE-200 microscope (Nikon).

Transmission electron microscopy. Overnight cultures of wild type *E. coli* BW25113 and Y324* mutant were diluted 1000-fold in fresh LB media and grown at 15°C in the presence of 4 μ g/ml vancomycin or without drug. Cells were grown

to early log phase (OD=0.2), washed in 50 mM HEPES (pH 6.8), and fixed in HEPES with 2% glutaraldehyde for one hour in the dark. Cells were washed, incubated with osmium tetroxide for 10 minutes, washed, and mixed with 2% noble agar (Sigma Aldrich). Agar cubes (~1 x 2 mm in size) were subjected to a 50%, 70%, 90%, and ~100% (2x) ethanol dehydration series. Samples were infiltrated with 1:1 ethanol:LR White resin (Sigma Aldrich), followed by LR White alone. The cubes were set in gelatin capsules, and cured at 60°C for 18 hours. Ultrathin sections were prepared on formvar-coated copper grids, stained with 2% uranyl acetate and lead citrate, washed, and imaged using a Philips CM-10 electron microscope (Philips).

Divalent cation suppression analysis. Overnight cultures of wild type *E. coli* BW25113 and Y324* mutant were diluted 1000-fold in fresh LB media and vancomycin suppression was determined by conducting standard checkerboard broth micro-dilution assays with nine serially diluted concentrations of vancomycin, and CaCl₂ or MgCl₂ (Sigma Aldrich). Checkerboards were incubated at 37°C (18 hours) and 15°C (72 hours) in the same growth conditions as outlined above.

Screening for vancomycin resistance. The *E. coli* Keio collection was pinned from frozen stocks on LB agar using 96-well pins in duplicate. These plates were then scaled to 1536 density using a Singer RoToR automated pinning system (Singer Instruments). Vancomycin was added to LB agar to a final concentration of 32 µg/ml, and the Keio collection was pinned at 1536 density onto these plates

and grown at 37°C (18 hours) and 15°C (72 hours). Plates were scanned in transmissive mode on an Epson Perfection V750-M scanner (Epson) and quantitatively analyzed using ImageJ. Plate images were background subtracted using a 50-pixel rolling ball radius and converted to a binary image using the Otsu algorithm to identify colony margins. With colony margins identified, the integrated density (light absorption) of each was calculated as an indicator of cell number. Edge effects were corrected using a double-pass method across columns and rows based on the median value⁵³. Strains grown at 15°C in the presence of vancomycin with growth at least 3σ greater than the mean were defined as resistant.

Suppressor mutant generation and sequencing. Overnight cultures of *E. coli* BW25113 were diluted 1000-fold in 10 ml of LB media containing 5 x MIC (40 µg/ml) of vancomycin and grown with shaking at 15°C until the media became turbid. Putative suppressors from this culture were streaked onto LB agar and LB agar supplemented with vancomycin to assess mutational stability and purify suppressor strains, respectively. A single suppressor strain was subsequently selected for resistance to vancomycin, and chromosomal DNA was purified for sequencing using a Qiagen Genra Puregene kit (Qiagen). Suppressor DNA was sequenced on an Illumina MiSeq (Illumina) platform and reads were aligned to the *E. coli* MG1655 chromosome (NC_000913) to identify the mutations responsible for vancomycin resistance.

Gel electrophoresis. Cells were grown in LB media at 37°C and 15°C until early log phase (OD=0.2), and equivalent amounts of cells based on OD were boiled in SDS-PAGE loading buffer for 10 minutes and subsequently treated with proteinase K at 55°C overnight. The whole cell lysates were resolved on NuPAGE Novex 4-12% Bis-Tris gradient gels (Life Technologies) and LPS was visualized by silver staining. Minor variations between wild type sample banding patterns can be attributed to slight differences in growth and/or silver staining efficiency between samples.

Isolation of LPS. Cultures of wild type *E. coli* BW25113 and the Y324* mutant were grown overnight at 37°C and 15°C, and cells were harvested by centrifugation prior to being lyophilized. Cell pellets were resuspended in 50 ml of 50 mM Tris-Cl pH 7.5, 5 mM EDTA per 5 g dry cell weight, and cells were disrupted by sonication followed by treatment with hen egg white lysozyme with stirring at 4°C for 16 hours. Total volume was adjusted to 100 ml per 5 g dry weight, adjusted to 10 mM MgCl₂, and the mixture was incubated at 37°C for 10 minutes. DNase and RNase were added each to 1 µg/ml and the mixture was incubated at 37°C for 10 minutes followed by 60°C for 20 minutes. To isolate LPS, an equal volume of 90% phenol was added to perform hot phenol-water extraction using the Westphal method⁵⁴. The extraction mixture was cooled and centrifuged at 10,000 x g for 15 minutes, the aqueous phase was collected, dialyzed against water, and lyophilized. The resulting crude LPS was purified by ultracentrifugation at 105,000 x g for 16 hours at 4°C.

Mild acid degradation of LPS. LPS samples were hydrolyzed with 2% acetic acid at 100°C for 1 to 2 hours, and the lipid precipitate was removed by centrifugation at 13,000 x g for 20 minutes. The carbohydrate-containing supernatant was fractionated by gel chromatography on a Sephadex G-50 superfine column (2.5 cm x 75 cm) in 50 mM pyridinium acetate buffer pH 4.5 at a flow rate of 0.6 ml/min to give high molecular mass polysaccharide (fraction I, presumably colanic acid), one or two core oligosaccharide fractions (fraction II in wild type *E. coli*; fractions IIa and IIb in the Y324* mutant), and low molecular weight compounds (fraction III). Elution was monitored by a differential refractometer. Lipid A was additionally purified by three extractions with 2:1:3 (v/v/v) chloroform/methanol/water mixture in order to remove membrane phospholipids.

Mass spectrometry. Negative-ion electrospray ionization mass spectrometry was performed using an amaZon SL ion-trap mass-spectrometer (Bruker) in the Advanced Analysis Centre at the University of Guelph. Fraction II samples were dissolved in a 1:1 (v/v) water/acetonitrile solution, and lipid A samples were dissolved in a 2:1 (v/v) chloroform/methanol solution. Samples were sprayed at a flow rate of 10 µl/min. Capillary entrance and exit voltages were set to 4 kV and 140 V, respectively; the drying gas temperature was 300°C. The spectra were charge deconvoluted using Bruker Compass DataAnalysis 4.2 software (Bruker). Mass numbers given refer to monoisotopic molecular masses.

Author Contributions

J.M.S., E.D.B. conceived and designed the project. J.M.S., S.F., O.G.O., C.B. performed experiments and analyzed data. J.M.S., S.F., O.G.O., C.W., E.D.B. wrote the manuscript, J.M.S., E.D.B. revised the manuscript.

Acknowledgements

This work was supported by the Natural Sciences and Engineering Research Council (Discovery Grant to E.D.B.), by grants from the Canadian Institutes of Health Research to E.D.B. and C.W., by salary awards to E.D.B. and C.W. from the Canada Research Chairs Program, by a fellowship from the Canadian Institutes of Health Research Drug Safety and Effectiveness Cross-Disciplinary Training Program to S.F., and by scholarships awarded to J.M.S. from the Canadian Institutes of Health Research and the Ontario Graduate Scholarships Program.

References

1. Nikaido, H. Molecular basis of bacterial outer membrane permeability revisited. *Microbiol Mol Biol Rev.* **67**, 593–656 (2003).
2. Bush, K. *et al.* Tackling antibiotic resistance. *Nat Rev Microbiol.* **9**, 894–896 (2011).
3. Perros, M. Infectious disease. A sustainable model for antibiotics. *Science* **347**, 1062–1064 (2015).
4. Payne, D. J., Gwynn, M. N., Holmes, D. J. & Pompliano, D. L. Drugs for bad bugs: confronting the challenges of antibacterial discovery. *Nat Rev Drug Discov.* **6**, 29–40 (2006).

5. Tommasi, R., Brown, D. G., Walkup, G. K., Manchester, J. I. & Miller, A. A. ESKAPEing the labyrinth of antibacterial discovery. *Nat Rev Drug Discov.* **14**, 529–542 (2015).
6. IMI. <https://www.imi.europa.eu/content/translocation> (2015).
7. Whitfield, C. & Trent, M. S. Biosynthesis and export of bacterial lipopolysaccharides*. *Annu Rev Biochem.* **83**, 99–128 (2014).
8. Stevenson, G. *et al.* Structure of the O antigen of *Escherichia coli* K-12 and the sequence of its rfb gene cluster. *J Bacteriol.* **176**, 4144–4156 (1994).
9. Heinrichs, D. E., Yethon, J. A. & Whitfield, C. Molecular basis for structural diversity in the core regions of the lipopolysaccharides of *Escherichia coli* and *Salmonella enterica*. *Mol Microbiol.* **30**, 221–232 (1998).
10. Raetz, C. R. & Whitfield, C. Lipopolysaccharide endotoxins. *Annu Rev Biochem.* **71**, 635–700 (2002).
11. Schneck, E. *et al.* Quantitative determination of ion distributions in bacterial lipopolysaccharide membranes by grazing-incidence X-ray fluorescence. *Proc Natl Acad Sci U.S.A.* **107**, 9147–9151 (2010).
12. Herrera, C. M., Hankins, J. V. & Trent, M. S. Activation of PmrA inhibits LpxT-dependent phosphorylation of lipid A promoting resistance to antimicrobial peptides. *Mol Microbiol.* **76**, 1444–1460 (2010).
13. Bishop, R. E. *et al.* Transfer of palmitate from phospholipids to lipid A in outer membranes of gram-negative bacteria. *EMBO J.* **19**, 5071–5080 (2000).
14. Reinés, M. *et al.* Molecular basis of *Yersinia enterocolitica* temperature-dependent resistance to antimicrobial peptides. *J Bacteriol.* **194**, 3173–3188 (2012).
15. Clements, A. *et al.* Secondary acylation of *Klebsiella pneumoniae* lipopolysaccharide contributes to sensitivity to antibacterial peptides. *J Biol Chem.* **282**, 15569–15577 (2007).
16. Vorachek-Warren, M. K., Carty, S. M., Lin, S., Cotter, R. J. & Raetz, C. R. H. An *Escherichia coli* mutant lacking the cold shock-induced palmitoleoyltransferase of lipid A biosynthesis: absence of unsaturated acyl chains and antibiotic hypersensitivity at 12 degrees C. *J Biol Chem.* **277**,

14186–14193 (2002).

17. Carty, S. M., Sreekumar, K. R. & Raetz, C. R. Effect of cold shock on lipid A biosynthesis in *Escherichia coli*. Induction At 12 degrees C of an acyltransferase specific for palmitoleoyl-acyl carrier protein. *J Biol Chem.* **274**, 9677–9685 (1999).
18. Frirdich, E. & Whitfield, C. Lipopolysaccharide inner core oligosaccharide structure and outer membrane stability in human pathogens belonging to the Enterobacteriaceae. *J Endotoxin Res.* **11**, 133–144 (2005).
19. Vaara, M. Outer membrane permeability barrier to azithromycin, clarithromycin, and roxithromycin in gram-negative enteric bacteria. *Antimicrob Agents Chemother.* **37**, 354–356 (1993).
20. Shlaes, D. M., Shlaes, J. H., Davies, J. & Williamson, R. *Escherichia coli* susceptible to glycopeptide antibiotics. *Antimicrob Agents Chemother.* **33**, 192–197 (1989).
21. Morones-Ramirez, J. R., Winkler, J. A., Spina, C. S. & Collins, J. J. Silver enhances antibiotic activity against gram-negative bacteria. *Sci Transl Med.* **5**, 190ra81 (2013).
22. Vaara, M. Antibiotic-supersusceptible mutants of *Escherichia coli* and *Salmonella typhimurium*. *Antimicrob Agents Chemother.* **37**, 2255–2260 (1993).
23. Liu, A. *et al.* Antibiotic sensitivity profiles determined with an *Escherichia coli* gene knockout collection: generating an antibiotic bar code. *Antimicrob Agents Chemother.* **54**, 1393–1403 (2010).
24. Stokes, J. M., Davis, J. H., Mangat, C. S., Williamson, J. R. & Brown, E. D. Discovery of a small molecule that inhibits bacterial ribosome biogenesis. *Elife* **3**, e03574 (2014).
25. Chatterjee, S. *et al.* Balhimycin, a new glycopeptide antibiotic with an unusual hydrated 3-Amino-4-oxoaldopyranose sugar moiety. *J Org Chem.* **59**, 3480–3484 (1994).
26. Kaplan, J., Korty, B. D., Axelsen, P. H. & Loll, P. J. The role of sugar residues in molecular recognition by vancomycin. *J Med Chem.* **44**, 1837–1840 (2001).
27. Kalan, L., Perry, J., Koteva, K., Thaker, M. & Wright, G. Glycopeptide

- Sulfation Evades Resistance. *J Bacteriol.* **195**, 167–171 (2012).
28. Zheng, B., Tomita, H., Inoue, T. & Ike, Y. Isolation of VanB-type *Enterococcus faecalis* strains from nosocomial infections: first report of the isolation and identification of the pheromone-responsive plasmids pMG2200, Encoding VanB-type vancomycin resistance and a Bac41-type bacteriocin, and pMG2201, encoding erythromycin resistance and cytolysin (Hly/Bac). *Antimicrob Agents Chemother.* **53**, 735–747 (2009).
 29. Marshall, C. G., Lessard, I. A. D., Park, I. S. & Wright, G. D. Glycopeptide antibiotic resistance genes in glycopeptide-producing organisms. *Antimicrob Agents Chemother.* **42**, 2215–2220 (1998).
 30. Barna, J. C. & Williams, D. H. The structure and mode of action of glycopeptide antibiotics of the vancomycin group. *Annu Rev Microbiol.* **38**, 339–357 (1984).
 31. Walsh, C. T., Fisher, S. L., Park, I. S., Prahalad, M. & Wu, Z. Bacterial resistance to vancomycin: five genes and one missing hydrogen bond tell the story. *Chem Biol.* **3**, 21–28 (1996).
 32. Clifton, L. A. *et al.* Effect of divalent cation removal on the structure of Gram-negative bacterial outer membrane models. *Langmuir* **31**, 404–412 (2014).
 33. Baba, T. *et al.* Construction of *Escherichia coli* K-12 in-frame, single-gene knockout mutants: the Keio collection. *Mol Syst Biol.* **2**, 2006:0008 (2006).
 34. Tatusov, R. L., Koonin, E. V. & Lipman, D. J. A genomic perspective on protein families. *Science* **278**, 631–637 (1997).
 35. Tatusov, R. L. *et al.* The COG database: an updated version includes eukaryotes. *BMC Bioinformatics* **4**, 41 (2003).
 36. Lu, M. & Kleckner, N. Molecular cloning and characterization of the pgm gene encoding phosphoglucomutase of *Escherichia coli*. *J Bacteriol.* **176**, 5847–5851 (1994).
 37. Paterson, G. K., Cone, D. B., Peters, S. E. & Maskell, D. J. The enzyme phosphoglucomutase (Pgm) is required by *Salmonella enterica* serovar Typhimurium for O-antigen production, resistance to antimicrobial peptides and in vivo fitness. *Microbiology* **155**, 3403–3410 (2009).
 38. Coyne, M. J., Russell, K. S., Coyle, C. L. & Goldberg, J. B. The

- Pseudomonas aeruginosa* algC gene encodes phosphoglucomutase, required for the synthesis of a complete lipopolysaccharide core. *J Bacteriol.* **176**, 3500–3507 (1994).
39. McKay, G. A., Woods, D. E., MacDonald, K. L. & Poole, K. Role of phosphoglucomutase of *Stenotrophomonas maltophilia* in lipopolysaccharide biosynthesis, virulence, and antibiotic resistance. *Infect Immun.* **71**, 3068–3075 (2003).
 40. West, N. P. *et al.* Role of phosphoglucomutase of *Bordetella bronchiseptica* in lipopolysaccharide biosynthesis and virulence. *Infect Immun.* **68**, 4673–4680 (2000).
 41. Mares, J., Kumaran, S., Gobbo, M. & Zerbe, O. Interactions of lipopolysaccharide and polymyxin studied by NMR spectroscopy. *J Biol Chem.* **284**, 11498–11506 (2009).
 42. Felek, S. *et al.* Phosphoglucomutase of *Yersinia pestis* is required for autoaggregation and polymyxin B resistance. *Infect Immun.* **78**, 1163–1175 (2010).
 43. Broeze, R. J., Solomon, C. J. & Pope, D. H. Effects of low temperature on in vivo and in vitro protein synthesis in *Escherichia coli* and *Pseudomonas fluorescens*. *J Bacteriol.* **134**, 861–874 (1978).
 44. Shajani, Z., Sykes, M. T. & Williamson, J. R. Assembly of Bacterial Ribosomes. *Annu Rev Biochem.* **80**, 501–526 (2011).
 45. Yethon, J. A., Heinrichs, D. E., Monteiro, M. A., Perry, M. B. & Whitfield, C. Involvement of waaY, waaQ, and waaP in the modification of *Escherichia coli* lipopolysaccharide and their role in the formation of a stable outer membrane. *J Biol Chem.* **273**, 26310–26316 (1998).
 46. Yethon, J. A., Vinogradov, E., Perry, M. B. & Whitfield, C. Mutation of the lipopolysaccharide core glycosyltransferase encoded by waaG destabilizes the outer membrane of *Escherichia coli* by interfering with core phosphorylation. *J Bacteriol.* **182**, 5620–5623 (2000).
 47. Shibayama, K., Ohsuka, S., Tanaka, T., Arakawa, Y. & Ohta, M. Conserved structural regions involved in the catalytic mechanism of *Escherichia coli* K-12 WaaO (RfaI). *J Bacteriol.* **180**, 5313–5318 (1998).
 48. Müller-Loennies, S., Lindner, B. & Brade, H. Structural analysis of oligosaccharides from lipopolysaccharide (LPS) of *Escherichia coli* K12

strain W3100 reveals a link between inner and outer core LPS biosynthesis. *J Biol Chem.* **278**, 34090–34101 (2003).

49. Nikaido, H. Preventing drug access to targets: cell surface permeability barriers and active efflux in bacteria. *Semin Cell Dev Biol.* **12**, 215–223 (2001).
50. Ray, M. K., Kumar, G. S. & Shivaji, S. Phosphorylation of lipopolysaccharides in the Antarctic psychrotroph *Pseudomonas syringae*: a possible role in temperature adaptation. *J Bacteriol.* **176**, 4243–4249 (1994).
51. Nikaido, H. Restoring permeability barrier function to outer membrane. *Chem Biol.* **12**, 507–509 (2005).
52. Ferguson, A. D. *et al.* Active transport of an antibiotic rifamycin derivative by the outer-membrane protein FhuA. *Structure* **9**, 707–716 (2001).
53. Mangat, C. S., Bharat, A., Gehrke, S. S. & Brown, E. D. Rank ordering plate data facilitates data visualization and normalization in high-throughput screening. *J Biomol Screen.* **19**, 1314–1320 (2014).
54. Westphal, O. & Jann, K. Bacterial lipopolysaccharides: extraction with phenol-water and further applications of the procedure. *Methods Carbohydr Chem.* **5**, 83–91 (1965).

Figure Legends

Figure 1. Vancomycin inhibits growth of *E. coli* in a temperature-dependent

manner. (a) Top: potency analysis of vancomycin against wild type *E. coli* at 42°C, 37°C, 30°C, 25°C, 20°C, and 15°C. Light to dark shaded symbols represent increasing temperatures from 20°C to 42°C. Open circles represent cells grown at 15°C. Bottom: potency analysis of vancomycin at 15°C against *E. coli* harboring pBAD30-*vanHBX* (filled circles) or empty pBAD30 plasmid (open circles). Black circles represent cultures induced with 0.2% arabinose. Grey circles represent no induction. All experiments were performed in duplicate and

varied by <10%. (b) Morphology of wild type *E. coli* grown at 15°C in the presence of increasing concentrations of vancomycin. Cells were grown to early log phase in the presence of vancomycin and stained with FM4-64 prior to visualization. (c) TEM of wild type *E. coli* grown at 15°C in the presence of DMSO (left) or 4 µg/ml vancomycin (right). Arrows indicate regions where the outer membrane and inner membrane have detached. Scale bars represent 1 µm. (d) Suppression of vancomycin activity at 37°C (red) and 15°C (blue) by titration of Ca²⁺ or Mg²⁺. See also Figure S1 and S2.

Figure 2. Genetic perturbations in outer membrane biosynthesis cause vancomycin resistance. (a) Vancomycin activity against the *E. coli* Keio collection at 15°C. All growth data is normalized to 1. Red circles show gene-deletion strains that grew 3σ or greater above the mean of the entire collection, as measured by integrated density. 41 strains were vancomycin resistant using this criterion (see Table S1). Inset shows replicate plot of normalized growth data. (b) Classification of 41 vancomycin resistant Keio strains based on clusters of orthologous groups. (c) Potency analysis of vancomycin against the Y324* mutant *E. coli* at 42°C, 37°C, 30°C, 25°C, 20°C, and 15°C. Light to dark shaded symbols represent increasing temperatures from 20°C to 42°C. Open circles represent cells grown at 15°C. All experiments were performed in duplicate and varied by <10%. (d) Morphology of the Y324* mutant *E. coli* grown at 15°C in the presence of increasing concentrations of vancomycin. Cells were grown to early

log phase in the presence of vancomycin and stained with FM4-64 prior to visualization. See also Figure S3 and S4.

Figure 3. LPS profiles of vancomycin-sensitive and -resistant *E. coli* strains.

Cells were grown in LB media at 37°C and 15°C until early log phase and equal amounts of proteinase K-treated whole-cell lysates were subjected to SDS-PAGE followed by silver staining. (a) A selection of vancomycin sensitive *E. coli* Keio mutants. Skp; periplasmic chaperone. LpxL/M; lipid A acylation. WaaJ/L/O/P; LPS core biosynthesis. (b) A selection of vancomycin resistant *E. coli* Keio mutants. GalU, Pgm; UDP-glucose biosynthesis. LpcA, RfaE, WaaB/F/G/Q/Y; LPS core biosynthesis. (c) Y324* mutant *E. coli* grown at 37°C and 15°C. (d) The structure of *E. coli* K-12 core OS and genes involved in its biosynthesis. Inner core is shown in red and outer core is shown in blue. Asterisks highlight biosynthetic genes that are functionally interdependent. The solid black line defines the distal region of outer core where loss-of-function mutations do not impact vancomycin susceptibility.

Figure 4. Modifications in LPS chemistry affect vancomycin activity in *E.*

***coli*.** Charge-deconvoluted negative-ion ESI mass spectra of core OS isolated from *E. coli* strains grown at 37°C (left column) and 15°C (right column). (a) Wild type *E. coli* fraction II. (b) Y324* mutant fraction IIa. (c) Y324* mutant fraction IIb. All core OS fractions were found to be heterogeneous in composition to some extent, and differed in the presence of Kdo in normal and anhydro forms (Δm 18 u), as well as the content of phosphate (Δm 80 u – blue bars),

phosphoethanolamine (Δm 123 u – orange bars), hexose (Δm 162 u – purple bars), and heptose (Δm 192 u – green bars). See also Figure S5 and S6.

Figure 5. Proposed structures of core OS from wild type and Y324* mutant

E. coli. (a) Core OS species found in fraction II in wild type and fraction IIa in the Y324* mutant. Note that at 15°C, core species contained an additional one or two phosphate groups at currently unknown positions. Furthermore, the abundance of glycoform I is significantly reduced in the Y324* mutant at 15°C relative to wild type. (b) Core OS species found in fraction IIb from the Y324* mutant. For all structures, inner core is shown in red and outer core is shown in blue.

Figure 6. Proposed model for vancomycin activity in *E. coli* at low growth

temperature. (a) X-ray structure of *E. coli* LPS isolated from PDB 1FI1. Lipid A is shown in pink, Kdo is shown in blue, and core OS is shown in green. At 15°C, lipid A would contain a palmitoleate acyl chain at the location marked by *. Additionally, our results show an additional one or two phosphates in core OS at currently unexplored locations. The maximum depth of core OS relative to lipid A is ~20Å (side view – right). (b) Simplified depiction of the cell surface in wild type and (c) vancomycin resistant *E. coli*. Grey circles represent divalent cations.

Supplemental Figure Legends

Figure S1 – related to Figure 1. Growth of *E. coli* at 37°C and 15°C. (a)

Growth curves of wild type *E. coli* in LB at 37°C (left) and 15°C (right). Overnight cultures were diluted 1000-fold in fresh LB media and grown in 96-well plates in a

final volume of 100 μ l with shaking at 250 rpm to obtain precise curves. While growth rates are reduced in the absence of shaking, no differences in culture densities during the various phases of growth are observed whether cells are grown with or without agitation. (b) Potency analysis of vancomycin against wild type *E. coli* at 37°C (black) and 15°C (grey) with shaking at 250 rpm. All experiments were performed in duplicate and varied by <10%.

Figure S2 – related to Figure 1. Temperature-dependent activity of glycopeptides against *E. coli*. (a) Potency analyses of teicoplanin class glycopeptides (top row) and vancomycin analogs (bottom row). Wild type *E. coli* was grown in the presence of each molecule at 37°C (black) and 15°C (grey). All experiments were performed in duplicate and varied by <10%. (b) Structures of all glycopeptides tested for temperature-dependent activity against *E. coli*.

Teicoplanins are along the top row and vancomycins along the bottom. (c) Effect of outgrowth temperature on *E. coli* harboring pBAD30-*vanHBX*. Cells harboring pBAD30-*vanHBX* (filled circles) or empty pBAD30 plasmid (open circles) were either outgrown at 37°C and grown with vancomycin at 15°C (grey) or outgrown at 15°C and grown with vancomycin at 37°C (black). All cultures were induced with 0.2% arabinose. All experiments were performed in duplicate and varied by <10%. (d) Potency analysis of vancomycin at 37°C against *E. coli* harboring pBAD30-*vanHBX* (filled circles) or empty pBAD30 plasmid (open circles). Black circles show cultures induced with 0.2% arabinose. Grey circles represent no induction. All experiments were performed in duplicate and varied by <10%.

Figure S3 – related to Figure 2. Phenotypic characterization of vancomycin resistant *E. coli* strains. (a) Screen of the *E. coli* Keio collection at 37°C in the presence of 32 µg/ml vancomycin (left), at 15°C without drug (middle), and at 37°C without drug (right). Cells were pinned on LB agar and grown for 72 hours at 15°C or 18 hours at 37°C at 1536 density in duplicate. All growth data is normalized to 1. Red circles show the growth of vancomycin resistant gene-deletion strains in different growth conditions. Insets show replicate plots of normalized growth data. (b) TEM of the Y324* mutant *E. coli* grown at 15°C in the presence of DMSO (left) or 4 µg/ml vancomycin (right). Scale bars represent 1 µm. (c) Suppression of vancomycin activity at 37°C (red) and 15°C (blue) by titration of Ca²⁺ or Mg²⁺ using checkerboard dilution assays. (d) Activity of structurally and functionally diverse antibiotics against wild type *E. coli* (filled circles) and Y324* mutant *E. coli* (open circles) grown at 37°C (black) and 15°C (grey). All experiments were performed in duplicate and varied by <10%.

Figure S4 – related to Figure 2. Antibiotic susceptibility of a core-OS deficient $\Delta rfaE$ strain of *E. coli*. Activity of structurally and functionally diverse antibiotics against wild type *E. coli* (filled circles) and a $\Delta rfaE$ strain of *E. coli* (open circles) grown at 37°C (black) and 15°C (grey). Note that similarly to the Y324* mutant, the $\Delta rfaE$ strain is resistant to balhimycin, displays increased resistance to hydrophobic antibiotics at 15°C relative to 37°C, and is highly sensitive to polymyxin B. All experiments were performed in duplicate and varied by <10%.

Figure S5 – related to Figure 4. Charge-deconvoluted negative-ion ESI mass spectra of core OS isolated from wild type *E. coli* and Y324* mutant. The left column shows mass spectra from cells grown at 37°C and the right column shows those from cells grown at 15°C. (a) Wild type *E. coli* fraction II. (b) Y324* mutant fraction IIa. (c) Y324* mutant fraction IIb. All core OS fractions were found to be heterogeneous in composition to some extent, and differed in the presence of Kdo in normal and anhydro forms, as well as the content of phosphate, phosphoethanolamine, hexose, and heptose. The mass numbers given refer to monoisotopic molecular masses.

Figure S6 – related to Figure 4. Charge-deconvoluted negative-ion ESI mass spectra of lipid A isolated from wild type *E. coli* and Y324* mutant. The left column shows mass spectra from cells grown at 37°C and the right column shows those from cells grown at 15°C. Top panels are data gathered from wild type cells and bottom are from the Y324* mutant. No substantial differences are observed between wild type and mutant strains at either growth temperature. The mass numbers given refer to monoisotopic molecular masses.

Table S1 – related to Figure 2. *E. coli* Keio strains that displayed resistance to vancomycin at 15°C.

Gene	COG	Function
<i>galU</i>	G	UTP-glucose-1-phosphate uridylyltransferase
<i>opgG</i>	G	Periplasmic protein; synthesis of osmoregulated periplasmic glucans
<i>opgH</i>	G	Membrane glycosyltransferase; synthesis of osmoregulated periplasmic glucans
<i>pgm</i>	G	Phosphoglucomutase
<i>ccmC</i>	H	ABC complex for formation and release of holoCcmE; membrane subunit
<i>gshB</i>	H	Glutathione synthetase
<i>gmr</i>	K	Cyclic di-GMP phosphodiesterase
<i>narL</i>	K	DNA-binding transcriptional dual regulator
<i>recQ</i>	K	ATP-dependent DNA helicase
<i>fadR</i>	K/I	DNA-binding transcriptional dual regulator
<i>fliA</i>	K/N	RNA polymerase; sigma 28 (sigma F) factor
<i>csgA</i>	M	Curlin major subunit
<i>lapA</i>	M	Lipopolysaccharide assembly protein LapA
<i>lpcA</i>	M	D-sedoheptulose 7-phosphate isomerase
<i>miaA</i>	M	Outer membrane protein; involved in preserving outer membrane lipid asymmetry
<i>miaC</i>	M	Phospholipid ABC transporter; periplasmic binding protein
<i>miaD</i>	M	Phospholipid ABC transporter; substrate binding protein
<i>miaE</i>	M	Phospholipid ABC transporter; integral membrane subunit
<i>miaF</i>	M	Phospholipid ABC transporter; ATP binding subunit
<i>wzzE</i>	M	Enterobacterial common antigen polysaccharide chain length modulation protein
<i>waaY</i>	M	Lipopolysaccharide core heptose (II) kinase
<i>fliC</i>	M/N	Flagellar biosynthesis; flagellin; filament structural protein
<i>lgoT</i>	M/G	Galactonate:H ⁺ symporter
<i>rfaE</i>	M/G	Fused heptose 7-phosphate kinase; heptose 1-phosphate adenyltransferase
<i>rfe</i>	M/G	Undecaprenyl-phosphate α -N-acetylglucosaminyl transferase
<i>rffH</i>	M/G	dTDP-glucose pyrophosphorylase
<i>waaB</i>	M/G	UDP-D-galactose:(glucosyl)lipopolysaccharide-1,6-D-galactosyltransferase
<i>waaF</i>	M/G	ADP-heptose:LPS heptosyltransferase II
<i>waaG</i>	M/G	Lipopolysaccharide glucosyltransferase I
<i>waaQ</i>	M/G	Lipopolysaccharide heptosyltransferase III
<i>yceG</i>	R	Protein involved in cytokinesis
<i>yegS</i>	R	Lipid kinase
<i>flxA</i>	S	Qin prophage; predicted protein
<i>racC</i>	S	Rac prophage; predicted protein
<i>yaiP</i>	S	Predicted glucosyltransferase
<i>ybfP</i>	S	Predicted protein
<i>ybjN</i>	S	Predicted oxidoreductase
<i>ycho</i>	S	Predicted invasin
<i>yhbG</i>	S	Predicted protein; hydrophobic drug sensitivity
<i>acrA</i>	U	AcrAB-TolC multidrug efflux system; membrane fusion protein
<i>tolC</i>	U	Outer membrane channel

Figure 1

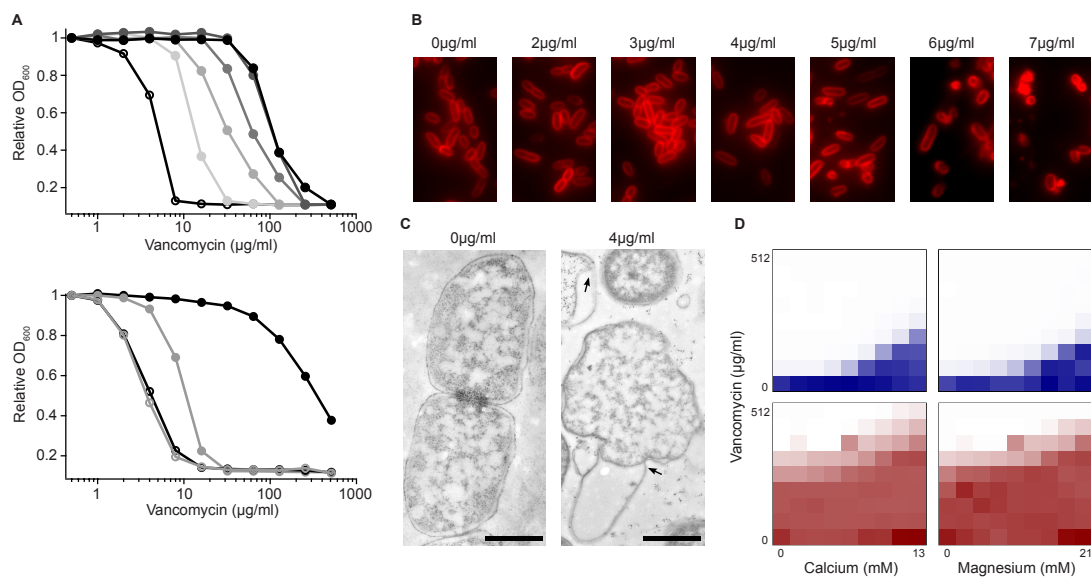


Figure 2

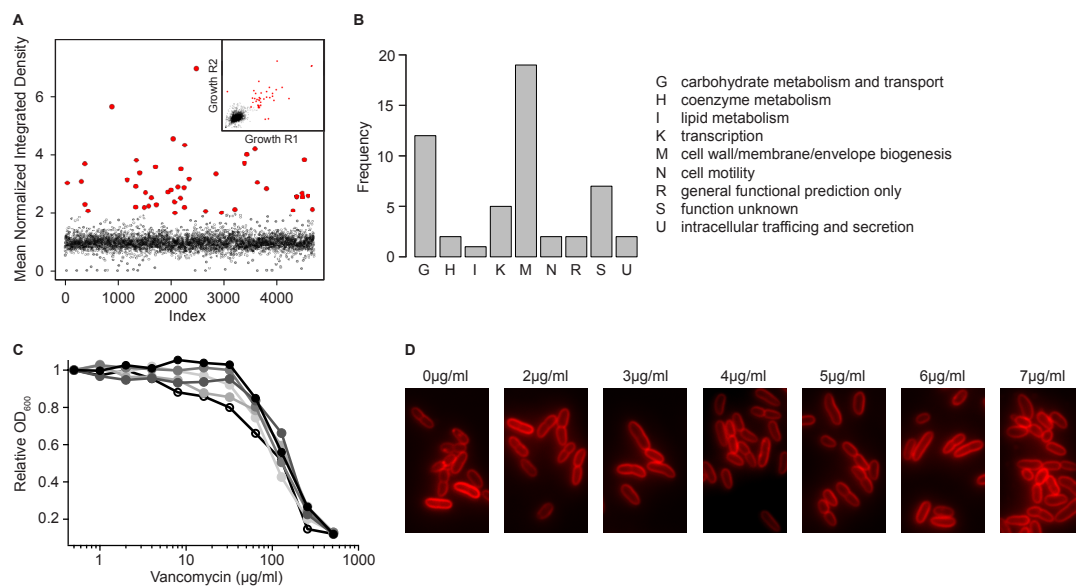


Figure 3

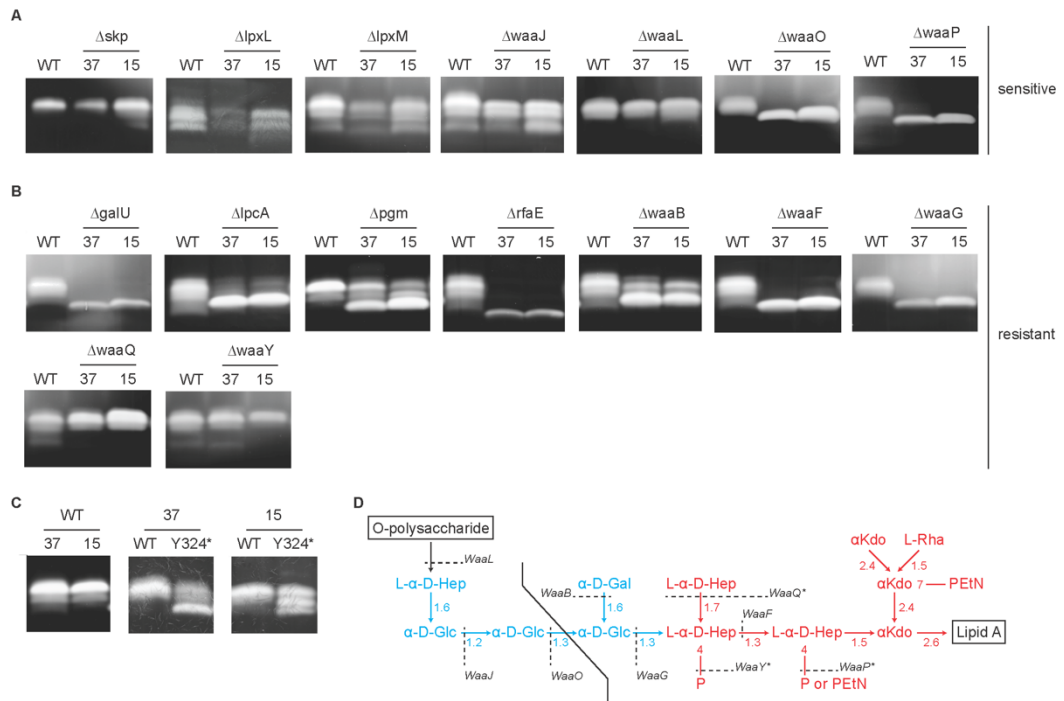


Figure 4

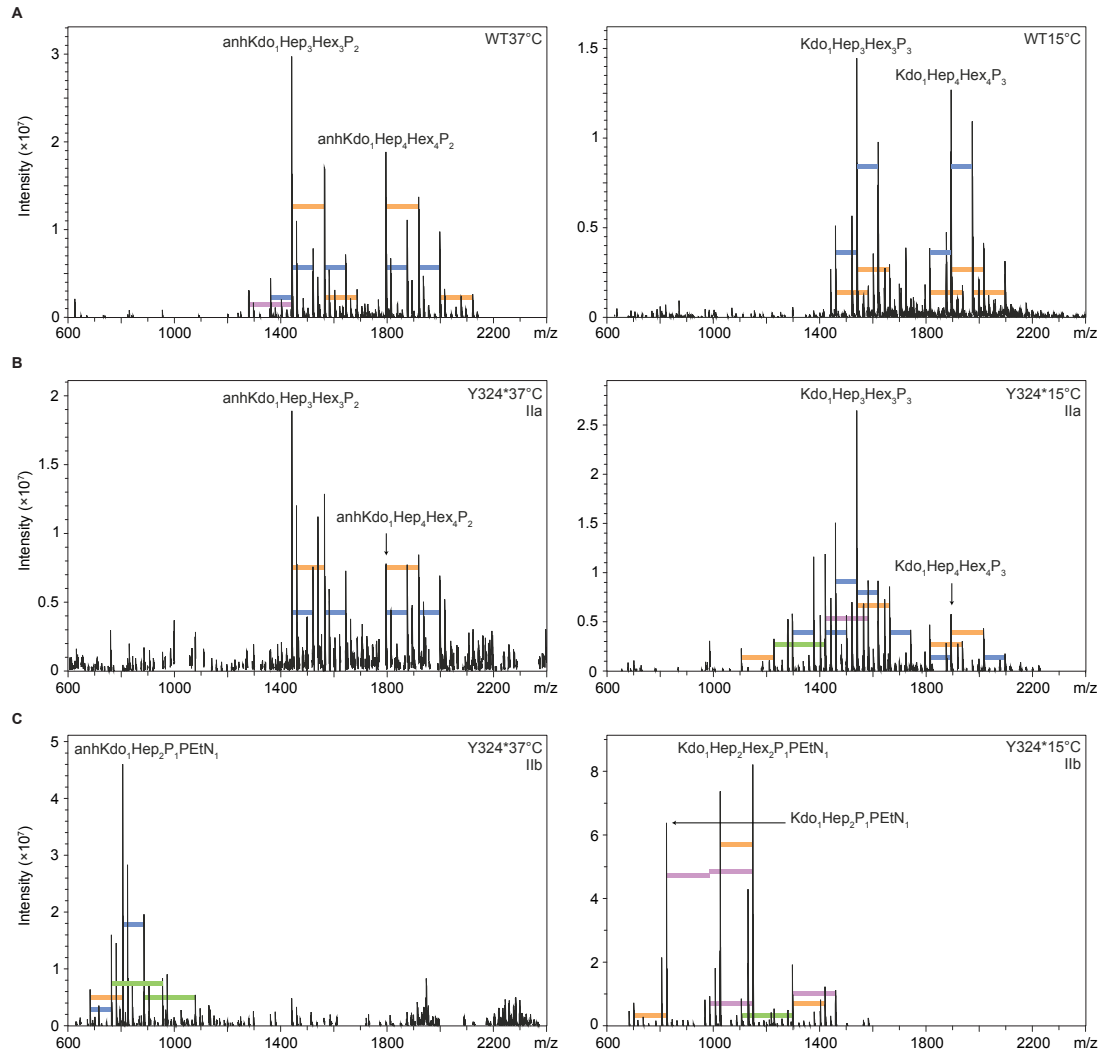


Figure 5

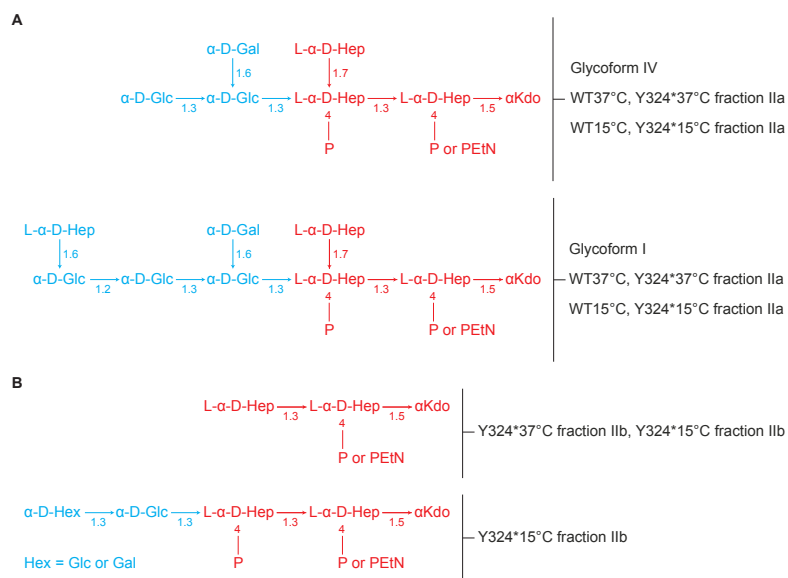


Figure 6

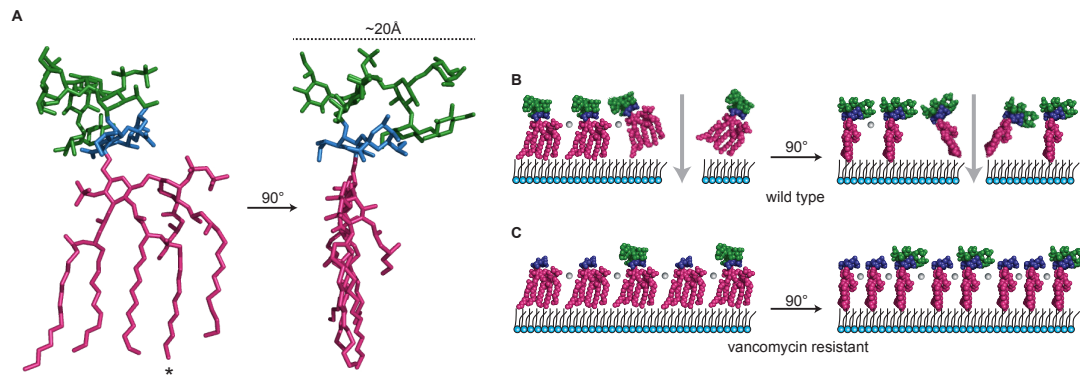


Figure S1

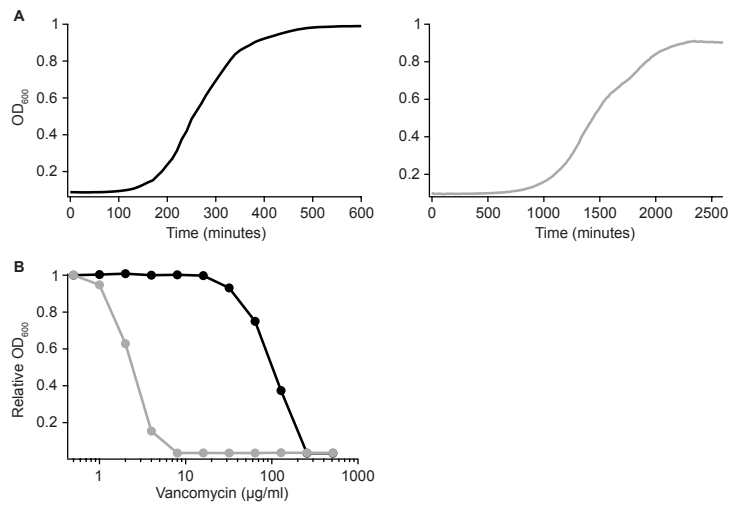


Figure S2

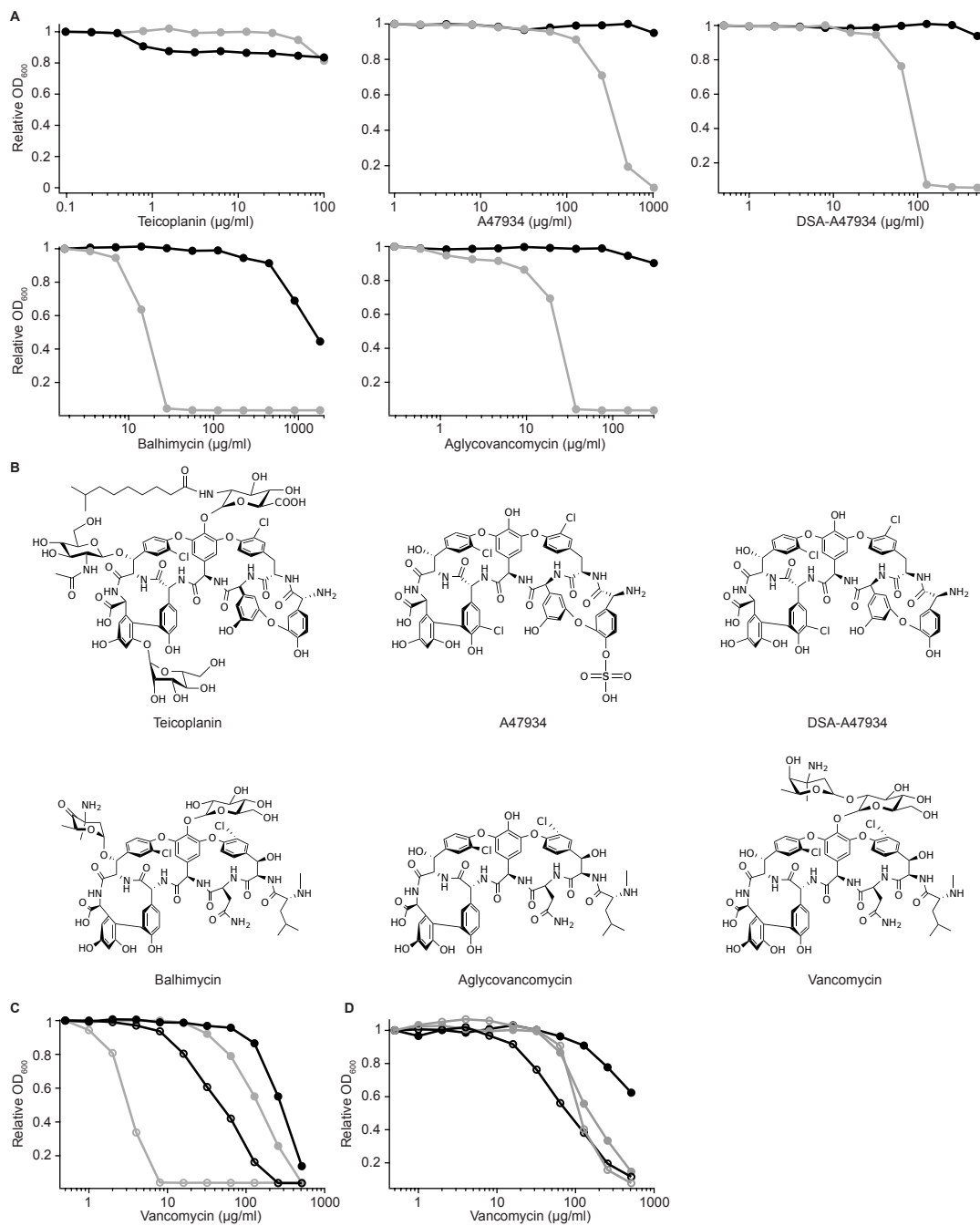


Figure S3

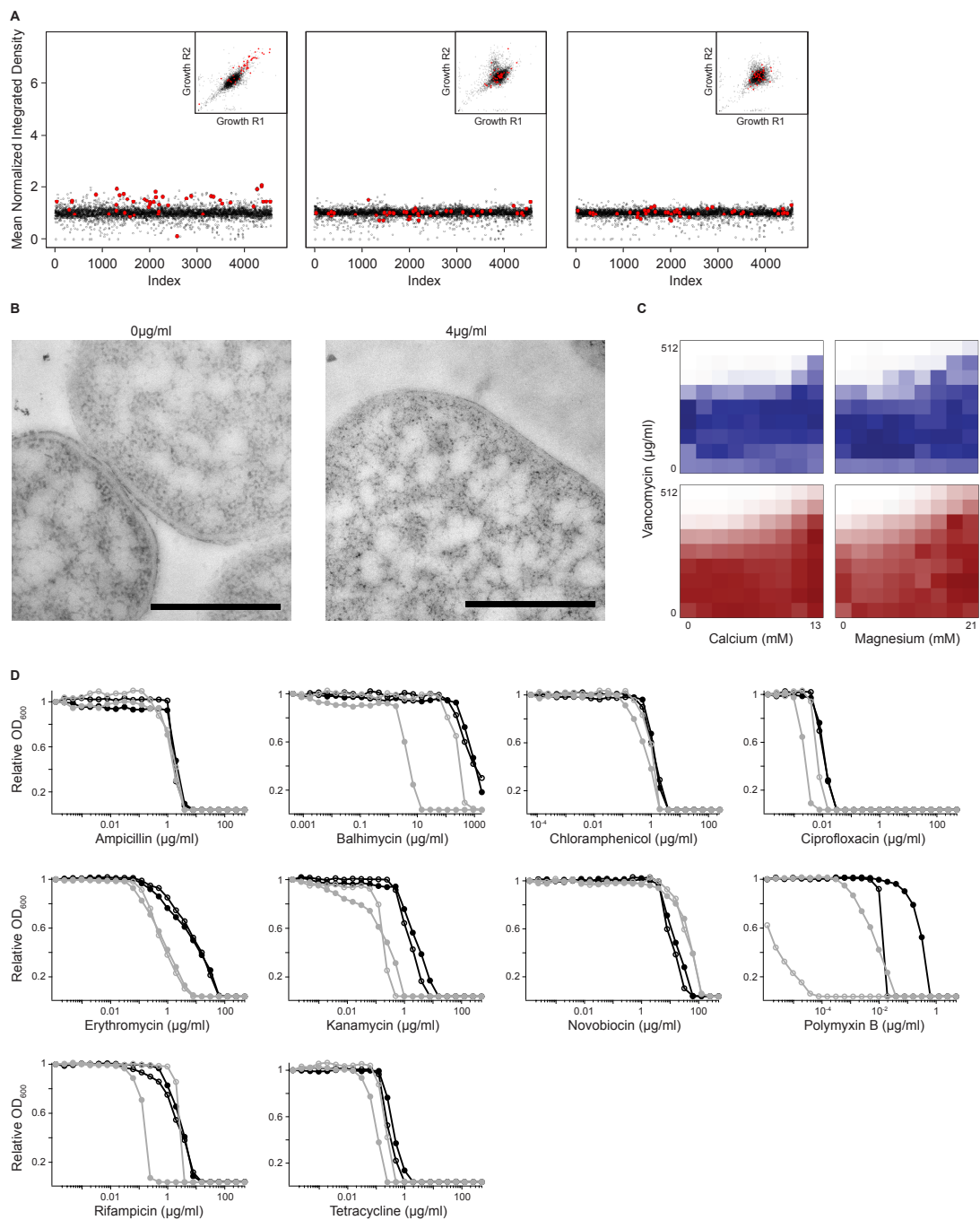


Figure S4

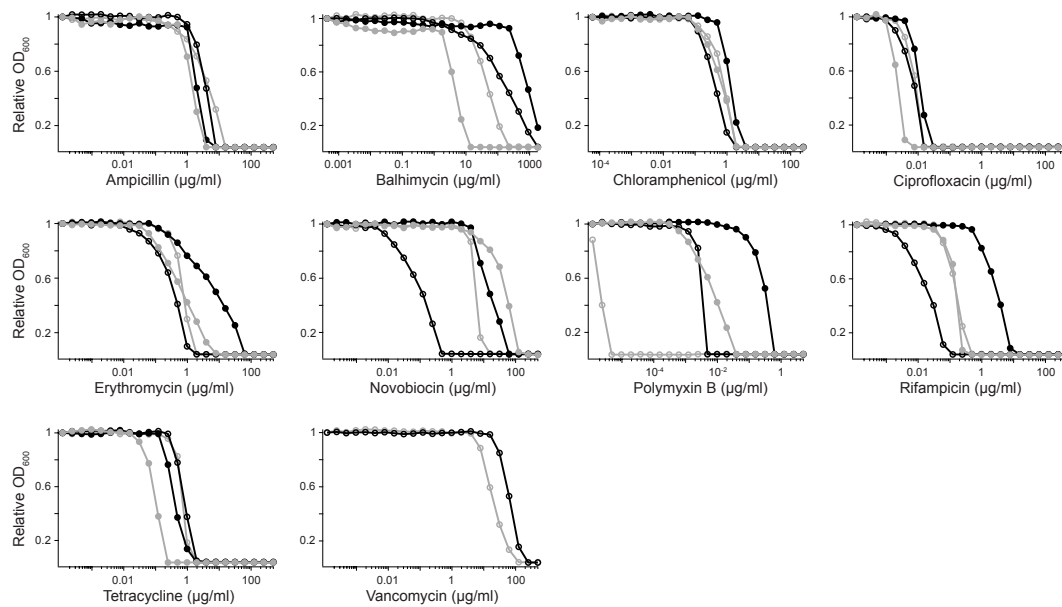


Figure S5

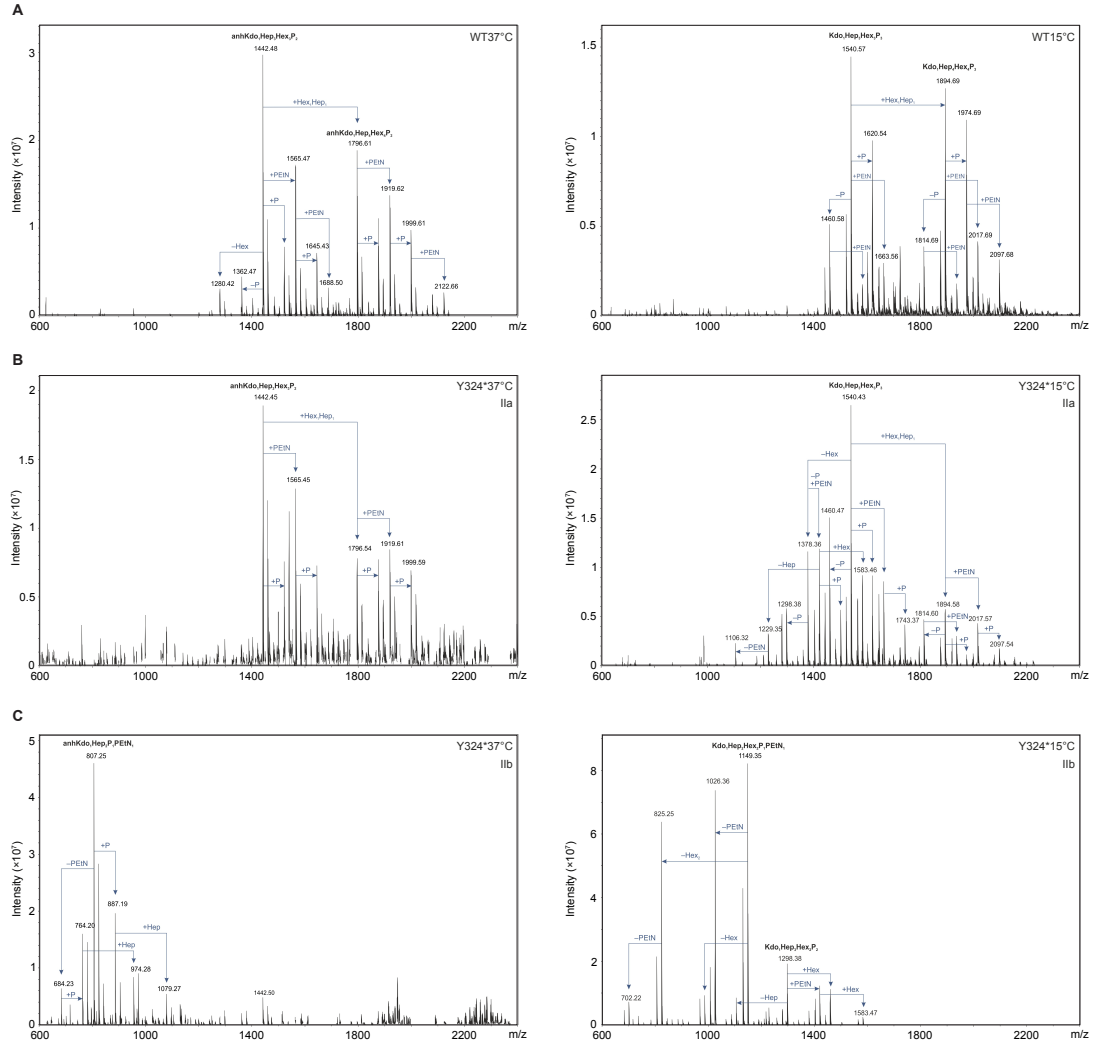
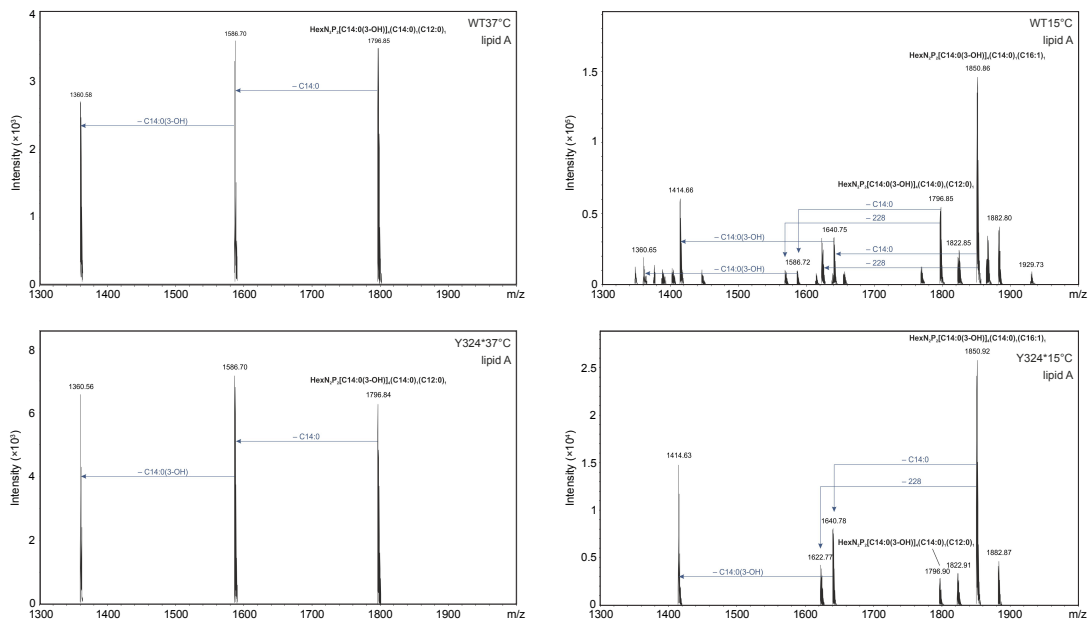


Figure S6



**CHAPTER V – An antiprotozoal drug overcomes *mcr-1* mediated colistin
resistance**

Preface

The work presented in this chapter is in preparation for submission, as of June 22, 2016:

Stokes JM, MacNair CR, Ilyas B, French S, Cote JP, Farha MA, Coombes BK, Brown ED. An antiprotozoal drug overcomes *mcr-1* mediated colistin resistance. *In preparation.*

I designed the vancomycin antagonism screening platform and conducted all *in vitro* antibiotic susceptibility assays. French S and Cote JP assisted in genetic screening experiments. French S performed atomic force microscopy. Ilyas B performed qRT-PCR. MacNair CR and Ilyas B assisted in murine infection models. I wrote the manuscript with input from all authors, particularly Farha MA.

The global dissemination of plasmid-borne colistin resistance threatens to cause a serious breach in our last line of defense against multidrug-resistant Gram-negative pathogens, and heralds the emergence of truly pan-resistant infections¹. To blame is the action of the *mcr-1* phosphoethanolamine (PEtN) transferase, which covalently modifies lipid A with PEtN, thereby reducing the affinity of polymyxins for lipopolysaccharide (LPS)^{2,3}. Addressing the rapidly diminishing number of treatment options for patients with Gram-negative infections is a public health priority, and begs for novel strategies to tackle multidrug-resistant Gram-negative pathogens^{4,5}. Difficulty in eradicating Gram-negative organisms is primarily due to their intrinsic resistance to many common antibiotics, largely afforded by the molecular architecture of their impermeable outer membrane⁶. As such, effective diffusion of most clinically useful antibiotics, which to date are targeted at intracellular processes, is inhibited. Herein, we describe the development of a novel screening platform tailored to specifically enrich for non-lethal outer-membrane active molecules, which would act as adjuvants to conventional antibiotics, by identifying compounds that antagonized the activity of vancomycin against *Escherichia coli* at low temperatures⁷. A subsequent counter screen further captured those molecules that retained activity in an *mcr-1* positive background. This approach identified the antiprotozoal drug pentamidine as an effective Gram-negative outer membrane perturbant.

Through interactions with LPS, pentamidine displayed potent synergy with canonical Gram-positive antibiotics against a wide scope of Gram-negative pathogens *in vitro*, as well as robust efficacy in a systemic *Acinetobacter baumannii* murine infection model at subclinical doses. Notably, the adjuvant activity of pentamidine persisted in cells expressing *mcr-1 in vitro* and *in vivo*. Overall, pentamidine and structurally analogous compounds represent important first-in-class molecules for the treatment of Gram-negative infections, particularly those harboring the *mcr-1* gene. Additionally, the widespread use of pentamidine as an antiprotozoal agent^{8,9} favorably positions this molecule for immediate clinical repurposing towards the treatment of antibiotic-resistant infections.

Previous work by our group has shown that *E. coli* becomes susceptible to vancomycin during periods of cold stress⁷. Paradoxically, this phenotype can be reversed through inactivation of genes involved in outer membrane biosynthesis, particularly those for the core oligosaccharide (core OS) of LPS. Given previous work has shown that genetic lesions in non-essential outer membrane biosynthesis machinery sensitize Gram-negative species to canonical Gram-positive antibiotics¹⁰, we reasoned that a low temperature vancomycin antagonism screening approach may enrich for non-lethal outer membrane perturbants. Indeed, a comparative analysis between *E. coli* gene deletion mutants that displayed vancomycin resistance at 15°C, and those that displayed enhanced sensitivity to the classical Gram-positive antibiotics erythromycin,

novobiocin, and/or rifampicin at 37°C, revealed unique similarities (Fig. 1a). Specifically, common among those strains that showed vancomycin resistance at 15°C, and antibiotic sensitivity at 37°C, were genes involved in outer membrane biosynthesis. Subsequent statistical analysis of all 41 gene deletion mutants that displayed vancomycin resistance at 15°C revealed a significant enrichment for genes involved in LPS and carbohydrate biosynthesis, as well those responsible for lipid metabolism and transport (Fig. 1b), all of which are essential to maintain outer membrane integrity.

Herein, we have leveraged these observations to develop a unique screening platform tailored to specifically detect non-lethal molecules that perturb outer membrane architecture. Indeed, compounds that can rescue *E. coli* in the presence of vancomycin at low temperature would enrich for perturbants of outer membrane integrity. Importantly, the sensitivity and specificity of this cold-dependent phenotype in capturing an outer membrane-centric target list renders it a powerful platform for drug screening, and far outpaces the more traditional antibiotic sensitivity screens which often lead to the identification of “nuisance” gene products¹¹.

Utilizing this approach, we carried out a screen of 1,440 previously approved drugs for those that suppressed the activity of vancomycin against *E. coli* at 15°C. Interestingly, only 3 hit compounds were identified, highlighting the specificity of this screening approach over more classical antibiotic potentiation screens¹². We followed up on these hits by assessing their ability to suppress

vancomycin activity at 15°C in a dose-dependent manner against wild-type *E. coli*, and subsequently counter screened for vancomycin suppression in *E. coli* expressing *mcr-1* to capture those active in this polymyxin-resistant background. Pentamidine, a clinically essential medicine for the treatment of pneumocystis pneumonia and West African trypanosomiasis, displayed the most potent suppression of vancomycin activity against wild type *E. coli* (Fig. 1c). Importantly, expression of *mcr-1* did not impair the ability of pentamidine to suppress vancomycin activity at low temperature (Fig. 1d).

Consistent with an ability to suppress vancomycin activity in the cold, atomic force microscopy of pentamidine-treated *E. coli* revealed a dramatic effect on outer membrane structure at 37°C. The surface topography of pentamidine-treated *E. coli* was characterized by undulations on the order of 40 nm in amplitude, whereas untreated *E. coli* remained largely uniform (Fig. 1e and Extended Data Fig. 1a-e). Interestingly, analysis of *E. coli* LPS upon treatment with pentamidine at 37°C failed to show inhibition of core OS biosynthesis (Extended Data Fig. 1f), suggesting that pentamidine may directly associate with the outer membrane to alter its architecture. Indeed, previous reports have shown that pentamidine and other aromatic diamidines display high affinity for purified lipid A *in vitro* ($K_d \sim 120$ nM)¹³⁻¹⁵, consistent with these observations.

Given its ability to disrupt outer membrane architecture, we reasoned pentamidine would act as an effective antibiotic adjuvant, sensitizing Gram-negative species to canonical Gram-positive antibiotics. Indeed, reminiscent to

the ability of polymyxin B nonapeptide (PMBn) to potentiate large molecular weight antibiotics through electrostatic associations with lipid A phosphate residues¹⁶⁻¹⁸, pentamidine similarly potentiated the activity of Gram-positive antibiotics against *E. coli* at 37°C (Fig. 2a). Specifically, pentamidine synergized with rifampicin, novobiocin, and erythromycin (fractional inhibitory concentration [FIC] index ≤ 0.5), all of which are hydrophobic, but not with the hydrophilic compound vancomycin. These data are consistent with antibiotic potentiation phenotypes previously observed with PMBn, where synergy with hydrophobic molecules was generally more pronounced than synergy with those that were hydrophilic¹⁹. Additionally, pentamidine failed to further enhance the activity of low molecular weight antibiotics that are able to passively diffuse through the outer membrane, or gain access to the cytoplasm through membrane porins (Extended Data Fig. 2a).

In lending support to the ability of pentamidine to disrupt outer membrane integrity through association with LPS, we tested the effect of exogenously adding LPS into the growth medium on the ability of pentamidine to potentiate rifampicin against *E. coli*. Addition of increasing concentrations of purified *E. coli* LPS to growth medium abolished pentamidine-dependent potentiation of rifampicin in a dose-dependent fashion (Fig. 2b and Extended Data Fig. 2b), suggesting binding of exogenous LPS to free pentamidine. Expectedly, the presence of exogenous LPS also suppressed the ability of PMBn to potentiate rifampicin (Extended Data Fig. 2c). Interestingly, both pentamidine and PMBn

failed to potentiate rifampicin when cells were grown in the presence of high concentrations of Mg^{2+} (Extended Data Fig. 2d), which assists in forming strong electrostatic interactions between adjacent LPS molecules²⁰. This observation suggests that both adjuvants can be competed from the cell surface by divalent cations, in agreement with a mechanism of antibiotic potentiation involving the disruption of lateral inter-LPS interactions. Additionally, pentamidine activated the PhoPQ two-component system, which is stimulated in Mg^{2+} -limiting conditions, and upon challenge with cationic peptides^{3,21} (Fig. 2c).

To gain further insight into the specific location where pentamidine associates with LPS, we analyzed the ability of pentamidine to potentiate rifampicin in each of 5 genetic backgrounds displaying various truncations of core OS (Fig. 2d and Extended Data Fig 2e). We observed that deeper truncations in core OS, or removal of core OS phosphate residues, resulted in more pronounced synergy, suggesting that pentamidine association with lipid A is a primary contributor to outer membrane disorganization and antibiotic potentiation. Indeed, a model whereby pentamidine disrupts lateral interactions between lipid A molecules is further supported by the observation that both terminal amidine groups are essential for pentamidine activity, and that increasing the inter-amidine distance or decreasing molecular flexibility proportionately increases rifampicin potentiation against *E. coli* (Table 1).

To evaluate the potentiation and spectrum exhibited by pentamidine against a wide variety of antibiotic-resistant Gram-negative pathogens, we

examined the *in vitro* activity of pentamidine in combination with rifampicin against a modest panel of clinical isolates. The ability of pentamidine to synergize with rifampicin persisted against a wide scope of antibiotic-resistant strains, including naturally polymyxin-resistant *Serratia* species, likely owing to the highly conserved chemistry of lipid A (Fig. 2e). The lack of potentiation against *Pseudomonas aeruginosa* may perhaps be rationalized by the presence of additional phosphate residues in core OS^{22,23}, decreasing the access of pentamidine to lipid A. However, an explanation for the absence of potentiation in *Proteus* and *Morganella* species remains elusive. Indeed, all *Serratia*, *Proteus*, and *Morganella* isolates tested were highly resistant to polymyxin B (data not shown). Further investigation is necessary to rationalize the varying activity of pentamidine in these genera in order to design analogs with full-spectrum coverage.

Where the incidence of polymyxin-resistant infections to date has been relatively rare, owing in part to the lack of horizontally-transferrable resistance determinants targeting this class of antibiotics, the recent global dissemination of the plasmid-borne *mcr-1* gene threatens the utility of the last-line polymyxins. In line with this resistance mechanism, we observed resistance to colistin – a clinically revived polymyxin²⁴ – (Extended Data Fig. 3a) and PMBn-dependent potentiation of rifampicin in *E. coli* expressing *mcr-1* (Fig. 3a). Notably, potentiation of rifampicin by pentamidine was not impacted by the expression of *mcr-1* (Fig. 3b and Extended Data Fig. 3b), suggesting that pentamidine is able to

associate with LPS in the presence of PEtN modifications on lipid A. Significantly, these phenotypes persisted in two environmental *E. coli* isolates harboring the *mcr-1* gene on natural plasmids (Fig. 3c, d and Extended Data Fig. 3c).

The broad *in vitro* efficacy of pentamidine in combination with Gram-positive antibiotics against diverse clinically relevant pathogens provided an opportunity to explore *in vivo* activity, and the therapeutic potential of repurposing pentamidine towards antibacterial use in the clinic. We used a systemic murine infection model of multidrug-resistant *A. baumannii* to test the efficacy of pentamidine in combination with novobiocin. Interestingly, the potency of pentamidine *in vitro* initially suggested that therapeutic concentrations *in vivo* may be inaccessible (Fig. 4a). However, we observed 100% survival of mice treated with 10 mg/kg pentamidine in combination with 5 mg/kg novobiocin (Fig. 4b), which represents 1/5th and 1/20th of human equivalent therapeutic doses, respectively. Accordingly, the majority of combination-treated mice contained no detectable *A. baumannii* in organ tissue at day 7 post-infection, highlighting bacterial cell clearance by combination therapy (Fig. 4c and Extended Data Fig. 4a-d). Importantly, mice displayed organ occupancy of $\sim 10^6$ CFU/ml/g at time of treatment (Extended Data Fig. 4e), showing that combination therapy cured an established infection, as opposed to acting prophylactically.

We next tested the efficacy of a combination of pentamidine and novobiocin in a systemic murine infection model of *A. baumannii* harboring the *mcr-1* gene on a natural plasmid (Extended Data Fig. 4f-i). Intriguingly, this

treatment succeeded only in modestly extending lifespan, but failed to rescue. Here, it is possible that the presence of PEtN on lipid A enhanced virulence through resistance to host cationic antimicrobial peptides, as has been described previously²⁵. Indeed, where administration of the bacteriostatic antibiotic novobiocin was sufficient to halt infection progression in *mcr-1* negative *A. baumannii*, we reasoned that clearance of an *mcr-1* positive infection would necessitate the administration of pentamidine with a bactericidal antibiotic such as rifampicin²⁶. Remarkably, co-administration of 10 mg/kg pentamidine and 4 mg/kg rifampicin rescued 2/3 of infected mice in a preliminary trial (Fig. 4d, e).

The acquisition of *mcr-1* by alarmingly common pathogens, such as carbapenem resistant Enterobacteriaceae²⁷, is resulting in the emergence of untreatable infections, and threatens to devastate healthcare practices worldwide. Here, we highlight the utility of a unique screening platform, and introduce a novel use for the antiprotozoal drug pentamidine as an antibiotic adjuvant for the treatment of *mcr-1* positive infections at sub-therapeutic doses. We posit that pentamidine and analogs thereof represent attractive leads as adjuvants to address the emerging threat of pan-resistant Gram-negative infections.

Methods

Genetic screening. The *E. coli* Keio collection²⁸ was pinned from frozen at 1536-density onto solid LB media using a Singer RoToR automated pinning system

(Singer Instruments). Media was supplemented with 64 $\mu\text{g/ml}$ erythromycin, 128 $\mu\text{g/ml}$ novobiocin, 8 $\mu\text{g/ml}$ rifampicin, or 32 $\mu\text{g/ml}$ vancomycin. All antibiotics were purchased from Sigma-Aldrich. Cells were grown at 37°C for 18 hours on LB containing erythromycin, novobiocin, or rifampicin; cells were grown at 15°C for 72 hours on LB containing vancomycin. After incubation, plates were scanned in transmissive mode on an Epson Perfection V750-M scanner (Epson) and quantitatively analyzed using ImageJ. Plate images were background subtracted using a 50-pixel rolling ball radius and converted to a binary image using the Otsu algorithm to identify colony margins. With colony margins identified, the integrated density (light absorption) of each was calculated as an indicator of cell number. Edge effects were corrected using a double-pass method across columns and rows based on the median value^{29,30}. Strains grown at 37°C in the presence of erythromycin, novobiocin, or rifampicin with growth at least 3σ less than the mean were defined as sensitive. Strains grown at 15°C in the presence of vancomycin with growth at least 3σ greater than the mean were defined as resistant. Genetic intersections between the various treatments were identified with the R statistical programming language³¹, and used to generate a 4-treatment Venn diagram. From the vancomycin resistant genetic subset of 41 strains, gene ontology (GO) terms were generated using EcoCyc pathway-tools³²⁻³⁴. This list was further refined to include transcriptional regulation and biosynthetic pathways using an enrichment analysis in EcoCyc pathway-tools.

Counts of the number of genes present for each GO term were compiled, along with p-values, to assess statistical enrichment for cellular processes.

Chemical screening. *E. coli* BW25113 was grown overnight in LB media and diluted 1/5000 into fresh LB containing 16 µg/ml vancomycin. 49.5 µl of cells were subsequently transferred to each well of a clear 384-well flat-bottom plate (Corning) using a Beckman Coulter Biomek FX^P laboratory automated workstation (Beckman Coulter). 0.5 µl of each molecule from a library of 1440 previously approved drugs was added to cells using a 96-head pin tool (V&P Scientific), in duplicate, such that the final screening concentration of each compound was 10 µM. Plates were immediately read at 600 nm using a Perkin Elmer EnVision plate reader (Perkin Elmer), then grown without shaking at 15°C for 96 hours. Plates were again read at 600 nm, and cell growth was calculated by subtracting the initial optical density (OD) of each well at time 0 from the final OD at 96 hours.

Checkerboard analyses. *E. coli* BW25113 was grown overnight in LB media and diluted 1/5000 into fresh LB. Vancomycin antagonism was determined by conducting standard checkerboard broth microdilution assays with 8 two-fold serially diluted concentrations of pentamidine (Sigma-Aldrich) and vancomycin against cells in a final volume of 100 µl. Plates were incubated without shaking at 15°C for 96 hours prior to reading at 600 nm. This duration was sufficient for untreated cultures to reach early-stationary phase. Antibiotic synergy was determined by diluting overnight cultures 1/10,000 and conducting checkerboard

broth microdilution assays with 8 two-fold serially diluted concentrations of various antibiotics in final volumes of 100 μ l. Plates were incubated at 37°C with continuous shaking in a Tecan Sunrise plate reader (Tecan), with reads at 600 nm taken every 10 minutes to monitor growth. At early-stationary phase for each strain, experiments were halted and final reads were used to generate checkerboard plots. For strains harboring the *mcr-1* gene, overnights were grown in the presence of 50 μ g/ml kanamycin (for *E. coli* BW25113 transformed with pDGP2:*mcr-1*), or 2 μ g/ml colistin (for all strains carrying natural plasmids). Core OS mutants used to analyze pentamidine-dependent rifampicin potentiation were gathered from the *E. coli* Keio collection, except for the Δ *waaC* strain, which was engineered using standard *E. coli* gene deletion techniques. Clinical isolates were curated from the Wright Clinical Collection. LPS purified from *E. coli* 0127:B8 (Sigma-Aldrich) or MgCl₂ (Sigma-Aldrich) was used in synergy inhibition experiments. Fractional inhibitory concentration (FIC) indices were calculated as described below. *MIC_a* is the minimum inhibitory concentration (MIC) of compound A alone; *MIC_{ac}* is the MIC of compound A in combination with compound B; *MIC_b* is the MIC of compound b alone; *MIC_{bc}* is the MIC of compound B in combination with compound A.

$$FIC_i = \frac{MIC_{ac}}{MIC_a} + \frac{MIC_{bc}}{MIC_b}$$

Antibiotic potency analyses. Cells were grown overnight in LB media, with or without selection as described above, and diluted 1/10,000 into fresh LB. Cells

were then introduced to 2-fold serial dilutions of antibiotic in a final volume of 100 μ l. Plates were incubated at 37°C with continuous shaking in a Tecan Sunrise plate reader (Tecan), with reads at 600 nm taken every 10 minutes to monitor growth. At early-stationary phase for each strain, experiments were halted and final reads were used to generate antibiotic potency plots. A conservative clinical MIC breakpoint for colistin of 2 μ g/ml was set by the Société Française de Microbiologie³⁵, and used to outline resistance in this study.

AFM sample preparation and imaging. Antibiotic treatments were prepared as described for antibiotic potency and checkerboard broth microdilution experiments. 50 μ l of mid-log culture (OD~0.5) was transferred to hydrophilic polycarbonate 0.2 μ m Millipore Isopore GTTP filters (Merck Millipore), on top of Kimwipes (Kimberly-Clark Professional) to absorb excess liquid across the filter. 50 μ l of 25 mM HEPES pH 7.0 was then passed over the culture and absorbed by a Kimwipe in order to flush extracellular salts from the LB medium. Once the liquid had been removed, the filter was quickly attached to a clean glass slide with a non-conductive double-sided adhesive tab. Samples were imaged using a Bruker BioScope Catalyst (Bruker), with a Nanoscope V controller. For each treatment, a 0.65 μ m thick Si₃N₄ triangular cantilever was used (Scan Asyst AIR, Bruker), with a symmetric tip and spring constant of about 0.4 N·m⁻¹. Scans were acquired at 25°C, with scan rates of 0.5 Hz and 512 samples per line (512 line) resolution, in PeakForce quantitative nanomechanical mapping (QNM) mode. Downstream image processing and analysis was performed using NanoScope

software (Bruker). Height images were flattened to compensate for cell curvature, and topographical sections were generated to accompany 2-dimensional and 3-dimensional reconstructions of surface texture.

LPS gel electrophoresis. *E. coli* BW25113 was grown overnight in LB media and diluted 1/10,000 into fresh LB containing various concentrations of pentamidine. Cells were grown at 37°C until early-log phase (OD~0.2), boiled in SDS-PAGE loading buffer for 10 minutes, and subsequently treated with proteinase K at 55°C overnight. The whole cell lysates were resolved on NuPAGE Novex 4-12% Bis-Tris gradient gels (Life Technologies) and LPS was visualized by silver staining. Minor variations between sample banding intensities can be attributed to slight differences in growth.

Quantitative reverse transcription PCR. Wild type *E. coli* BW25113 and *E. coli* BW25113 Δ *phoP* were grown overnight in LB media and diluted 1/5000 into 10 ml of LB supplemented with antibiotics as described. Cells were grown to mid-log phase (OD~0.5) and pelleted by centrifugation. Cells were then lysed in 2 ml TRIzol (Life Technologies) and incubated at room temperature for 5 minutes, or frozen at -20°C for later processing. Phase separation was performed by phenol-chloroform extraction. 200 μ l chloroform (Biobasic) was vigorously mixed with 1 ml TRIzol, followed by centrifugation at 12,000xg for 15 minutes at 4°C. The aqueous phase was collected, and RNA was isolated by isopropanol-ethanol extraction. The aqueous phase was mixed with 500 μ l of 100% isopropanol (Biobasic) per 1 ml of TRIzol reagent. After incubation at room temperature for 10

minutes, RNA was pelleted by centrifugation at 12,000xg for 15 minutes at 4°C. RNA was then washed with 75% ethanol and centrifuged once more under the same conditions. The resulting pellet was allowed to air dry for 10 minutes to remove any remaining ethanol, and resuspended in 100 µl of RNase free water (Ambion). RNA was subject to DNase I treatment (Ambion) for 30 minutes at 37°C, followed by DNase inactivation. The RNA was then re-purified from DNase I by a subsequent isopropanol-ethanol wash step. RNA was mixed with isopropanol at -20°C for 30 minutes, pelleted by centrifugation, washed once with 75% ethanol, re-pelleted, and resuspended in water. Prior to cDNA synthesis, RNA from all isolates was adjusted to identical concentrations. 600 ng total RNA from each sample was used for reverse transcription using the Quanta Biosciences qScript cDNA supermix (Quanta Biosciences), as well as for a no RT control. First strand cDNA was diluted 1/10 prior to qRT-PCR, which was conducted in 96-well format using the Light cycler 480 (Roche) with SYBR Green (PerfeCTa SYBR green supermix, Quanta Biosciences). Primers JS02F and JS02R were used to amplify *mgtA*, which is upregulated in response to PhoPQ activation³⁶, and JS03F and JS03R were used to amplify the housekeeping gene *rsmC*. Cycle threshold values were used to calculate RNA concentrations based on a standard curve for each primer pair. RNA concentrations for *mgtA* were then normalized to the RNA concentrations of *rsmC*. Experiments were conducted in technical and biological duplicates. JS02F – 5'cggtggtagtgccagaaaat3'; JS02R –

5'gtctcttttggcggatcaag3'; JS03F – 5'gaaattctggggcgaataca3'; JS03R –
5'ctttcacctcgaaaagacg3'.

Murine infection models. 7 to 9-week old C57BL/6 mice (Taconic Biosciences) were infected intraperitoneally with $\sim 3 \times 10^6$ CFU of *A. baumannii* clinical isolate B80510 with 5% porcine mucin. Cells were transformed with a natural plasmid isolated from *E. coli* strain N15-02866 for the *mcr-1* positive infection model. Infections were allowed to establish for 2 hours, and treatments were administered intraperitoneally as described. Phenotypic murine endpoint was determined using a 5-point body condition score analyzing weight loss, decrease in body temperature, respiratory distress, hampered mobility, and hunched posture. Experimental endpoint was defined as 7-days post-infection. At phenotypic or experimental endpoints, mice were sacrificed and organ tissues were dissected using sterile technique and placed into 1 ml sterile PBS at 4°C. Blood was acquired via cheek puncture and collected into sterile 2 ml heparinized tubes (BD Scientific). Organs were then homogenized using a high-throughput tissue homogenizer (ATS Scientific), serially diluted in PBS, and plated onto solid LB supplemented with 20 µg/ml chloramphenicol. Plates were incubated overnight at 37°C and colonies were quantified to determine organ load.

References

1. McGann, P. *et al.* *Escherichia coli* harboring *mcr-1* and *bla*CTX-M on a novel IncF plasmid: first report of *mcr-1* in the USA. *Antimicrob. Agents Chemother.* AAC.01103–16 (2016).

2. Liu, Y.Y. *et al.* Emergence of plasmid-mediated colistin resistance mechanism MCR-1 in animals and human beings in China: a microbiological and molecular biological study. *Lancet Infect. Dis.* **16**, 161–168 (2015).
3. Needham, B. D. & Trent, M. S. Fortifying the barrier: the impact of lipid A remodelling on bacterial pathogenesis. *Nat. Rev. Microbiol.* **11**, 467–481 (2013).
4. Bush, K. *et al.* Tackling antibiotic resistance. *Nat. Rev. Microbiol.* **9**, 894–896 (2011).
5. Brown, E. D. & Wright, G. D. Antibacterial drug discovery in the resistance era. *Nature* **529**, 336–343 (2016).
6. Nikaido, H. Molecular basis of bacterial outer membrane permeability revisited. *Microbiol. Mol. Biol. Rev.* **67**, 593–656 (2003).
7. Stokes, J. M. *et al.* Cold stress makes *Escherichia coli* susceptible to glycopeptide antibiotics by altering outer membrane integrity. *Cell Chem. Biol.* **23**, 267–277 (2016).
8. Curi, D. A. *et al.* IV pentamidine for *Pneumocystis jiroveci* pneumonia prophylaxis in pediatric allogeneic stem cell transplant patients. *Bone Marrow Transplant.* (2016). doi:10.1038/bmt.2016.133
9. Sands, M., Kron, M. A. & Brown, R. B. Pentamidine: A Review. *Rev. Infect. Dis.* **7**, 625–634 (1985).
10. Delcour, A. H. Outer membrane permeability and antibiotic resistance. *Biochim. Biophys. Acta* **1794**, 808–816 (2009).
11. Liu, A. *et al.* Antibiotic sensitivity profiles determined with an *Escherichia coli* gene knockout collection: generating an antibiotic bar code. *Antimicrob. Agents Chemother.* **54**, 1393–1403 (2010).
12. Taylor, P. L., Rossi, L., De Pascale, G. & Wright, G. D. A forward chemical screen identifies antibiotic adjuvants in *Escherichia coli*. *ACS Chem. Biol.* **7**, 1547–1555 (2012).
13. David, S. A., Bechtel, B., Annaiah, C., Mathan, V. I. & Balaram, P. Interaction of cationic amphiphilic drugs with lipid A: implications for development of endotoxin antagonists. *Biochim. Biophys. Acta* **1212**, 167–175 (1994).

14. David, S. A., Mathan, V. I. & Balaram, P. Interactions of linear dicationic molecules with lipid A: structural requisites for optimal binding affinity. *J. Endotoxin Res.* **2**, 325–336 (1995).
15. David, S. A. Towards a rational development of anti-endotoxin agents: novel approaches to sequestration of bacterial endotoxins with small molecules. *J. Mol. Recognit.* **14**, 370–387 (2001).
16. Vaara, M. & Vaara, T. Polycations as outer membrane-disorganizing agents. *Antimicrob. Agents Chemother.* **24**, 114–122 (1983).
17. Viljanen, P. & Vaara, M. Susceptibility of gram-negative bacteria to polymyxin B nonapeptide. *Antimicrob. Agents Chemother.* **25**, 701–705 (1984).
18. Vaara, M. *et al.* A novel polymyxin derivative that lacks the fatty acid tail and carries only three positive charges has strong synergism with agents excluded by the intact outer membrane. *Antimicrob. Agents Chemother.* **54**, 3341–3346 (2010).
19. Ofek, I. *et al.* Antibacterial synergism of polymyxin B nonapeptide and hydrophobic antibiotics in experimental gram-negative infections in mice. *Antimicrob. Agents Chemother.* **38**, 374–377 (1994).
20. Clifton, L. A. *et al.* Effect of divalent cation removal on the structure of Gram-negative bacterial outer membrane models. *Langmuir* **31**, 404–412 (2015).
21. Olaitan, A. O., Morand, S. & Rolain, J. M. Mechanisms of polymyxin resistance: acquired and intrinsic resistance in bacteria. *Front. Microbiol.* **26**, 5:643 (2014).
22. Bystrova, O. V. *et al.* Structural studies on the core and the O-polysaccharide repeating unit of *Pseudomonas aeruginosa* immunotype 1 lipopolysaccharide. *Eur. J. Biochem.* **269**, 2194–2203 (2002).
23. Knirel, Y. A. *et al.* Structural analysis of the lipopolysaccharide core of a rough, cystic fibrosis isolate of *Pseudomonas aeruginosa*. *Eur. J. Biochem.* **268**, 4708–4719 (2001).
24. Falagas, M. E. & Kasiakou, S. K. Colistin: the revival of polymyxins for the management of multidrug-resistant gram-negative bacterial infections. *Clin. Infect. Dis.* **40**, 1333–1341 (2005).

25. Trent, M. S., Stead, C. M., Tran, A. X. & Hankins, J. V. Diversity of endotoxin and its impact on pathogenesis. *J. Endotoxin Res.* **12**, 205–223 (2006).
26. Pachón-Ibáñez, M. E. *et al.* Efficacy of rifampin and its combinations with imipenem, sulbactam, and colistin in experimental models of infection caused by imipenem-resistant *Acinetobacter baumannii*. *Antimicrob. Agents Chemother.* **54**, 1165–1172 (2010).
27. Du, H., Chen, L., Tang, Y.-W. & Kreiswirth, B. N. Emergence of the mcr-1 colistin resistance gene in carbapenem-resistant Enterobacteriaceae. *Lancet Infect. Dis.* **16**, 287–288 (2016).
28. Baba, T. *et al.* Construction of *Escherichia coli* K-12 in-frame, single-gene knockout mutants: the Keio collection. *Mol. Syst. Biol.* **2**, 2006.0008 (2006).
29. Mangat, C. S., Bharat, A., Gehrke, S. S. & Brown, E. D. Rank ordering plate data facilitates data visualization and normalization in high-throughput screening. *J. Biomol. Screen.* **19**, 1314–1320 (2014).
30. French, S. *et al.* A robust platform for chemical genomics in bacterial systems. *Mol. Biol. Cell* **27**, 1015–1025 (2016).
31. Ihaka, R. & Gentleman, R. R: A language for data analysis and graphics. *J. Comp. Graph. Stat.* **5**, 299–314 (1996).
32. Keseler, I. M. *et al.* EcoCyc: fusing model organism databases with systems biology. *Nucleic Acids Res.* **41**, D605–D612 (2013).
33. Karp, P. D. Pathway databases: a case study in computational symbolic theories. *Science* **293**, 2040–2044 (2001).
34. Karp, P. D. *et al.* Pathway tools version 19.0 update: software for pathway/genome informatics and systems biology. *Brief. Bioinform.* bbv079 (2015).
35. Hasman, H. *et al.* Detection of mcr-1 encoding plasmid-mediated colistin-resistant *Escherichia coli* isolates from human bloodstream infection and imported chicken meat, Denmark 2015. *Euro Surveill.* **20**(49) (2015).
36. Groisman, E. A. The pleiotropic two-component regulatory system PhoP-PhoQ. *J. Bacteriol.* **183**, 1835–1842 (2001).

Acknowledgements

We thank Catrien Bouwman and Dr. Chris Whitfield from the University of Guelph for core OS analysis of *E. coli*; Arthur Sieron and Dr. Gerard Wright from McMaster University for the pDGP2:*mcr-1* plasmid; and Kali Iyer (formerly in the lab of E.D.B.) for assistance with murine infection experiments. This work was supported by the Natural Sciences and Engineering Research Council (Discovery Grant to E.D.B.), by a grant from Cystic Fibrosis Canada to E.D.B., by a Canadian Institutes of Health Research Foundation Grant to E.D.B., by project grants from the Canadian Institutes of Health Research to E.D.B. and B.K.C., by salary awards to E.D.B. and B.K.C. from the Canada Research Chairs Program, by a fellowship from the Fonds de recherche en santé du Québec to J.P.C., by a fellowship from the Canadian Institutes of Health Research DSECT Program to S.F., by a scholarship from the Ontario Graduate Scholarships Program to C.R.M., and by scholarships awarded to J.M.S. from the Canadian Institutes of Health Research and the Ontario Graduate Scholarships Program.

Author Contributions

J.M.S., C.R.M., B.I., S.F., J.P.C., B.K.C., and E.D.B. designed experiments; J.M.S. designed the vancomycin suppression screening platform; S.F., J.P.C., and J.M.S. performed genetic screens; J.M.S. performed the chemical screen; S.F. performed atomic force microscopy; J.M.S. performed *in vitro* antibiotic susceptibility assays; B.I. performed qRT-PCR experiments; J.M.S. engineered

the *mcr-1* positive *E. coli* and *A. baumannii* strains; C.R.M., B.I., and B.K.C. designed *in vivo* infection model experiments; C.R.M., B.I., and J.M.S. performed *in vivo* infection model experiments; J.M.S., M.A.F., and E.D.B. wrote the manuscript with input from all authors.

Figure Legends

Figure 1. A vancomycin antagonism screening platform identifies pentamidine. **a**, Venn diagram showing the number of gene deletion mutants that displayed sensitivity to novobiocin (blue), rifampicin (red), and/or erythromycin (yellow) at 37°C, and/or resistance to vancomycin (grey) at 15°C. The *E. coli* Keio collection was grown on solid LB media containing each antibiotic and colony size was determined by transmissive scanning³⁰. Bold numbers highlight the genes that displayed sensitivity to any combination of novobiocin, rifampicin, or erythromycin, as well as resistance to vancomycin. **b**, 41 gene deletion mutants that displayed resistance to vancomycin at 15°C were classified based on gene ontology (GO), biosynthetic pathway, or promoter activation, and statistical enrichment was calculated using EcoCyc pathway-tools³²⁻³⁴. The 8 most statistically enriched, non-redundant GO, biosynthetic pathway, and promoter activation classifications are shown. **c**, Checkerboard broth microdilution assay showing dose-dependent vancomycin suppression by pentamidine against wild type *E. coli* grown at 15°C for 96 hours. Dark regions represent higher cell density. **d**, Same as in **c**, except cells were transformed with

the pGDP2 plasmid containing *mcr-1*. **e**, Atomic force microscopy of wild type *E. coli* grown at 37°C in the presence of 25 µg/ml pentamidine. The white box (left) highlights the region scanned to obtain high-resolution topographical images of the cell surface (right). Scans were acquired at 25°C, with scan rates of 0.5 Hz and 512 samples per line resolution in PeakForce quantitative nanomechanical mapping (QNM) mode. Height images were flattened to compensate for cell curvature, and topographical sections were generated to accompany 2-dimensional and 3-dimensional reconstructions of surface texture.

Figure 2. Pentamidine potentiates Gram-positive antibiotics in Gram-negative pathogens. **a**, Checkerboard broth microdilution assays between pentamidine and rifampicin, novobiocin, erythromycin, or vancomycin against wild type *E. coli* at 37°C. Dark regions represent higher cell density. **b**, Purified *E. coli* LPS (2 mg/ml) was added to growth medium, and wild type *E. coli* was grown in the presence of varying concentrations of pentamidine and rifampicin at 37°C. Dark regions represent higher cell density. **c**, Dose-dependent activation of the PhoPQ two-component regulatory system by pentamidine. Wild type *E. coli* (blue) and *E. coli* Δ *phoP* (pink) were grown at 37°C until mid-log phase (OD~0.5), and transcript levels of *mgtA*, which is directly controlled by PhoPQ³⁶, were quantified relative to the housekeeping gene *rsmC* using quantitative reverse transcription PCR. Experiments were performed in technical and biological duplicates. Error bars represent standard error of means. **d**, Pentamidine-dependent rifampicin potentiation against *E. coli* displaying various truncations in core OS. Cells were

grown at 37°C and FIC indices were calculated using checkerboard broth microdilution assays as described in Methods. White letters indicate the Waa core OS biosynthetic gene that is responsible for addition of the corresponding residue. WaaY (pink) is necessary for the addition of phosphate to heptose II (pink). Loss of WaaP (*) prevents the addition of both core OS phosphates (*), as well as side-chain heptose III (*). Dark blue represents outer core OS; mid blue represents inner core OS; light blue represents 3-deoxy-D-manno-oct-2-ulosonic acid residues. **e**, Pentamidine-dependent potentiation of rifampicin against a spectrum of antibiotic-resistant Gram-negative clinical isolates using checkerboard broth microdilution assays. The FIC index cutoff defining synergy was set to ≤ 0.5 . Blue shows members of the Xanthomonadales; pink shows members of the Pseudomonadales; green shows members of the Enterobacteriales. At least 4 non-clonal isolates from each genus were tested with exception of *Salmonella* (*), for which only 1 clinical isolate was obtained.

Figure 3. Pentamidine is an adjuvant in Gram-negative organisms

containing *mcr-1*. **a**, Checkerboard broth microdilution assays showing dose-dependent rifampicin potentiation by PMBn against wild type *E. coli* (left) and *E. coli* containing the *mcr-1* gene on the pGDP2 plasmid (right). The FIC index increases from ≤ 0.09 to ≤ 0.5 in the presence of *mcr-1*. **b**, Checkerboard broth microdilution assays showing dose-dependent rifampicin potentiation by pentamidine against wild type *E. coli* (left) and *E. coli* containing the *mcr-1* gene on the pGDP2 plasmid (right). The FIC index is 0.25 irrespective of the presence

of *mcr-1*. **c**, PMBn-dependent potentiation of rifampicin against two environmental isolates of *mcr-1* positive *E. coli*, N15-02865 (left) and N15-02866 (right), both of which were isolated from contaminated meat samples. **d**, Pentamidine-dependent potentiation of rifampicin against *mcr-1* positive *E. coli* strains N15-02865 (left) and N15-02866 (right). All experiments were performed at 37°C. Dark regions represent higher cell density.

Figure 4. Pentamidine potentiates Gram-positive antibiotics against wild type and *mcr-1* positive *A. baumannii* in systemic murine infection models.

a, Checkerboard broth microdilution assay showing dose-dependent novobiocin potentiation by pentamidine against *A. baumannii* clinical isolate B80510 grown at 37°C. Dark regions represent higher cell density. **b**, Pentamidine-dependent potentiation of novobiocin in a systemic *A. baumannii* murine infection model. $\sim 3 \times 10^6$ CFU was injected intraperitoneally, and treatments were administered at 2-hours and 16-hours post-infection (arrows). Treatment groups of n=10 included PBS vehicle (black), 10 mg/kg pentamidine (pink), 5 mg/kg novobiocin (green), or a combination of 10 mg/kg pentamidine and 5 mg/kg novobiocin (blue). Phenotypic endpoint was defined using a body condition score as described in Methods. Experimental endpoint was defined as 7-days post-infection. **c**, Bacterial load in the spleen at phenotypic or experimental endpoint was determined by selective plating on chloramphenicol. Black lines represent geometric mean of the bacterial load for each treatment group. **d**, Checkerboard broth microdilution assay showing dose-dependent rifampicin potentiation by

pentamidine against *A. baumannii* B80510 containing the *mcr-1* gene on a natural plasmid isolated from *E. coli* strain N15-02866. Cells were grown at 37°C. Dark regions represent higher cell density. **e**, Pentamidine-dependent potentiation of novobiocin in a preliminary systemic *mcr-1* positive *A. baumannii* murine infection model. $\sim 3 \times 10^6$ CFU was injected intraperitoneally, and treatments were administered at 2-hours and 16-hours post-infection (arrows). Treatment groups of n=3 included PBS vehicle (black) 10 mg/kg pentamidine (pink), 4 mg/kg rifampicin (green), or a combination of 10 mg/kg pentamidine and 4 mg/kg rifampicin (blue). Phenotypic endpoint was defined using a body condition score as described in Methods. Experimental endpoint was defined as 7-days post-infection.

Extended Data Figure Legends

Extended Data Figure 1. Cell surface analyses of *E. coli* treated with outer-membrane active molecules. **a**, Atomic force micrographs of wild type *E. coli* grown in LB at 37°C to mid-log phase (OD~0.5). The white box (far left) highlights the region scanned to obtain high-resolution topographical images of the cell surface (right). Scans were acquired at 25°C, with scan rates of 0.5 Hz and 512 samples per line resolution in PeakForce quantitative nanomechanical mapping (QNM) mode. Height images were flattened to compensate for cell curvature, and topographical sections were generated to accompany 2-dimensional and 3-dimensional reconstructions of surface texture. **b**, Atomic force micrographs of

wild type *E. coli* grown to mid-log phase in LB supplemented with pentamidine were acquired as in **a. c**, Atomic force micrographs of wild type *E. coli* grown to mid-log phase in LB supplemented with polymyxin B were acquired as in **a. d**, Atomic force micrographs of wild type *E. coli* grown to mid-log phase in LB supplemented with 0.5 mM EDTA were acquired as in **a. e**, Potency analyses of pentamidine (left) and polymyxin B (right) against wild type *E. coli* grown at 37°C in biological duplicate. Hashed lines represent the concentrations of each molecule that were used for the acquisition of atomic force micrographs. **f**, Core OS composition of wild type *E. coli* grown in the presence of pentamidine. Cells were grown at 37°C until early-log phase (OD~0.2), and proteinase K-treated whole-cell lysates were subjected to SDS-PAGE followed by silver staining. DMSO was used as a solvent control.

Extended Data Figure 2. Pentamidine-dependent potentiation of antibiotics

against *E. coli*. **a**, Checkerboard broth microdilution assays between pentamidine and various structural classes of Gram-negative active antibiotics against wild type *E. coli* at 37°C. Dark regions represent higher cell density. **b**, Purified *E. coli* LPS was added to growth medium, and wild type *E. coli* was grown in the presence of varying concentrations of pentamidine and rifampicin at 37°C. LPS was added to final concentrations of 0.25 mg/ml (left), 0.5 mg/ml (middle), and 1 mg/ml (right). Dark regions represent higher cell density. **c**, Purified *E. coli* LPS (2 mg/ml) was added to growth medium, and wild type *E. coli* was grown in the presence of varying concentrations of PMBn and rifampicin at

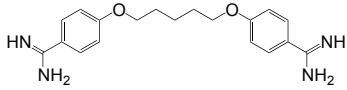
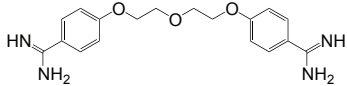
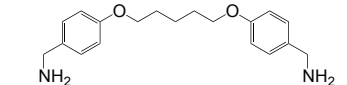
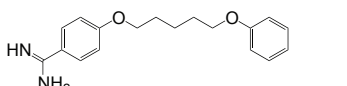
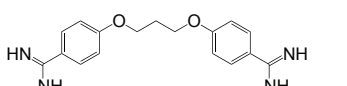
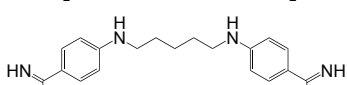
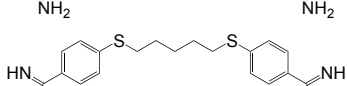
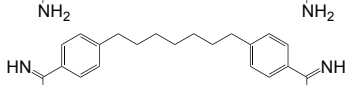
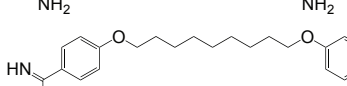
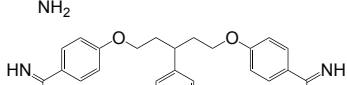
37°C. Dark regions represent higher cell density. **d**, Checkerboard broth microdilution assays between pentamidine and rifampicin (left) or PMBn and rifampicin (right) against wild type *E. coli* in LB media supplemented with 21 mM Mg²⁺. Cells were grown at 37°C. Dark regions represent higher cell density. **e**, Structure of wild type *E. coli* core OS and genes involved in its biosynthesis. Asterisks highlight biosynthetic genes that are functionally interdependent. Note that *E. coli* BW25113 does not contain O-polysaccharide.

Extended Data Figure 3. Sensitivity of *mcr-1* positive *E. coli* to colistin. a, Potency analyses of colistin against wild type *E. coli* (pink) and *E. coli* expressing *mcr-1* from the pGDP2 plasmid (blue). Cells were grown at 37°C in duplicate. **b**, Potency analyses of pentamidine against wild type *E. coli* (pink) and *E. coli* expressing *mcr-1* from the pGDP2 plasmid (blue). Cells were grown at 37°C in duplicate. **c**, Potency analyses of colistin against *E. coli* isolate N15-02865 (pink) and N15-02866 (blue). Cells were grown at 37°C in duplicate. Hashed lines represent the clinical MIC breakpoint for colistin (2 µg/ml).

Extended Data Figure 4. *In vivo* efficacy of pentamidine against *A. baumannii*. Bacterial loads in the lung (**a**), liver (**b**), kidney (**c**), and blood (**d**) at phenotypic or experimental endpoint were determined by selective plating on chloramphenicol. Black lines represent geometric mean of the bacterial load for each treatment group. **e**, Bacterial loads of *A. baumannii* in various organ tissues at 2-hours post infection with ~3x10⁶ CFU injected intraperitoneally (n=2). Note that all organs harvested contained ~10⁶ CFU/ml/g, showing full organ occupancy

at time of initial treatment. **f**, Potency analyses of colistin against wild type *A. baumannii* B80510 (pink) and *A. baumannii* B80510 containing the *mcr-1* gene on a natural plasmid isolated from *E. coli* strain N15-02866 (blue). Cells were grown at 37°C in duplicate. Hashed line represent the clinical MIC breakpoint for colistin (2 µg/ml). **g**, Checkerboard broth microdilution assay showing dose-dependent novobiocin potentiation by pentamidine against *A. baumannii* clinical isolate B80510 containing the *mcr-1* gene on a natural plasmid isolated from *E. coli* strain N15-02866. Cells were grown at 37°C. Dark regions represent higher cell density. **h**, Pentamidine-dependent potentiation of novobiocin in a systemic *mcr-1* positive *A. baumannii* murine infection model. $\sim 3 \times 10^6$ CFU was injected intraperitoneally, and treatments were administered at 2-hours and 16-hours post-infection (arrows). Treatment groups of n=5 or n=6 included PBS vehicle (black), 10 mg/kg pentamidine (pink), 5 mg/kg novobiocin (green), or a combination of 10 mg/kg pentamidine and 5 mg/kg novobiocin (blue). Phenotypic endpoint was defined using a body condition score as described in Methods. **i**, Bacterial load in the spleen at phenotypic endpoint was determined by selective plating on chloramphenicol. Black lines represent geometric mean of the bacterial load for each treatment group.

Table 1. Activity of pentamidine analogs against *E. coli*.

Structure	MIC _A	MIC _{AC}	MIC _R	MIC _{RC}	FIC Index
	200	25	12	1.5	0.25
	>200	100	12	6	<1
	>200	100	12	1.5	<0.63
	100	50	12	0.2	0.52
	200	25	12	3	0.38
	>200	50	12	1.5	<0.38
	50	6	12	0.8	0.19
	100	6	12	0.8	0.13
	25	1.5	12	0.2	0.08
	>200	6	12	0.2	0.05

FIC indices were calculated against *E. coli* using checkerboard broth microdilution assays with maximum concentrations of analog and rifampicin set to 200 µg/ml and 12 µg/ml, respectively. MIC_A is the minimum inhibitory concentration (MIC) of each analog alone; MIC_{AC} is the MIC of each analog in combination with rifampicin; MIC_R is the MIC of rifampicin alone; MIC_{RC} is the MIC of rifampicin in combination with each analog.

Figure 1

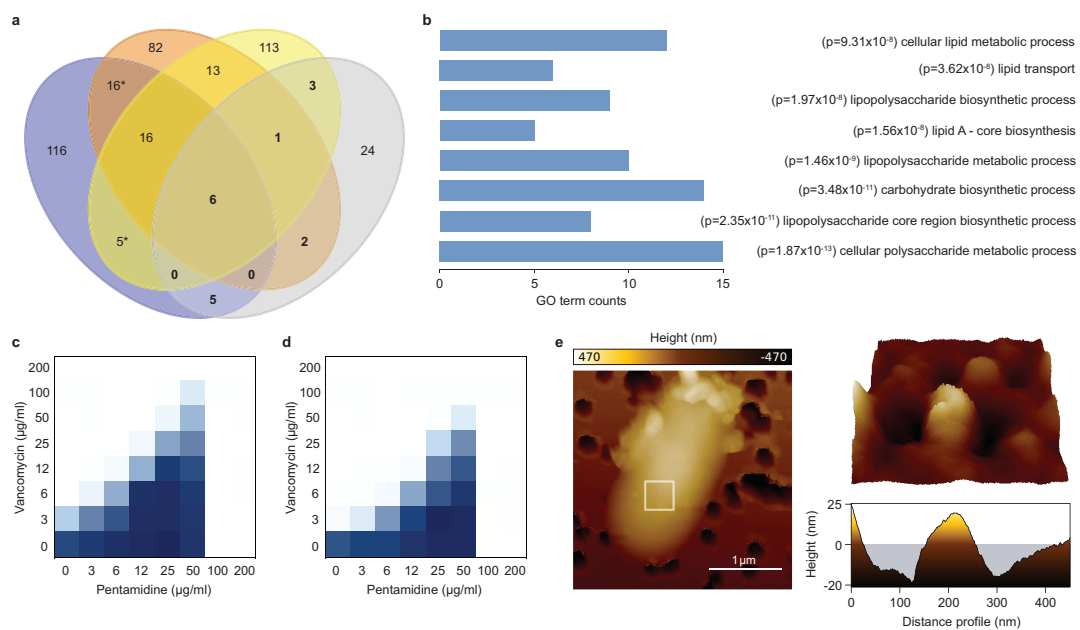


Figure 2

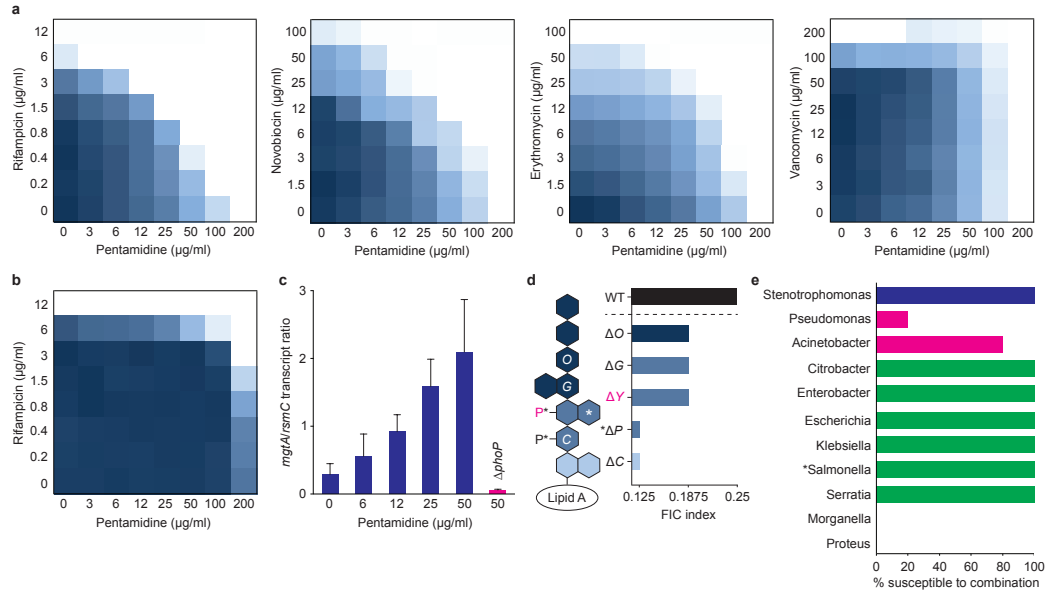


Figure 3

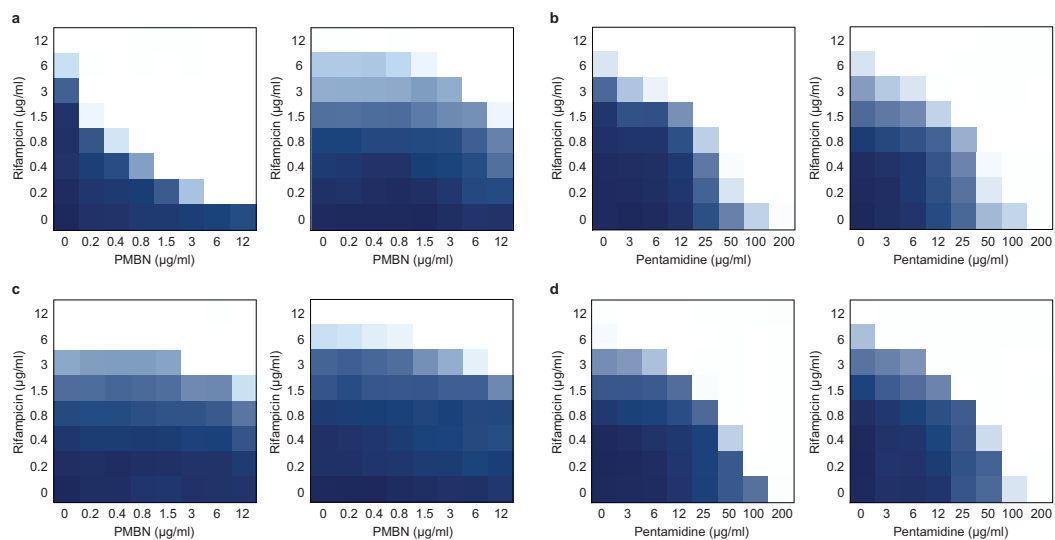
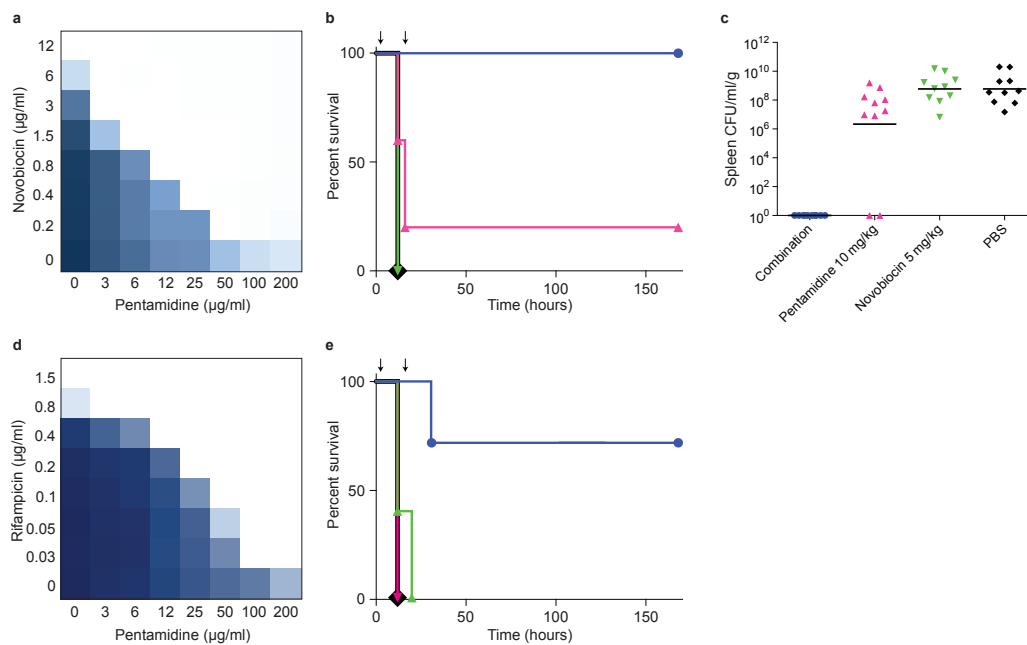
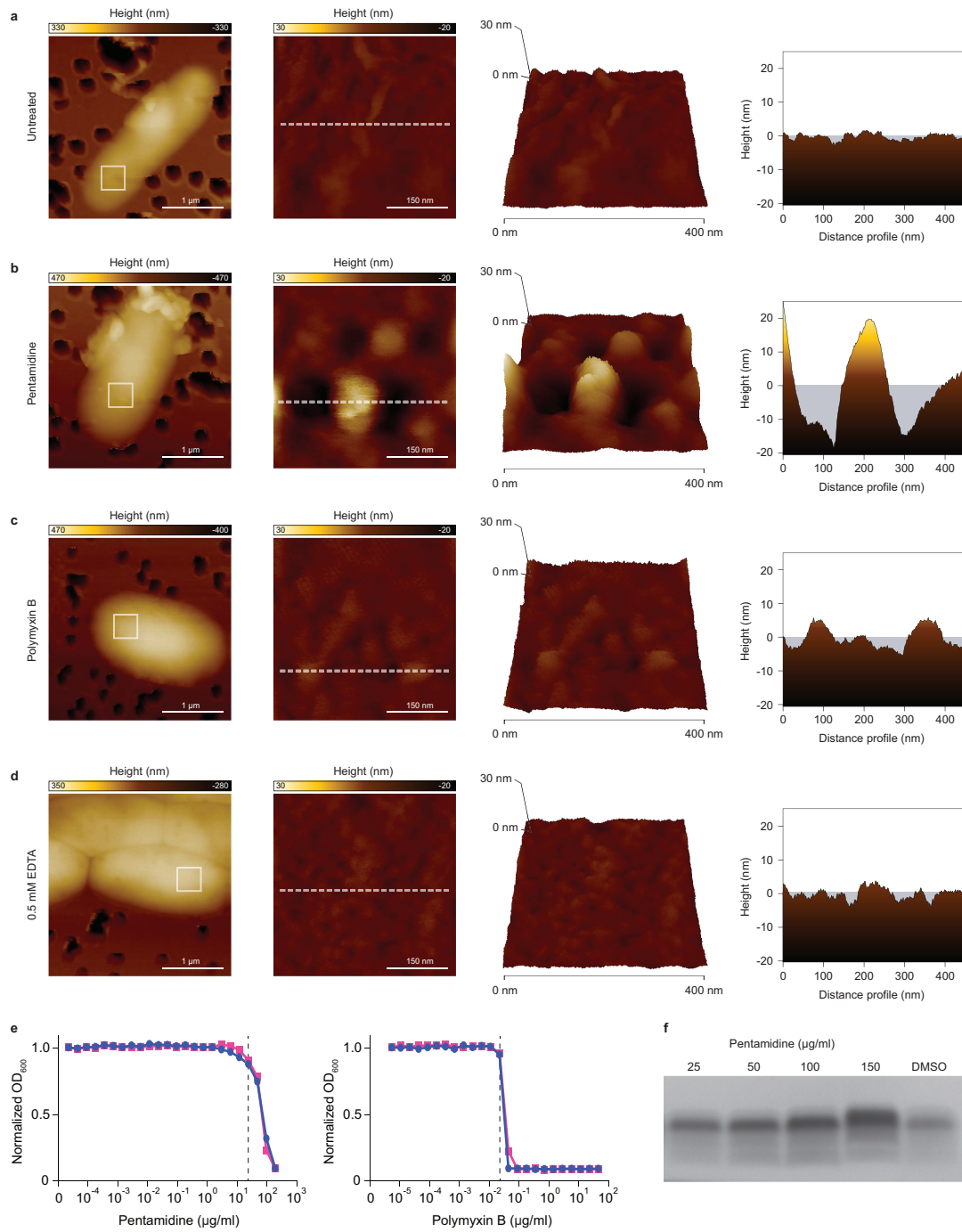


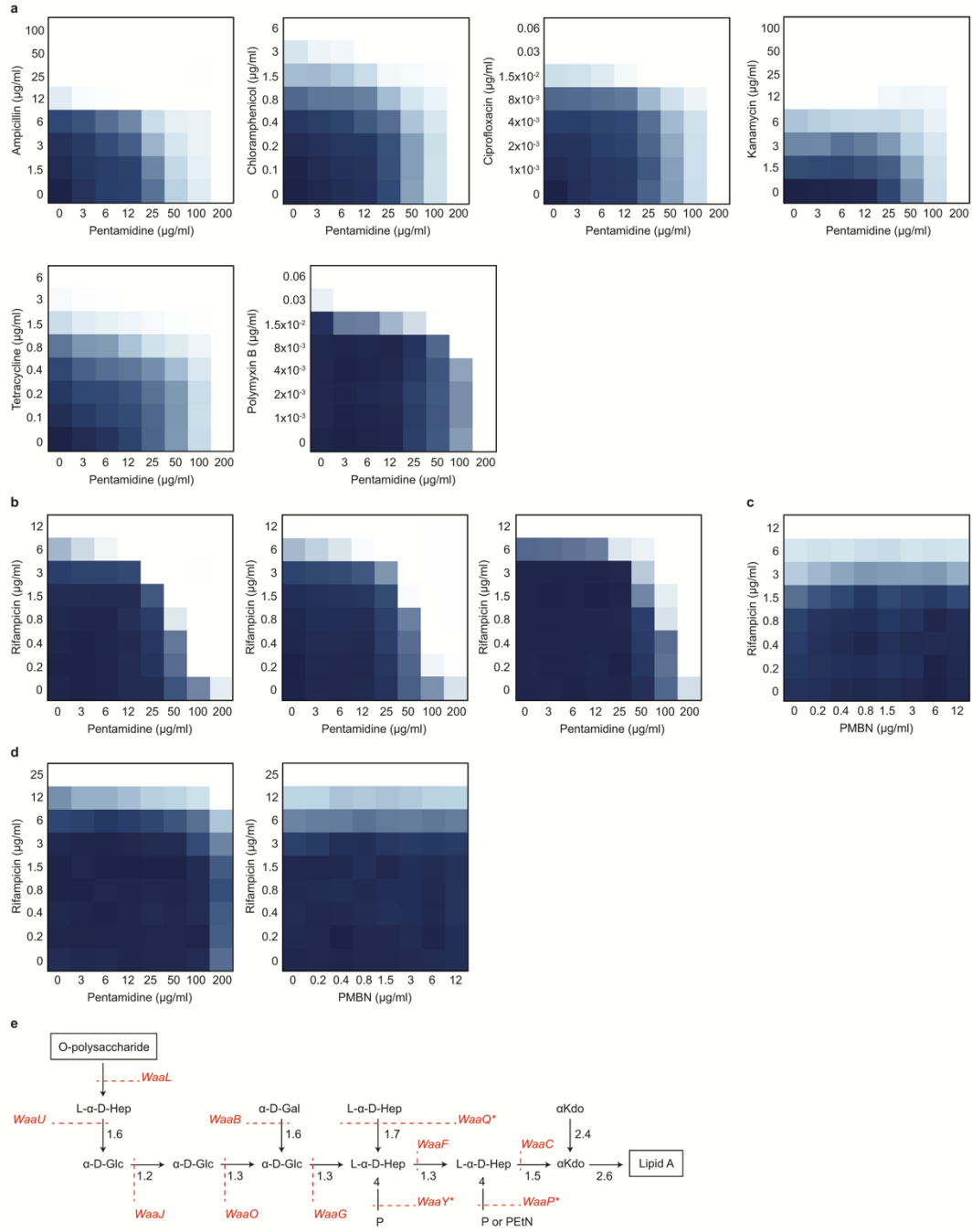
Figure 4



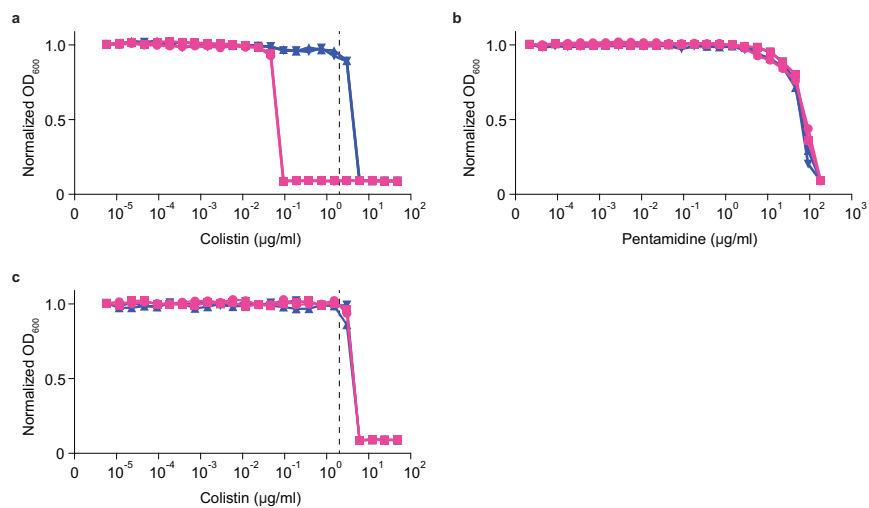
Extended Data Figure 1



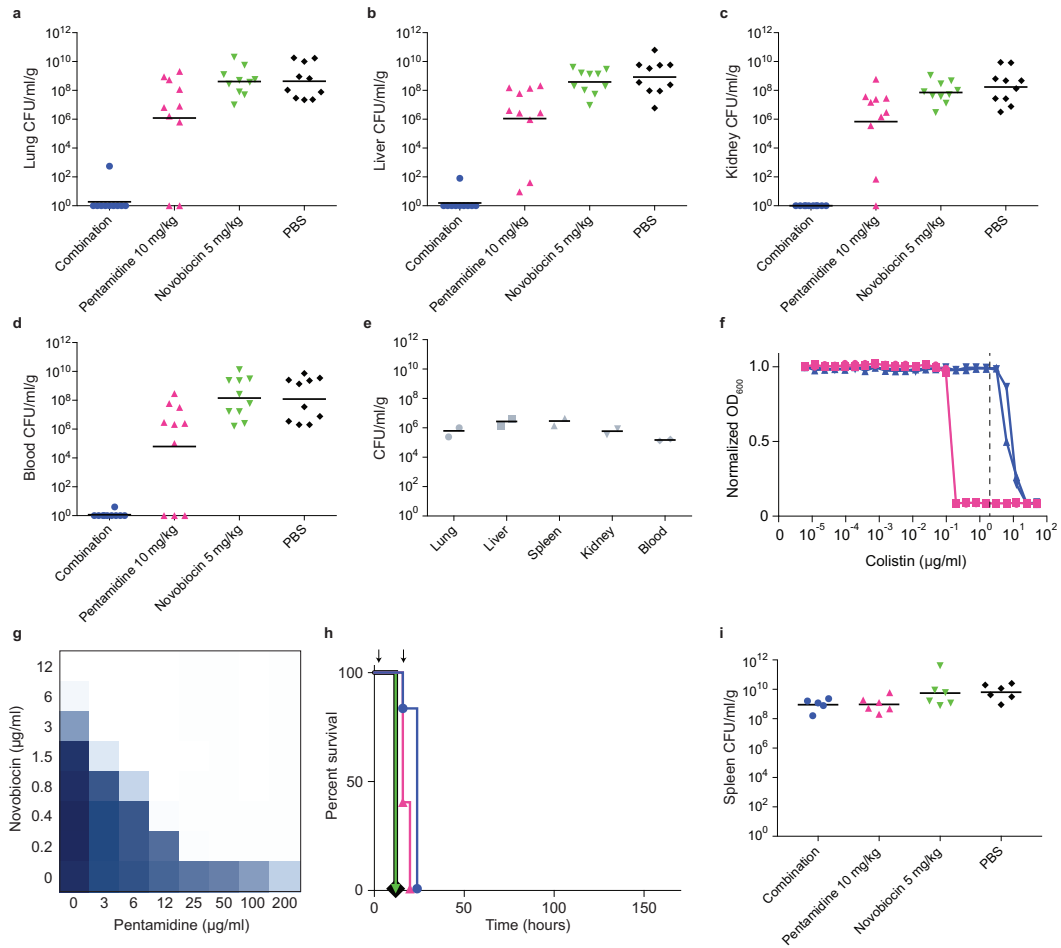
Extended Data Figure 2



Extended Data Figure 3



Extended Data Figure 4



CHAPTER VI – Conclusions

Suggestions for future research

The work presented herein, although wide in scope, begins to highlight the utility of exploiting the bacterial cold shock response in small molecule probe and antibiotic development. Chapter 2 describes the discovery and characterization of the first small molecule inhibitor of bacterial ribosome biogenesis, and strongly suggests a role for translation initiation factor IF2 in the assembly of both 30S and 50S subunits at low temperature¹. Chapter 3 builds on these observations by theorizing the benefits of small molecules in understanding the molecular events underlying ribosome assembly, and illuminating the drawbacks of conventional genetic approaches that have defined the investigation of this process *in vivo*². Chapter 4 introduces a tangential discussion of the idiosyncratic cold-dependent activity of vancomycin against *Escherichia coli*. Here, we reveal an interesting paradox where mutations that impeded Gram-negative outer membrane biosynthesis caused resistance to vancomycin³. Lastly, in chapter 5 we use the vancomycin sensitivity and resistance phenotypes of chapter 4 to develop a screening platform designed to enrich for non-lethal perturbants of the outer membrane. This screening approach subsequently resulted in the discovery of a novel antibiotic adjuvant capable of potentiating Gram-positive antibiotics against Gram-negative pathogens *in vitro* and *in vivo*.

Together, these investigations have allowed me to gain a deep appreciation for 2 divergent cellular components. It is worth noting here that a statement claiming my complete mastery of either ribosome biogenesis or outer

membrane permeability would be an insult to the giants upon whose shoulders I have stood. However, I will humbly state that I can sustain a reasonably intelligent conversation on both topics, and therefore feel sufficiently knowledgeable to propose a number of avenues for future investigation.

Is ribosome biogenesis an attractive drug target?

To this point, I have discussed the importance of small molecule inhibitors of ribosome biogenesis primarily in the context of biological probes. My avoidance of discussions regarding these molecules as antibiotics stems from minor uncertainties in my position. On one hand, this process is essential for life, metabolically demanding, and highly complex, the latter suggesting that there are many potentially druggable targets therein. However, the essentiality and obligatory complexity of this process has produced a dynamic assembly mechanism defined by pathway redundancies and non-linear relationships between maturation events, likely increasing the difficulty of discovering clinically useful inhibitors.

Chapter 3 includes a discussion of the various molecular events within ribosome biogenesis that, in theory, could be targeted by small molecules. These include (a) preventing rRNA transcription or processing, (b) sterically blocking r-protein/rRNA interactions, and (c) inhibiting the function of ribosome assembly factors. Targeted inhibition of rRNA transcription is an active area of study for the treatment of hyperproliferative disorders in humans, since eukaryotic RNA

polymerase I is solely responsible for rRNA synthesis. In bacteria, however, a single RNA polymerase transcribes all RNA species, thereby hampering the possibility for rRNA transcription-specific small molecule inhibitors. rRNA processing, on the other hand, may be an attractive target due to the essentiality of RNase E. This ribonuclease may be particularly interesting due to the fact that it is responsible for some of the earliest maturation events during ribosome biogenesis, namely the processing of pre-16S and pre-5S rRNA species – in addition to mRNA and tRNA⁴. Early rRNA processing may be considered one of the more predictable steps during ribosome assembly, which quickly increases in complexity as maturation progresses. For the reason that subunit assembly pathways become increasingly complex as ribosome biogenesis advances⁵, I believe that attempting to inhibit more stereotypical maturation steps, such as individual rRNA folding or r-protein/rRNA recognition events – whether or not they are mediated by ribosome biogenesis factors – will necessitate a combination therapy involving multiple compounds with distinct targets. While currently-identified genetic interactions between ribosome biogenesis factors are beginning to illuminate this possibility⁶, much more research is necessary to understand which combinations of perturbations are sufficient to completely prevent the biosynthesis of translationally competent subunits.

However, as I mention periodically throughout chapters 1 – 3, a small number of essential ribosome biogenesis factors exist that may make suitable targets for mono-therapeutic antibiotics. For instance, in chapter 3 I discuss the

essential 30S biogenesis factor Era, and at first consideration one may assume that this would make an ideal target towards the development of lethal ribosome biogenesis inhibitors. However, recall that since the early 1990s this GTPase has been associated with numerous functions within the cell, including acclimation to heat shock, ppGpp production, carbon source metabolism, and protein translation⁷⁻⁹. Ironically then, it may be that eventual small molecule inhibition of essential assembly factors such as Era may not prevent cell growth due to inhibition of ribosome biogenesis, but rather that of alternative cellular functions. Indeed, it will be interesting to observe whether other essential assembly factors are indispensable due to functions outside of ribosome biogenesis, or whether these govern unique bottlenecks within the assembly process.

If we assume the discovery of a ribosome biogenesis inhibitor with therapeutic potential – whether a single molecule or a combination – one must question what effects this may have on the cell. It is likely that specifically and completely preventing ribosome biogenesis would result in what may be termed delayed stasis. For example, work dating to the late 1990s has shown that conditional repression of the essential r-proteins L28 and L33 abruptly halts 50S subunit maturation, and causes the accumulation of a non-native 50S precursor¹⁰. Interestingly, upon repression, growth of this culture assumes arithmetically as opposed to exponentially. This is because growth is limited to the existing pool of translationally competent ribosomes, and with each successive division the ribosome concentration per cell is decreased by half. The

result of this is a decrease in growth rate by a factor of 2 with each division cycle, until the culture enters stasis. Interestingly, the observations with L28/L33 repression, as well as my own with lamotrigine, show that *E. coli* undergoes between 4 and 5 divisions before entering stasis. As a basic scientist, the suggestion that an enigmatic mechanism preventing cells from dividing to death is intriguing, and surely worth investigation. However, from the perspective of a drug discoverer, one may have a preference for molecules that display a more rapid and direct route to cell lethality.

Is ribosome biogenesis appealing from an antibiotic discovery viewpoint? As a mono-therapeutic target, perhaps with the exception of the early-functioning RNase E, perhaps not. However, until such a molecule – or combination of molecules – that functions at 37°C is discovered and tested against a relevant pathogen *in vivo*, this is highly speculative. Indeed, previous work has shown that deletion of the non-essential 30S biogenesis factor RsgA in *Staphylococcus aureus* attenuates virulence, suggesting that non-essential ribosome assembly factors may represent potential anti-virulence targets¹¹. Furthermore, the possibility remains that inhibition of ribosome assembly may potentiate antibiotics with alternative functions. Since this process is intimately coupled to protein translation, combinations of inhibitors targeting both assembly and translation may make for potentially synergistic combination therapies. Additionally, combinations of ribosome biogenesis inhibitors with compounds that perturb metabolism may also result in synergy due to the large metabolic demand of the

assembly process. Therefore, I encourage the discovery of a large collection of functionally diverse ribosome biogenesis inhibitors not only in the context of highly precise biological probes, as discussed in chapters 2 and 3, but also in the context of attempting to make this central process rich for antibiotic development. Essential for the success of the latter goal, continuing studies of ribosome biogenesis should integrate systems-level approaches so that we may more thoroughly understand how this process relates to other aspects of the cell. Indeed, systems biology has yet to be sufficiently adopted by those interested in ribosome biogenesis, surely to our detriment in both understanding fundamental cell physiology, as well as discovering new antibiotics.

How should we target the Gram-negative outer membrane?

My venture into the Gram-negative outer membrane stemmed from a curiosity of the temperature-dependent activity of vancomycin against *E. coli*. Indeed, the paper that comprises chapter 4 was never intended to form the foundation of a small molecule screening platform for outer membrane active compounds; it was a basic science paper intended to highlight a paradoxical phenomenon. The fact that we have been able to leverage the cold sensitivity of *E. coli* to vancomycin is extremely exciting, and has forced upon me a world for which I had little interest at the start of my graduate studies.

A number of recent publications from the pharmaceutical sector have highlighted their difficulties in identifying Gram-negative-active compounds^{12,13}.

As is discussed in chapter 1, this stems largely from the observation that hydrophobic compounds tend to potently inhibit enzyme targets, yet these molecules generally display poor permeability through the outer membrane. The opposing forces governing *in vitro* versus *in vivo* activity act as a stern reminder of our poor understanding of how molecules traverse this surface. Indeed, however unnecessary, one must urge investigators to continue to study the Gram-negative cell surface with the goal of creating chemical rules that will marry potent *in vitro* activity with a high rate of penetration through the cell envelope. One method to accomplish this may involve systematically curating a large collection of molecules – perhaps on the order of $\sim 10^3$ – with varying *in vitro* and *in vivo* potencies, and taking a cheminformatics approach to elucidate the chemical characteristics that maximize both. Indeed, this method may initially necessitate the absence of efflux mechanisms, but this is a variable that can be subsequently introduced.

Admittedly, this may be a decades-long problem to solve, but is a worthwhile effort towards the development of novel antibacterial therapies for Gram-negative infections. In the near-term, compounds that perturb native outer membrane composition will likely play a critical role in expanding the therapeutic utility of current antibiotics. As discussed in chapter 5, polymyxin B nonapeptide is an analog of polymyxin B that lacks the fatty acyl tail present on polymyxin B and colistin¹⁴. This hydrophobic chain provides the latter 2 molecules the ability to depolarize the inner membrane, causing lysis. However, while polymyxin B

nonapeptide lacks intrinsic bactericidal activity, its ability to disrupt the outer membrane through electrostatic association with lipid A allows for potent antibiotic potentiation¹⁵. Unsurprisingly, structural analogs of polymyxin B nonapeptide are currently in preclinical development, however the emergence of plasmid-borne polymyxin resistance determinants already threatens their potential clinical utility. Therefore, future work should aim to enhance our repertoire of molecules capable of perturbing native outer membrane structure.

The vancomycin suppression screen described herein is a powerful tool towards this goal. Indeed, through a screen of just 1,440 molecules, we have already identified pentamidine as an adjuvant capable of potentiating large hydrophobic molecules against a myriad of Gram-negative pathogens. The observation that pentamidine is able to overcome *mcr-1*-mediated polymyxin resistance may be the result of good fortune, as opposed to an inherent trait unintentionally built into the screening platform. However, it will be interesting to see whether other molecules identified through this method are also insensitive to current polymyxin-resistance mechanisms. Indeed, such investigations should not be too distant, since some 140,000 synthetic molecules have recently been subjected to this screen. Upon selection of the most promising hits from this effort, I suggest that screens of natural product extracts ensue. Polymyxin B and colistin are natural products produced by the soil-dwelling Gram-positive bacterium *Paenibacillus polymyxa*, and I posit that other molecules that disrupt

the outer membrane directly, or through inhibition of core OS biosynthesis, may be discovered through the vancomycin suppression platform.

Importantly, where this screen falls short is in identification of molecules that target essential steps in LPS biosynthesis, namely the first 7 steps of the Raetz pathway¹⁶, and transfer of LPS from the inner membrane to the cell surface¹⁷. Since LpxC and LptD are the only essential LPS biosynthetic enzymes against which whole cell-active small molecules have been discovered, lipid A biosynthesis and LPS transport are cellular processes ripe for antibiotic development. While inhibitors of these enzymes may be discovered through *in vitro* approaches, downstream efforts are likely to be hindered due to poor cell permeability. Therefore, I suggest that cell-based phenotypes be elucidated that can engage these targets. One interesting phenotype that may be leveraged towards this goal is the non-essentiality of LPS in *Acinetobacter baumannii*^{18,19}. Understanding this fascinating anomaly may facilitate its transfer to lab strains of *E. coli*, which would allow for a screen where one identifies molecules that inhibit the growth of wild type cells, but not those carrying the machinery necessary to render LPS non-essential.

The unique LPS dispensability phenotype displayed by *A. baumannii* brings us to the last aspect of the outer membrane that, to me, makes this an extremely attractive target for the development of next-generation antibiotics – evolutionary divergence. Indeed, differences in LPS chemistry have been observed across species, and this begs the question of whether compounds that

recognize specific chemical patterns may be identified. In this manner, treatments can be developed that target individual pathogens while avoiding commensal bacteria, which we are now understanding to be critical to human health²⁰. For example, cationic antimicrobial peptides that bind to lipid A phosphate residues have recently been observed to spare the commensal Gram-negative *Bacteroides thetaiotaomicron*²¹. This is likely the result of co-evolution, where this bacterium has evolved to dephosphorylate lipid A at the 4' position, decreasing antimicrobial peptide affinity. Indeed, future efforts aimed at identifying novel outer membrane-targeting molecules should consider the evolutionarily-guided mechanisms through which the host immune system recognizes pathogens, yet disregards human flora.

Concluding remarks

The work presented herein has aimed to increase our understanding of ribosome assembly and Gram-negative outer membrane permeability. Where ribosome biogenesis remains poorly understood, chemical tools will surely help to illuminate the molecular details underlying this process. Indeed, the use of lamotrigine has already implicated translation initiation factor IF2 in the assembly process, a function that had eluded observation for decades. In the long-term, I am hopeful that investigators can leverage forthcoming ribosome assembly inhibitors towards the development of a new functional class of antibiotics; I like

to believe that our cold-sensitivity approach serves as an intellectually budding proof-of-principle towards this challenging goal.

However, due to our understanding of the effects of outer membrane perturbation on antibiotic susceptibility, it is my opinion that molecules targeting LPS are of more immediate clinical utility. I am cautiously optimistic that our vancomycin suppression screening platform will uncover molecules with therapeutic potential, since a small screen of just 1,440 compounds has already revealed pentamidine. Therefore, I urge investigators to maximize the utility of this approach, and significantly improve its capabilities, perhaps taking into account some of the ideas I mentioned above. This being stated, Richard Feynman wrote in *The Meaning of It All*, “But see that the imagination of nature is far, far greater than the imagination of man”, so perhaps you should look there for inspiration too.

References

1. Stokes, J. M., Davis, J. H., Mangat, C. S., Williamson, J. R. & Brown, E. D. Discovery of a small molecule that inhibits bacterial ribosome biogenesis. *Elife* **3**, e03574 (2014).
2. Stokes, J. M. & Brown, E. D. Chemical modulators of ribosome biogenesis as biological probes. *Nat Chem Biol.* **11**, 924–932 (2015).
3. Stokes, J. M. *et al.* Cold stress makes *Escherichia coli* susceptible to glycopeptide antibiotics by altering outer membrane integrity. *Cell Chem Biol.* **23**, 267–277 (2016).
4. Mackie, G. A. RNase E: at the interface of bacterial RNA processing and decay. *Nat Rev Microbiol.* **11**, 45–57 (2013).

5. Mulder, A. M. *et al.* Visualizing ribosome biogenesis: parallel assembly pathways for the 30S subunit. *Science* **330**, 673–677 (2010).
6. Shajani, Z., Sykes, M. T. & Williamson, J. R. Assembly of Bacterial Ribosomes. *Annu Rev Biochem.* **80**, 501–526 (2011).
7. Gollop, N. & March, P. E. A GTP-binding protein (Era) has an essential role in growth rate and cell cycle control in *Escherichia coli*. *J Bacteriol.* **173**, 2265–2270 (1991).
8. Britton, R. A. *et al.* Cell cycle arrest in Era GTPase mutants: a potential growth rate-regulated checkpoint in *Escherichia coli*. *Mol Microbiol.* **27**, 739–750 (1998).
9. Sayed, A., Matsuyama, S. I. & Inouye, M. Era, an essential *Escherichia coli* small G-protein, binds to the 30S ribosomal subunit. *Biochem Biophys Res Commun.* **264**, 51–54 (1999).
10. Maguire, B. A. & Wild, D. G. The roles of proteins L28 and L33 in the assembly and function of *Escherichia coli* ribosomes in vivo. *Mol Microbiol.* **23**, 237–245 (1997).
11. Campbell, T. L., Henderson, J., Heinrichs, D. E. & Brown, E. D. The yjeQ Gene Is Required for Virulence of *Staphylococcus aureus*. *Infect Immun.* **74**, 4918–4921 (2006).
12. Tommasi, R., Brown, D. G., Walkup, G. K., Manchester, J. I. & Miller, A. A. ESKAPEing the labyrinth of antibacterial discovery. *Nat Rev Drug Discov.* **14**, 529–542 (2015).
13. Brown, D. G., May-Dracka, T. L., Gagnon, M. M. & Tommasi, R. Trends and exceptions of physical properties on antibacterial activity for Gram-positive and Gram-negative pathogens. *J Med Chem.* **57**, 10144–10161 (2014).
14. Viljanen, P. & Vaara, M. Susceptibility of gram-negative bacteria to polymyxin B nonapeptide. *Antimicrob Agents Chemother.* **25**, 701–705 (1984).
15. Vaara, M. Agents that increase the permeability of the outer membrane. *Microbiol Rev.* **56**, 395–411 (1992).
16. Whitfield, C. & Trent, M. S. Biosynthesis and export of bacterial lipopolysaccharides*. *Annu Rev Biochem.* **83**, 99–128 (2014).

17. Okuda, S., Sherman, D. J., Silhavy, T. J., Ruiz, N. & Kahne, D. Lipopolysaccharide transport and assembly at the outer membrane: the PEZ model. *Nat Rev Microbiol.* **14**, 337–345 (2016).
18. Bojkovic, J. *et al.* Characterization of an *Acinetobacter baumannii* lptD deletion strain: permeability defects and response to inhibition of lipopolysaccharide and fatty acid biosynthesis. *J Bacteriol.* **198**, 731–741 (2015).
19. Moffatt, J. H. *et al.* Colistin resistance in *Acinetobacter baumannii* is mediated by complete loss of lipopolysaccharide production. *Antimicrob Agents Chemother.* **54**, 4971–4977 (2010).
20. Cho, I. & Blaser, M. J. The human microbiome: at the interface of health and disease. *Nat Rev Genet.* **13**, 260–270 (2012).
21. Cullen, T. W. *et al.* Gut microbiota. Antimicrobial peptide resistance mediates resilience of prominent gut commensals during inflammation. *Science* **347**, 170–175 (2015).